

# R&T

## 1999 Research & Technology



**Glenn Research  
Center at Lewis Field**

**Cleveland, Ohio  
NASA/TM-2000-209639**

**About the cover:**

- Top right: Cloud particle sizing probes in Glenn's Icing Research Tunnel; NASA Twin Otter icing research aircraft; and right wing of NASA Twin Otter showing Supercooled Large Droplet ice accretion and cloud-particle sizing probe (pp. 82–83).
- Center: VentureStar reusable launch vehicle, which will use a titanium aluminide metallic thermal protection system (pp. 99–100).
- Bottom left: Glenn's cool flame experiment aboard NASA's KC–135 reduced-gravity aircraft studies very weak flames that spontaneously occur at temperatures as low as 120 °C and can develop into conventional hot flames under certain conditions (pp. 141–143).

# Research & Technology 1999



National Aeronautics and  
Space Administration

**Glenn Research Center**  
Cleveland, Ohio 44135-3191

**NASA/TM—2000-209639**

Trade names or manufacturers' names are used in this report for identification only. This usage does not constitute an official endorsement, either expressed or implied, by the National Aeronautics and Space Administration.

Available from

NASA Center for Aerospace Information  
7121 Standard Drive  
Hanover, MD 21076  
Price Code: A09

National Technical Information Service  
5285 Port Royal Road  
Springfield, VA 22100  
Price Code: A09



# Introduction

The NASA Glenn Research Center at Lewis Field is responsible for developing and transferring critical technologies that address national priorities in aerospace propulsion and space applications in partnership with U.S. industries, universities, and other Government institutions.

As NASA's premier center for aerospace propulsion and power, our role is to develop, demonstrate, and transfer relevant technologies to U.S. industry for commercialization. As NASA's designated Center of Excellence in Turbomachinery, we develop new and innovative technologies that improve the reliability, performance, efficiency, affordability, capacity, and environmental compatibility of aerospace propulsion systems. We also

maintain a science and technology development role in communications, space power, onboard propulsion, and microgravity fluid physics and combustion. We are committed to enabling U.S.-based aerospace and nonaerospace industries to benefit directly from the technologies developed through our programs. Our goal is to maximize the benefit of our efforts to the Nation and to optimize the return on each taxpayer's investment.

Over 3300 civil service employees and support service contractor personnel staff Glenn. Scientists and engineers comprise more than half of our workforce, with technical specialists, skilled workers, and an administrative staff supporting them. We aggressively strive for technical excellence through continuing education, expanded diversity in our workforce, and continuous improvement in our management and business practices so that we can extend the edge of aeronautics, space, and aerospace technology.

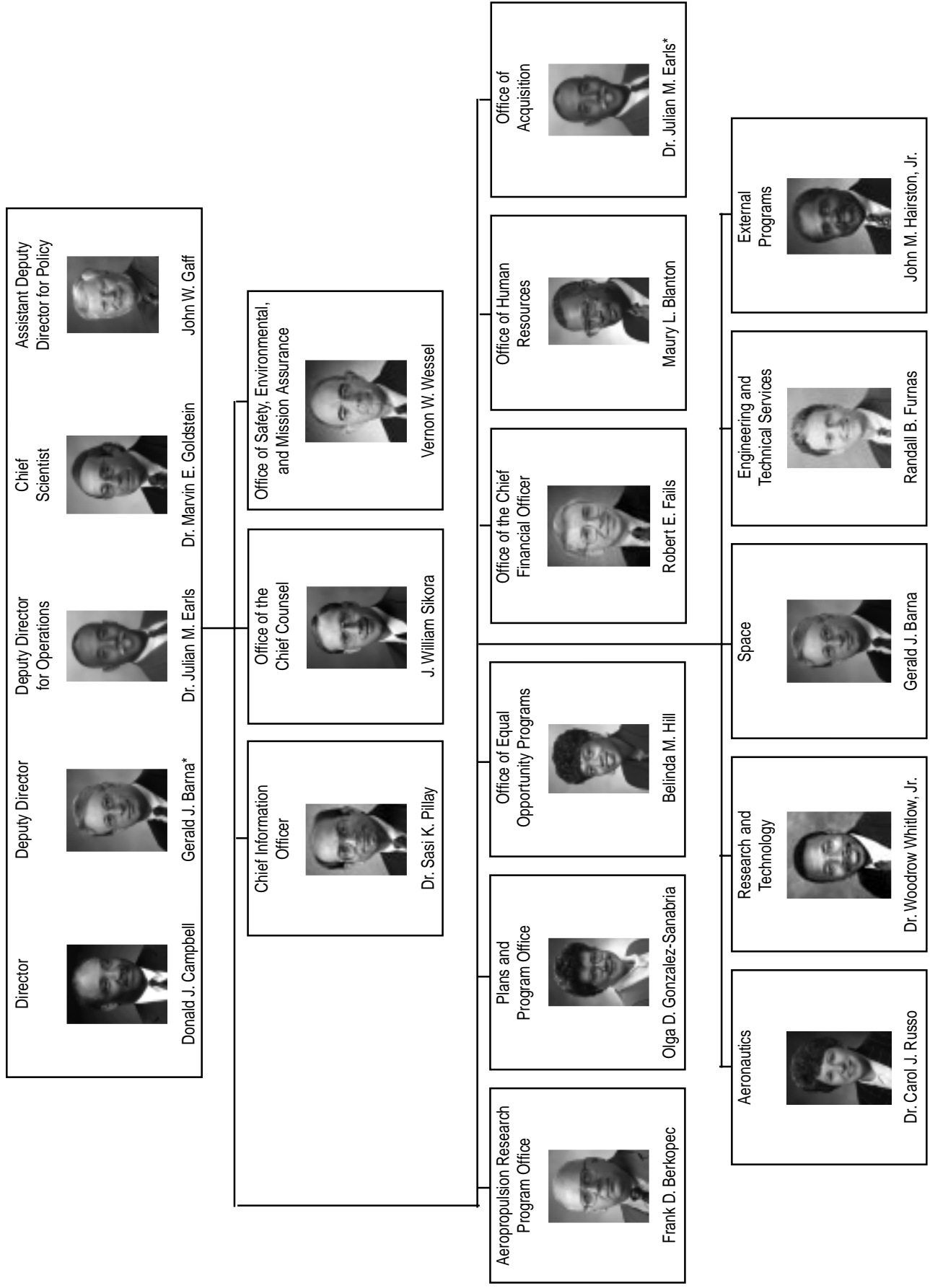
The Glenn Research Center is a unique facility located in the southwest corner of Cleveland, Ohio. Situated on 350 acres of land adjacent to the Cleveland Hopkins International Airport, Glenn comprises more than 140 buildings, including 24 major facilities and over 500 specialized research and test facilities. Additional facilities are located at the Plum Brook Station, which is about 50 miles west of Cleveland.

Our end product is knowledge. This report will help make this knowledge fully available to potential users—the aircraft engine industry, the space industry, the energy industry, the automotive industry, the aerospace industry, and others. It is organized so that a broad cross section of the community can readily use it. Each article begins with a short introductory paragraph that should prove to be a valuable tool for the layperson. These articles summarize the progress made during the year in various technical areas and portray the technical and administrative support associated with Glenn's technology programs.

We hope that the information is useful to all. If additional information is desired, readers are encouraged to contact the researchers identified at the end of each article and to visit NASA Glenn on the World Wide Web at <http://www.grc.nasa.gov>. This document is available on the World Wide Web (<http://www.grc.nasa.gov/WWW/RT/>).

  
Donald J. Campbell  
Director

# NASA Glenn Research Center Senior Management



\*Acting



# Quality Council

**Gerald J. Barna**  
Acting Deputy Director  
Director of Space



**Dr. Woodrow Whitlow, Jr.**  
Director of Research  
and Technology



**Donald J. Campbell**  
Director



**Donald R. Strelbing**  
President AFGE



**Virginia A. Cantwell**  
President LESA



**Dennis M. Sender**  
Special Assistant to  
the Quality Council



**Dr. Julian M. Earls**  
Deputy Director for  
Operations



**Dr. Carol J. Russo**  
Director of  
Aeronautics



**Robert E. Falls**  
Chief Financial Officer



**Christopher J. Pestak**  
Support Service  
Contractor Liaison



**Randall B. Furnas**  
Director of Engineering  
and Technical Services



**John M. Hairston, Jr.**  
Director of  
External Programs



**Dr. Marvin E. Goldstein**  
Chief Scientist



The Quality Council was established in October 1992 to adopt and implement a Total Quality (TQ) plan for the Center (now NASA Glenn). It is composed of Executive Council members as well as the president of the American Federation of Government Employees (AFGE), Local 2812, and the president of the Lewis Engineers and Scientists Association (LESA), IPFTE Local 28. A representative of major onsite support service contractors serves as a liaison.

February 2000

# Contents

## Aeronautics

### *Propulsion Systems Analysis*

Noise-Reduction Benefits Analyzed for Over-the-Wing-Mounted Advanced Turbofan Engines .....	2
Integrated Supportability Analysis and Cost System Enhanced .....	3

## Research and Technology

### *Materials*

Very Long Term Oxidation of Titanium Aluminides Investigated .....	6
Directionally Solidified NiAl-Based Alloys Studied for Improved Elevated-Temperature Strength and Room-Temperature Fracture Toughness .....	8
Creep Properties of NiAl-1Hf Single Crystals Re-Investigated .....	9
Constituent-Based Life Models Being Developed for SiC/SiC Composites .....	11
Silicon Nitride Rocket Thrusters Test Fired Successfully .....	12
Directionally Solidified Ceramics Produced .....	13
Electric Plasma Arc-Lamp Combustor Liner Durability Test System Developed .....	14
Affordable, Robust Ceramic Joining Technology (ARCJoinT) Given 1999 R&D 100 Award ....	15
Atomistic Method Applied to Computational Modeling of Surface Alloys .....	16
System Being Developed to Measure the Rotordynamic Characteristics of Air Foil Bearings ..	17
Surface Coatings in Egyptian Art Characterized Through Spectroscopy .....	18
Shelf Life of PMR Polyimide Monomer Solutions and Prepregs Extended .....	19
Resin Transfer Moldable Polyimides Developed for High-Temperature Applications .....	20
Erosion Coatings for High-Temperature Polymer Composites: A Collaborative Project With Allison Advanced Development Company .....	22
Near-Net-Shape Processing of Sintered Fibrous Ceramics Achieved .....	23
Formation of Leading-Edge Pinholes in the Space Shuttle Wings Investigated .....	24
Diagnostic Techniques Used to Study Chemical-Vapor-Deposited Diamond Films .....	26
Turbine Airfoil With CMC Leading-Edge Concept Tested Under Simulated Gas Turbine Conditions .....	28
Thermal Conductivity Change Kinetics of Ceramic Thermal Barrier Coatings Determined by the Steady-State Laser Heat Flux Technique .....	29

### *Power and On-Board Propulsion Technology*

SAVANT—Solar Array Verification and Analysis Tool Demonstrated .....	32
Chemical Fabrication Used to Produce Thin-Film Materials for High Power-to-Weight-Ratio Space Photovoltaic Arrays .....	33
High-Efficiency Multibandgap Solar Cell Being Developed .....	34
Prototype Lithium-Ion Battery Developed for Mars 2001 Lander .....	35
Nickel-Hydrogen Battery Cell Life Test Program Update for the International Space Station .....	36
4.5-kW Hall Effect Thruster Evaluated .....	38
Advanced Monopropellant Thruster Technology Tested .....	39
Ion Thruster Used to Propel the Deep Space 1 Spacecraft to Comet Encounters .....	40
High-Temperature Superconductive Cabling Investigated for Space Solar Power Satellites ...	41
Facility Designed and Built to Investigate the Combined Effects of Contaminant and Atomic Oxygen on a Light-Transmitting Surface .....	42
Large-Area Atomic Oxygen Facility Used to Clean Fire-Damaged Artwork .....	43
Insights Developed Into the Damage Mechanism of Teflon FEP Thermal Control Material on the Hubble Space Telescope .....	45

Contaminated Solar Array Handrail Samples Retrieved From Mir Analyzed .....	46
Steady-State Vacuum Ultraviolet Exposure Facility With Automated Lamp Calibration and Sample Positioning Fabricated .....	48
Environmental Exposure Conditions for Teflon FEP on the Hubble Space Telescope Investigated .....	49
Effects of Carbon Structure and Surface Oxygen on Carbon's Performance as the Anode in Lithium-Ion Battery Determined .....	50
Portable Infrared Reflectometer Designed and Manufactured for Evaluating Emittance in the Laboratory or in the Field .....	51
Electronics Demonstrated for Low-Temperature Operation .....	52
Automated Reflectance Measurement System Designed and Fabricated to Determine the Limits of Atomic Oxygen Treatment of Art Through Contrast Optimization .....	53
Automated Multiple-Sample Tray Manipulation Designed and Fabricated for Atomic Oxygen Facility .....	54
Adaptive Vibration Reduction System Shown to Effectively Eliminate Vibrations for the Stirling Radioisotope Power System .....	55
 <b><i>Instrumentation and Controls</i></b>	
Deep Etching Process Developed for the Fabrication of Silicon Carbide Microsystems .....	57
Packaging Technology Developed for High-Temperature SiC Sensors and Electronics .....	58
Hydrogen Sensors Demonstrated on the Shuttle .....	59
Temperature Distribution Within a Defect-Free Silicon Carbide Diode Predicted by a Computational Model .....	60
Temperature Correction of Pressure-Sensitive Paints Simplified .....	61
Surge Flow in a Centrifugal Compressor Measured by Digital Particle Image Velocimetry .....	62
Engine-Scale Combustor Rig Designed, Fabricated, and Tested for Combustion Instability Control Research .....	63
Aerospike Engine Post-Test Diagnostic System Delivered to Rocketdyne .....	65
 <b><i>Communications Technology</i></b>	
Internet Protocol Suite Enhanced for Satellite-Based Networks .....	66
Three-Dimensional Electron Optics Model Developed for Traveling-Wave Tubes .....	67
Modular Low-Heater-Power Cathode/Electron Gun Assembly for Microwave and Millimeter Wave Traveling Wave Tubes .....	68
Digital Channel Simulator Developed and Tested .....	69
ACTS High-Speed VSAT Demonstrated .....	71
 <b><i>Turbomachinery and Propulsion Systems</i></b>	
Accuracy of Numerical Simulations of Tip Clearance Flow in Transonic Compressor Rotors Improved Dramatically .....	73
Wave Rotor Technology Tested Successfully .....	74
Turbine Blade and Endwall Heat Transfer Measured in NASA Glenn's Transonic Turbine Blade Cascade .....	75
Solid Hydrogen Formed for Atomic Propellants .....	77
Atomic Rocket Vehicle Performance Improved .....	78
Extensive Testing Conducted for the Advanced Subsonics Technology Regional Engine Combustor Program .....	79
Ice Accretions on Modern Airfoils Investigated .....	79
Interactive Software System Developed to Study How Icing Affects Airfoil Performance (Phase 1 Results) .....	81
Supercooled Large Droplet Icing Flight Research Program .....	82
Software Released by LEWICE 2.0 Ice Accretion Software Development Project .....	84

Mt. Washington Icing Sensors Project (MWISP) Tests Technologies for Remote Sensing of Icing Conditions .....	85
Aircraft Icing Educational and Training Videos Produced for Pilots .....	86
Inlet Unstart Propulsion Integration Wind Tunnel Test Program Completed for High-Speed Civil Transport .....	87
CFD Software for Aerospace Applications Available From the NPARC Alliance .....	88
Screech Noise Generation From Supersonic Underexpanded Jets Investigated .....	89
Propellant Densification Ground Testing Conducted for Launch Vehicles .....	90
DRAGON Grid: A Three-Dimensional Hybrid Grid Generation Code Developed .....	92

### ***Structures and Acoustics***

Thermoelastic Stress Analysis: An NDE Tool for the Residual Stress Assessment of Metallic Alloys .....	93
Composite Flywheels Assessed Analytically by NDE and FEA .....	94
Time-Dependent Reversible-Irreversible Deformation Threshold Determined Explicitly by Experimental Technique .....	97
Benchmark Testing of the Largest Titanium Aluminide Sheet Subelement Conducted .....	98
Titanium Aluminide Technologies Successfully Transferred From HSR Program to RLV VentureStar Program .....	99
Test Standard Developed for Determining the Life Prediction Parameters of Advanced Structural Ceramics at Elevated Temperatures .....	100
Nonlinearity and Strain-Rate Dependence in the Deformation Response of Polymer Matrix Composites Modeled .....	101
Strain Measurement System Developed for Biaxially Loaded Cruciform Specimens .....	102
Damage Resistance of Titanium Aluminide Evaluated .....	103
CEMCAN Software Enhanced for Predicting the Properties of Woven Ceramic Matrix Composites .....	104
GENOA-PFA: Progressive Fracture in Composites Simulated Computationally .....	105
New Technology—Large-Area Three-Dimensional Surface Profiling Using Only Focused Air-Coupled Ultrasound—Given 1999 R&D 100 Award .....	107
Propulsion Aeroelastic Analysis Developed for Flutter and Forced Response .....	108
Optical Measurements of Axial and Tangential Steady-State Blade Deflections Obtained Simultaneously .....	109
Structural Simulations of Engine-Airframe Systems Being Improved .....	110
Curved Thermopiezoelectric Shell Structures Modeled by Finite Element Analysis .....	111
Novel Vibration Damping of Ceramic Matrix Composite Turbine Blades Developed for RLV Applications .....	111
Cascade Optimization Strategy With Neural Network and Regression Approximations Demonstrated on a Preliminary Aircraft Engine Design .....	113
Effects of Various Heat Treatments on the Ballistic Impact Properties of Inconel 718 Investigated .....	114
Failure Accommodation Tested in Magnetic Suspension Systems for Rotating Machinery ...	115
Acoustics and Thrust of Separate Flow Exhaust Nozzles With Mixing Devices Investigated for High Bypass Ratio Engines .....	116
New High-Temperature Turbine Seal Rig Fabricated .....	117
Experimental and Analytical Determinations of Spiral Bevel Gear-Tooth Bending Stress Compared .....	118
Gear Durability Shown To Be Improved by Superfinishing .....	120
Pressure-Balanced, Low-Hysteresis Finger Seal Developed and Tested .....	122
Thermal Barriers Developed for Solid Rocket Motor Nozzle Joints .....	123

# Space

## ***Space Communications***

Seven Years of ACTS Technology Verification Experiments Reviewed .....	128
Advanced Communications Technology Satellite (ACTS) Used for Inclined Orbit Operations .....	129
Satellite Broadcast of Graphical Weather Data Flight Tested .....	130
Proposal Drafted for Allocating Space-to-Space Frequencies in the GPS Spectrum Bands ...	131
Low-Cost Tracking Ground Terminal Designed To Use Cryogenically Cooled Electronics ....	133
Feasibility Activities Completed for the Direct Data Distribution (D <sup>3</sup> ) Experiment .....	134
Antennas Designed for Advanced Communications for the Air Traffic Management (AC/ATM) Project .....	135

## ***Microgravity Science***

Burning Plastics Investigated in Space for Unique U.S./Russian Cooperative Project .....	137
Novel High Gas-Temperature Calibration System Demonstrated .....	138
Flame Design—A Novel Approach Developed to Produce Clean, Efficient Diffusion Flames .....	140
Cool Flames and Autoignition: Thermal-Ignition Theory of Combustion Experimentally Validated in Microgravity .....	141
Fiber-Optic Imaging Probe Developed for Space Used to Detect Diabetes Through the Eye .....	143
Nucleate Boiling Heat Transfer Studied Under Reduced-Gravity Conditions .....	146
Boiling on Microconfigured Composite Surfaces Enhanced .....	148
Bubbly Suspension Generated in Low Gravity .....	149
Growth and Morphology of Supercritical Fluids Studied in Microgravity on Mir .....	151
Density Relaxation of Liquid-Vapor Critical Fluids Examined in Earth's Gravity .....	152
Diffusing Wave Spectroscopy Used to Study Foams .....	153
Concept Defined for the International Space Station's Fluids and Combustion Facility .....	154
Hubble Space Telescope Program on STS-95 Supported by Space Acceleration Measurement System for Free Flyers .....	155
Physics of Hard Spheres Experiment: Significant and Quantitative Findings Made .....	157
Colloidal Gelation-2 and Colloidal Disorder-Order Transition-2 Investigations Conducted on STS-95 .....	160

## ***Power and Propulsion***

Power System Options Evaluated for the Radiation and Technology Demonstration Mission .....	163
Solar Power System Evaluated for the Human Exploration of Mars .....	164
Power Systems Evaluated for Solar Electric Propulsion Vehicles .....	166

# Engineering and Technical Services

## ***Facilities and Test Engineering***

New Compressor Added to Glenn's 450-psig Combustion Air System .....	170
Two-Dimensional Bifurcated Inlet Variable Cowl Lip Test Completed in 10- by 10-Foot Supersonic Wind Tunnel .....	170
Reflective Focused Schlieren System Improved for Use in 10- by 10-Foot Supersonic Wind Tunnel .....	172

***Engineering Design and Analysis***

Ultrasonic Waves in Water Visualized With Schlieren Imaging ..... 173  
Mars Spark Source Prototype Developed ..... 174  
Reduced-Noise Gas Flow Design Guide Developed as a Noise-Control Design Tool for  
Meeting Glenn’s Hearing Conservation and Community Noise Goals ..... 176  
New Web Server—the Java Version of *Tempest*—Produced ..... 177

**Appendixes**

Definitions of NASA Headquarters Program Offices ..... 179  
Definitions of Programs and Projects ..... 180  
Index of Authors and Contacts ..... 182

# Aeronautics



# Propulsion Systems Analysis

## Noise-Reduction Benefits Analyzed for Over-the-Wing-Mounted Advanced Turbofan Engines

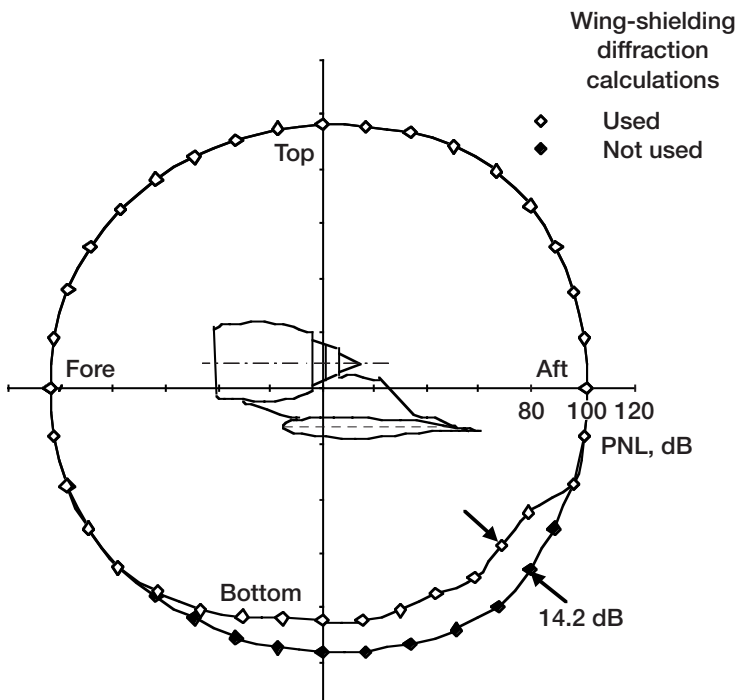
As we look to the future, increasingly stringent civilian aviation noise regulations will require the design and manufacture of extremely quiet commercial aircraft. Also, the large fan diameters of modern engines with increasingly higher bypass ratios pose significant packaging and aircraft installation challenges. One design approach that addresses both of these challenges is to mount the engines above the wing. In addition to allowing the performance trend towards large diameters and high bypass ratio cycles to continue, this approach allows the wing to shield much of the engine noise from people on the ground.

With older technology engines, jet noise was prominent and fan inlet noise was high. Investigations with such engines showed limited noise-reduction benefits from mounting engines above the wing. Experimental wing shielding tests in the 1970's demonstrated reductions of less than 3 dB because the wing chord was not sufficiently large to shield both ends of the engine. Jet noise was particularly difficult to shield efficiently because it is a distributed source downstream of the wing. However, the overall noise signature of advanced turbofan engines with highly loaded, wide-chord fan blades will be dominated by fan discharge noise that can be effectively shielded by the wing. Also, modern, high-pressure cores and high bypass ratio cycles extract significant energy from the core airflow, which tends to reduce primary jet noise. Consequently, designers anticipate that, with fan

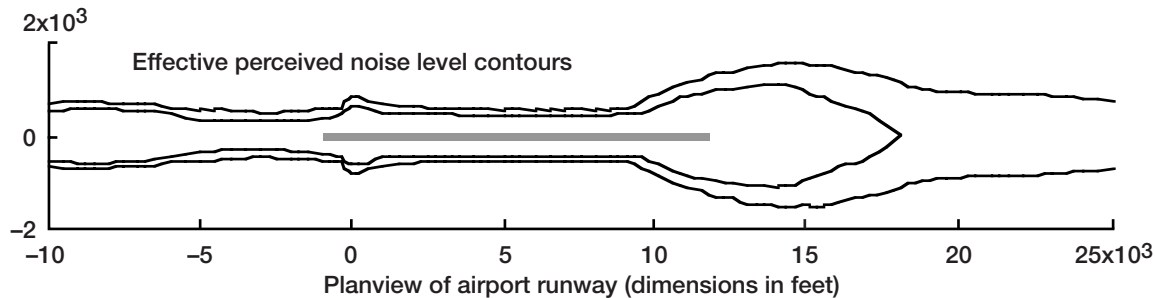
discharge noise dominating modern turbofans and with jet noise becoming less prominent, wing shielding will be much more effective than it was in the past. Mounting the engines above the wing will also allow designers to install increasingly larger diameter engines more easily and will allow the performance trend toward high bypass ratio cycles to continue.

The Propulsion Systems Analysis Office at the NASA Glenn Research Center at Lewis Field conducted independent analytical research to estimate the noise reduction potential of mounting advanced turbofan engines above the wing. Certification noise predictions were made for a notional long-haul commercial quadjet transport. A large quad was chosen because, even under current regulations, such aircraft sometimes experience difficulty in complying with certification noise requirements with a substantial margin. Also, because of its long wing chords, a large airplane would receive the greatest advantage of any noise-shielding benefit.

Fan inlet and discharge source noises were predicted using actual experimental acoustic data measured from fan rig tests conducted at Glenn's 9- by 15-Foot Low-Speed Wind Tunnel. Then, existing analytical models were used to calculate jet, core, and airframe noise sources and propagation effects. A classic partial-barrier diffraction analysis was used to predict the apparent attenuation of the source noise due to wing shielding.



Perceived noise level (PNL) variation in pitch angle with respect to an engine/wing assembly.



*Reduction in airport noise "footprint" area resulting from wing shielding. Shown are the 90-dB effective perceived noise level contours around the airport runway, with and without wing shielding diffraction calculations.*

Effective perceived noise levels were calculated for listening points on the ground. In certification parlance, the airplane in this study is 45 cumulative dB below current regulations, 10 cumulative dB of which may be attributed to wing barrier shielding. This compares favorably with the certification noise levels of current large quadjets, which are only approximately 10 cumulative dB below current regulations.

**Find out more about this research on the World Wide Web:**  
<http://www-psao.grc.nasa.gov/Library/Abstracts/ISABE.html>

**Glenn contact:**

Jeffrey J. Berton, (216) 977-7031,  
 Jeffrey.J.Berton@grc.nasa.gov

**Author:** Jeffrey J. Berton

**Headquarters program office:** OAST

**Programs/Projects:** Noise and  
 Emissions Reduction Initiative

## Integrated Supportability Analysis and Cost System Enhanced

In recent years, the NASA Glenn Research Center at Lewis Field had recognized the need for propulsion system designs that would not only enhance performance but improve reliability and reduce system life-cycle costs. To deal with these issues, Glenn, in cooperation with GE Aircraft Engines, created the Enhanced Integrated Supportability Analysis and Cost System (ISACS+).

GE developed the ISACS computer code in the early 1990's to simulate operation and support for the U.S. Air Force F-16 engine program. In 1996, Glenn's Propulsion Systems Analysis Office (PSAO) obtained the software from GE and entered into a 3-year Space Act Agreement whereby GE provided consulting support and Glenn's PSAO directed and coordinated the enhancement of the software. Glenn contracted with Technology Support Corporation of Cary, North Carolina, to perform this task. Funding for the enhanced ISACS (ISACS+) was provided by NASA Headquarters' Office of Safety & Mission Assurance and Office of Aero-Space Technology through Glenn's Office of Safety and Assurance Technologies and PSAO, respectively.

ISACS+, operating in the MS Windows NT/95 environment, enables analysts to model a fleet of military or commercial aircraft and engines to

determine the effects of engine reliability, maintainability, and logistics support on system safety and life-cycle cost. The ISACS+ model will support trade studies during the various design phases and through the full-scale production and fielding of aircraft to help designers and engineers meet the specified mission requirements at a minimum life-cycle cost. For aircraft engines in the field, ISACS+ can help maintenance planners specify the most economical maintenance support infrastructure. This would include providing information on when to repair, buy, and store individual parts and forecasting such things as labor utilization, support equipment, and demand for consumables at each maintenance center for a fleet of aircraft.

In addition, ISACS+ can be used to manage risk by tracking and monitoring propulsion system and component usage. This usage history is used to schedule repairs to reduce risk and maintenance costs and to formulate warranty plans by identifying high-risk areas and predicting failure rates and repair intervals.

ISACS+ will enhance Glenn's capability to analyze the effects of various propulsion technologies on the reliability, maintainability, and life-cycle cost of advanced propulsion systems as they are applied to future fleets of aircraft. Outside NASA, military planners, engine and airframe manufacturers, and commercial airlines could use ISACS+ for trade studies, planning, and cost-estimating activities. The code could be modified to model space, ground, and sea transportation systems as well as any product requiring periodic maintenance.

The ISACS+ program software was completed in July 1999 and is available for anyone to use. The Technology Support Corporation plans to further develop and market the code and to provide documentation and customer assistance for its users starting in October 1999.

**Glenn contacts:**

Brijendra Singh, (216) 977-7019,  
Brijendra.Singh@grc.nasa.gov; and  
Alban D. Seigneur, (216) 433-3807,  
Alban.D.Seigneur@grc.nasa.gov

**Author:** Alban D. Seigneur

**Headquarters program office:**

OSMA, OAST

**Programs/Projects:**

Three Pillar Goals Study, UEET

# Research and Technology



# Materials

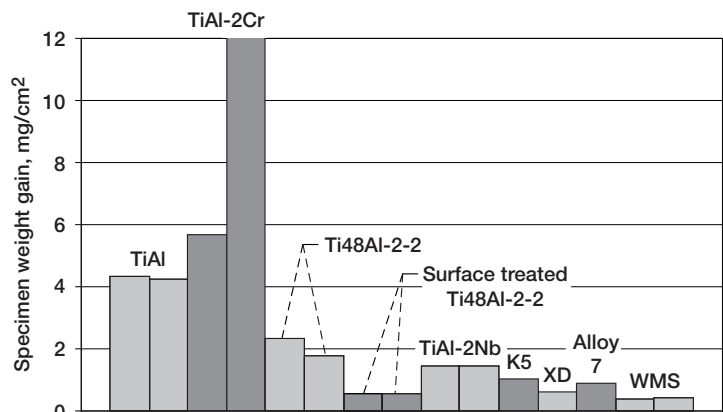
## Very Long Term Oxidation of Titanium Aluminides Investigated

Titanium aluminides (TiAl) are of great interest for intermediate-temperature (600 to 850 °C) aerospace and power-generation applications because they offer significant weight savings over today's nickel alloys. TiAl alloys are being investigated for low-pressure turbine blade applications, exhaust nozzle components, and compressor cases in advanced subsonic and supersonic engines (ref. 1).

Significant progress has been made in understanding the fundamental aspects of the oxidation behavior of binary TiAl alloys (refs. 2 and 3). However, most of this work has concentrated on short term (<1000 hr), high-temperature (900 to 1000 °C) exposures. Also, there is not much data available in the literature regarding the oxidation behavior of the quaternary and higher order engineering alloys. This is especially true for the very long term, low-temperature conditions likely to be experienced during aerospace applications.

An investigation at the NASA Glenn Research Center at Lewis Field was undertaken to characterize the long-term oxidation behavior of various model and advanced titanium aluminides for periods up to 7000 hr at 704 °C in air using a high-resolution field emission scanning electron microscope. Also, a unique surface treatment technique (ref. 4) developed to improve the oxidation resistance of TiAl was evaluated. The alloys included in this investigation are listed in the table. The table also shows typical alloy compositions and the specific weight changes and scale thickness measured for each alloy after exposure to 700 °C for 7000 hr in air.

The response to the long-term exposure is reflected in the specimen weight gained for the different alloy compositions (see the bar chart and



Specimen weight gain for model and advanced  $\gamma$ -TiAl alloys after isothermal exposure to 704 °C for 7000 hr in air. Duplicate tests were done for TiAl, TiAl-2Cr, Ti48Al-2-2, surface-treated Ti48Al-2-2, and TiAl-2Nb. (This figure is shown in color in the online version of this article: <http://www.grc.nasa.gov/WWW/RT1999/5000/5120loci.html>.)

COMPOSITIONS, WEIGHT GAINED, AND SCALE THICKNESS FOR MODEL AND ENGINEERING TiAl ALLOYS EXPOSED TO 700 °C FOR 7000 HR IN AIR

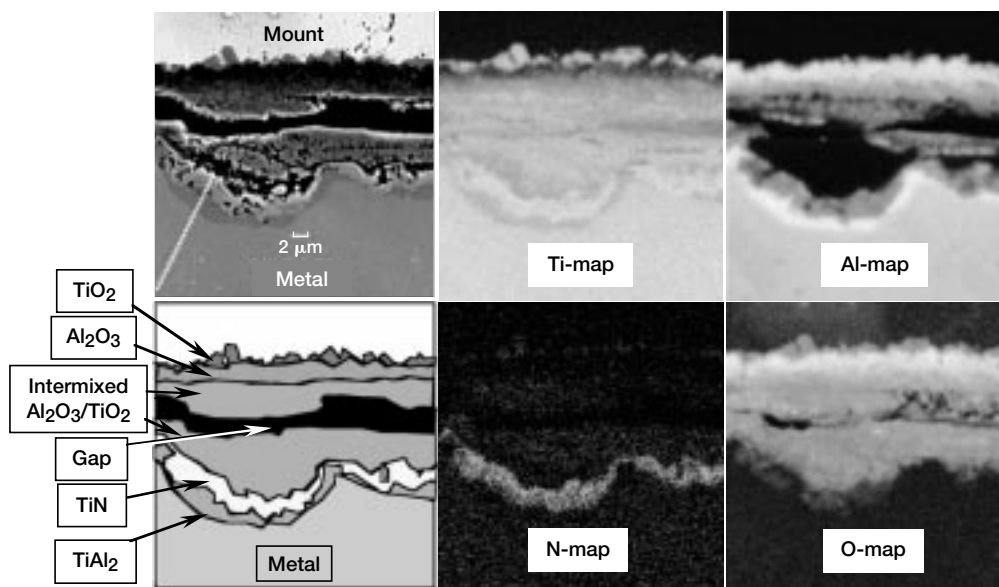
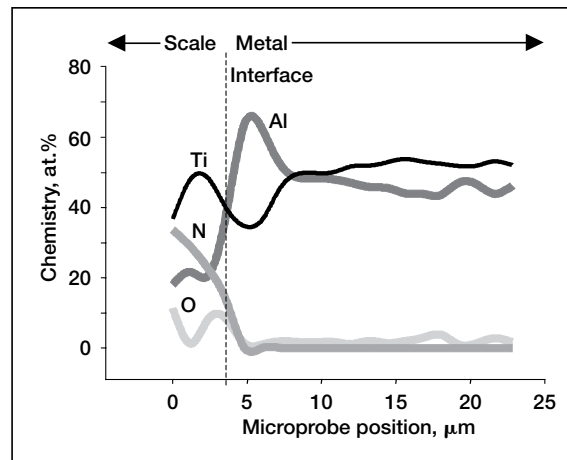
Alloy	Composition, at.%						Weight change/area, mg/cm <sup>2</sup>	Scale thickness, $\mu$ m
	Al	Ti	Cr	Nb	Mn	W		
TiAl <sup>a</sup>	48.07	51.93	----	----	----	----	4.28	20
TiAl-2Cr <sup>b</sup>	47.99	50.01	2.00	----	----	----	10.29	150
TiAl-2Nb	47.99	50.01	----	2.00	----	----	1.43	12
TiAl-2Cr-2Nb	48.03	47.97	2.00	2.00	----	----	2.04	15
Surface-treated TiAl-2Cr-2Nb	48.03	47.97	2.00	2.00	----	----	.57	6
XD	47.39	49.24	2.04	1.14	0.21	----	.86	9
K5	46.5	48.3	2	3	----	0.2	1.05	6
Alloy 7	46	48	----	5	----	1	.4	5
WMS	47	50	----	2	1	.5	.61	4

<sup>a</sup>Spalled.

<sup>b</sup>Reacted with alumina boat.

the table). The binary TiAl alloy is the only alloy where the scale did not adhere but tended to spall off. Cr, which is normally added to the alloy for enhanced mechanical properties, was extremely detrimental to oxidation resistance. The presence of Nb as a ternary or quaternary addition was extremely beneficial, minimizing the weight gained even when Cr was present in the alloy. The TiAl-2Cr-2Nb alloy benefited further from phosphoric acid surface treatment (ref. 4), which significantly reduced the oxidation rate. The more advanced alloys, which contain a higher number of added elements, showed reduced oxidation rates.

All the alloys formed complex alloy scales that required detailed microscopy analyses. Microprobe spectrometry and high-resolution scanning microscopy were used to reveal the key features of the alloy scales. The following figure shows



Typical microstructure, elemental maps, and linescans observed in a binary TiAl alloy after exposure to 704 °C for 7000 hr in air. (This figure is shown in color in the online version of this article: <http://www.grc.nasa.gov/WWW/RT1999/5000/5120locchi.html>.)

a typical cross-section describing the complex multilayered scale as well as elemental maps and linescan plots describing the chemistry variations through the scale thickness for a binary TiAl alloy. These microstructural differences are being used to explain and predict the oxidation response that advanced TiAl alloys will exhibit in actual service.

#### References

1. Bartolotta, P.A.; and Krause, D.L.: Titanium Aluminide Applications in the High Speed Civil Transport. NASA TM-1999-209071, 1999. (Available online: <http://gltrs.grc.nasa.gov/cgi-bin/GLTRS/browse.pl?/1999/TM-1999-209071.html>)
2. Locci, I.E., et al.: Very Long Term Oxidation of Ti-48Al-2Cr-2Nb at 704 °C in Air. Scripta Mat., vol. 37, no. 6, 1997, pp. 761-766.
3. Brady, M.P., et al.: The Oxidation and Protection of Gamma Titanium Aluminides. JOM, vol. 48, no. 11, 1996, pp. 46-50.
4. Retallick, W.B.; Brady, M.P.; and Humphrey, D.L.: Phosphoric Acid Surface Treatment for Improved Oxidation Resistance of Gamma Titanium Aluminides. Intermetallics, vol. 6, issue 4, 1998, pp. 335-337.

#### Institute for Computational Mechanics in Propulsion (ICOMP) contact:

Dr. Ivan E. Locci, (216) 433-5009,  
Ivan.E.Locci@grc.nasa.gov,  
<http://polly.grc.nasa.gov/MDWeb/People/MSLOCC.html>

#### Glenn contact:

Dr. James L. Smialek, (216) 433-5500,  
James.L.Smialek@grc.nasa.gov

**Authors:** Dr. Ivan E. Locci, Michael P. Brady, Dr. James L. Smialek, and William B. Retallick

**Headquarters program office:** OAST

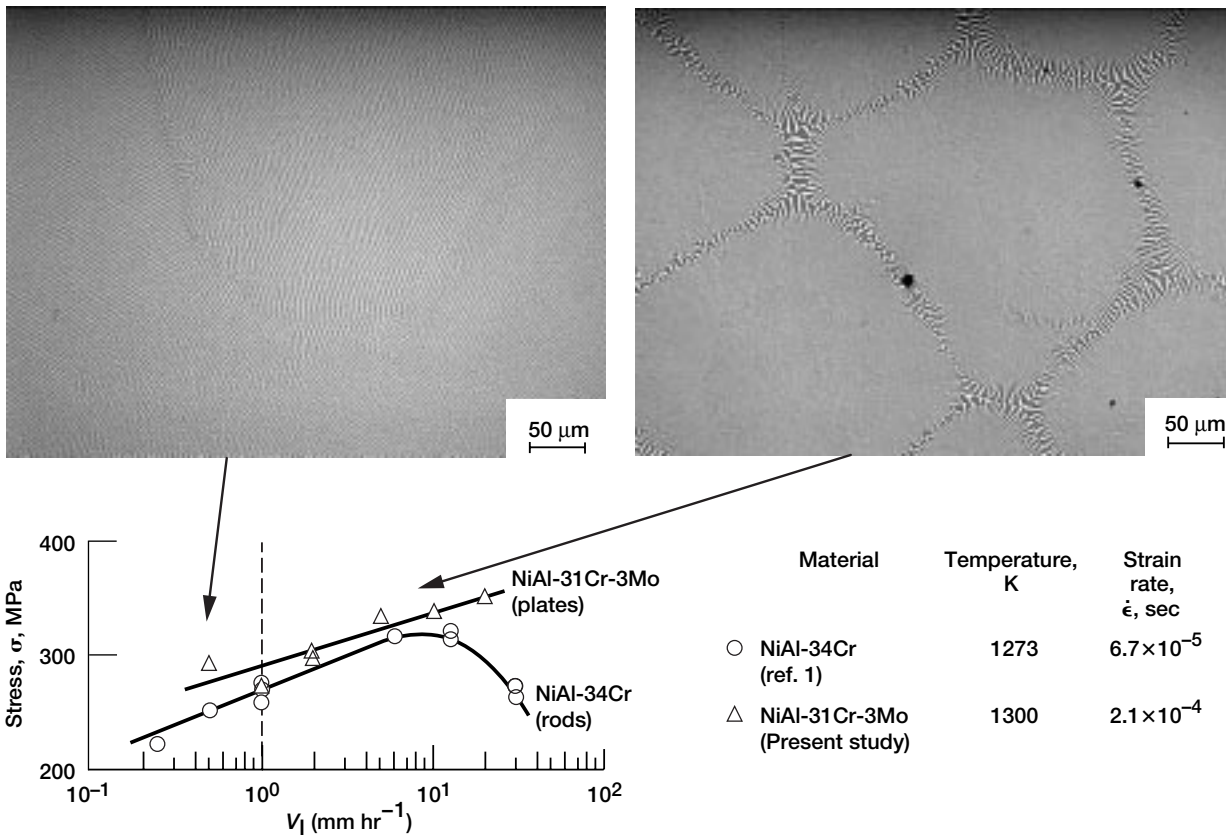
**Programs/Projects:** HSCT, UEET, RLV

# Directionally Solidified NiAl-Based Alloys Studied for Improved Elevated-Temperature Strength and Room-Temperature Fracture Toughness

Efforts are underway to replace superalloys used in the hot sections of gas turbine engines with materials possessing better mechanical and physical properties. Alloys based on the intermetallic NiAl have demonstrated potential; however, they generally suffer from low fracture resistance (toughness) at room temperature and from poor strength at elevated temperatures. Directional solidification of NiAl alloyed with both Cr and Mo has yielded materials with useful toughness and elevated-temperature strength values.

The intermetallic alloy NiAl has been proposed as an advanced material to extend the maximum operational temperature of gas turbine engines by several hundred degrees centigrade. This intermetallic alloy displays a lower density (~30-percent less) and a higher thermal conductivity (4 to 8 times greater) than conventional superalloys as well as good high-temperature oxidation resistance. Unfortunately, unalloyed NiAl has poor elevated-temperature strength (~50 MPa at 1027 °C) and low room-temperature fracture toughness (about 5 MPa√m).

Directionally solidified NiAl eutectic alloys are known to possess a combination of high elevated-temperature strength and good room-temperature fracture toughness. Research (refs. 1 and 2) has demonstrated that a NiAl matrix containing a uniform distribution of very thin Cr plates alloyed with Mo possessed both increased fracture toughness and elevated-temperature creep strength. Although attractive properties were obtained, these alloys were formed at low growth rates ( $\leq 19$  mm/hr), which are considered to be economically unviable. Hence, an investigation



Top: Unetched optical microstructure perpendicular to the growth direction of Ni-33Al-31Cr-3Mo. Left: Directional solidification at 12.7 mm/hr results in planar eutectic grains. Right: Directional solidification at 127 mm/hr results in radial eutectic cells. Bottom: Elevated-temperature flow strength of directionally solidified NiAl-based eutectic alloys as a function of growth rate for tests conducted at ~1027 °C and a strain rate of  $\sim 10^{-4}$  sec<sup>-1</sup>.

was warranted of the strength and toughness behavior of NiAl-(Cr,Mo) directionally solidified at faster growth rates. If the mechanical properties did not deteriorate with increased growth rates, directional solidification could offer an economical means to produce NiAl-based alloys commercially for gas turbine engines.

An investigation at the NASA Glenn Research Center at Lewis Field was undertaken to study the effect of the directional solidification growth rate on the microstructure, room-temperature fracture toughness, and strength at 1027 °C of a Ni-33Al-31Cr-3Mo eutectic alloy. The directionally solidified rates varied between 7.6 and 508 mm/hr (ref. 3). Essentially fault-free, alternating (Cr, Mo)/NiAl lamellar plate microstructures (left photograph) were formed during growth at and below 12.7 mm/hr, whereas cellular microstructures (right photograph) with the (Cr, Mo) phase in a radial spokelike pattern were developed at faster growth rates. The compressive strength at 1027 °C continuously increased with increasing growth rate and did not indicate a maxima as was reported for directionally solidified Ni-33Al-34Cr (see the graph). Surprisingly, samples with the lamellar plate microstructure (left photograph) possessed a room-temperature fracture toughness of  $\sim 12 \text{ MPa}\sqrt{\text{m}}$ , whereas all the alloys with a cellular microstructure had a toughness of about  $17 \text{ MPa}\sqrt{\text{m}}$ . These results are significant since they clearly demonstrate that Ni-33Al-31Cr-3Mo can be directionally solidified at much faster growth rates without any observable deterioration in its mechanical properties. Thus, the potential to produce strong, tough NiAl-based eutectics at commercially acceptable growth rates exists. Additional testing and alloy optimization studies are underway.

## References

1. Cline, H.E.; and Walter, J.L.: The Effect of Alloy Additions on the Rod-Plate Transition in the Eutectic NiAl-Cr. *Metall. Trans.*, vol. 1, 1970, pp. 2907–2917.
2. Johnson, D.R., et al.: Processing and Mechanical Properties of In-Situ Composites From the NiAl-Cr and NiAl-(Cr,Mo) Eutectic Systems. *Intermetallics*, vol. 3, issue 2, 1995, pp. 99–113.
3. Whittenberger, J.D., et al.: Effect of Growth Rate on Elevated Temperature Plastic Flow and Room Temperature Fracture Toughness of Directionally Solidified NiAl-31Cr-3Mo. *Intermetallics*, vol. 7, issue 10, 1999, pp. 1159–1168.

**Glenn contact:** Dr. Sai V. Raj, (216) 433–8195, Sai.V.Raj@grc.nasa.gov

**Authors:** Dr. J. Daniel Whittenberger, Dr. Sai V. Raj, Dr. Ivan E. Locci, and Jonathan A. Salem

**Headquarters program office:** OAST

**Programs/Projects:** HITEMP

**Special recognition:** A paper based on this work appeared in a special edition of the journal *Intermetallics* in honor of Prof. G. Sauthoff's 60th birthday (ref. 3).

## Creep Properties of NiAl-1Hf Single Crystals Re-Investigated

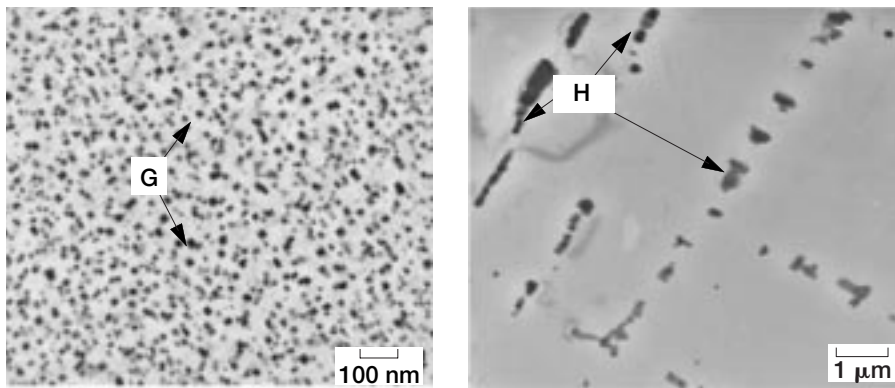
NiAl-1Hf single crystals have been shown to be quite strong at 1027 °C, with strength levels approaching those of advanced Ni-based superalloys. Initial testing, however, indicated that the properties might not be reproducible. Study of the 1027 °C creep behavior of four different NiAl-1Hf single-crystal ingots subjected to several different heat treatments indicated that strength lies in a narrow band. Thus, we concluded that the mechanical properties are reproducible.

Recent investigations (ref. 1) of the intermetallic NiAl have confirmed that minor alloying additions combined with single-crystal growth technology can produce elevated-temperature strength levels approaching those of Ni-based superalloys. For example, General Electric alloy AFN-12 {Ni-48.5(at.%) Al-0.5Hf-1Ti-0.05Ga} has a creep rupture strength equivalent to Rene'80 combined with a  $\sim 30$ -percent lower density, a fourfold improvement in thermal conductivity, and the ability to form a self-protective alumina scale in aggressive environments.

Although the compositions of strong NiAl single crystals are relatively simple, the microstructures are complex and vary with the heat treatment

and with small ingot-to-ingot variations in the alloy chemistry (ref. 2). In addition, initial testing (ref. 3) suggested a strong dependence between microstructure and creep strength. If these observations were true, the ability to utilize NiAl single-crystal rotating components in turbine machinery could be severely limited.

To investigate the possible limitations in the creep response of high-strength NiAl single crystals, the NASA Glenn Research Center at Lewis Field initiated an indepth investigation (ref. 4) of the effect of heat treatment on the microstructure and subsequent 1027 °C creep

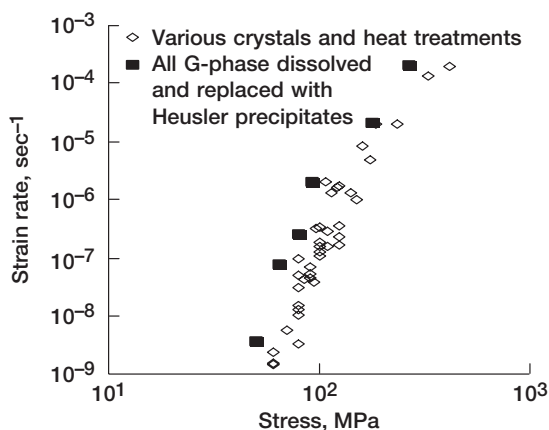


Bright field transmission electron microscopy images of phases observed in [001]-oriented single crystal NiAl-1Hf alloys. Left: Solution treated and air cooled. Right: Solution treated, furnace cooled, plus aged at 1127 °C for 20 hr.

behavior of [001]-oriented NiAl-1Hf with a nominal chemistry of Ni-47.5Al-1Hf-0.5Si. This alloy was selected since four ingots, grown over a number of years and possessing slightly different compositions, were available for study. Specimens taken from the ingots were subjected to several heat treatment schedules, examined by transmission electron microscopy, and tested in both compression and tension.

An example of the microstructure found in a [001]-oriented NiAl-1Hf specimen after a solution treatment at 1317 °C for 50 hr followed by air cooling is illustrated in the image on the left, where the NiAl matrix contains a uniform distribution of nanometer-scale G-phase ( $\text{Ni}_{16}\text{Hf}_6\text{Si}_7$ ) precipitates. Other heat treating schedules produced microstructures with nanometer-sized G-phase cubes and plates or, in an extreme case, produced a microstructure with all the G-phase converted to Heusler ( $\text{Ni}_2\text{AlHf}$ ) particles (indicated by "H" in the right image).

The results of 1027 °C creep strength and strain rate testing are illustrated in the following graph, which summarizes data from tensile and compressive testing of samples cut from all four NiAl-1Hf ingots and subjected to a variety of heat treatment schedules. With one exception, all the strength values lie in a narrow band that spans six orders of magnitude in strain rate.



Comparison of 1027 °C creep properties for [001]-oriented NiAl-1Hf crystals taken from several ingots and subjected to different heat treatments.

The only factor that produced results outside of this band was the heat treatment schedule that dissolved all the G-phase and replaced it with Heusler precipitates.

The results portrayed in this figure lead to the important practical conclusion that the elevated-temperature creep properties of NiAl-1Hf single crystals are reproducible and are not affected by small varia-

tions in alloy chemistry from ingot to ingot or by different initial distributions of G-phase in the heat-treated alloy. The only variable in this study that produced a significant and deleterious effect on mechanical strength was a post-solution heat treatment that led to the complete disappearance of the G-phase in favor of Heusler precipitates.

## References

1. Darolia R.; and Walston, W.S.: Development and Characterization of High Strength NiAl Single Crystal Alloys. First International Symposium on Structural Intermetallics 1997, TMS, Warrendale, PA, 1997, pp. 585–594.
2. Locci, I.E., et al.: Microstructure and Phase Stability of Single Crystal NiAl Alloyed With Hf and Zr. *J. Mater. Res.*, vol. 11, no. 12, 1996, pp. 3024–3038.
3. Walston, W.S.; and Darolia, R.: Intermetallic HPT Technology Development. Final Report, WL-TR-96-2118, WPAFB, OH, July 1996. (Available from WL/POTT, Wright-Patterson AFB.)
4. Whittenberger, J.D., et al: 1300 K Creep Behavior of [001] Oriented Ni-49Al-1Hf (at.%) Single Crystals. *Mater. Sci. Eng. A*, A268, no. 1, 1999, pp. 165–183.

**Glenn contact:** Dr. J. Daniel Whittenberger, (216) 433-3196, John.D.Whittenberger@grc.nasa.gov

**Authors:** Dr. J. Daniel Whittenberger, Dr. Ivan E. Locci, Dr. Ram Darolia, and Dr. Randy R. Bowman

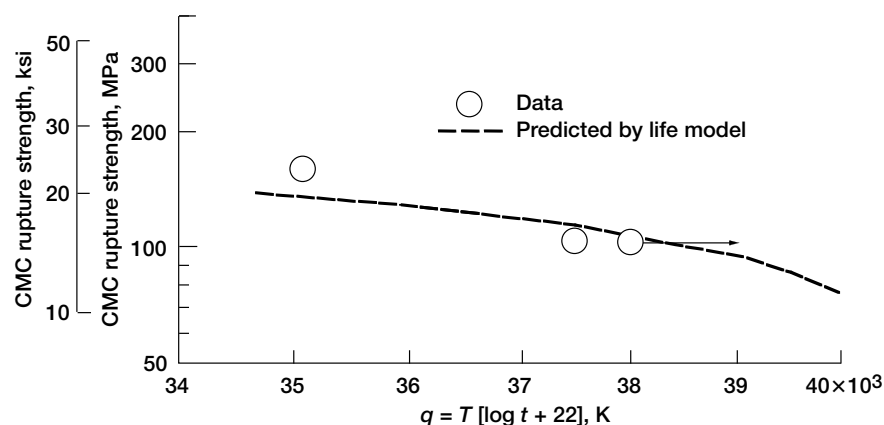
**Headquarters program office:** OAST

**Programs/Projects:** HITEMP

# Constituent-Based Life Models Being Developed for SiC/SiC Composites

For the successful utilization of ceramic matrix composites (CMC) as hot-section components in advanced aeropropulsion engines, the CMC constituents will need to be tailored and optimized to meet all the critical property demands of each component. Under the High-Speed Research (HSR) and Advanced High-Temperature Engine Materials Technology (HITEMP) Programs, the NASA Glenn Research Center at Lewis Field initiated research to develop mechanistic models for key CMC thermostructural properties. These models would describe the effects of different constituent factors (composition, geometry, and volume fraction) and of potential application conditions (stress, time, temperature, and environment) on these properties. Particular focus was placed on both analytical and numerical modeling of state-of-the-art SiC/SiC composites where the primary load-bearing constituents are stoichiometric SiC fibers in a complex multiphase SiC matrix produced by chemical vapor infiltration and melt infiltration.

Recent studies have resulted in computer-based numerical models for the elastic modulus, thermal expansion, and thermal conductivity properties of the SiC/SiC system (ref. 1). Additional studies have generated analytical and empirical models for the time dependence of composite rupture strength at temperatures above 2200 °F (1200 °C), where CMC's have an important thermostructural advantage over current nickel-based superalloys. These life models utilize thermal activation theory and fiber stress-rupture results measured at Glenn to generate Larson-Miller ( $L-M$ ) plots of fiber rupture strength versus  $q$ , a single time- and temperature-dependent parameter (ref. 2). Assuming a worse case in which the SiC matrix is cracked, rupture is then controlled by the time-dependent fracture characteristics of the fiber bundles bridging the matrix cracks. With this as the controlling mechanism, one can then use simple composite theory and the fiber  $L-M$  plots to predict CMC rupture strength versus the  $q$  parameter (ref. 3).



Time- and temperature-dependent rupture strength for a state-of-the-art SiC/SiC composite.

The dashed line shows the predicted rupture strength of a SiC/SiC composite that is reinforced by a state-of-the-art stoichiometric SiC fiber. For the  $q$  parameter, time is in hours and temperature in kelvin. To generate these predictions, a two-dimensional 0°/90° composite with ~16 percent fiber in the applied stress direction and an air test environment were assumed. As such, it is possible to compare the model predictions against limited stress-rupture data for this CMC as shown by the data points. The good agreement confirms the rupture model at least for the selected CMC and test conditions. Thus for this particular SiC/SiC composite, one can estimate a 1000-hr rupture strength of ~12 ksi at 2400 °F ( $T = 1588$  K and  $q = 39\,700$  K). At lower CMC application stresses, the SiC matrix is typically uncracked, so both the fiber and matrix constituents share the composite load. In this case, CMC rupture is controlled by the constituent with the longest rupture time based on the creep rate of the composite. Measured Monkman-Grant plots of rupture time versus creep rate for the two SiC constituents have been used to develop CMC life models for this important application condition (ref. 4). NASA and DOD are currently using this information to establish application and material goals for more advanced CMC's that can be used at even higher temperatures.

## References

1. Mital, S.K., et al.: Micromechanics-Based Modeling of Thermal and Mechanical Properties of an Advanced SiC/SiC Composite Material. NASA TM-206295, 1998. (Available from Glenn's HSR or UEET Project Office.)

2. Yun, H.M.; and DiCarlo, J.A.: Time/Temperature Dependent Tensile Strength of SiC and Al<sub>2</sub>O<sub>3</sub>-Based Fibers. Proceedings of the Advances in Ceramic Matrix Composites III Symposium, vol. 74, 1996, pp. 17–25.
3. DiCarlo, J.A.; and Yun, H.M.: Status of Advanced SiC Fibers for 2400 °F CMC. NASA/CP–1999-208915, HITEMP Review 1999, paper no. 42, pp. 1–11. (Available from Glenn’s Subsonic Systems Office.)
4. DiCarlo, J.A.; and Yun, H.M.: Factors Controlling Stress-Rupture of Fiber-Reinforced Ceramic Composites. Proceedings of ICCM–12, Paris, France, 1999.

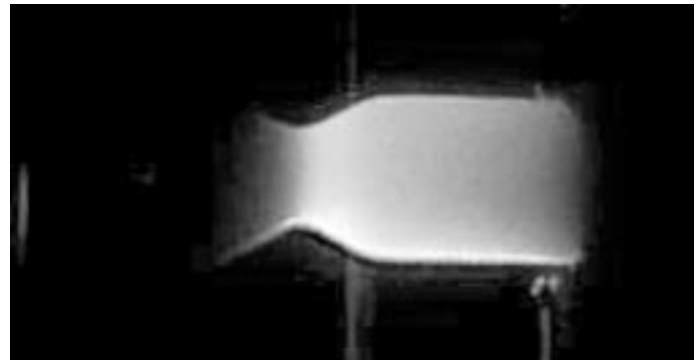
**Glenn contact:** Dr. James A. DiCarlo,  
(216) 433–5514,  
James.A.DiCarlo@grc.nasa.gov

**Authors:** Dr. James A. DiCarlo and  
Hee Mann Yun

**Headquarters program office:** OAST

**Programs/Projects:** HSR, EPM, HITEMP

## Silicon Nitride Rocket Thrusters Test Fired Successfully



*Silicon nitride thruster. Left: Mounted in test stand. Right: Being tested with H<sub>2</sub>/O<sub>2</sub> propellants.*

In-situ-toughened silicon nitride offers high strength, low density, and good thermal shock resistance. In previous research on flat coupons at the NASA Glenn Research Center at Lewis Field, it was identified as one of the few monolithic ceramic materials capable of surviving the severe thermal shock and thermal gradients generated in hydrogen/oxygen rocket engines. To demonstrate this capability in a complex configuration, a team from Glenn and Case Western Reserve University used advanced rapid prototyping technology to fabricate a 1-in.-diameter, single-piece combustion chamber/nozzle (thruster) component. Compliant seals were used to attach the net-shape-fabricated uncooled thruster to a water-cooled metallic propellant injector assembly. Then, the thruster was successfully hot-fire tested with hydrogen/oxygen propellant. The thruster survived five cycles including a 5-min cycle to a 2400 °F material temperature. Silicon nitride can now be considered a viable candidate for some small rocket thruster applications. The research is expected to continue with increasingly larger and more complex geometries being fabricated and tested in a broad range of rocket engine operating conditions.

**Glenn contact:** Dr. Andrew J. Eckel,  
(216) 433–8185,  
Andrew.J.Eckel@grc.nasa.gov

**Author:** Dr. Andrew J. Eckel

**Headquarters program office:** OAST

**Programs/Projects:** Propulsion  
Systems R&T, Space Transportation

## Directionally Solidified Ceramics Produced

Multiphase, interpenetrating structures are an alternative route to obtaining structural ceramic materials with adequate strength, toughness, and stability for high-temperature aerospace applications. The eutectic architecture, a continuous-reinforcing phase within a higher volume phase or matrix, can be described as a naturally occurring, in situ composite. The phases of a eutectic are thermodynamically compatible at high homologous temperatures. Strong and stable materials have been produced. Toughness, however, remains a technical obstacle. The potential for producing materials with enhanced toughness along with adequate strength and stability was demonstrated using the laser-heated float zone (LHFZ) growth method at the NASA Glenn Research Center at Lewis Field.

LHFZ growth at Glenn provides a means to efficiently produce and record the underlying growth phenomena associated with two-phase structures. To initiate directional solidification, a seed of single-crystal sapphire ( $\langle 0001 \rangle$  direction) was lowered onto the molten liquid until wetting occurred and then withdrawn at a constant rate. Neither the crystal nor the source rod was rotated. The materials produced were tested mechanically in tension, and the resulting microstructure was examined with a scanning electron microscope.

Both the inherent properties of the constituent phases and the properties of the interface between them affect the mechanical behavior and the fracture surfaces. The following scanning electron micrographs show the microstructures of two different materials that were tested to failure in tension. In the left micrograph, the flat fracture surface is typical of a material that is strong but has low toughness. In the right micrograph, the crack is effectively deflected at the interface between the two phases, achieving higher toughness at moderately lower strength levels. Conducting mechanical tests to determine the high-temperature properties of these materials is the next step in determining their eventual suitability.

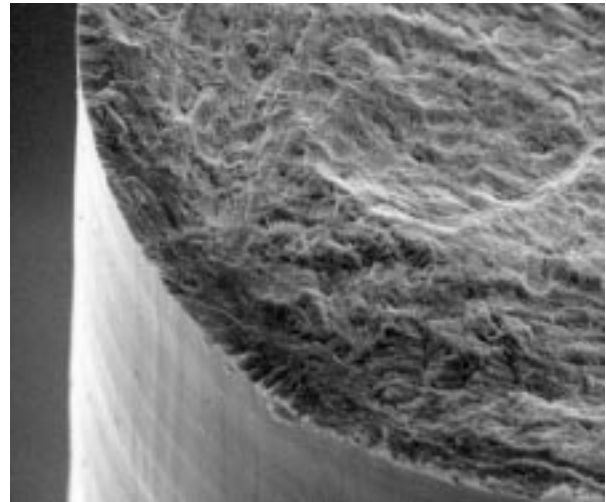
**Glenn contact:** Dr. Serene C. Farmer, (216) 433-3289, Serene.C.Farmer@grc.nasa.gov

**Case Western Reserve University contact:** Dr. Ali Sayir, (216) 433-6254, Ali.Sayir@grc.nasa.gov

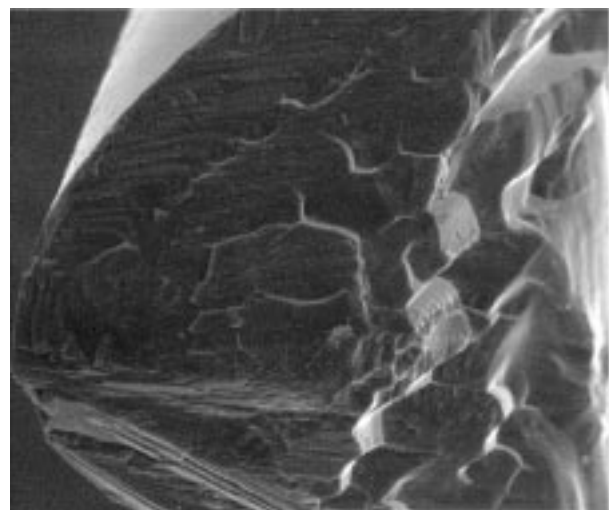
**Authors:** Dr. Serene C. Farmer and Dr. Ali Sayir

**Headquarters program office:** OAST

**Programs/Projects:** HITEMP



10  $\mu\text{m}$



100  $\mu\text{m}$

*Top: Fracture surface showing moderate surface roughness. Bottom: Enhanced toughness material showing a stepped fracture surface caused by a strong tendency to deflect cracks at two-phase boundaries.*

# Electric Plasma Arc-Lamp Combustor Liner Durability Test System Developed

Silicon carbide matrix composites are candidate materials for high-temperature combustor liners. Because through-the-thickness thermal gradients are the primary cause of stress on combustor liners, a unique test facility was developed at the NASA Glenn Research Center at Lewis Field to simulate in-service pure thermal stress distributions in fiber-reinforced silicon carbide cylinders. It was developed initially under Phase II of the High-Speed Research Program.

This test stand can accommodate 8-in.-long test cylinders that have outer diameters of 4 in. and a wall thickness of about 0.08 to 0.12 in. One cylinder at a time is loaded vertically into the test stand. Water-cooled plates enclose the open ends of the cylinder and provide cooling. Load plates on the exterior side of the water-cooled plates provide support and compression loads.

To evaluate a combustor liner material's potential performance, researchers induce thermal gradients with an axisymmetric, direct-current, electric arc within the cylinder while refrigerated air at a rate of 1.5 lb/sec impinges on the outside surface of the cylinder. The achievable through-the-thickness thermal gradient is predicted to be in excess of 200 °C. The 8-in. long, 0.5-in.-diameter plasma arc emits full spectrum visible light; radiant intensity exceeds 300 W/cm<sup>2</sup> to produce temperatures in excess of 1500 °C on materials with emissivity near unity. Because the system does not rely upon the combustion of fuels to achieve the related thermal conditions, ancillary environmental reactions with the sample are eliminated.

The system incorporates a standard mechanical test frame, which can impose constant as well cyclical axial stresses up to 2200 lb upon the test piece. Silicon-carbide-fiber-reinforced silicon carbide matrix composite cylinders were instrumented with thin-film thermocouples to obtain through-the-thickness thermal flux measurements. Inside wall temperatures reached 1200 °C with only 250 A of current. One of the special features of this configuration is the creation of hoop stress states within the cylinder, which up to this point have not been obtainable in planar coupon tests.

This facility will allow various operational modes, including accelerated tests of thermal transients simulating the effects of repeated engine ignition as well as prescribed thermal and mechanical histories to simulate various duty cycle profiles. Tests can now be performed on thermal-barrier-coated metallic liners and ceramic composite liners that require a combination of high heat flux and controlled mechanical stresses.



*Electric plasma arc-lamp combustor liner durability test system.*

**Glenn contact:**

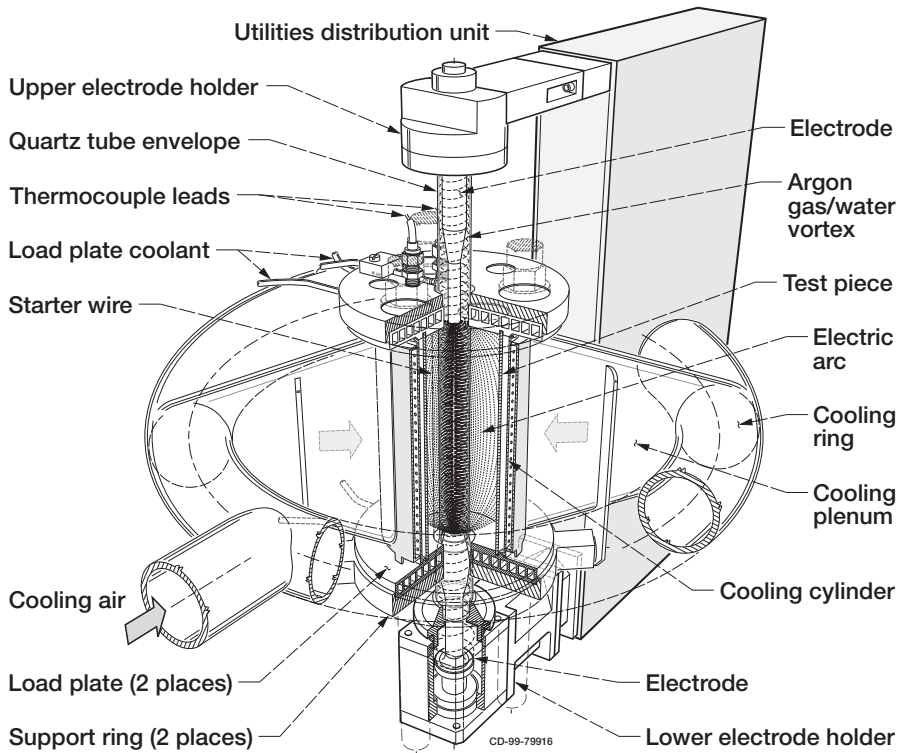
Dr. Jon C. Goldsby, (216) 433-8250,  
Jon.C.Goldsby@grc.nasa.gov

**U.S. Army Vehicle Technology Center  
contact:** Michael C. Halbig, (216) 433-  
2651, Michael.C.Halbig@grc.nasa.gov

**Authors:** Dr. Jon C. Goldsby and  
Michael C. Halbig

**Headquarters program office:** OAST

**Programs/Projects:**  
HSR Phase II, UEET



*Test facility for inducing through-the-thickness thermal gradients.*

## Affordable, Robust Ceramic Joining Technology (ARCJoinT) Given 1999 R&D 100 Award

Advanced ceramics and fiber-reinforced ceramic matrix composites with high strength and toughness, good thermal conductivity, thermal shock resistance, and oxidation resistance are needed for high-temperature structural applications in advanced high-efficiency and high-performance engines, space propulsion components, and land-based systems. The engineering designs of these systems require the manufacturing of large parts with complex shapes, which are either quite expensive or impossible to fabricate. In many instances, it is more economical to build complex shapes by joining together simple geometrical shapes. Thus, joining has been recognized as an enabling technology for the successful utilization of advanced ceramics and fiber-reinforced composite components in high-temperature applications. However, such joints must retain their structural integrity at high temperatures and must have mechanical strength and environmental stability comparable to those of the bulk materials. In addition, the joining technique should be robust, practical, and reliable.

ARCJoinT, which is based on the reaction-forming approach, is unique in terms of producing joints with tailorable microstructures. The formation of joints by this approach is attractive since the thermomechanical properties of the joint interlayer can be tailored to be very close to those of the base materials. In addition, high-temperature fixturing is not needed to hold the parts at the infiltration temperature. The joining process begins with the application of a carbonaceous mixture in the joint area, holding the items to be joined in a fixture, and curing at 110 to 120 °C for 10 to 20 min. This

step fastens the pieces together. Then, silicon or a silicon alloy in tape, paste, or slurry form is applied around the joint region and heated to 1250 to 1425 °C (depending on the type of infiltrant) for 10 to 15 min. The molten silicon or silicon-refractory metal alloy reacts with carbon to form silicon carbide with controllable amounts of silicon and other phases as determined by the alloy composition. Joint thickness can be readily controlled through adjustments of the properties of the carbonaceous paste and the applied fixturing force.

The following photograph shows various shapes of silicon-carbide-based ceramics and fiber-reinforced composites that have been joined using ARCJoinT. Thermo-mechanical and thermochemical



*Various ceramics and composites joined using ARCJoinT.*

characterization of joints is underway for a wide variety of silicon-carbide-based advanced ceramics and fiber-reinforced composites under the hostile environments that will be encountered in engine applications.

## Atomistic Method Applied to Computational Modeling of Surface Alloys

The formation of surface alloys is a growing research field that, in terms of the surface structure of multicomponent systems, defines the frontier both for experimental and theoretical techniques. Because of the impact that the formation of surface alloys has on surface properties, researchers need reliable methods to predict new surface alloys and to help interpret unknown structures. The structure of surface alloys and when, and even if, they form are largely unpredictable from the known properties of the participating elements. No unified theory or model to date can infer surface alloy structures from the constituents' properties or their bulk alloy characteristics. In spite of these severe limitations, a growing catalogue of such systems has been developed during the last decade, and only recently are global theories being advanced to fully understand the phenomenon.

None of the methods used in other areas of surface science can properly model even the already known cases. Aware of these limitations, the Computational Materials Group at the NASA Glenn Research Center at Lewis Field has developed a useful, computationally economical, and physically sound methodology to enable the systematic study of surface alloy formation in metals. This tool has been tested successfully on several known systems for which hard experimental evidence exists (refs. 1 and 2) and has been used to predict ternary surface alloy formation (results to be published: Garces, J.E.; Bozzolo, G.; and Mosca, H.: Atomistic Modeling of Pd/Cu(100) Surface Alloy Formation. Surf. Sci., 2000 (in press); Mosca, H.; Garces J.E.; and Bozzolo, G.: Surface Ternary Alloys of

ARCJoinT, which was developed by researchers at the NASA Glenn Research Center at Lewis Field, received R&D Magazine's prestigious R&D 100 Award in 1999.

**For more information, visit the Ceramics Branch on the World Wide Web:** <http://www.grc.nasa.gov/WWW/Ceramics/homepage.htm>

**Dynacs Engineering Corporation, Inc., contact:**

Dr. Mrityunjay Singh, (216) 433-8883, Mrityunjay.Singh@grc.nasa.gov

**Author:** Dr. Mrityunjay Singh

**Headquarters program office:** OAST

**Program/Projects:** CTO, SRF

**Special recognition:**  
1999 R&D 100 Award

(Cu,Au)/Ni(110). (Accepted for publication in Surf. Sci., 2000.); and Garces, J.E.; Bozzolo, G.; Mosca, H.; and Abel, P.: A New Approach for Atomistic Modeling of Pd/Cu(110) Surface Alloy Formation. (Submitted to Appl. Surf. Sci.)). Ternary alloy formation is a field yet to be fully explored experimentally.

The computational tool, which is based on the BFS (Bozzolo, Ferrante, and Smith) method for the calculation of the energetics, consists of a small number of simple PC-based computer codes that deal with the different aspects of surface alloy formation. Two analysis modes are available within this package.

(1) The first mode provides an atom-by-atom description of real and virtual stages during the process of surface alloying, based

on the construction of catalogues of configurations where each configuration describes one possible atomic distribution. BFS analysis of this catalogue provides information on accessible states, possible ordering patterns, and details of island formation or film growth. More importantly, it provides insight into the evolution of the system. Software developed by the Computational Materials Group allows for the study of an arbitrary number of elements forming surface alloys, including an arbitrary number of surface atomic layers.

(2) The second mode involves large-scale temperature-dependent computer simulations that use the BFS method for the energetics and provide information on the dynamic processes during surface alloying. These simulations require the implementation of Monte-Carlo-based codes with high efficiency within current workstation environments.

This methodology capitalizes on the advantages of the BFS method: there are no restrictions on the number or type of elements or on the type of crystallographic structure considered. This removes any restrictions in the definition of the configuration catalogues used in the analytical calculations, thus allowing for the study of arbitrary ordering patterns, ultimately leading to the actual surface alloy structure. Moreover, the Monte Carlo numerical technique used for the large-scale simulations allows for a detailed visualization of the simulated process, the main advantage of this type of analysis being the ability to understand the underlying features that drive these processes. Because of the simplicity of the BFS method for the energetics used in these calculations, a detailed atom-by-atom analysis can be performed at any point in the simulation, providing necessary insight on the details of the process.

The main objective of this research program is to develop a tool to guide experimenters in understanding and interpreting often unexpected results in alloy formation experiments. By reducing the computational effort without losing physical accuracy, we expect that powerful simulation tools will be developed in the immediate future, which will allow material scientists to easily visualize and analyze processes at a level not achievable experimentally.

## System Being Developed to Measure the Rotordynamic Characteristics of Air Foil Bearings

Because of the many possible advantages of oil-free engine operation, interest in using air-lubricated foil-bearing technology in advanced oil-free engine concepts has recently increased. The Oil-Free Turbomachinery Program at the NASA Glenn Research Center at Lewis Field has partially driven this recent push for oil-free technology. The program's goal of developing an innovative, practical, oil-free gas turbine engine for aero-propulsion began with the development of NASA's high-temperature solid-lubricant coating, PS304. This coating virtually eliminates the life-limiting wear that occurs during the startup and shutdown of the bearings. With practically unlimited life, foil air bearings are now very attractive to rotating machinery designers for use in turbomachinery. Unfortunately, the current knowledge base of these types of bearings is limited. In particular, the

### References

1. Bozzolo, G.; Ferrante, J.; and Ibanez-Meier, R.: Semi-Empirical Analysis of Surface Alloy Formation. Proceedings of the 1995 15th European Conference on Surface Science, vols. 352-354, 1996, p. 577-582.
2. Bozzolo, G., et al.: Surface Segregation in Multicomponent Systems: Modeling of Surface Alloys and Alloy Surfaces. *Comp. Mat. Sci.*, vol. 15, 1999, pp. 169-195.

### Additional references are available via the World Wide Web:

[http://www.grc.nasa.gov/WWW/SurfSci/bfs/bfs\\_index.html](http://www.grc.nasa.gov/WWW/SurfSci/bfs/bfs_index.html)

### Ohio Aerospace Institute contact:

Dr. Guillermo H. Bozzolo,  
(440) 962-3103 or (216) 433-5824,  
Guillermo.H.Bozzolo@grc.nasa.gov

### Glenn contact:

Dr. Phillip B. Abel, (216) 433-6063,  
Phillip.B.Abel@grc.nasa.gov

**Authors:** Dr. Guillermo H. Bozzolo and Dr. Phillip B. Abel

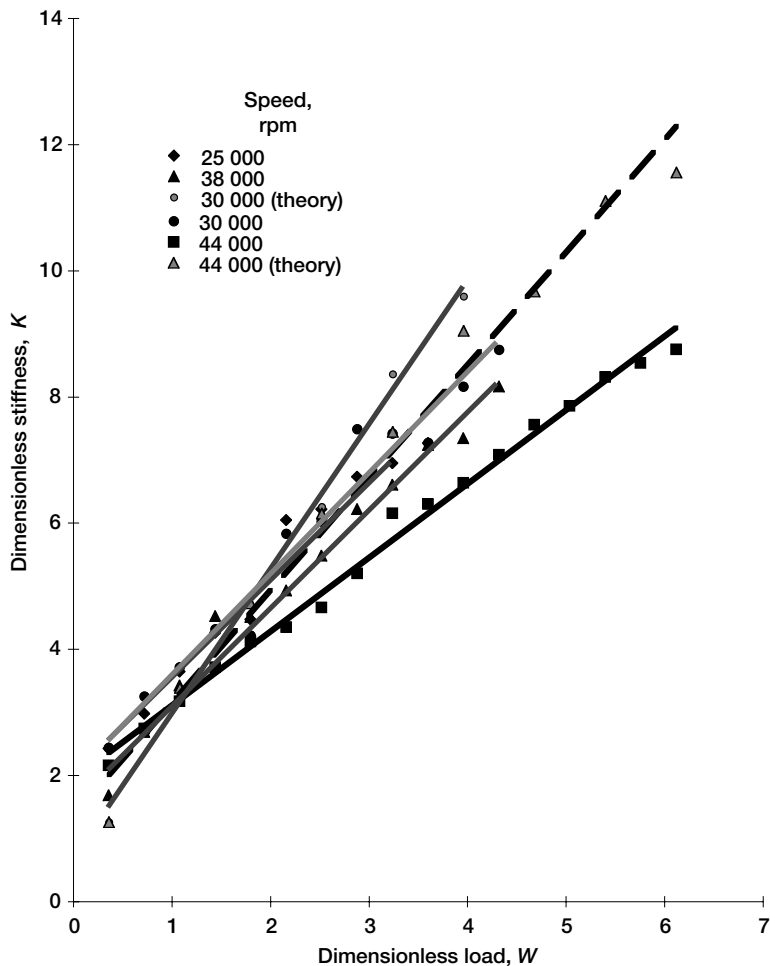
**Headquarters program office:** OAST

**Programs/Projects:** HITEMP, P&PM

**Special recognition:** NASA Honor Award given to the Computational Materials Group; reference 2 named Glenn Research Center's Distinguished Paper of the Year for 1999.

understanding of how these types of bearings contribute to the rotordynamic stability of turbomachinery is insufficient for designers to design with confidence.

Recent work in oil-free turbomachinery has concentrated on advancing the understanding of foil bearings. A high-temperature fiber-optic displacement probe system and measurement method were



Effect of speed and load on bearing stiffness.

developed to study the effects of speed, load, temperature, and other environmental issues on the stiffness characteristics of air foil bearings. Since high-temperature data are to be collected in future testing, the testing method was intentionally simplified to minimize the need for expensive test hardware. The method measures the displacement induced upon a bearing in response to an applied perturbation load. The

early results of these studies, which are shown in the accompanying figure, indicate trends in steady state stiffness that suggest stiffness increases with load and decreases with speed. It can be seen, even from these data, that stiffness is not expected to change by orders of magnitude over the normal operating range of most turbomachinery; a promising sign for their eventual integration into oil-free turbomachines. Planned future testing will generate similar plots for stiffness changes with temperature and geometry, as well as damping data. The data collected by this method represent a critical step toward understanding how to successfully apply foil air bearings to future oil-free turbomachinery systems.

**Case Western Reserve University contact:**

Samuel A. Howard, (216) 433-6076, Samuel.A.Howard@grc.nasa.gov

**Glenn contacts:** Dr. Christopher DellaCorte, (216) 433-6056, Christopher.DellaCorte@grc.nasa.gov; and Dr. Mark J. Valco, (216) 433-3717, Mark.J.Valco@grc.nasa.gov

**Authors:** Samuel A. Howard, Dr. Christopher DellaCorte, and Dr. Mark J. Valco

**Headquarters program office:** OAST  
**Programs/Projects:** P&PM, SGE

## Surface Coatings in Egyptian Art Characterized Through Spectroscopy

For objects dating back dozens of centuries, very few records of their construction and composition remain. Yet it is extremely important to have accurate information regarding the surface chemistry of art objects when preservation or restorative techniques are applied. Furthermore, it is essential that the object not be substantially consumed during characterization. To this end, the Cleveland Museum of Art has partnered with the microspectroscopy laboratory at the NASA Glenn Research Center at Lewis Field to characterize the surface coating of their prized Egyptian antiquities.

Microsamples from the relief of the *Nome Gods Bearing Offerings*, coffin lids, the bust of *Amenhotep III Wearing the Blue Crown* (see "Collection/Egyptian highlights tour" at <http://www.cma-oh.org/> for art objects), and other art objects were characterized by

Fourier Transform Infrared Spectroscopy (FT-IR) to determine the composition and, if possible, identify deterioration products associated with centuries of aging. The characterization is complex because the artisans selectively applied multiple varnishes in various locations of a given object. The different surface coatings appear to have been chosen on the basis of aesthetics, such as color and gloss, rather than protection. The process of identifying the original surface composition is further complicated by the treatments used by early restorers, such as impregnation of painted materials with beeswax or paraffin, materials also used by the original artisans.

FT-IR clearly distinguishes wax from plant resin materials, but it is not possible at this time to determine if the wax is from an original application or a restorative measure. There are many applications of various plant resins in the construction of art objects. In the case of the bust of Amenhotep III, several sections of carved stone were glued together. The nose sustained damage and was restored with putty. The bust was finished by the application of various colored pigments and varnish. Plant resin applications include putty for restoration or disguising artisan flaws, binder for the various pigments of paint, and varnish to hold the paint in place or provide a glossy appearance. It is difficult to identify the exact plant providing various resins; however, in many cases it is possible with the use of FT-IR, in combination with optical microscopy and fluorescence to differentiate between different resins applied to an object. Finally, animal materials such as hides were used to formulate glues and other liquids that were used in art objects. Animal materials are distinguishable from waxes and resins, but at this time, we have not identified any in the Egyptian art works that we are examining.

The spectra obtained from coatings on the Nome gods relief, a Nefertiti portrait, and three dummy jars are virtually identical, suggesting that the

coatings were of similar material. The quality of the spectra obtained from the bust of Amenhotep are distorted because of contamination or age degradation, but several key peaks in the spectra indicate that this coating is a varnish similar to that on other objects. Aside from the academic value of accurately identifying the methods of construction, this information is crucial when attempts are made to reconstruct the original appearance of an object with poorly preserved decorative layers.

**These art objects are depicted on the World Wide Web:**

<http://www.cma-oh.org>, (see the "Collection/Egyptian highlights tour")

**Glenn contact:**

Dr. Kenneth W. Street, (216) 433-5032, [Kenneth.W.Street@grc.nasa.gov](mailto:Kenneth.W.Street@grc.nasa.gov)

**Author:** Dr. Kenneth W. Street

**Headquarters program office:** OAST

**Programs/Projects:**

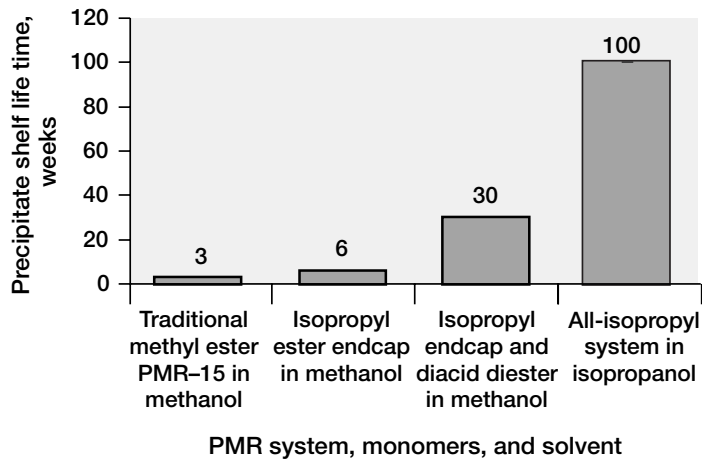
Technology Transfer

## Shelf Life of PMR Polyimide Monomer Solutions and Prepregs Extended

PMR (Polymerization of Monomeric Reactants) technology was developed in the mid-1970's at the NASA Glenn Research Center at Lewis Field for fabricating high-temperature stable polyimide composites. This technology allowed a solution of polyimide monomers or prepreg (a fiber, such as glass or graphite, impregnated with PMR polyimide monomers) to be thermally cured without the release of volatiles that cause the formation of voids—unlike the non-PMR technology used for polyimide condensation type resins. The initial PMR resin introduced as PMR-15 is still commercially available and is used worldwide by aerospace industries as the state-of-the-art resin for high-temperature polyimide composite applications. PMR-15 offers easy composite processing, excellent composite mechanical property retention, a long lifetime at use temperatures of 500 to 550 °F, and relatively low cost. Later, second-generation PMR resin versions, such as PMR II-50 and VCAP-75, offer improvements in the upper-use temperature (to 700 °F) and in the useful life at temperature without major compromises in processing and property retention but with significant increases in resin cost. Newer versions of nontoxic (non-methylene dianiline) PMR resins, such as BAX PMR-15, offer similar advantages as

originally found for PMR-15 but also with significant increases in resin cost. Thus, the current scope of the entire PMR technology available meets a wide range of aeronautical requirements for polymer composite applications.

A major problem with PMR technology is that PMR polyimide monomer solutions and prepregs all suffer from a short shelf life. State-of-the-art PMR-15 has a maximum shelf life of 3 weeks at room temperature. Second-generation versions of PMR monomer solutions and prepregs and newer nontoxic versions of



*PMR-15 solution stability as a function of time to precipitate.*

non-methylene dianiline PMR monomer solutions and preregs exhibit an even shorter shelf life—over an order of magnitude less than that of state-of-the-art PMR-15. This problem has plagued industry since PMR's inception until now. Researchers at Glenn recently discovered that PMR's shelf life is dramatically improved by using secondary alcohols (preferably isopropanol) instead of conventional primary alcohols (methanol or ethanol) to both esterify the PMR monomer mix and dissolve it. In-house researchers also found that PMR monomer solutions and preregs made with this alternative ester approach are less reactive during comparable storage and handling temperatures without affecting typical curing temperatures. The graph illustrates PMR-15's extended shelf life at room temperature when the new alternative ester approach is used. In the best case, using an all isopropyl system, a thirty-three-fold increase in shelf life is seen before the PMR-15 solution forms precipitates. For second-generation and nontoxic PMR monomer solutions and preregs, the shelf life improvement is about an order of magnitude. Thus, this discovery has widespread application to improve the shelf life of many PMR systems.

This method of improving PMR shelf life could also offer several additional advantages over conventional PMR technology because of its greater temperature stability, providing an increased tolerance to the mishandling of PMR solutions and preregs. These advantages translate into (1) reduced shipping and handling costs by eliminating the need for refrigeration, (2) reduced variability between PMR monomer batches that results in more consistent processability, (3) improved hot-melt PMR prepreg manufacturing, (4) reduced scrap rates, (5) improved safety because isopropanol is less toxic than methanol and ethanol, and (6) improved adaptability to some processing techniques such as solvent-assisted resin transfer molding. Further work is ongoing to exploit all these advantages.

**U.S. Army Research Laboratory at Glenn contact:**

Dr. William B. Alston, (216) 433-3220, William.B.Alston@grc.nasa.gov

**Dynacs Engineering Co., Inc., contact:**

Daniel A. Scheiman, (216) 433-3223, Daniel.A.Scheiman@grc.nasa.gov

**Authors:** Dr. William B. Alston and Daniel A. Scheiman

**Headquarters program office:** OAST

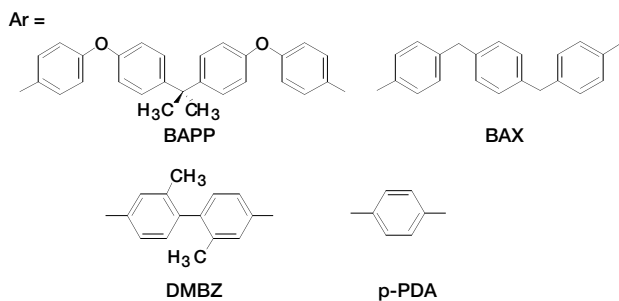
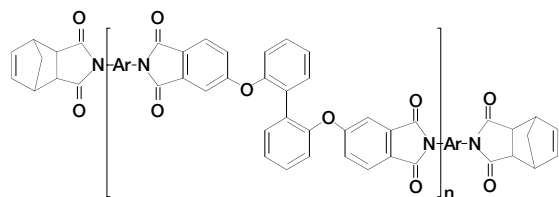
**Programs/Projects:** HITEMP

## Resin Transfer Moldable Polyimides Developed for High-Temperature Applications

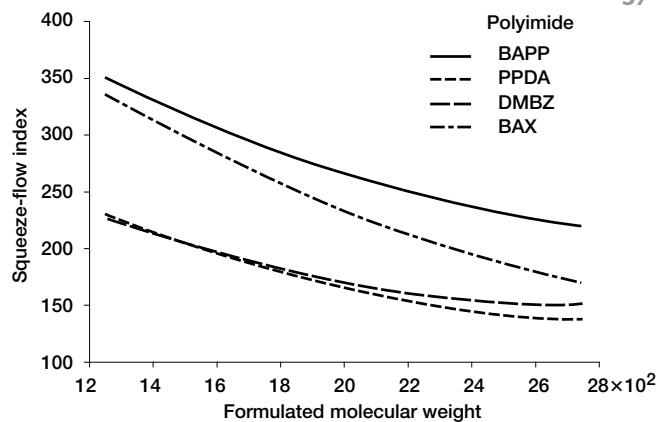
High-temperature polyimides, such as PMR-15 (which was developed at the NASA Glenn Research Center at Lewis Field), are becoming an increasingly important class of materials for a variety of aerospace applications, such as aircraft engine components and propulsion and airframe components for reusable launch vehicles (RLV's). Because of their high specific strength and low density, use of these materials in place of more traditional aerospace materials, such as titanium, can significantly reduce component and vehicle weight, leading to reductions in fuel consumption (and pollutants), increases in payload and passenger capacity, and improvements in vehicle performance.

Typical methods for fabricating components from these high-temperature materials are fairly labor intensive and costly. More cost-effective methods,

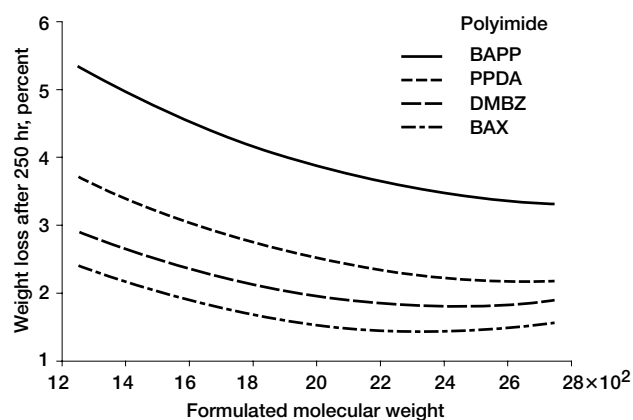
such as resin transfer molding (RTM), have been developed and successfully employed with low-temperature polymers (use temperatures no higher than 400 °F). RTM processing can lead to as much as a 50-percent reduction in manufacturing costs over traditional fabrication methods. In the RTM technique, a preform, made by weaving or braiding fiber reinforcements, is infiltrated with molten polymer, and the resulting



Low-melt-viscosity PMR polyimides.



Melt flow of PMR polyimides.



Weight Loss after 250 hr at 550 °F (290 °C) of low-melt-viscosity PMR polyimides.

structure is cured at elevated temperatures. To successfully fill the mold and wet out all of the fibers in the preform, the molten polymer must have a melt viscosity no higher than 1000 centipoise (cP)—about the consistency of castor oil. High-temperature polymers, such as PMR-15, have melt viscosities on the order of 200,000 cP—the consistency of peanut butter. The challenge is to develop new polymers that not only have melt viscosities low enough to enable RTM processing but have the stability and properties necessary for operation at temperatures above 450 °F (232 °C).

A recent collaboration between researchers in Glenn’s Polymers Branch and the University of Akron’s Institute of Polymer Science led to the development of a new family of PMR polyimides (see the chemical diagrams) with melt viscosities low enough for RTM processing. Melt viscosities of these imide oligomers were measured by pressing 0.5 g of resin powder between two 12- by 12-in. sheets of Kapton in a heated press (500 °F, 260 °C) at 170-psi pressure. Areas of the resulting resin “spots” (Squeeze Flow Index) were measured and are shown in the top graph as a function of formulated molecular weight. Those resins with Squeeze Flow Indexes greater than 220 cm<sup>2</sup> have melt viscosities below 1000 cP. Most of the resins prepared from BAPP and BAX diamines have melt viscosities low enough for RTM processing. Neat resin samples were molded from these imide oligomers at 316 °C and postcured for 16 hr at 325 °C. Weight losses

for these samples after 250 hr of aging in air at 550 °F (290 °C) are shown in the bottom graph. Resin samples prepared from the BAX diamine showed the lowest weight losses of all samples tested and indicate good long-term stability at or near 550 °F. Further work is underway to evaluate these materials in carbon-fiber-reinforced composites.

**Glenn contacts:** Dr. Michael A. Meador, (216) 433-9518, Michael.A.Meador@grc.nasa.gov; Christopher Gariepy, (216) 433-3187, Christopher.Gariepy@grc.nasa.gov; and Dr. Mary Ann Meador, (216) 433-3221, Maryann.Meador@grc.nasa.gov

**Author:** Dr. Michael A. Meador

**Headquarters program office:** OAST

**Programs/Projects:** RLV

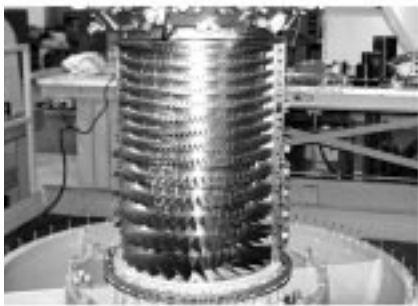
# Erosion Coatings for High-Temperature Polymer Composites: A Collaborative Project With Allison Advanced Development Company



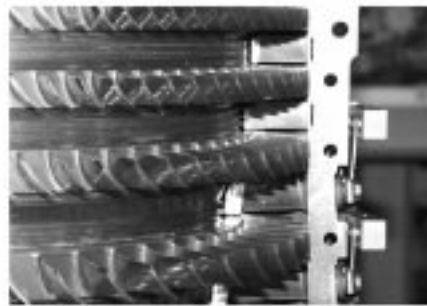
AE 2100 Inlet Housing/Shroud/Guide Vane



AE 3007 Fan



AE 3007 Rotor Assembly Compressor Case Removed



AE 3007 Rotor Assembly/Stator Vane

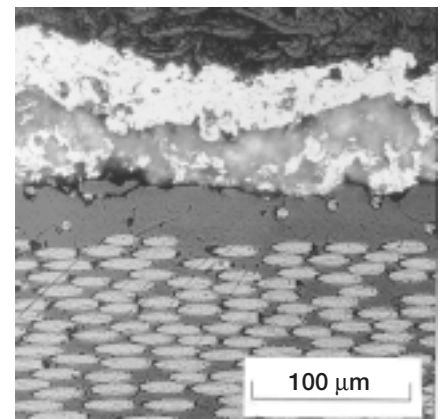
*Erosion coating applications in gas turbines.*

The advantages of replacing metals in aircraft turbine engines with high-temperature polymer matrix composites (PMC's) include weight savings accompanied by strength improvements, reduced part count, and lower manufacturing costs. Successfully integrating high-temperature PMC's into turbine engines requires several long-term characteristics. Resistance to surface erosion is one rarely reported property of PMC's in engine applications because PMC's are generally softer than metals and their erosion resistance suffers. Airflow rates in stationary turbine engine components typically exceed 2.3 kg/sec at elevated temperatures and pressures. In engine applications, as shown in the following photos, the survivability of PMC components is clearly a concern, especially when engine and component life-cycle requirements become longer.

Although very few publications regarding the performance of erosion coatings on PMC's are available—particularly in high-temperature applications—the use of erosion-resistant coatings to significantly reduce wear on metallic substrates is well documented. In this study initiated by the NASA Glenn Research Center at Lewis Field, a low-cost (less than \$140/kg) graphite-fiber-reinforced T650–35/PMR–15 sheet-molding compound was investigated with various coatings. This sheet-molding compound has been compression molded into many structurally complicated components, such as shrouds for gas turbine inlet housings and gearboxes. Erosion coatings

developed for PMC's in this study consisted of a two-layered system: a bondcoat sprayed onto a cleaned PMC surface, followed by an erosion-resistant, hard topcoat sprayed onto the bondcoat as shown in following photomicrograph. Six erosion coating systems were evaluated for their ability to withstand harsh thermal cycles, erosion resistance (ASTM G76–83 “Standard Practice for Conducting Erosion Tests by Solid Particle Impingement Using Gas Jets”) using  $Al_2O_3$ , and adhesion to the graphite fiber polyimide composite (ASTM D 4541–95 “Pull Off Strength of Coatings”).

Glenn and Allison Advanced Development Company collaborated to optimize erosion coatings for gas turbine fan and compressor applications. All the coating systems survived aggressive thermal cycling without spalling. During erosion tests (see the photo on the following page), the most promising coating systems tested had  $Cr_3C_2$ -NiCr and WC-Co as the hard topcoats. In all cases, these coating systems performed significantly better than that with a TiN hard

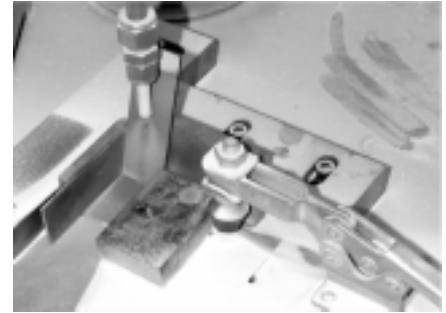


*Erosion coating/T650–35/PMR–15.*

topcoat. When material depth (thickness) loss is considered, the  $\text{Cr}_3\text{C}_2$ -NiCr and WC-Co coating systems provided, on average, an erosion resistance 8.5 times greater than that for the uncoated PMR-15/T650-35 composite. Similarly,  $\text{Cr}_3\text{C}_2$ -NiCr and WC-Co coating systems adhered to the PMC substrate during tensile tests significantly better than systems containing a TiN topcoat. Differences in topcoats of  $\text{Cr}_3\text{C}_2$ -NiCr and WC-Co were determined by considering issues such as cost and environmental impact. The preferred erosion-resistant coating system for PMR-15/T650-35 has WC-Co as the hard topcoat. This system provides the following benefits in comparison to the coating system with  $\text{Cr}_3\text{C}_2$ -NiCr topcoat: lower powder material cost (15 to 20 percent), environmentally friendly materials ( $\text{Cr}_3\text{C}_2$ -NiCr is hazardous), and higher deposition yield (10 to 15 percent), which results in less waste.

#### Bibliography

Naik, S.K., et al.: Erosion Coatings for High Temperature Polymer Composites. Proceedings of the 44th International SAMPE Symposium, vol. 44, book 1, 1999, pp. 68-81.



*Erosion rig.*

#### Glenn contact:

Dr. James K. Sutter, (216) 433-3226,  
James.K.Sutter@grc.nasa.gov

**Author:** Dr. James K. Sutter

**Headquarters program office:** OAST

#### Programs/Projects:

Propulsion Systems R&T, HITEMP

## Near-Net-Shape Processing of Sintered Fibrous Ceramics Achieved

A variety of sintered fibrous ceramic (SFC) materials have been developed over the last 50 years as thermal barrier materials for reentry applications. SFC materials typically exhibit very low thermal conductivities combined with low densities and good thermal stability up to 2500 °F. These materials have flown successfully on the space shuttle orbiters since the 1960's. More recently, the McDonnell Douglas Corporation successfully used SFC tiles as a heat shield on the underside of its DC-X test vehicle. For both of these applications, tiles are machined from blocks of a specific type of SFC called an alumina-enhanced thermal barrier (AETB). The sizes of these blocks have been limited by the manufacturing process. In addition, as much as 80 to 90 percent of the material can be lost during the machining of tiles with significant amounts of curvature. To address these problems, the NASA Glenn Research Center at Lewis Field entered a cooperative contract with the Boeing Company to develop a vacuum-assisted forming process that can produce large (approximately 4 ft<sup>2</sup>), severely contoured panels of AETB while saving costs in comparison to the conventional cast-and-machine billet process.

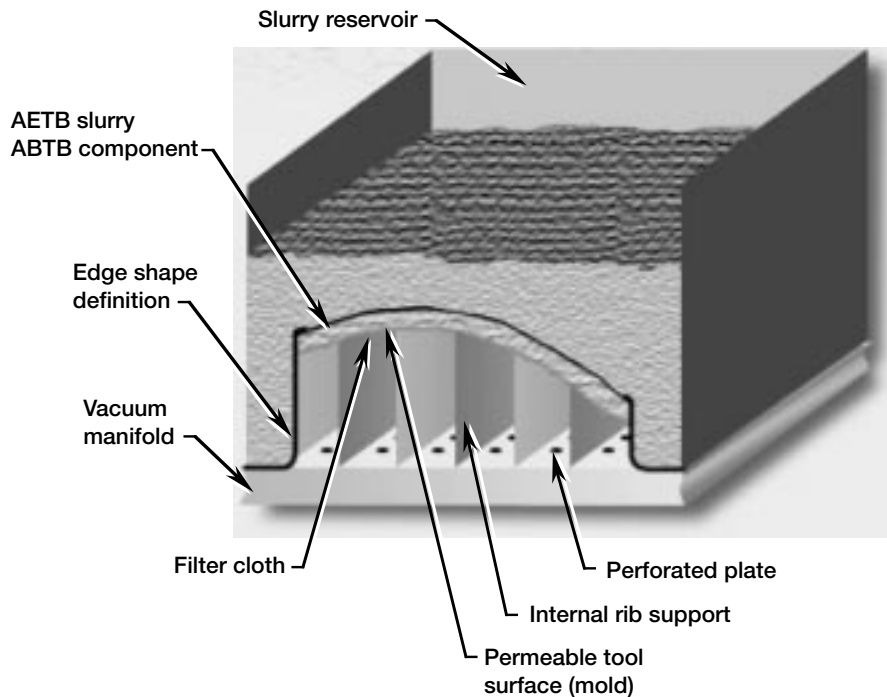
For shuttle use, AETB is slurry cast, drained, and fired to form square billets conforming to the shape of the filtration box. The billets are then cut into tiles of the appropriate size for thermally protecting the space shuttle. Processing techniques have limited the maximum size of AETB billets to 21.5 in.<sup>2</sup> by 6.5-in. thick, but the space shuttles use discrete heat shield tiles

no more than 8 to 12 in.<sup>2</sup> However, in other applications, large, complex shapes are needed, and the tiling approach is undesirable.

For such applications, vacuum-assisted forming can produce large parts with complex shapes while reducing machining waste and



*2- by 2-ft AETB panel with complex curvature manufactured by the vacuum-assisted forming process.*



*Depiction of vacuum cooling and equipment.*

eliminating cemented joints between bonded billets. Because it allows contoured shapes to be formed, material utilization is inherently high. Initial estimates show that the amount of material lost during machining can be reduced by 50 percent or more. In addition, a fiber alignment favorable for minimum heat transfer is maintained for all panel shapes since the fibers are aligned parallel to the contoured surface of the forming tool or mold. The vacuum-assisted forming process can complete the entire forming operation in a matter of minutes and can produce multiple parts whose size is limited only by the size of the forming tool. To date,

panels as large as 2 ft<sup>2</sup> have been demonstrated (see the preceding photo).

The vacuum-assisted forming process starts with the fabrication of a permeable forming tool, or mold, with the proper part contour. This reusable tool is mounted over an internal rib support structure, as depicted in the diagram, such that a vacuum can be pulled on the bottom portion of the tool. AETB slurry is then poured over and around the tool, liquid is drawn from the slurry, and the part forms over the tool surface. The part is then dried, fired, and finished machined. Future plans include an evaluation of the need for additional coatings and surface-toughness treatments to extend the durability and performance of this material.

**Glenn contact:** Dr. Paul W. Angel, (216) 433-8008, Paul.W.Angel@grc.nasa.gov

**Author:** Dr. Paul W. Angel

**Headquarters program office:** OAST

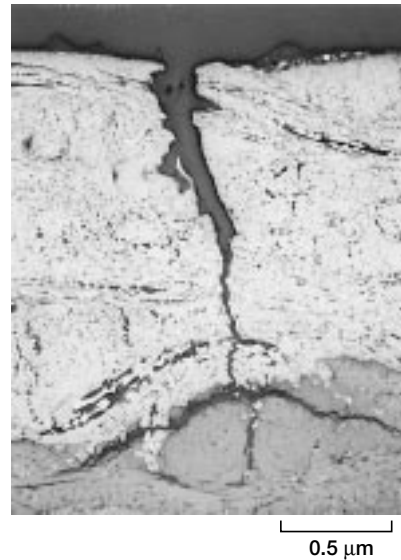
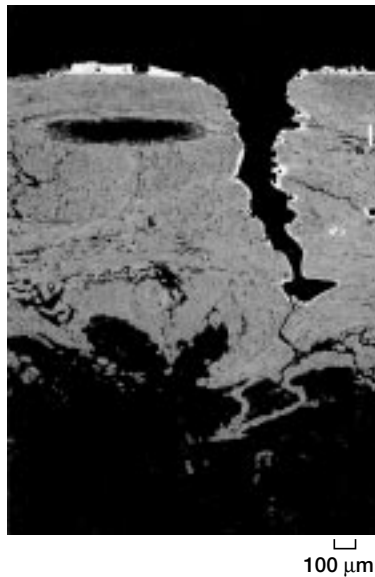
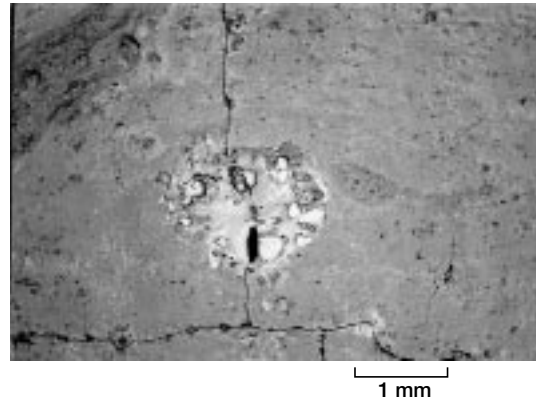
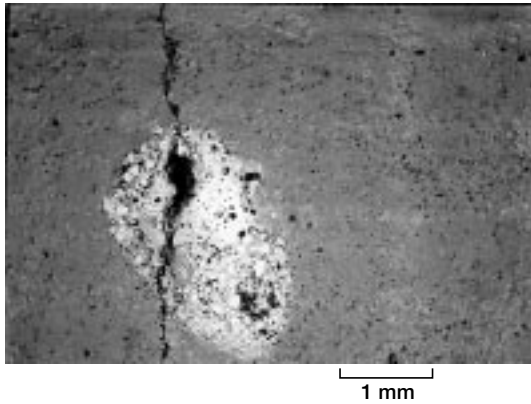
**Programs/Projects:** AAP, PHSV

## Formation of Leading-Edge Pinholes in the Space Shuttle Wings Investigated

The space shuttle wing leading edge and nose cap are composed of a carbon/carbon composite that is protected by silicon carbide. The coefficient of thermal expansion mismatch leads to cracks in the silicon carbide. The outer coating of the silicon carbide is a sodium-silicate-based glass that becomes fluid at the shuttles' high reentry temperatures and fills these cracks.

Small pinholes roughly 0.1 mm in diameter have been observed on these materials after 12 or more flights. These pinholes have been investigated by researchers at the NASA Johnson Space Center, Rockwell International, the Boeing Company, Lockheed Martin Corporation, and the NASA Glenn Research Center at Lewis Field to determine the possible sources and the extent of damage.

A typical pinhole is illustrated in the following photomicrographs (on the left). These pinholes are found primarily on the wing leading edges and not on the nose cap, which is covered when the orbiter is on the launch pad. The pinholes are generally associated with a bead of zinc-rich glass. Examination of the orbiter and launch structure indicates that weathering paint on the launch structure leads to deposits of zinc-containing paint



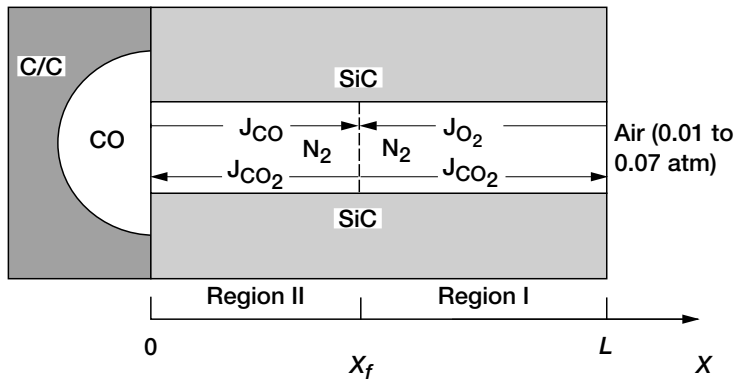
*Top: Pinhole from OV-102 wing leading-edge panel 12 RH; 15 flights. Bottom: Cross-sectional view (backscattered electron image).*

*Top: Pinhole from OV-102 wing leading-edge panel 12 RH; 15 flights. Bottom: Cross-sectional view with optical microscope.*

flakes on the wing leading edge. These may become embedded in the crevices of the wing leading edge and form the observed zinc-rich glass.

Laboratory experiments indicate that zinc oxide reacts vigorously with the glass coating on the silicon carbide. Thus, it is likely that this is the reaction that leads to pinhole formation (Christensen, S.V.: Reinforced Carbon/Carbon Pin Hole Formation Through Zinc Oxide Attack. Rockwell International Internal Letter, RDW-96-057, May 1996). Cross-sectional examination of pinholes suggests that they are enlarged thermal expansion mismatch cracks. This is illustrated in the photomicrographs on the right. A careful microstructural analysis indicates that the pinhole walls consist of layers of zinc-containing glass. Thus, pinholes are likely formed by zinc oxide particles lodging in crevices and forming a corrosive zinc-rich glass that enlarges existing cracks (ref. 1).

Having established the likely source of the pinholes, we next needed to model the damage (ref. 2). Our concern was that if a pinhole went through the silicon carbide to the carbon/carbon substrate, oxygen would have a clear path to oxidize the carbon at high temperatures. This possibility was examined with studies in a laboratory furnace. An ultrasonic drill was used to make artificial pinholes in a sample of protected carbon/carbon. After exposure, the specimens were



Model for the oxidation of a carbon/carbon composite at the bottom of a pinhole in a SiC coating.

weighed and cross-sectioned to quantify the extent of oxidation below the pinhole.

The results at higher temperatures showed good agreement with a simple diffusion-control model. This model is based on the two-step oxidation of carbon to carbon monoxide and carbon dioxide. The fluxes are illustrated in the final figure. The model indicates a strong dependence on pinhole diameter. For smaller diameters and short times, the oxidation of carbon is very limited.

## Diagnostic Techniques Used to Study Chemical-Vapor-Deposited Diamond Films

The advantages and utility of chemical-vapor-deposited (CVD) diamond as an industrial ceramic can only be realized if the price and quality are right. Until recently, this technology was of interest only to the academic and basic research community. However, interest has grown because of advances made by leading CVD diamond suppliers (ref. 1):

- (1) Reduction of the cost of CVD polycrystalline diamond deposition below \$5/carat (\$8/cm<sup>2</sup>)
- (2) Installation of production capacity
- (3) Epitaxial growth of CVD single-crystal diamond

Thus, CVD diamond applications and business are an industrial reality. At present, CVD diamond is produced in the form of coatings or wafers. CVD diamond film technology offers a broader technological potential than do natural and high-pressure synthetic diamonds because size, geometry, and eventually cost will not be as limiting. Now that they are cost effective, diamond coatings—with their extreme properties—can be used in a variety of applications. Diamond coatings can improve many of the surface properties of engineering substrate materials, including erosion, corrosion, and wear resistance. Examples of actual and potential applications, from microelectromechanical systems to the wear parts of diamond coatings and

### References

1. Jacobson, N.S.: Space Shuttle Pinhole Formation Mechanism Studies. NASA/TM-1998-208659. (Available online: <http://gltrs.grc.nasa.gov/cgi-bin/GLTRS/browse.pl?1998/TM-1998-208659.html>)
2. Jacobson, N.S., et al.: Oxidative Attack of Carbon/Carbon Substrates Through Coating Pinholes. Carbon vol. 37, no. 3, 1999, pp. 411-419.

**Glenn contact:** Dr. Nathan S. Jacobson, (216) 433-5498, Nathan.S.Jacobson@grc.nasa.gov

**NASA Johnson contact:** Dr. Donald M. Curry, (281) 483-8865, donald.m.curry1@jsc.nasa.gov

**Author:** Dr. Nathan S. Jacobson

**Headquarters program office:** OSF

**Programs/Projects:** Space Shuttle Leading Edge Structural Subsystem

related superhard coatings are described in reference 2. For example, diamond coatings can be used as a chemical and mechanical barrier for the space shuttles' check valves, particularly on the guide pins and seat assemblies (see the following figure and ref. 3).

To achieve satisfactory surface and bulk properties of coatings and films, researchers must optimize deposition parameters through the study of the physical, chemical, and structural changes of coatings and films as a function of deposition parameters (ref. 4). These parameters must not only give the appropriate initial level of surface and bulk properties but must also provide durable coatings and films.

For a material to be recognized as diamond it must have all of the following characteristics (refs. 1 and 4):

- (1) A crystalline diamond morphology and microstructure visible by electron microscopy
- (2) A single-phase diamond crystal line structure detectable by x-ray or electron diffraction
- (3) A clear, sharp diamond peak at  $1332\text{ cm}^{-1}$  in a Raman spectrum
- (4) Carbon content
- (5) A low equilibrium coefficient of friction (0.01 to 0.05) in air

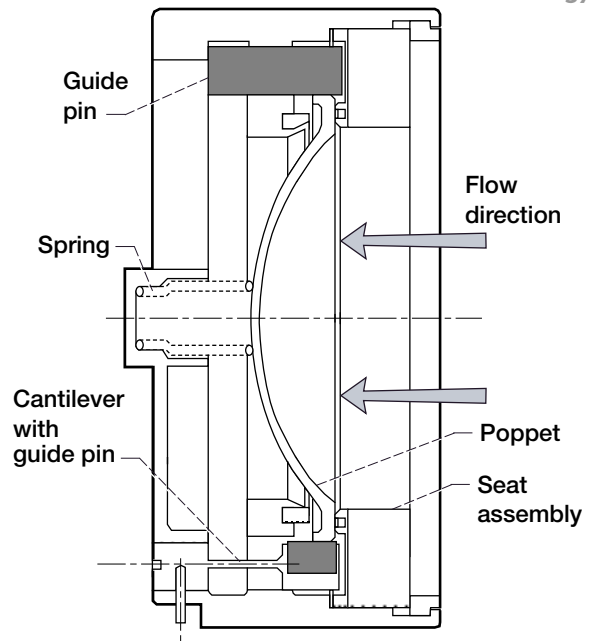
Diagnostic techniques, including friction measurement, have been highlighted in an important case study of microwave-plasma-assisted CVD diamond films (ref. 4) at the NASA Glenn Research Center at Lewis Field. The work focused attention primarily on the nature, character, and quality of the CVD diamond films. Diagnostic techniques included

- (1) Scanning electron microscopy and transmission electron microscopy to determine surface morphology, microstructure, and grain size
- (2) Surface profilometry and atomic force microscopy to measure surface roughness and determine surface morphology
- (3) Rutherford backscattering and elastic recoil spectroscopy to determine the composition (including hydrogen content)
- (4) Raman spectroscopy to characterize the atomic bonding state and quality
- (5) X-ray diffraction to determine the crystal orientation
- (6) Friction examination to determine the coefficient of friction and surface properties

The commercial potential of diamond films has been clearly established, and a number of applications have been identified through university, industry, and Government research studies. A combination of diagnostic techniques can provide the technical information required for understanding the characteristics and properties of diamond films, which are important to their application in specific component systems and environments (refs. 1, 4, and 5).

**References**

1. Miyoshi, K.: Chemical-Vapor-Deposited Diamond Films, chapter 9. NASA/TM-1999-107249, 1999. (Available online: <http://gltrs.grc.nasa.gov/cgi-bin/GLTRS/browse.pl?/1999/TM-1999-107249-CH9.html>)
2. Miyoshi, K., et al.: Tribological Characteristics and Applications of Superhard Coatings: CVD Diamond, DLC, and c-BN. NASA/TM-1999-209189, 1999. (Available online: <http://gltrs.grc.nasa.gov/cgi-bin/GLTRS/browse.pl?/1999/TM-1999-209189.html>)
3. Miyoshi, K.: Aerospace Mechanisms and Tribology Technology: Case Studies, chapter 7. NASA/TM-1999-107249, 1999. (Available online: <http://gltrs.grc.nasa.gov/cgi-bin/GLTRS/browse.pl?/1999/TM-1999-107249-CH7.html>)



*Potential application of CVD diamonds for valves such as the guide pins and seat assemblies in the space shuttles' check valves.*

4. Miyoshi, K.: Surface Diagnostics in Tribology Technology and Advanced Coatings Development. NASA/TM-1999-208527, 1999. (Available online: <http://gltrs.grc.nasa.gov/cgi-bin/GLTRS/browse.pl?/1999/TM-1999-208527.html>)
5. Miyoshi, K.: Surface Design and Engineering Toward Wear-Resistant, Self-Lubricating Diamond Films and Coatings. NASA/TM-1999-208905, 1999. (Available online: <http://gltrs.grc.nasa.gov/cgi-bin/GLTRS/browse.pl?/1999/TM-1999-208905.html>)

**Glenn contact:** Dr. Kazuhisa Miyoshi, (216) 433-6078, [Kazuhisa.Miyoshi@grc.nasa.gov](mailto:Kazuhisa.Miyoshi@grc.nasa.gov)

**Author:** Dr. Kazuhisa Miyoshi

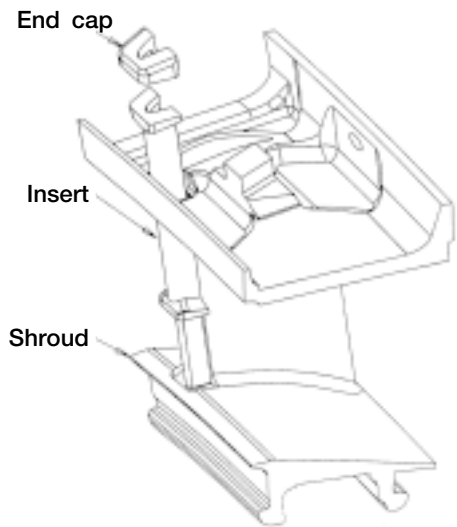
**Headquarters program office:** OAST

**Programs/Projects:** Ultrasafe, P&PM

# Turbine Airfoil With CMC Leading-Edge Concept Tested Under Simulated Gas Turbine Conditions

Silicon-based ceramics have been proposed as component materials for gas turbine engine hot-sections. When the Navy's Harrier fighter experienced engine (Pegasus F402) failure because of leading-edge durability problems on the second-stage high-pressure turbine vane, the Office of Naval Research came to the NASA Glenn Research Center at Lewis Field for test support in evaluating a concept for eliminating the vane-edge degradation. The High Pressure Burner Rig (HPBR) was selected for testing since it could provide temperature, pressure, velocity, and combustion gas compositions that closely simulate the engine environment. The study focused on equipping the stationary metal airfoil (Pegasus F402) with a ceramic matrix composite (CMC) leading-edge insert and evaluating the feasibility and benefits of such a configuration. The test exposed the component, with and without the CMC insert, to the harsh engine environment in an unloaded condition, with cooling to provide temperature relief to the metal blade underneath.

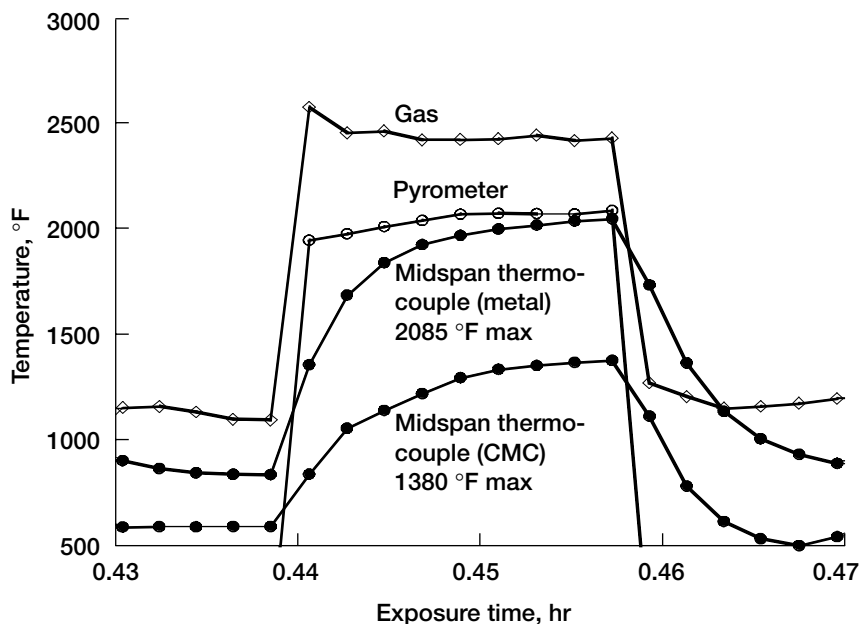
The insert was made using an AlliedSignal Composites, Inc., enhanced HiNicalon (Nippon Carbon Co. LTD., Yokohama, Japan) fiber-reinforced silicon carbide composite (SiC/SiC CMC) material fabricated via chemical vapor infiltration. This insert was 45-mils thick and occupied a recessed area in the leading edge and shroud of the vane. It was designed to be free floating with an end cap design. The HPBR tests provided a comparative evaluation of the temperature response and leading-edge durability and included cycling the airfoils between simulated idle, lift, and cruise flight conditions. In addition, the airfoils were air-cooled, uniquely instrumented, and exposed to the exact set of internal and external conditions, which included gas temperatures in excess of 1370 °C (2500 °F).



*Airfoil with integrated CMC leading-edge concept.*

In addition to documenting the temperature response of the metal vane for comparison with the CMC, a demonstration of improved leading-edge durability was a primary goal. First, the metal vane was tested for a total of 150 cycles. Both the leading edge and trailing edge of the blade exhibited fatigue cracking and burn-through similar to the failures experienced in service by the F402 engine. Next, an airfoil, fitted with the ceramic leading edge insert, was exposed for 200 cycles. The temperature response of those HPBR cycles indicated a reduced internal metal temperature, by as much as 600 °F at the midspan location for the same surface temperature (2100 °F). After testing, the composite insert appeared intact, with no signs of failure on either the vane's leading or trailing edge. Only a slight oxide scale, as would be expected, was noted on the insert.

Overall, the CMC insert performed similarly to a thick thermal barrier coating. With a small air gap between the metal and the SiC/SiC



*Temperature response during HPBR test cycle of the baseline metal airfoil in comparison to that equipped with the CMC leading-edge insert.*

leading edge, heat transfer from the CMC to the metal alloy was low, effectively lowering the temperatures. The insert's performance has proven that an uncooled CMC can be engineered and designed to withstand the thermal up-shock experienced during the severe lift conditions in the Pegasus engine. The design of the leading-edge insert, which minimized thermal stresses in the SiC/SiC CMC, showed that the CMC/metal assembly can be engineered to be a functioning component.

AlliedSignal Composites, Inc., and NASA Glenn thank the Office of Naval Research for their support of this ongoing program through ONR Contract N00014-96-C-0149.

### **Bibliography**

Robinson, R.C.; and Hatton, K.S.: SiC/SiC Leading Edge Turbine Airfoil Tested Under Simulated Gas Turbine Conditions. NASA/CR-1999-209314, 1999. (Available online: <http://gltrs.grc.nasa.gov/cgi-bin/GLTRS/browse.pl?/1999/TM-1999-209314.html>)

**Dynacs Engineering Company, Inc., contact:**

R. Craig Robinson, (216) 433-5547,  
Raymond.C.Robinson@grc.nasa.gov

**Glenn contact:** Leslie A. Greenbauer-Seng, (216) 433-6781,  
Leslie.A.Greenbauer-Seng@grc.nasa.gov

**Authors:** R. Craig Robinson and  
Kenneth S. Hatton

**Headquarters program office:** OAST

**Programs/Projects:** Propulsion  
Systems R&T, HITEMP (via Interagency  
Space Act Agreement (SAA3-145) with  
Office of Naval Research)

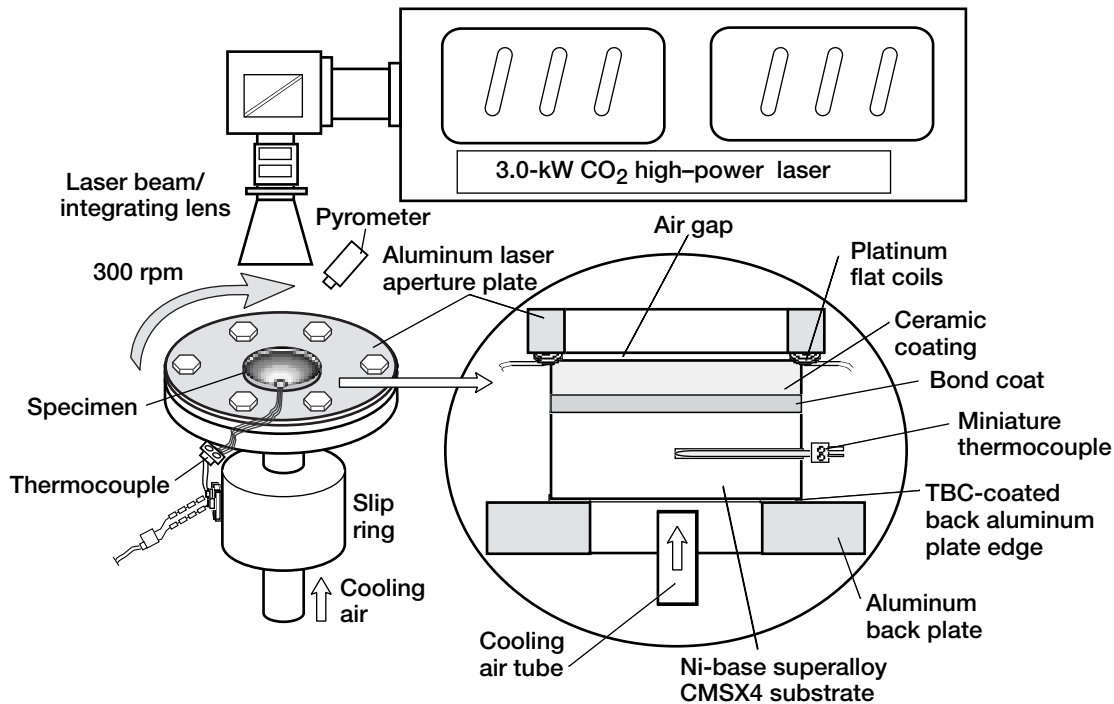
## **Thermal Conductivity Change Kinetics of Ceramic Thermal Barrier Coatings Determined by the Steady-State Laser Heat Flux Technique**

Ceramic thermal barrier coatings (TBC's) are being developed for advanced gas turbine engine components to improve engine efficiency and reliability. However, the durability of the coating systems remains a crucial issue under the increased operating temperatures and extended hot exposure times that will be encountered in next-generation engines. The temperature-dependent change kinetics of the coating thermal conductivity are among the most important parameters required for coating design and life prediction. Increase in thermal conductivity due to ceramic sintering can reduce thermal coating insulation and increase bond coat/substrate oxidation. Therefore, the determination of the thermal conductivity change kinetics of thermal barrier coatings at high temperatures is of great importance.

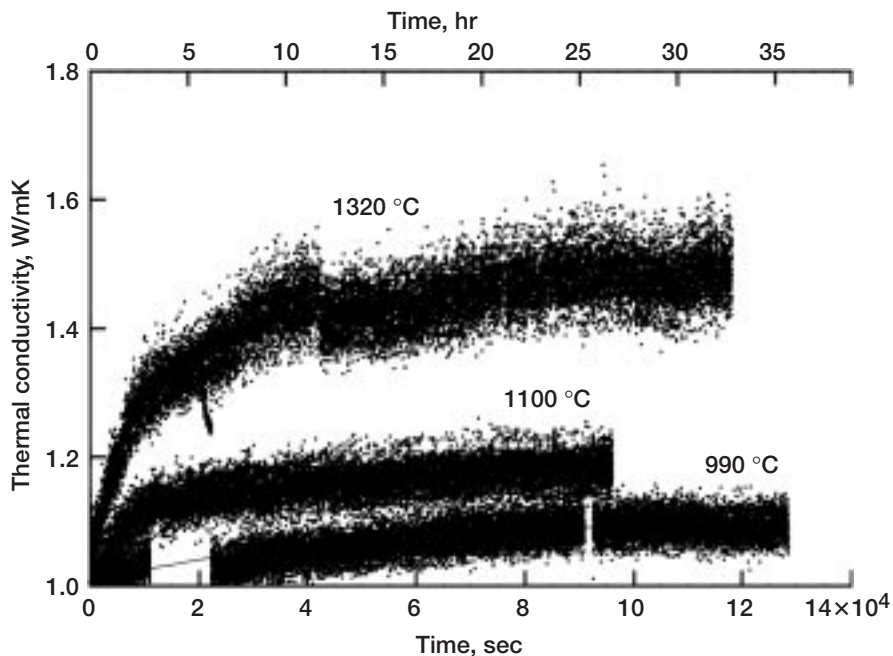
A steady-state laser heat flux technique has been developed at the NASA Glenn Research Center at Lewis Field to obtain critical thermal conductivity data of ceramic thermal barrier coatings under the temperature and thermal gradients that are realistically expected to be encountered in advanced engine systems (ref. 1). The following schematic diagram shows the laser thermal conductivity rig used in this technique. This test rig consists of a 3.0-kW CO<sub>2</sub> continuous-wave laser (wavelength, 10.6 μm), a motor-driven rotating test station, and temperature measurement instruments such as a thermography system and infrared pyrometers. The laser surface heating and the backside air cooling determine appropriate steady-state temperature gradients across the coating systems. An integrating ZnSe lens combined with the specimen rotation can ensure a uniform laser power distribution for the specimen heating. Overall thermal conductivity changes can, thus, be continuously monitored in real

time by measuring the temperature difference across the ceramic coating.

In this study, thermal conductivity change kinetics of a plasma-sprayed, 254-μm-thick ZrO<sub>2</sub>-8 wt %Y<sub>2</sub>O<sub>3</sub> ceramic coating were obtained at high temperatures. During the testing, the temperature gradients across the coating system were carefully measured by the surface and back pyrometers and an embedded miniature thermocouple in the substrate. The actual heat flux passing through the coating system was determined from the metal substrate temperature drop (measured by the embedded miniature thermocouple and the back pyrometer) combined with one-dimensional heat transfer models. The radiation heat loss and laser absorption corrections of the ceramic coating were considered in the calculations by incorporating the coating's measured total

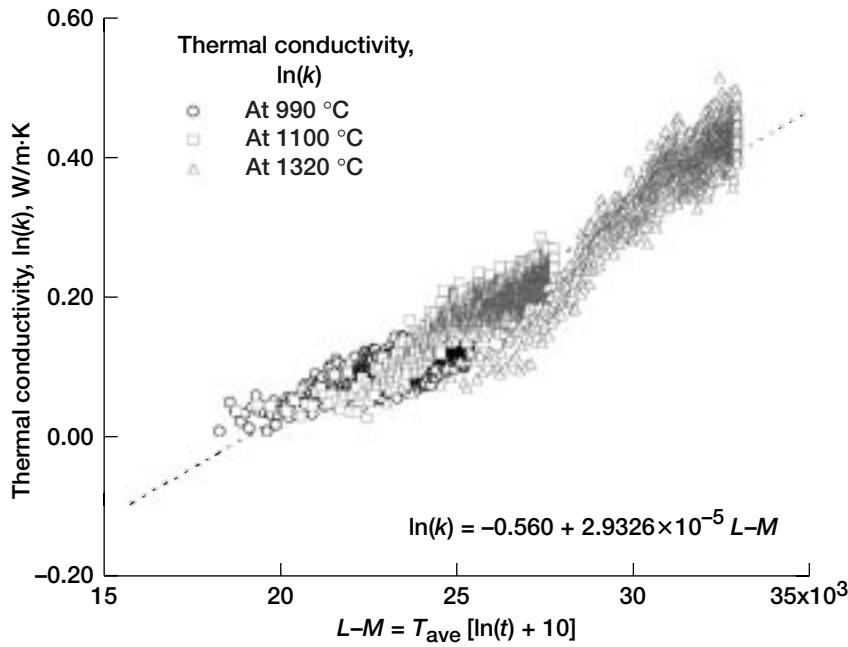


Laser high heat flux rig for determining the thermal conductivity change kinetics of thermal barrier coatings. During the test, the ceramic surface and the metal backside temperatures are measured by infrared pyrometers. The metal substrate midpoint temperature can be obtained by an embedded miniature type-K thermocouple. The interfacial temperatures and the actual heat flux passing through the thermal barrier coating system are, therefore, determined under the steady-state laser heating conditions by one-dimensional heat transfer models (ref. 1).



Overall thermal conductivity change kinetics of the  $ZrO_2$ - $Y_2O_3$  thermal barrier coating determined by real-time laser heat flux testing.

emissivity and reflectivity. From the test results shown in the graph to the left, a significant thermal conductivity increase was observed during the laser steady-state high heat flux testing. For the  $ZrO_2$ -8 wt % $Y_2O_3$  coating, the overall thermal conductivity increased from an initial value of 1.0 W/m-K to 1.15, 1.19, and 1.5 W/m-K after 30 hr of testing at surface temperatures of 990, 1100, and 1320 °C, respectively. The effects of heating time and temperature on the overall ceramic thermal conductivity are approximately described by the  $\ln(k)$  versus Larson-Miller relationship as shown in the following graph. The average slope of the Larson-Miller plot for the  $ZrO_2$ - $Y_2O_3$  coating was about  $2.93 \times 10^{-5}$  for the thermal barrier coating system. The increase in thermal conductivity in the thermal barrier coating systems was attributed to sintering-



Ceramic thermal conductivity  $\ln(k)$  as a function of Larson-Miller ( $L-M$ ) parameter ( $L-M = T_{ave} [\ln(t) + C]$ , where  $t$  is the heating time in seconds,  $T_{ave}$  is the average temperature in the ceramic coating in kelvin, and  $C$  is a fitting constant that equals 10 in this study). The effects of heating time and temperature on the overall ceramic thermal conductivity are approximately described by the conductivity to Larson-Miller relationship.

induced microporosity gradients under the laser-imposed high thermal gradient conditions (refs. 1 and 2). The test technique provides a viable way to obtain coating data for use in the design, development, stress modeling, and life prediction of various thermal barrier coating applications.

**References**

1. Zhu, D.; and Miller, R.A.: Thermal Conductivity and Elastic Modulus Evolution of Thermal Barrier Coatings Under High Heat Flux Conditions. NASA/TM-1999-209069, 1999. (Available online: <http://gltrs.grc.nasa.gov/cgi-bin/GLTRS/browse.pl?/1999/TM-1999-209069.html>)
2. Zhu, D.; and Miller, R.A.: Determination of Creep Behavior of Thermal Barrier Coatings Under Laser Imposed High Thermal and Stress Gradient Conditions. J. Materials Res., vol. 14, no. 1, 1999, pp. 146-141.

**Glenn contacts:**

Dr. Dongming Zhu, (216) 433-5422, Dongming.Zhu@grc.nasa.gov; and Dr. Robert A. Miller, (216) 433-3298, Robert.A.Miller@grc.nasa.gov

**Authors:** Dr. Dongming Zhu and Dr. Robert A. Miller

**Headquarters program office:** OAST

**Programs/Projects:** HITEMP, EPM

# Power and On-Board Propulsion Technology

## SAVANT—Solar Array Verification and Analysis Tool Demonstrated

The photovoltaics (PV) industry is now being held to strict specifications, such as end-of-life power requirements, that force them to overengineer their products to avoid contractual penalties. Such overengineering has been the only reliable way to meet such specifications. Unfortunately, it also results in a more costly process than is probably necessary. In our conversations with the PV industry, the issue of cost has been raised again and again. Consequently, the Photovoltaics and Space Environment Effects branch at the NASA Glenn Research Center at Lewis Field has been developing a software tool to address this problem. SAVANT, Glenn's tool for solar array verification and analysis is in the technology demonstration phase. Ongoing work has proven that more efficient and less costly PV designs should be possible by using SAVANT to predict the on-orbit life-cycle performance.

The ultimate goal of the SAVANT project is to provide a user-friendly computer tool to predict PV on-orbit life-cycle performance. This should greatly simplify the tasks of scaling and designing the PV power component of any given flight or mission. By being able to predict how a particular PV article will perform, designers will be able to balance mission power requirements (both beginning-of-life and end-of-life) with survivability concerns such as power degradation due to radiation and/or contamination. Recent comparisons with actual flight data from the Photovoltaic Array Space Power Plus Diagnostics (PASP Plus) mission validate this approach (see the graph).

Until now, there has been no reliable, simple way to design a PV article with respect to how life-cycle performance would be affected by factors such as radiation-induced performance degradation. The current state of the art consists of large amounts of information divided among several books. Even with this information at hand, it can take an expert from 3 weeks to 2 months to perform a partial analysis of PV life-cycle performance versus radiation degradation (as an example). SAVANT can perform the same analysis in less than 5 minutes. This technology demonstration tool vastly improves the current state of the art with respect to PV design and should allow industry to meet specifications without overengineering their products. This tool is being developed in-house in cooperation with the Ohio Aerospace Institute and the Naval Research Laboratories.

**Glenn contact:**

Ricaurte Chock, (216) 433-8057,  
ronin@grc.nasa.gov

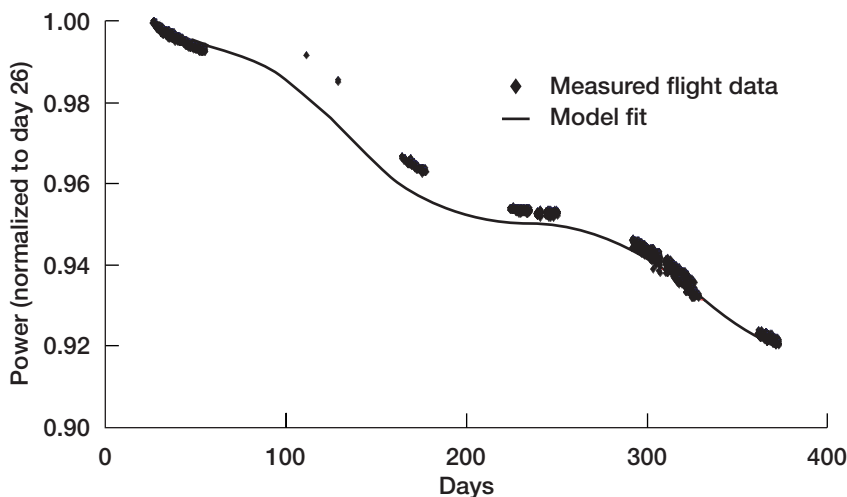
**Author:** Ricaurte Chock

**Headquarters program office:**

OSS (ATMS)

**Programs/Projects:** Photovoltaic

technology in space, CETDP



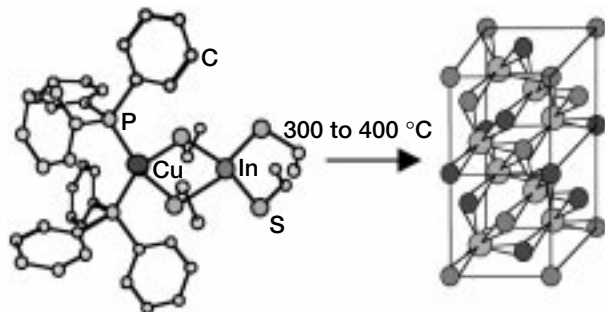
*Normalized power output versus day of mission for the PASP Plus GaAs (Gallium Arsenide) cell experiment.*

# Chemical Fabrication Used to Produce Thin-Film Materials for High Power-to-Weight-Ratio Space Photovoltaic Arrays

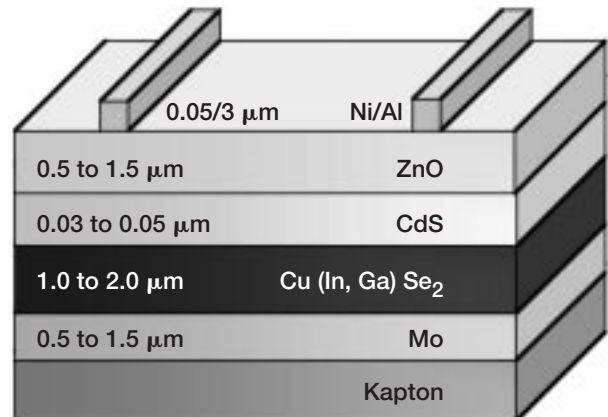
The key to achieving high specific power (watts per kilogram) space solar arrays is the development of a high-efficiency, thin-film solar cell that can be fabricated directly on a flexible, lightweight, space-qualified durable substrate such as Kapton (DuPont) or other polyimide or suitable polymer film. Cell efficiencies approaching 20 percent at AM0 (air mass zero) are required. Current thin-film cell fabrication approaches are limited by either (1) the ultimate efficiency that can be achieved with the device material and structure or (2) the requirement for high-temperature deposition processes that are incompatible with all presently known flexible polyimide or other polymer substrate materials. Cell fabrication processes must be developed that will produce high-efficiency cells at temperatures below 400 °C, and preferably below 300 °C to minimize the problems associated with the difference between the coefficients of thermal expansion of the substrate and thin-film solar cell and/or the decomposition of the substrate.

A chemically based approach at the NASA Glenn Research Center at Lewis Field is enabling the development of such a process: deposition of thin-film solar cell materials via a chemical spray process (using advanced single-source precursors) or electrochemical deposition directly onto molybdenum-coated Kapton or other suitable substrates (see the top figure). A single-source precursor containing all the required atoms (copper, indium, and sulfur, or copper, indium, gallium, and selenium, see the next figure) in chemical coordination will enable the use of low deposition temperatures that are compatible with the substrate of choice. Electrochemical deposition enables the precise stoichiometry control required to produce materials with fine-tuned bandgaps.

Work in collaboration with Professor William Buhro and Jennifer Hollingsworth at Washington University (St. Louis, Missouri) (ref. 1) has resulted in low-temperature chemical spray vapor deposition to produce  $\text{CuInS}_2$  thin films from an optimized single-source precursor. A combination of low-temperature electrochemical deposition and chemical bath deposition was



Decomposition of single-source precursor to produce  $\text{CuInS}_2$ .

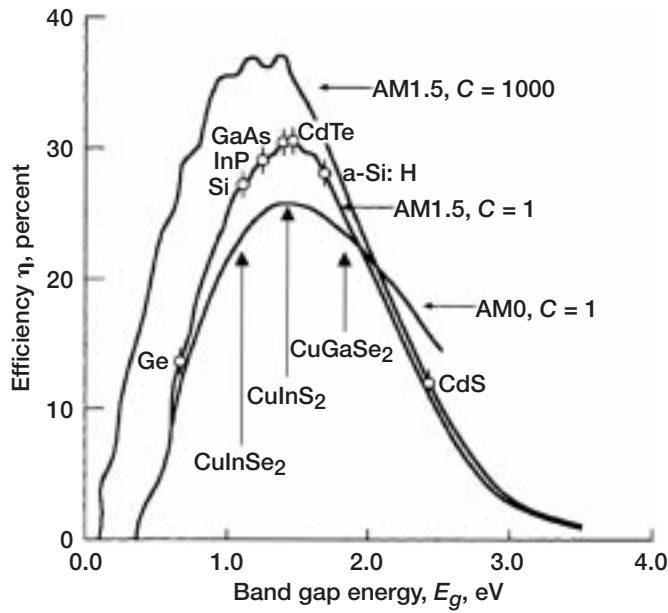


Thin-film solar cell deposited on Kapton substrate.

used to produce  $\text{ZnO/CdS/CuInSe}_2$  thin-film photovoltaic solar cells on lightweight flexible plastic substrates. This work was performed at Glenn with onsite research faculty Professor Ryne Raffaele (Rochester Institute of Technology) and NASA Glenn Research Associates Dr. Jerry Harris and Dr. David Hehemann (Kent State University) (ref. 2). One potential device configuration to achieve an efficiency at AM0 of 20 percent or better is based on a copper indium diselenide/copper indium disulfide/copper gallium diselenide ( $\text{CuInSe}_2/\text{CuInS}_2/\text{CuGaSe}_2$ ) three-junction multiple-bandgap structure. The bandgaps of these three materials are shown in the final figure in relation to the optimal efficiencies to be realized as a function of wavelength for the solar spectrum in space (AM0) and on the surface of Earth (AM1.5).

**Find out more about this research on the World Wide Web:**

<http://powerweb.grc.nasa.gov/pvsee/programs/>



Predicted efficiency versus bandgap for thin-film photovoltaic materials for solar spectra in space (AM0) and on the surface of the Earth (AM1.5) at 300 K.

## References

1. Hollingsworth, J.A.; Hepp, A.F.; and Buhro, W.E.: Spray CVD of Copper Indium Sulfide Films: Control of Microstructure and Crystallographic Orientation. *Chem. Vapor Deposition*, vol. 3, no. 3, 1999, pp. 105–108.
2. Raffaele, R.P., et al.: Electrodeposited Cds on CIS pn Junctions. *Solar Energy Materials and Solar Cells*, vol. 57, 1999, pp. 167–178.

## Glenn contact:

Dr. Aloysius F. Hepp, (216) 433–3835, Aloysius.F.Hepp@grc.nasa.gov

**Authors:** Dr. Aloysius F. Hepp, Dr. George C. Rybicki, Professor Ryne P. Raffaele, Dr. Jerry D. Harris, Dr. David G. Hehemann, Jennifer A. Hollingsworth, and Professor William E. Buhro

**Headquarters program office:** OSS

**Programs/Projects:** CETDP, SSP

## High-Efficiency Multibandgap Solar Cell Being Developed

Current high-efficiency solar cells are based on lattice-matched materials, specifically indium gallium phosphide (InGaP) on gallium arsenide (GaAs) on germanium (Ge). These materials were chosen more for their lattice constant (spacing between atoms) than their ability to efficiently convert the solar spectrum. Theoretical analysis indicates that the optimum efficiency for a multijunction solar cell would utilize very different bandgap cells. Unfortunately, no group of materials satisfies both the lattice-match and optimum bandgap requirements. The projected efficiency of the current state-of-the-art dual-junction InGaP/GaAs solar cell is ~29 percent (at air mass zero, AM0). If the optimum bandgaps could be utilized, the projected efficiency would increase to ~33 percent.

The use of lattice-mismatched materials has been avoided because the mismatch generates performance-robbing defects. Several novel buffer-layer concepts are being developed to mitigate these problems. Under a Small Business Innovation Research contract with the NASA Glenn Research Center at Lewis Field, Essential Research is developing an optimized dual-junction, lattice-mismatched solar cell based on indium aluminum gallium phosphide (InGaAlP) on indium gallium arsenide (InGaAs). These devices are lattice matched to each other, but lattice mismatched to either GaAs or Ge substrates. A novel InGaAs buffer layer has been demonstrated that effectively reduces the deleterious effects of lattice

mismatching. Current test devices have projected efficiencies of 26 percent at AM0. Three- and four-junction bandgap-optimized, lattice-mismatched solar cells are also being developed.

NASA Glenn and the Ohio State University are exploring the use of silicon substrates for III–V photovoltaic devices through a novel silicon germanium (SiGe) buffer layer developed by Professor Fitzgerald at Massachusetts Institute of Technology (MIT) and Amberwave. Researchers have long wanted to use silicon for such devices because of silicon's low cost, low mass, and high strength. Unfortunately, the large lattice mismatch (4 percent) and the difference in thermal expansion

coefficient between Si and GaAs have so far prevented the demonstration of high-efficiency III-V devices on Si. MIT and Ohio State have recently demonstrated world-record lifetimes (10 nsec) for AlGaAs/GaAs double heterostructures grown on the SiGe/Si substrates. In addition, they have measured dislocation densities in GaAs grown on these substrates of  $<10^{-6}$  cm<sup>-2</sup>. These results provide encouragement that transitioning these high-efficiency III-V cells to low-cost, lightweight Si substrates may soon be possible.

**Glenn contacts:**

David M. Wilt, (216) 433-6293, David.M.Wilt@grc.nasa.gov; and Dr. Dennis J. Flood, (216) 433-2303, Dennis.J.Flood@grc.nasa.gov

**Author:** David M. Wilt

**Headquarters program office:** OAST

**Programs/Projects:** Solar-powered NASA missions, commercial satellite power systems, SBIR

## Prototype Lithium-Ion Battery Developed for Mars 2001 Lander

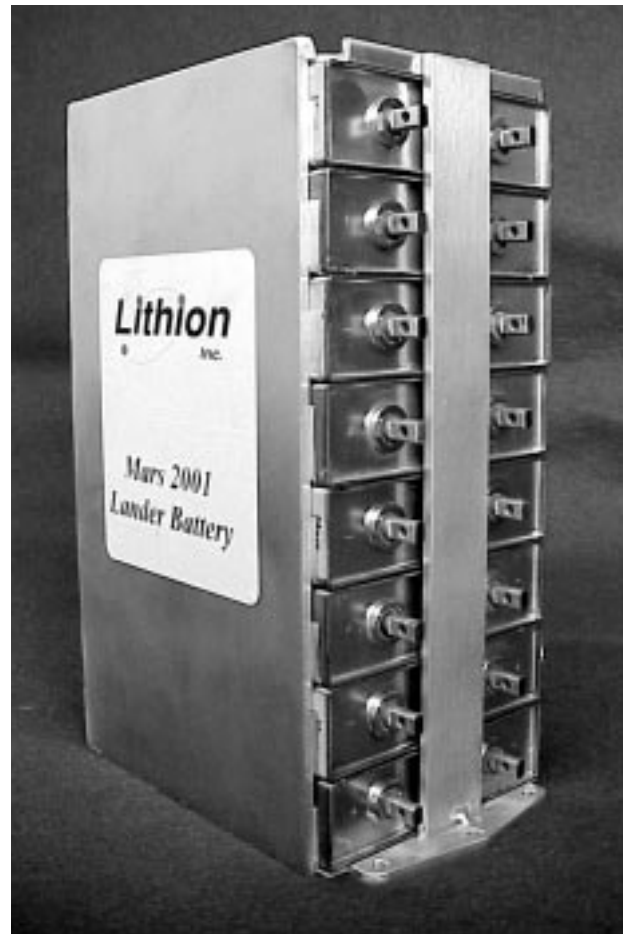
In fiscal year 1997, NASA, the Jet Propulsion Laboratory, and the U.S. Air Force established a joint program to competitively develop high-power, rechargeable lithium-ion battery technology for aerospace applications. The goal was to address Department of Defense and NASA requirements not met by commercial battery developments.

from low-capacity (7 to 20 A-hr) and low-voltage (14 to 28 V) systems for planetary landers and rovers to systems for aircraft that require up to 270 V and for

This advanced lithium-ion battery chemistry is of interest for the following reasons:

- (1) It has a high cell voltage—3.6-V closed-circuit voltage compared with 1.3 V for conventional alkaline chemistries. Consequently, the battery can achieve a desired system voltage with fewer cells and, hence, reduced system complexity and lower manufacturing and assembly costs.
- (2) It has a high theoretical specific energy density—750 W-hr/kg, approximately twice that of conventional alkaline cells. The improvements in specific energy (watt-hours per kilogram) and energy density (watt-hours per liter) realized by this battery system can enhance any mission that uses rechargeable batteries for energy storage and can enable missions that have critical weight and/or volume margins.
- (3) It incorporates environmentally safe materials and has safe battery operation. Because of the way the battery operates, there is no danger of lithium fires or of environmental hazards associated with the disposal of the used batteries.
- (4) It operates over a wide range of temperatures centered on the ambient temperature. This flexibility simplifies thermal system design and expands the envelope of operational parameters under which the battery can be used.

Under this program, contracts have been awarded to Yardney Technical Products, Eagle-Picher Technologies, LLC, BlueStar Advanced Technology Corporation, and SAFT America, Inc., to develop cylindrical and prismatic cell and battery systems for a variety of NASA and U.S. Air Force applications. The battery systems being developed range



Prototype 25 A-hr, 28-V lithium-ion battery selected for Mars 2001 Lander.

Unmanned Aerial Vehicles that require capacities up to 200 A-hr. Low-Earth-orbit and geosynchronous-orbit spacecraft pose additional challenges to system operation with long cycle life (>30,000 cycles) and long calendar life (>10 years), respectively.

Technical and program management advisory groups have been established to coordinate program and technical management activities and to verify and validate test results from the individual contractors. The NASA Glenn Research Center at Lewis Field has members on both committees and has supported the contracts with NASA's Office of Space Science, Cross-Enterprise Technology Development Program Funding. Additional funding support for the program has come from NASA's Office of Space Science, Mars 2001 Program Office; U.S. Air Force offices; and other Department of Defense agencies.

The initial work on lithium-ion battery development focused on the development of a battery to power the lander for the Mars 2001 mission. The challenge has been to develop a battery with high specific energy and energy density that could operate at the temperature extremes expected for the Mars mission (-20 to 40 °C). Under this program, Yardney and BlueStar successfully developed batteries that could meet the mission

requirements for the Mars 2001 Lander. On the basis of a performance evaluation of the cells delivered to date, Yardney Technical Products was selected as the vendor for the Mars 2001 mission. The prototype 25 A-hr, 28-V battery developed by Yardney Technical Products has a specific energy of 123 W-hr/kg at 20 °C and of 85 W-hr/kg at the low end of the temperature range, -20 °C.

**Glenn contact:**

Michelle A. Manzo, (216) 433-5261, fax (216) 433-6160, Michelle.A.Manzo@grc.nasa.gov

**Author:** Michelle A. Manzo

**Headquarters program office:** OSS

**Programs/Projects:**

Mars 2001 Lander, CETDP, UAV

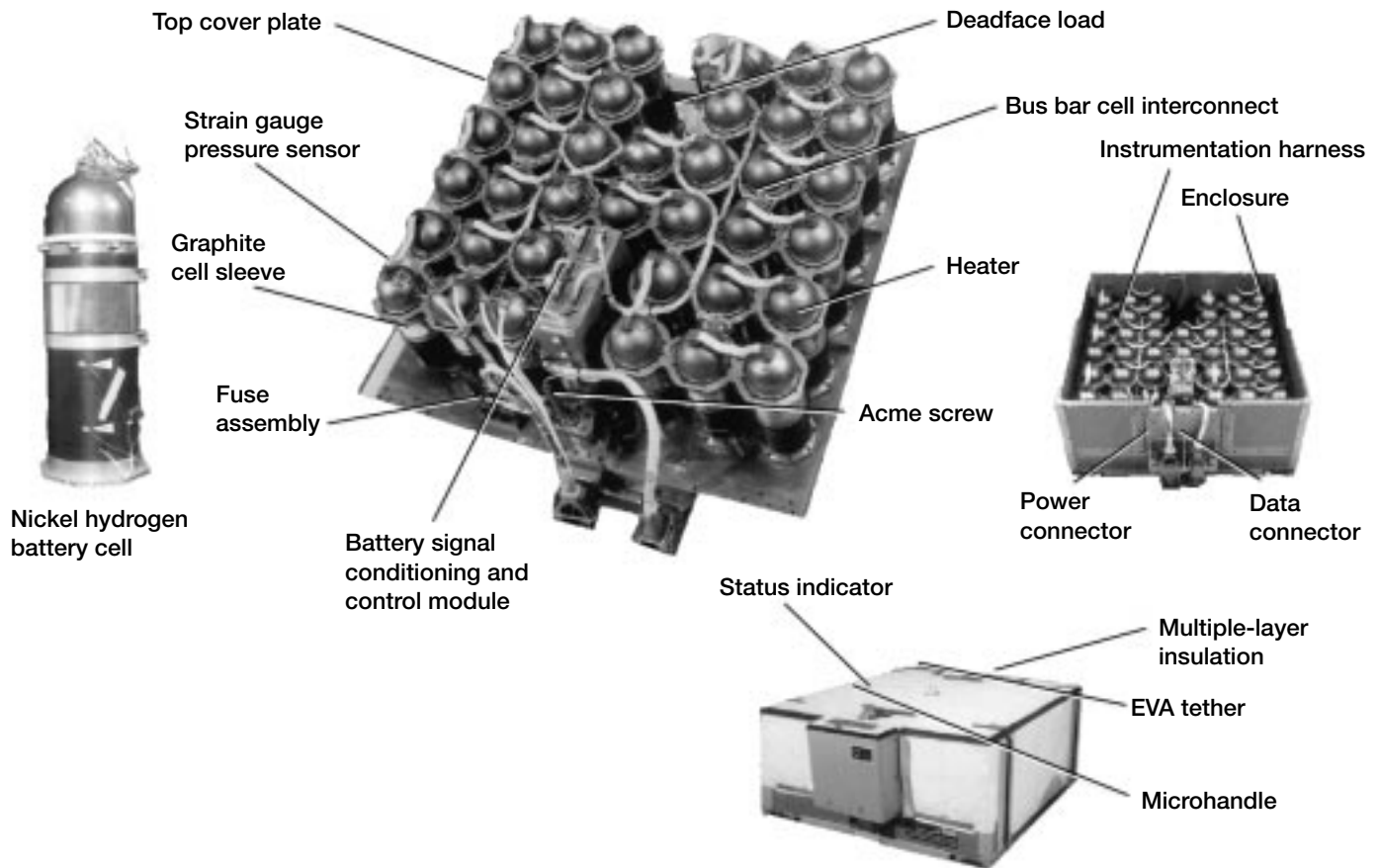
## Nickel-Hydrogen Battery Cell Life Test Program Update for the International Space Station

NASA and Boeing North America are responsible for constructing the electrical power system for the International Space Station (ISS), which circles the Earth every 90 minutes in a low Earth orbit (LEO). For approximately 55 minutes of this orbit, the ISS is in sunlight, and for the remaining 35 minutes, the ISS is in the Earth's shadow (eclipse). The electrical power system must not only provide power during the sunlight portion by means of the solar arrays, but also store energy for use during the eclipse. Nickel-hydrogen (Ni/H<sub>2</sub>) battery cells were selected as the energy storage systems for ISS. Each battery Orbital Replacement Unit (ORU) comprises 38 individual series-connected Ni/H<sub>2</sub> battery cells, and there are 48 battery ORU's on the ISS. On the basis of a limited Ni/H<sub>2</sub> LEO data base on life and performance characteristics, the NASA Glenn Research Center at Lewis Field commenced testing through two test programs: one in-house and one at the Naval Surface Warfare Center in Crane, Indiana.

Under the in-house test program, Glenn constructed a Ni/H<sub>2</sub> battery cell test facility with an automated data acquisition system to assess the performance of cells from different vendors. The resulting 39-cell test matrix consisted of 13 different battery cell configurations. The cells were placed on a LEO endurance life test at a 35-percent depth-of-discharge (DOD) stress condition at either -5 or 10 °C. As of September 1999, 29 cells had completed over 5 years of life testing (29,200 charge and discharge cycles). Currently, there are 16 cells in active operation. The number of life cycles tested ranged from 50,100 (8.5 years) to 59,800 (10.25 years) in LEO.

To verify the ISS operational life requirement of 6.5-year life at 35-percent DOD, researchers are testing a statistically significant number of Ni/H<sub>2</sub> battery cells at the Naval Surface Warfare Center. The test matrix contains cells from three different manufacturers. All battery cell endurance life testing is being performed in either 10-, 8-, or 5-cell series-connected test packs at 35- or 60-percent DOD and operating temperatures of -5 or 10 °C.

All 100 Ni/H<sub>2</sub> cells from Yardney Technical Products have failed. Battery pack failures tested at the 35-percent DOD condition ranged from 37,000 to 48,300 cycles (6.3 to 8.3 years). Failures of packs tested at the higher 60-percent DOD stress condition ranged from 420 to 4750 cycles (1 to 10 months). The 112 Ni/H<sub>2</sub> cells from



*International Space Station battery Orbital Replacement Unit.*

Gates Aerospace Batteries were also tested at the Naval Surface Warfare Center facility to benchmark their performance. Thirty of the Gates cells were used to assess the impact of potassium hydroxide electrolyte concentration with various charge management schemes. Packs tested at the 60-percent DOD condition exhibited failures ranging from 7500 to 36,900 cycles (1.3 to 6.3 years). Because of funding limitations, the packs operating at 35-percent DOD were terminated. At that time, the various packs had accumulated from 24,600 to 42,000 cycles (4.2 to 7.2 years). The 120 Eagle-Picher Industries, Inc., Ni/H<sub>2</sub> cells have only shown failures at the 60-percent DOD operating point. Pack failures ranged from 6200 to 40,200 cycles (1.1 to 6.9 years). Packs operating at 35-percent DOD, which continue to cycle, now range from 42,200 to 46,400 cycles (7.2 to 7.9 years). Forty-eight of the Eagle-Picher cells are undergoing a special charge control study. Some of the cells are being charged using the ISS baseline charge profile, which incorporates a constant current charge followed by a taper charge to 100-percent state of charge. The other cells are being charged at a constant current terminating at either a 90 or 94-percent state of charge.

Through a competitive down-selection process, Eagle-Picher is the sole supplier of Ni/H<sub>2</sub> battery cells for the ISS. The results to date provide the necessary confidence in achieving a 38,000 cycle (6.5 years) LEO

life for Ni/H<sub>2</sub> battery cells at the 35-percent DOD operating condition, which is the design point for the International Space Station. In general, prolonged cycle life is achieved by selecting a properly designed battery cell configuration, incorporating the reduced 26-percent potassium hydroxide electrolyte concentration, and by using the ISS baseline charge control methodology of taper charging.

**Glenn contact:**

Thomas B. Miller, (216) 433-6300,  
Thomas.B.Miller@grc.nasa.gov

**Author:** Thomas B. Miller

**Headquarters program office:** OSF

**Programs/Projects:** ISS

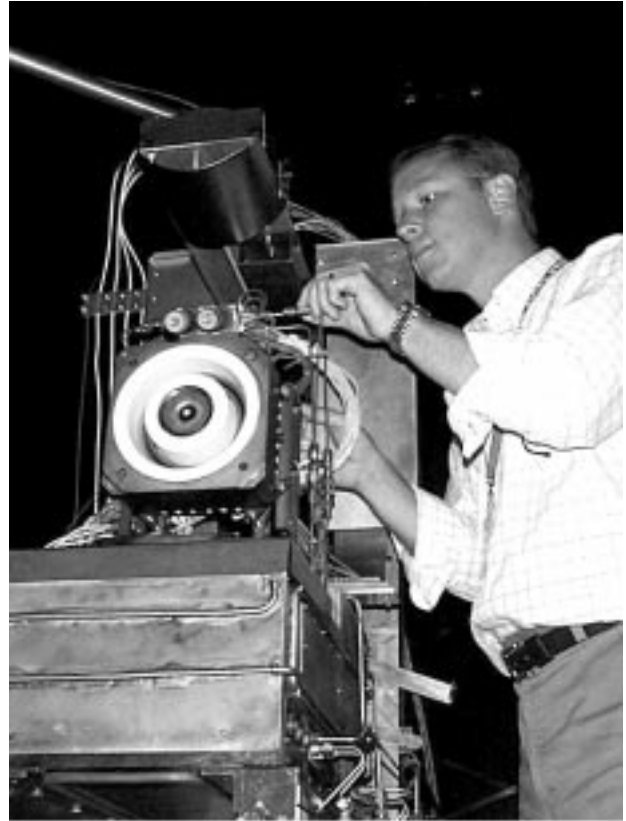
## 4.5-kW Hall Effect Thruster Evaluated

As part of an Interagency Agreement with the Air Force Research Lab (AFRL), a space simulation test of a Russian SPT-140 Hall Effect Thruster was completed in September 1999 at Vacuum Facility 6 at the NASA Glenn Research Center at Lewis Field. The thruster, shown in the photo, was subjected to a three-part test sequence that included thrust and performance characterization, electromagnetic interference, and plume contamination. SPT-140 is a 4.5-kW thruster developed under a joint agreement between AFRL, Atlantic Research Corp, and Space Systems/Loral, and was manufactured by the Fakal Experimental Design Bureau of Russia. All objectives were satisfied, and the thruster performed exceptionally well during the 120-hr test program, which comprised 33 engine firings.

The Glenn testing provided a critical contribution to the thruster development effort, and the large volume and high pumping speed of this vacuum facility was key to the test's success. The low background pressure ( $1 \times 10^{-6}$  torr) provided a more accurate representation of space vacuum than is possible in most vacuum chambers. The facility had been upgraded recently with new cryogenic pumps and sputter shielding to support the active electric propulsion program at Glenn. The Glenn test team was responsible for all test support equipment, including the thrust stand, power supplies, data acquisition, electromagnetic interference measurement equipment, and the contamination measurement system.

The test program provided a comprehensive evaluation of thruster operation in preparation for future flight opportunities. The performance test measured thrust over a wide variety of operating conditions and background pressures to develop an extensive thruster performance map. The electromagnetic interference test characterized interference caused by thruster operation over a wide range of communication antenna frequencies. The contamination test evaluated plume effects on representative satellite surface samples, such as solar cell cover glasses and optical solar reflectors, during 100 hours of continuous thruster operation.

Early review of the test data indicates very positive results for all test phases. The breadth and success of this test effort will provide a convincing argument for future flight considerations for this thruster technology. Potential applications include orbit station keeping, repositioning, low-Earth-orbit to geosynchronous-Earth-orbit transfer, and deep space maneuvers.



*Installation of the SPT-140 on the thrust measurement stand.*

**Glenn contacts:**

Lee S. Mason, (216) 977-7106,  
Lee.S.Mason@grc.nasa.gov; and  
Robert S. Jankovsky, (216) 977-7515,  
Robert.S.Jankovsky@grc.nasa.gov

**Author:** Lee S. Mason

**Headquarters program office:** OAST

**Programs/Projects:** CETDP, STR

## Advanced Monopropellant Thruster Technology Tested

A new family of environmentally friendly, low-freezing-point, high-density monopropellants is being developed under a NASA Glenn technology program. New monopropellant technology would greatly benefit a range of small (<100 kg) satellites and spacecraft missions. These monopropellants are mixtures of hydroxylammonium nitrate (HAN), fuel, and water. Primex Aerospace Company, under contract to the NASA Glenn Research Center at Lewis Field, tested a 1-lbf thruster using a HAN-based monopropellant formulation. Over 8000 sec of total test time was accumulated on a single thruster using the blowdown duty cycle typical of state-of-the-art monopropellant systems.

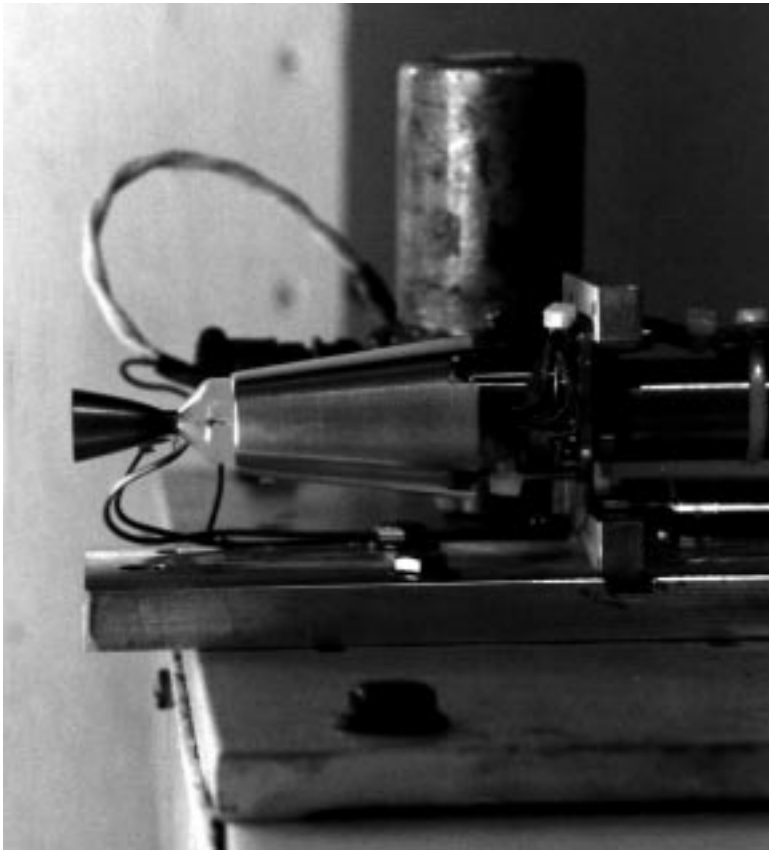
HAN-based monopropellants contain HAN as the oxidizer component (typically 60 wt %), a fuel component, and water. These monopropellants represent a range of formulations, with a corresponding range of characteristics and performance levels. Because they do not pose a shock or vapor hazard, their handling procedures are much simpler than those for hydrazine ( $N_2H_4$ ). HAN-based formulations generally have lower freezing points than  $N_2H_4$ , some as low as  $-35\text{ }^\circ\text{C}$ , greatly reducing the thermal management requirements for power-limited spacecraft. Although the specific impulse performance of the first-generation formulations is lower than that of hydrazine (190 versus 220 sec), these formulations are also 40-percent

denser. This results in a density-specific impulse at least 20 percent better than  $N_2H_4$ , offering greater packing efficiency for volume-constrained spacecraft.

A NASA-sponsored technology program at Primex Aerospace Company addressed the propellant development and thruster development of HAN-based monopropellants. This technology work involved laboratory-thruster testing of a range of amines, acids, and alcohols as fuel components in the HAN formulation; material compatibility testing with common aerospace materials; thermal stabilization; a strand-burning investigation; reactor development, including the screening of catalysts, injectors, and bed configurations; and life testing of a 4.5-N thruster.

Testing was conducted with a formulation (60 wt % HAN, 26 wt % glycine, and 14 wt % water) compatible with off-the-shelf catalysts. The catalyst bed was preheated to  $315\text{ }^\circ\text{C}$ . Two series of steady-state tests were conducted, accumulating a total of 8000 sec of hot-fire life with 21 cold starts over a full range of feed pressures (2965 to 930 kPa). At the end of 8000 sec, the pressure had degraded approximately 7.5 percent from the original chamber pressure. Pulse mode testing was also conducted, with on times ranging from 0.100 to 300 sec, for duty cycles ranging from 0.5 to 100 percent.

The next-generation formulations will provide higher specific impulse values ( $> 240\text{ sec}$ ), which will reduce propellant system mass fractions by up to 25 percent, while still maintaining the nontoxic and thermal benefits. Candidate



*1-lbf HAN-glycine monopropellant thruster firing.*

formulations have already been tested in a laboratory reactor and will be further developed in 2000. Since HAN-based formulations generally have higher molecular weights than  $N_2H_4$ , higher combustion temperatures are required to achieve  $N_2H_4$ -like performance. This will require the development of high-temperature catalyst materials or noncatalytic decomposition methods.

**Glenn contact:** Brian D. Reed, (216) 977-7489, Brian.D.Reed@grc.nasa.gov

**Author:** Brian D. Reed

**Headquarters program office:** OSS

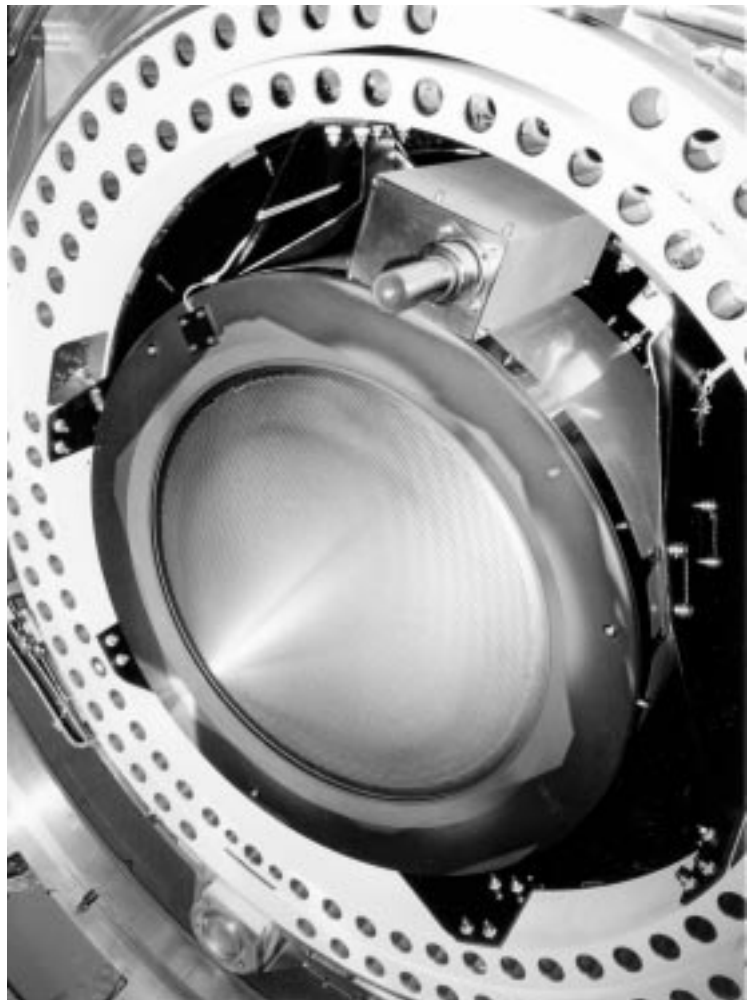
**Programs/Projects:**  
On-Board Propulsion

## Ion Thruster Used to Propel the Deep Space 1 Spacecraft to Comet Encounters

The NASA Solar Electric Propulsion Technology Applications Readiness (NSTAR) Project provided a xenon ion propulsion system to the Deep Space 1 (DS1) spacecraft to validate the propulsion system as well as perform primary propulsion for asteroid and comet encounters. The On-Board Propulsion Branch of the NASA Glenn Research Center at Lewis Field developed engineering model versions of the 30-cm-diameter ion thruster and the 2.5-kW power processor unit (PPU). Glenn then transferred the thruster and PPU technologies to Hughes Electron Dynamics and managed the contract, which supplied two flight sets of thrusters and PPU's to the Deep Space 1 spacecraft and to a ground-based life verification test at the Jet Propulsion Laboratory (JPL). In addition to managing the DS1 spacecraft development, JPL was responsible for the NSTAR Project management, thruster life tests, the feed system, diagnostics, and propulsion subsystem integration. The ion propulsion development team included NASA Glenn, JPL, Hughes Electronics, Moog Inc., and Spectrum Astro Inc.

The overall NSTAR subsystem dry mass, including thruster, PPU, controller, cables, and the xenon storage and feed system, is 48 kg. The mass of the xenon stored onboard DS1 was about 81 kg, and the spacecraft wet mass was approximately 500 kg.

The DS1 spacecraft was launched on October 24, 1998, and on July 29, 1999, it flew within 16 miles of the small asteroid Braille (formerly 1992KD) at a relative speed of 35,000 mph. As of November 1999, the ion propulsion system had performed flawlessly for nearly 149 days of thrusting. NASA has approved an extension to the mission, which will allow DS1 to continue thrusting to encounters with two comets in 2001. The DS1 optical and plasma diagnostic instruments will be used to investigate the comet and space environments. The spacecraft is scheduled to fly past the dor-



*Flight ion thruster mounted to the Deep Space 1 spacecraft gimbal assembly.*

mant comet Wilson-Harrington in January 2001 and the very active comet Borrelly in September 2001, at which time approximately 500 days of ion engine thrusting will have been completed.

**Bibliography**

Sovey, J.: An Ion Propulsion System for NASA's Deep Space Missions. AIAA Paper 99-4612, 1999.

Rawlin, V.K., et al.: NSTAR Flight Thruster Qualification Testing. AIAA Paper 98-3936, July 1998.

**Glenn contacts:** James S. Sovey, (216) 977-7454, James.S.Sovey@grc.nasa.gov; and Vincent K. Rawlin, (216) 977-7462, Vincent.K.Rawlin@grc.nasa.gov

**Author:** James S. Sovey

**Headquarters program offices:** OSS, OAST

**Programs/Projects:** New Millennium, NSTAR, Deep Space 1, AST

## High-Temperature Superconductive Cabling Investigated for Space Solar Power Satellites

NASA has been directed by Congress to take a fresh look at the Space Solar Power (SSP) concept that was studied by the Department of Energy and NASA about 20 years ago. To summarize, the concept involves (1) collecting solar energy and converting it to electrical energy via photovoltaic arrays on satellites in Earth orbit, (2) conducting the electricity to the microwave transmitting portion of the satellite, and (3) transmitting the power via microwave transmitters (or possibly via lasers) to ground power station antennas located on the surface of the Earth. One Sun Tower SSP satellite concept is illustrated here. This figure shows many photovoltaic arrays attached to a "backbone" that conducts electricity down to a wireless transmitter, which is pointed toward the Earth. Other variations on this concept use multiple backbones to reduce the overall length of the satellite structure. In addition, non-Sun-Tower concepts are being considered.

The objective of the work reported here was to determine the benefits to the SSP concept of using high-temperature superconductors (HTS) to conduct the electricity from the photovoltaic arrays to the wireless power

transmitters. Possible benefits are, for example, reduced mass, improved efficiency, and improved reliability. Dr. James Powell of Plus Ultra Technologies, Inc., of Stony Brook, New York, is conducting the study, and it is being managed by the NASA Glenn Research Center at Lewis Field via a task-order contract through Scientific Applications International Corp. (SAIC).

Specific tasks included in the contract were to

- (1) Review the state of the art of HTS wire and cables, particularly the work that is being done by the Department of Energy and its contractors
- (2) Compare differences in SSP satellite mass, size, reliability, and efficiency when superconducting and nonsuperconducting cables are used between the solar arrays and wireless power transmitters
- (3) Consider the benefits of using superconductors to reduce the losses involved in distributing the power over the microwave transmitter surface to the individual transmitters
- (4) Consider possible applications of HTS for the ground power station



*Space solar power Sun Tower conceptual design.*

(5) Address practicality issues of deployment, maintenance, and vulnerability to space debris and to spacecraft charging due to space plasma.

Thus far, it appears practical to have a massively parallel Sun Tower architecture in which low-voltage (~80 V) direct-current transmission lines run directly from each solar panel to the radiofrequency transmitter without requiring power converters. This architecture would use conventional aluminum conductors for local solar panel power collection and distribution, a high-temperature superconducting (HTS) subtransmission line from the solar panel to the Sun Tower "backbone," and a low-temperature superconductor (LTS) transmission line along the Sun Tower backbone. The 77-K superconductors based on thin yttrium barium copper oxide (YBCO) films have yet not been produced in the length and current capability required. The 35-K superconductors based on bismuth strontium calcium copper oxide (BSCCO) wires appear to be suitable for the Sun Tower. Multifilament, multikilometer Nb<sub>3</sub>Sn conductor wires with 10<sup>6</sup> A/cm<sup>2</sup> capability at 6 K are commercially available. In addition, a new concept, termed magnetically inflated cable, has been developed for a lightweight, highly rigid, automatically deployable backbone structure for the Sun Tower.

Items still to be completed under the current contract are complete reports on (1) the status of HTS and LTS technologies and their applicability to

SSP, (2) evaluation of Sun Tower transmission and distribution options including preparation of weight budgets for the various transmission and distribution options, and (3) evaluation of the magnetically inflated cable concept, including weight and refrigeration budgets for systems based on this concept.

**Glenn contacts:**

Roy C. Tew, (216) 433-8471, Roy.C.Tew@grc.nasa.gov; and Albert J. Juhasz, (216) 433-6134, Albert.J.Juhasz@grc.nasa.gov

**Authors:**

Roy C. Tew and Albert J. Juhasz

**Headquarters program office:**

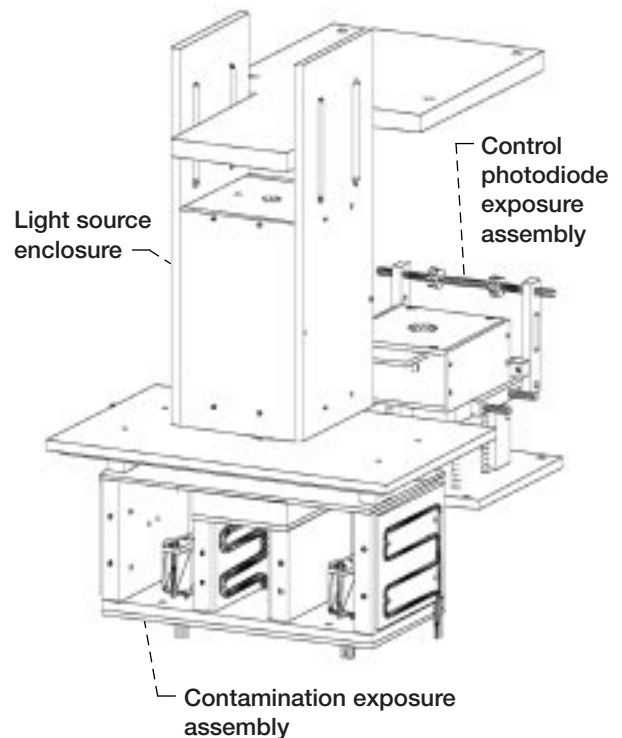
OSS (ATMS)

**Programs/Projects:** SERT, CETDP

## Facility Designed and Built to Investigate the Combined Effects of Contaminant and Atomic Oxygen on a Light-Transmitting Surface

A need exists to investigate changes in the transparency of a light-transmitting surface during simultaneous exposure to a contaminant and an atomic oxygen (AO) flux. This mechanism may be responsible for the degradation of the light-transmitting surfaces of both photovoltaic cells and photodiodes currently in use on many low-Earth-orbit spacecraft. To address this need, researchers from the Electro-Physics Branch of the NASA Glenn Research Center at Lewis Field built such a test system within their AO beam facility. This facility produces an effective AO flux of  $1.4 \times 10^{16}$  atoms/cm<sup>2</sup>/sec and contains a three-axis positioning system that provides the motion capability necessary for test operations.

During testing, a target surface is held directly within the AO beam and close to two contaminant effusion cells. The effusion cells are shielded from the AO beam, and the outgassing contaminant is constrained to move across the target surface when heat is applied to either of the reservoirs. A light source is periodically moved over the target surface, and the transmitted light intensity is checked with a photodiode located below the target. This light source is also periodically checked with a separate photodiode, which is protected from contamination and AO exposure, to allow adjustments necessary to maintain a consistent light intensity.



*Contamination test fixture hardware.*

The test fixture hardware was designed to allow a wide variation of test parameters while providing necessary protection for vital system components. The temperatures of four separate regions are controlled by balancing the heating and cooling elements. These regions are each of the contaminant reservoirs, the target surface, and the enclosure surrounding (but not in contact with) the target surface.

A software program was designed to provide automated turnkey control and data acquisition capability for the entire duration of an exposure test. This program controls two electrometers for photodiode measurements (light intensity control and contaminant buildup assessment), the three-axis positioning system, closed-loop proportional integral differential (PID) temperature controllers for regulating the four separate regions, and a solenoid valve to provide water cooling.

The program performs an automated exposure test after being initialized with the PID controller parameters, PID temperature set points, temperature versus time plot parameters, light source intensity level, test cycle time, and number of cycles. In addition, it monitors many system conditions for quality and safety, and aborts the test if any condition exceeds user-supplied values.

**Glenn contacts:**

Bruce A. Banks, (216) 433-2308, Bruce.A.Banks@grc.nasa.gov; and Sharon K. Rutledge (216) 433-2219, Sharon.K.Rutledge@grc.nasa.gov

**Dynacs Engineering Company, Inc., contacts:**

Edward A. Sechkar (216) 433-2299, Edward.A.Sechkar@grc.nasa.gov; and Thomas J. Stueber (216) 433-2218, Thomas.J.Stueber@grc.nasa.gov

**Authors:**

Edward A. Sechkar, Thomas J. Stueber, Sharon K. Rutledge, and Bruce A. Banks

**Headquarters program office:**

OSS (ATMS)

**Programs/Projects:** LEO environment simulation and optical surfaces durability for ISS and other LEO spacecraft

## Large-Area Atomic Oxygen Facility Used to Clean Fire-Damaged Artwork

In addition to completely destroying artwork, fires in museums and public buildings can soil a displayed artwork with so much accumulated soot that it can no longer be used for study or be enjoyed by the public. In situations where the surface has not undergone extensive charring or melting, restoration can be attempted. However, soot deposits can be very difficult to remove from some types of painted surfaces, particularly when the paint is fragile or flaking or when the top surface of the paint binder has been damaged. Restoration typically involves the use of organic solvents to clean the surface, but these solvents may cause the paint layers to swell or leach out. Also, immersion of the surface or swabbing during solvent cleaning may move or remove pigment through mechanical contact, especially if the fire damage extends into the paint binder.

A noncontact technique of removing organic deposits from surfaces was developed out of NASA research on the effects of oxygen atoms on various materials. Atomic oxygen is present in the atmosphere surrounding the Earth at the altitudes where satellites typically orbit. It can react chemically with surface coatings or deposits that contain carbon. In the reaction, the carbon is converted to carbon monoxide and some carbon dioxide. Water vapor is also a byproduct of the reaction if the surface contains carbon-hydrogen bonds. To study this reaction, NASA developed Earth-based facilities to produce atomic oxygen for material exposure and testing.

A vacuum facility designed and built by the Electro-Physics Branch of the NASA Glenn Research Center at Lewis Field to provide atomic oxygen over a large area for studying reactions in low Earth orbit has been used to successfully clean several full-size paintings. (This facility can accommodate paintings up to 1.5 by 2.1 m. The atomic oxygen plasma is produced between two large parallel aluminum plates using a radiofrequency power source operating at roughly 400 W. Atomic oxygen is generated uniformly over this area at an operating pressure of 1 to 5 mtorr.

The left photo shows a painting that was damaged in an arson fire. The right photo shows the same painting after it was cleaned with



*Left: Fire-damaged painting. Right: Restored painting.*

atomic oxygen. Because cleaning with atomic oxygen is a dry process, there is less risk of the paint surface leaching out or swelling. In addition, because the atomic oxygen reaction is confined to the surface, risk to the underlying paint or canvas is minimized. With careful use, including pre-treatment of an edge or corner to ensure the safeness of the paint for atomic oxygen cleaning, it can be used as an additional conservation tool. The technique appears to have great potential for removing heavy soot and char from the surface of fire-damaged art and may allow previously unrestorable works of art to be restored.

**For more information, visit the Electro-Physics Branch on the World Wide Web:**  
<http://www.grc.nasa.gov/WWW/epbranch/ephome.htm>

**Glenn contacts:**

Bruce A. Banks, (216) 433-2308,  
[Bruce.A.Banks@grc.nasa.gov](mailto:Bruce.A.Banks@grc.nasa.gov); and  
Sharon K. Rutledge, (216) 433-2219,  
[Sharon.K.Rutledge@grc.nasa.gov](mailto:Sharon.K.Rutledge@grc.nasa.gov)

**Dynacs Engineering Company, Inc., contacts:**

Edward A. Sechkar, (216) 433-2299,  
[Edward.A.Sechkar@grc.nasa.gov](mailto:Edward.A.Sechkar@grc.nasa.gov); and  
Thomas J. Stueber, (216) 433-2218,  
[Thomas.J.Stueber@grc.nasa.gov](mailto:Thomas.J.Stueber@grc.nasa.gov)

**Authors:** Sharon K. Rutledge, Bruce A. Banks, Thomas J. Stueber, and Edward A. Sechkar

**Headquarters program office:**  
OSS (ATMS)

**Programs/Projects:**  
Art restoration, art conservation

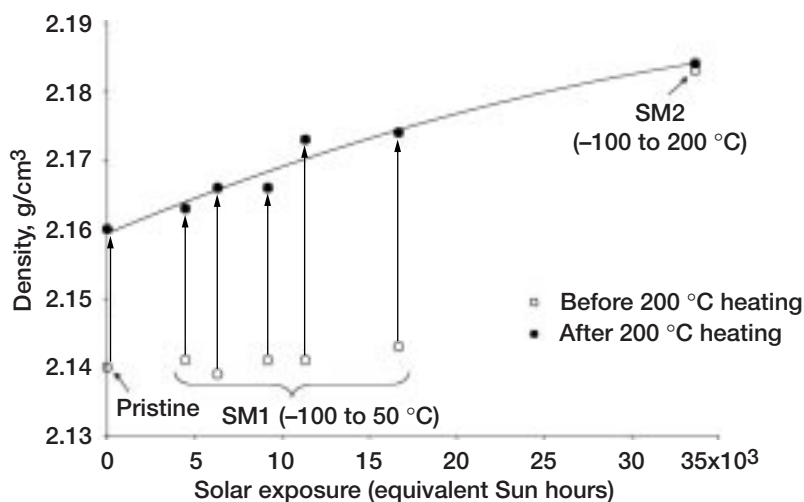
# Insights Developed Into the Damage Mechanism of Teflon FEP Thermal Control Material on the Hubble Space Telescope

Metalized Teflon FEP (DuPont; fluorinated ethylene propylene) thermal control material on the Hubble Space Telescope (HST) has been found to degrade in the space environment. Teflon FEP thermal control blankets retrieved during the first servicing mission were found to be embrittled on solar-facing surfaces and to contain microscopic cracks (the FEP surface is exposed to the space environment). During the second servicing mission, astronauts noticed that the FEP outer layer of the multilayer insulation blanketing covering the telescope was cracked in many locations. Large cracks were observed on the light shield, forward shell, and equipment bays. A tightly curled piece of cracked FEP from the light shield was retrieved during the second mission. This piece was severely embrittled, as witnessed by ground testing. A Failure Review Board was organized by NASA Goddard Space Flight Center to determine the mechanism causing the multilayer insulation degradation. This board included members of the Electro-Physics Branch of the NASA Glenn Research Center at Lewis Field.

Density measurements of the retrieved materials obtained under the review board's investigations indicated that FEP from the first servicing mission was essentially unchanged from pristine FEP but that the second servicing mission FEP had increased in density in comparison to pristine FEP (ref. 1). The results were consistent with crystallinity measurements taken using x-ray diffraction and with results from solid-state nuclear magnetic resonance tests (see the table and ref. 1). Because the second servicing mission FEP was embrittled and its density and crystallinity had increased in comparison to pristine FEP, board researchers expected that the first servicing mission FEP, which was also embrittled, would also have increased in crystallinity and density, but it did not. Because the retrieved second servicing mission material curled while in space, it experienced a

higher temperature extreme during thermal cycling (estimated at 200 °C) than the first servicing mission material (estimated at 50 °C). Therefore, Glenn initiated and conducted an investigation of the effects of heating pristine FEP and FEP that had been exposed on the Hubble Space Telescope. Samples of pristine and first and second servicing mission FEP were heated to 200 °C and evaluated for changes in density and morphology. We hoped that the results would help explain why FEP degrades in the Hubble Space Telescope space environment.

Elevated-temperature exposure was found to have a major impact on the density of the retrieved materials. The graph shows the density of pristine FEP and Hubble Space Telescope FEP (retrieved during both servicing missions) prior to and after ground laboratory heating to 200 °C for 7 to 9 days. The density of the pristine and first servicing mission FEP increased with heating at 200 °C, with an increase in density that corresponded to an increase in solar exposure. Nuclear magnetic resonance characterization of polymer morphology was consistent with the density results. Both techniques showed that the as-received first servicing mission FEP is structurally similar to pristine FEP and that the second servicing mission FEP is more tightly packed or crystalline. Heating at 200 °C changed the morphology of pristine FEP and first servicing mission FEP, with the first servicing mission FEP undergoing a greater change than pristine FEP. Heating at 200 °C produced no further change in second servicing mission FEP.



Density of pristine FEP and FEP retrieved from the Hubble Space Telescope during the first (SM1) and second (SM2) servicing missions, prior to and after ground laboratory heating at 200 °C for 7 to 9 days.

SUMMARY OF FAILURE REVIEW BOARD FINDINGS

[See ref. 1.]

Property	Pristine FEP	First servicing mission FEP, 11,339 ESH <sup>a</sup>	Second servicing mission FEP, 33,638 ESH <sup>a</sup>
	Very ductile	Brittle microscopic cracks	Brittle macroscopic cracks
Tensile property, percent elongation to failure	363	156	≈0
Density, g/cm <sup>3</sup>	2.140	2.138	2.184
X-ray diffraction crystallinity, percent	28.5	29.5	46.5
Nuclear magnetic resonance, T <sub>1ρ</sub> (C) <sup>b</sup>	35	33	41
Nuclear magnetic resonance, T <sub>CF</sub> peak, <sup>c</sup> msec	2	2	≈1

<sup>a</sup>ESH, equivalent Sun hours.

<sup>b</sup>T<sub>1ρ</sub>(C), <sup>13</sup>C relaxation in the rotating frame.

<sup>c</sup>T<sub>CF</sub> peak, cross-polarization time for intensity maximum.

These results, along with analyses of x-ray exposed and thermal-cycled FEP, provided insight into the damage mechanism of Teflon FEP in space. The results indicate that irradiation of Teflon FEP in space causes chain scission, resulting in FEP embrittlement. Heating at the nominal temperatures experienced on the Hubble Space Telescope did not change the density or crystallinity of FEP. But heating at the levels experienced by the retrieved curled second servicing mission sample allowed increased mobility of the space-environment-induced scissioned short chains, with resulting increased crystallinity and density. The percent crystallinity of second servicing mission FEP was found to be 27-percent higher than that of pristine FEP. Heating of pristine FEP at 200 °C also increased the crystallinity and density, but the increases were not as great as for the heated space-exposed samples, which experienced chain scission due to irradiation in space.

**Find out more about this research on the World Wide Web:**

<http://www.grc.nasa.gov/WWW/epbranch/ephome.htm>

**References**

1. Townsend, J.A., et al.: Hubble Space Telescope Metallized Teflon FEP Thermal Control Materials: On-Orbit Degradation and Post-Retrieval Analysis. High Perform. Polym., vol. 11, no. 1, 1999, pp. 81–99.

**Glenn contact:**

Kim K. de Groh, (216) 433–2297, [Kim.K.deGroh@grc.nasa.gov](mailto:Kim.K.deGroh@grc.nasa.gov)

**Authors:**

Kim K. de Groh, Dr. James R. Gaier, Rachele L. Hall, Mary Jo Norris, Dr. Matthew P. Espe, and Daveen R. Cato

**Headquarters project office:**

OSS (ATMS)

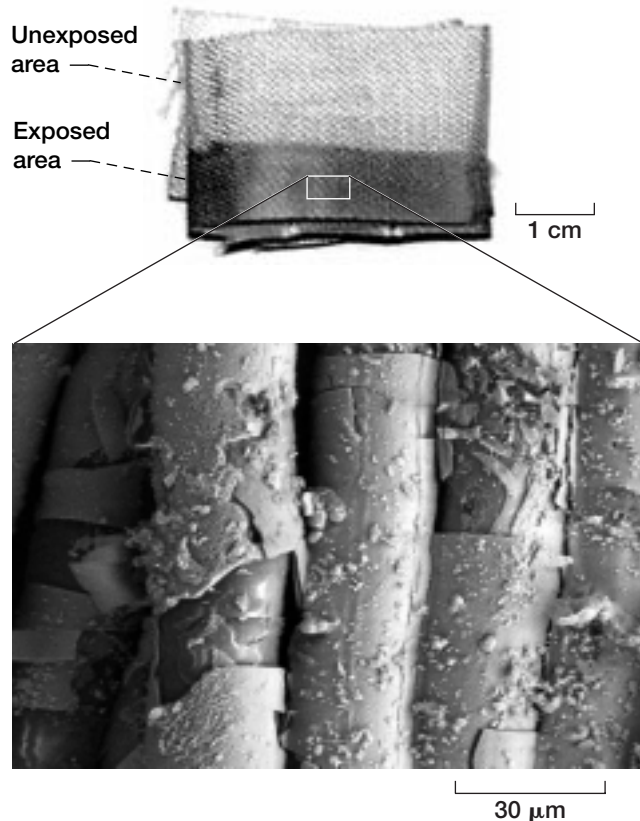
**Programs/Projects:** HST

## Contaminated Solar Array Handrail Samples Retrieved From Mir Analyzed

In January 1998 during the shuttle STS–89 mission, an eight-section Russian solar array panel was retrieved after more than 10 years of exposure to the orbital space environment on Mir. The array was deployed June 16, 1987, and removed on November 3, 1997. It had been actively used as a source of electrical power for 8 years. This operational array had been located on the Mir core module, located directly above the Kvant-2 module. Its retrieval provided a unique opportunity to study the effects of the low-Earth-orbit environment on a functional solar array.

The intact solar array underwent scientific inspections and preliminary tests by a joint team of U.S. and Russian investigators to evaluate the effects of long-term space exposure. Upon initial examination, significant contamination was observed over most components of the array. One panel, panel 8, was provided to the U.S. scientists for further evaluation.

As part of the U.S. investigations, two solar array handrail samples from panel 8 were evaluated for contamination at the NASA Glenn Research Center at Lewis Field. One is a section of a rigid handrail, and the other is a section of woven fabric tape that was overwrapped around a flexible handhold. Both the flexible handhold woven fabric and the rigid handrail were significantly darkened after 10 years of space exposure. They were evaluated with optical microscopy, field



*Flexible handhold fabric tape from the Russian solar array retrieved after 10 years of exposure to the low-Earth-orbit space environment on Mir. A very thick ( $\approx 1.6\text{-}\mu\text{m}$ ) brown oxidized silicon contaminant layer developed during the 10-yr space exposure.*

emission scanning electron microscopy (FESEM), and energy-dispersive spectroscopy. Solar absorptance and room-temperature emittance values also were obtained. The returned contaminated solar array segment is very similar in design to the solar arrays being supplied by the Russians for the International Space Station. Therefore, it was desirable to determine what the contaminants on various surfaces are and what the sources of the contamination were.

Optical microscopy and FESEM imaging showed that the brown stained areas have thick layers of contamination that have crazed and spalled-off the surfaces in some regions. An area where the cross section of the contaminant is visible in FESEM imaging shows the film to be approximately  $1.6\text{-}\mu\text{m}$  thick. The figure shows contaminated (space-exposed) and uncontaminated (protected) areas of the flexible handhold fabric along with a high-magnification FESEM image showing the thick contaminant layer coating the fabric fibers. The contaminant caused a 41-percent

increase in the solar absorptance of the flexible handhold fabric. Energy-dispersive spectroscopy revealed that the brown contaminant on both samples is composed of oxidized silicon with very little carbon content. There is no silicon present on the unexposed fabric overwrap, and very small amounts in the white paint. Therefore, the contaminant layer on both handrail samples is attributed to silicone contamination from other spacecraft materials that were oxidized by atomic oxygen while in orbit. A significant source of the silicone contamination has been determined to be from the solar array itself, specifically from the silicone compounds used to laminate the solar array panel. FESEM images of the handhold fabric show areas where the contaminant layer has spalled off the organic fibers and atomic oxygen erosion has occurred. This implies that flakes of the thick contaminant coating spalled off while in space and became a source of particulate contamination.

**Find out more about this research on the World Wide Web:**

<http://www.grc.nasa.gov/WWW/epbranch/ephome.htm>

**Glenn contact:**

Kim K. de Groh, (216) 433-2297,  
Kim.K.deGroh@grc.nasa.gov

**Authors:**

Kim K. de Groh and Terry R. McCue

**Headquarters project office:**

OSS (ATMS)

**Programs/Projects:** ISS

# Steady-State Vacuum Ultraviolet Exposure Facility With Automated Lamp Calibration and Sample Positioning Fabricated

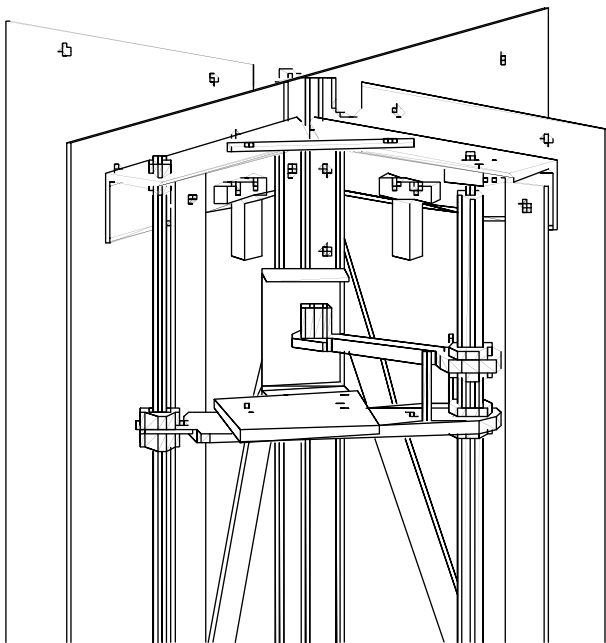
The Next Generation Space Telescope (NGST) will be placed in an orbit that will subject it to constant solar radiation during its planned 10-year mission. A sunshield will be necessary to passively cool the telescope, protecting it from the Sun's energy and assuring proper operating temperatures for the telescope's instruments. This sunshield will be composed of metalized polymer multilayer insulation with an outer polymer membrane (12 to 25  $\mu\text{m}$  in thickness) that will be metalized on the back to assure maximum reflectance of sunlight. The sunshield must maintain mechanical integrity and optical properties for the full 10 years. This durability requirement is most challenging for the outermost, constantly solar-facing polymer membrane of the sunshield. One of the potential threats to the membrane material's durability is from vacuum ultraviolet (VUV) radiation in wavelengths below 200 nm. Such radiation can be absorbed in the bulk of these thin polymer membrane materials and degrade the polymer's optical and mechanical properties. So that a suitable membrane material can be selected that demonstrates durability to solar VUV radiation, ground-based testing of candidate materials must be conducted to simulate the total 10-year VUV exposure expected during the Next Generation Space Telescope mission.

The Steady State Vacuum Ultraviolet exposure facility was designed and fabricated at the NASA Glenn Research Center at Lewis Field to provide unattended 24-hr exposure of candidate materials to VUV radiation of 3 to 5 times the Sun's intensity in the wavelength range of 115 to 200 nm. The facility's chamber, which maintains a pressure of approximately  $5 \times 10^{-6}$

torr, is divided into three individual exposure cells, each with a separate VUV source and sample-positioning mechanism. The three test cells are separated by a water-cooled copper shield plate assembly to minimize thermal effects from adjacent test cells. Part of the interior sample positioning mechanism of one test cell is shown in the illustration.

Of primary concern in VUV exposure is the maintenance of constant measured radiation intensity so that the sample's total exposure can be determined in equivalent Sun hours. This is complicated by the fact that a VUV lamp's intensity degrades over time, necessitating a decrease in the distance between the test samples and the lamp. The facility overcomes this challenge by periodically measuring the lamp's intensity with a cesium-iodide phototube and adjusting the sample distance as required to maintain constant exposure intensity. Sample positioning and periodic phototube location under the lamp are both achieved by a single lead-screw assembly. The lamps can be isolated from the main vacuum chamber for cleaning or replacement so that samples are not exposed to the atmosphere during a test.

This facility is operated by Glenn's Electro-Physics Branch and controlled through a computer program that automates lamp calibration, sample positioning, and test duration. The program also monitors system conditions for quality and safety and will abort a test if necessary.



*Interior sample positioning mechanism.*

**For more information, visit the Electro-Physics Branch on the World Wide Web:**  
<http://www.grc.nasa.gov/WWW/epbranch/ephome.htm>

**Glenn contacts:** Joyce A. Dever, (216) 433-6294, [Joyce.A.Dever@grc.nasa.gov](mailto:Joyce.A.Dever@grc.nasa.gov); and Bruce A. Banks, (216) 433-2308, [Bruce.A.Banks@grc.nasa.gov](mailto:Bruce.A.Banks@grc.nasa.gov)

**Dynacs Engineering Company, Inc., contacts:**  
 Edward A. Sechkar, (216) 433-2299, [Edward.A.Sechkar@grc.nasa.gov](mailto:Edward.A.Sechkar@grc.nasa.gov); and Thomas J. Stueber, (216) 433-2218, [Thomas.J.Stueber@grc.nasa.gov](mailto:Thomas.J.Stueber@grc.nasa.gov)

**Authors:**  
 Edward A. Sechkar, Thomas J. Stueber, Bruce A. Banks, and Joyce A. Dever

**Headquarters program office:**  
 OSS (ATMS)

**Programs/Projects:**  
 NGST, VUV exposure, LEO simulation

## Environmental Exposure Conditions for Teflon FEP on the Hubble Space Telescope Investigated

The Hubble Space Telescope (HST) was launched into low Earth orbit on April 24, 1990. During the first servicing mission in December 1993 (3.6 years after launch), multilayer insulation (MLI) blankets were retrieved from the two magnetic sensing systems located on the light shield. Retrieval of one of the solar arrays during this mission also provided MLI blanket material from the solar array drive arm. These MLI materials were analyzed in ground-based facilities, and results indicate that the space-facing outer layer of the MLI, aluminized Teflon FEP (DuPont; fluorinated ethylene propylene), was beginning to degrade. Close inspection of the FEP revealed through-the-thickness cracks in areas with the highest solar exposure and stress concentration. During the second servicing mission in February 1997 (6.8 years after launch), astronauts observed and documented severe cracking in the outer layer of the MLI blankets on both the solar-facing and anti-solar-facing surfaces. During this second mission, some material from the outer layer of the light shield MLI was retrieved and subsequently analyzed in ground-based facilities.

After the second servicing mission, a Failure Review Board was convened by NASA Goddard Space Flight Center to address the MLI degradation problem on HST. Members of the Electro-Physics Branch of the NASA Glenn Research Center at Lewis Field participated on this board. To determine possible degradation mechanisms, board researchers needed to consider all environmental constituents to which the FEP MLI surfaces were exposed. On the basis of measurements, models, and predictions, environ-

EXPOSURE CONDITIONS FOR TEFLON FEP ON THE HUBBLE SPACE TELESCOPE

FEP surface on HST	Light shield (HST body)				Solar array drive arm
Exposure duration on HST, yr	3.6 (SM1 <sup>a</sup> )	6.8 (SM2 <sup>a</sup> )	10	20	3.6
Thermal cycles	19,700	37,100	55,000	110,000	19,700
Thermal cycling temperature range, °C					
Solar-facing	-100 to 50	-100 to 50	-100 to 50	-100 to 50	-100 to >100
Anti-solar-facing	-200 to -10	-200 to -10	-200 to -10	-200 to -10	-100 to >100
Total solar exposure hours on solar-facing surfaces	16,670	33,638	50,000	100,000	20,056
Total solar exposure hours on anti-solar-facing surfaces	4477	3364	5000	10,000	6260
X-ray (0.1 to 0.8 nm) fluence, J/m <sup>2</sup>	175	252	302	700	223
X-ray (0.1 to 0.8 nm) dose at 64 μm, krads	47	68	81	189	60
X-ray (0.05 to 0.4 nm) fluence, J/m <sup>2</sup>	12	16	19	47	15
X-ray (0.05 to 0.4 nm) dose at 64 μm, krads	1.0	1.4	1.7	4.2	1.3
Trapped proton fluence >40 keV, #/cm <sup>2</sup>	8.0×10 <sup>9</sup>	2.0×10 <sup>10</sup>	2.8×10 <sup>10</sup>	5.9×10 <sup>10</sup>	8.0×10 <sup>9</sup>
Trapped proton dose at 64 μm, krads	0.81	2.0	2.9	6.1	0.81
Trapped electron fluence > 40 keV, #/cm <sup>2</sup>	1.4×10 <sup>13</sup>	2.0×10 <sup>13</sup>	2.7×10 <sup>13</sup>	6.0×10 <sup>13</sup>	1.4×10 <sup>13</sup>
Trapped electron dose at 64 μm, krads	147	201	283	624	147
Plasma proton fluence, #/cm <sup>2</sup>	1.1×10 <sup>19</sup>	1.6×10 <sup>19</sup>	2.3×10 <sup>19</sup>	5.0×10 <sup>19</sup>	1.1×10 <sup>19</sup>
Plasma electron fluence, #/cm <sup>2</sup>	3.2×10 <sup>19</sup>	4.7×10 <sup>19</sup>	6.6×10 <sup>19</sup>	1.4×10 <sup>20</sup>	3.2×10 <sup>19</sup>
Atomic oxygen fluence, atoms/cm <sup>2</sup>	<3.1×10 <sup>20</sup>	<3.2×10 <sup>20</sup>	<6.0×10 <sup>20</sup>	<1.1×10 <sup>21</sup>	1.2×10 <sup>20</sup>

<sup>a</sup>First (SM1) and second (SM2) servicing missions.

mental exposure conditions for FEP surfaces on HST were estimated for various time periods from launch in 1990 through 2010, the planned end-of-life for HST. The table summarizes these data—including the number and temperature ranges of thermal cycles; equivalent Sun hours; fluence and absorbed radiation dose from solar event x rays; fluence and absorbed dose from solar wind protons and electrons trapped in Earth's magnetic field; fluence of plasma electrons and protons; and atomic oxygen fluence.

The conclusions of the HST MLI Failure Review Board were based on the combined evidence of HST damage, data obtained from ground-based experiments, and understanding of the environmental exposure conditions for FEP exposed to the HST environment (ref. 1):

"The observations of HST MLI and ground testing of pristine samples indicate that thermal cycling with deep-layer damage from electron and proton radiation are necessary to cause the observed Teflon® FEP embrittlement and the propagation of cracks along stress concentrations. Ground testing and analysis of retrieved MLI indicate that damage increases with the combined total dose of electrons, protons, UV and x-rays along with thermal cycling."

An understanding of how the degradation of FEP on HST correlates with the environmental exposure conditions is important to spacecraft designers for predicting the lifetime of FEP components being used on spacecraft and for designing improved materials and MLI systems that will be durable in the space environment.

## Effects of Carbon Structure and Surface Oxygen on Carbon's Performance as the Anode in Lithium-Ion Battery Determined

Four carbon materials (C1, C2, C3, and C4) were tested electrochemically at the NASA Glenn Research Center at Lewis Field to determine their performance in lithium-ion batteries. They were formed as shown in the figure on the next page. This process caused very little carbon loss. Products C1 and C3 contained very little oxygen because of the final overnight heating at 540 °C. Products C2 and C4, on the other hand, contained small amounts of basic oxide. The electrochemical test involved cycles of lithium intercalation and deintercalation using C/saturated LiI-50/50 (vol %) ethylene carbonate (EC) and dimethyl carbonate (DMC)/Li half cell. The cycling test, which is summarized in the table, resulted in three major conclusions.

(1) The capacity of the carbon with a basic oxide surface converges to a constant value quickly (within 4 cycles), possibly because the oxide prevents solvent from entering the carbon structure and, therefore, prolongs the carbon's cycle life.

### Find out more about this research on the World Wide Web:

<http://www.grc.nasa.gov/WWW/epbranch/ephome.htm>

### Reference

1. Townsend, J.A., et al.: Hubble Space Telescope Metallized Teflon FEP Thermal Control Materials: On-Orbit Degradation and Post-Retrieval Analysis. High Perform. Polym., vol. 11, no. 1, 1999, pp. 81–99.

### Glenn contact:

Joyce A. Dever, (216) 433–6294,  
Joyce.A.Dever@grc.nasa.gov

### Goddard contact:

Jacqueline A. Townsend, (301) 286–6685,  
Jacqueline.A.Townsend.1@gssc.nasa.gov

### Authors:

Joyce A. Dever, Kim K. de Groh, Bruce A. Banks, Jacqueline A. Townsend, Janet L. Barth, Shaun Thomson, Teri Gregory, and William J. Savage

### Headquarters program office:

OSS (ATMS)

**Programs/Projects:** HST

(2) Under certain conditions, the disordered carbon can store more lithium than its precursor.

(3) These samples and their precursor can intercalate at 200 mA/g and deintercalate at a rate of 2000 mA/g without significant capacity loss.

### Glenn contact:

Ching-cheh Hung, (216) 433–2302,  
Ching-cheh.Hung@grc.nasa.gov

**Author:** Ching-cheh Hung

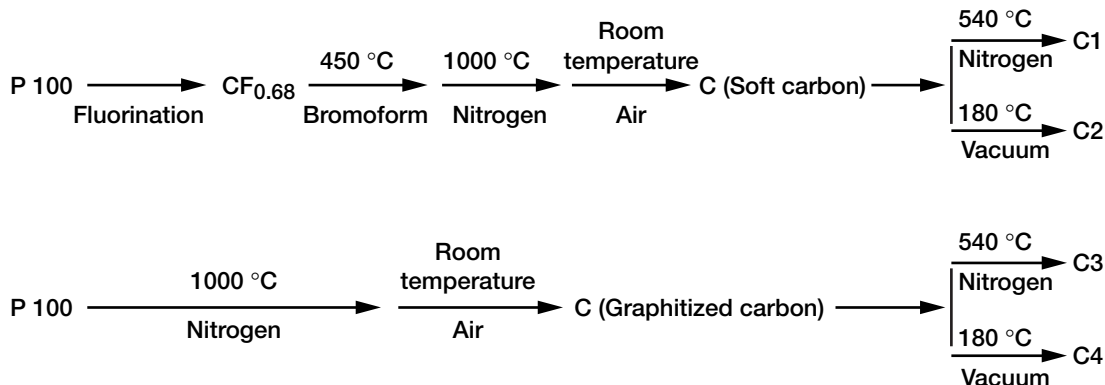
### Headquarters program office:

OSS (ATMS)

**Programs/Projects:** Space Power

CAPACITIES OF THE CARBON MATERIALS TO STORE AND RELEASE LITHIUM

	Capacity, mA-hr/g					
	1st cycle		4th cycle		High current density (After more than four cycles)	
	Intercalation 10 mA/g	Deintercalation 10 mA/g	Intercalation 10 mA/g	Deintercalation 10 mA/g	Intercalation 200 mA/g	Deintercalation 2000 mA/g
C1	487	280	288	268	—	—
C2	310	208	197	197	161	163
C3	249	223	224	219	—	—
C4	257	245	245	244	194	232



Preparation of carbon samples.

## Portable Infrared Reflectometer Designed and Manufactured for Evaluating Emittance in the Laboratory or in the Field

The optical properties of materials play a key role in spacecraft thermal control. In space, radiant heat transfer is the only mode of heat transfer that can reject heat from a spacecraft. One of the key properties for defining radiant heat transfer is emittance, a measure of how efficiently a surface can reject heat in comparison to a perfect black body emitter. Heat rejection occurs in the infrared region of the spectrum, nominally in the

range of 2 to 25  $\mu\text{m}$ . To calculate emittance, one obtains the reflectance over this spectral range, calculates spectral absorbance by difference, and then uses Kirchhoff's Law and the Stefan-Boltzmann equation to calculate emittance.



Portable infrared reflectometer for evaluating emittance.

A new portable infrared reflectometer, the SOC-400t, was designed and manufactured to evaluate the emittance of surfaces and coatings in the laboratory or in the field. It was developed by Surface Optics Corporation under a contract with the NASA Glenn Research Center at Lewis Field to replace the Center's aging Gier-Dunkle DB-100 infrared reflectometer. The specifications for the new instrument include a wavelength range of 2 to 25  $\mu\text{m}$ ; reflectance repeatability of  $\pm 1$  percent; self-calibrating, near-normal

spectral reflectance measurements; a full scan measurement time of 3.5 min, a sample size of 1.27 cm (0.5 in.); a spectral resolution selectable from 4, 8, 16, or 32  $\text{cm}^{-1}$ ; and optical property characterization utilizing an automatic integration to calculate total emittance in a selectable temperature range.

The computer specified to drive the software is a laptop with a menu-driven operating system for setup and operation, a full data base manager, and a full data analysis capability through MIDAC Grams/32 software (MIDAC Corporation, Irvine, California). Spectral scanning is achieved through the use of a Fourier Transform Infrared Michelson interferometer. In addition, the reflectometer's size and weight make it conducive to portable operation. Although most of the planned uses for the instrument are expected to be in the laboratory, some field operations are anticipated. The only requirement for field operation is a source of power (115 V alternating current).

Glenn took delivery of this world-unique, portable infrared reflectometer in January 1999. It is a resounding success, and an evaluation of thermal control materials for NASA and aerospace customers is currently underway.

**Find out more on the World Wide Web:** <http://www.grc.nasa.gov/WWW/epbranch/ephome.htm>

**Glenn contact:** Dr. Donald A. Jaworske, (216) 433-2312, Donald.A.Jaworske@grc.nasa.gov

**Author:** Dr. Donald A. Jaworske

**Headquarters program office:** OSS (ATMS)

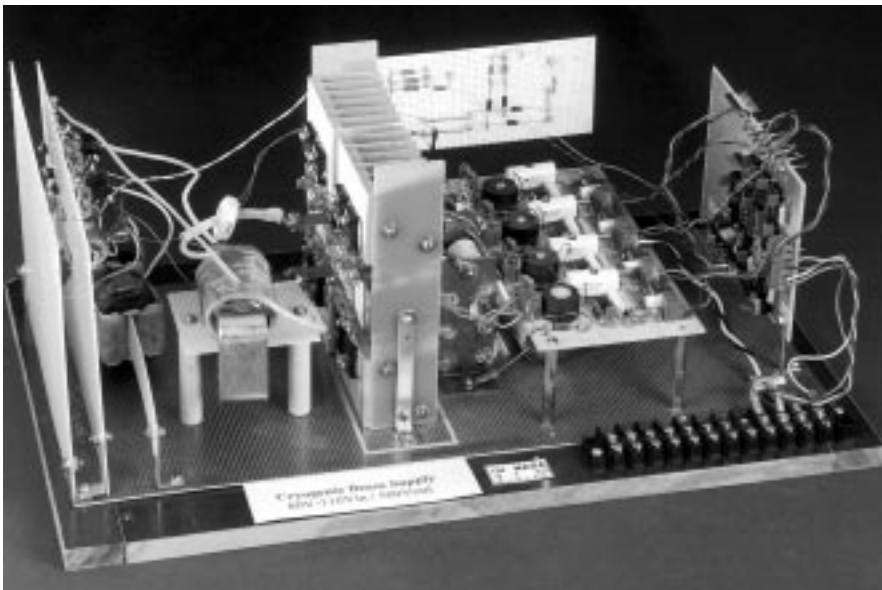
**Programs/Projects:** Space Power, ISS, Aerospace Industry

## Electronics Demonstrated for Low-Temperature Operation

The operation of electronic systems at cryogenic temperatures is anticipated for many NASA spacecraft, such as planetary explorers and deep space probes. For example, an unheated interplanetary probe launched to explore the rings of Saturn would experience an average temperature near Saturn of about  $-183\text{ }^{\circ}\text{C}$ . Electronics capable of low-temperature operation in the harsh deep space environment also would help improve circuit

performance, increase system efficiency, and reduce payload development and launch costs.

An ongoing research and development program on low-temperature electronics at the NASA Glenn Research Center at Lewis Field is focusing on the design of efficient power systems that can survive and exploit the advantages of low-temperature environments. The targeted systems, which are mission driven, include converters, inverters, controls, digital circuits, and special-purpose circuits. Initial development efforts successfully demonstrated the low-temperature operation and cold-restart of several direct-current/direct-current (dc/dc) converters based on different types of circuit design, some with superconducting inductors. The table lists some of these dc/dc converters with their properties, and the photograph shows a high-voltage, high-power dc/dc converter designed for an ion-propulsion system for low-temperature operation.



*High-voltage, 1-kW dc/dc converter designed for low-temperature ion propulsion system.*

PROPERTIES OF CERTAIN CONVERTERS DESIGNED FOR  
LOW-TEMPERATURE OPERATION AT GLENN

Circuit type	Voltage, V		Power, W	Frequency, kHz	Efficiency	
	Input	Output			At 25 °C	At -190 °C
Buck	42	28	175	50	—	—
Boost	24	48	150	50	—	95.9
Multiresonant Buck	48	28	55	200	93.9	94.8
High-voltage full-bridge	80 to 110	500	825	50	90.18	92.19
Three-level buck-boost	42	120	180	50	95.7	94.9
Push-pull	30	5	10	40	—	—

The development efforts of advanced electronic systems and the supporting technologies for low-temperature operation are being carried out in-house and through collaboration with other Government agencies, industry, and academia. The Low Temperature Electronics Program supports missions and development programs at NASA's Jet Propulsion Laboratory and Goddard Space Flight Center. The developed technologies will be transferred to commercial end users for applications such as satellite infrared sensors and medical diagnostic equipment.

Find out more about this research on the World Wide Web:

<http://www.grc.nasa.gov/WWW/epbranch/ephome.htm>

**Glenn contact:**

Richard L. Patterson, (216) 433-8166, Richard.L.Patterson@grc.nasa.gov

**Authors:** Richard L. Patterson, Ahmad Hammoud, and Scott S. Gerber

**Headquarters program office:** OSS

**Programs/Projects:** New Millennium, NASA Electronic Parts and Packaging, JPL Failure Detection and Prevention

## Automated Reflectance Measurement System Designed and Fabricated to Determine the Limits of Atomic Oxygen Treatment of Art Through Contrast Optimization

Atomic oxygen generated in ground-based research facilities has been used to not only test erosion of candidate spacecraft materials but as a noncontact technique for removing organic deposits from the surfaces of artwork. NASA has patented the use of atomic oxygen to remove carbon-based soot contamination from fire-damaged artwork.

The process of cleaning soot-damaged paintings with atomic oxygen requires exposures for variable lengths of time, dependent on the condition of a painting. Care must be exercised while cleaning to prevent the removal of pigment. The cleaning process must be stopped as soon as visual inspection or surface reflectance measurements indicate that cleaning is complete. Both techniques rely on optical comparisons of known bright locations against known dark locations on the artwork being cleaned. Difficulties arise with these techniques when either a known bright or dark location cannot be determined readily. Furthermore, dark locations will lighten with excessive exposure to atomic oxygen. Therefore, an automated test instrument to quantitatively characterize cleaning progression was designed and developed at the NASA Glenn Research Center at Lewis Field to determine when atomic oxygen cleaning is complete.

This reflectance camera scans a painting, vertically and horizontally, with a 30-W white light Cole-Parmer Fiber Optic Illuminator System (Cole-Parmer Instrument Company, Vernon Hills, Illinois)



Reflectance camera with atomic-oxygen-treated painting.

and records diffuse reflectance with a UDT Sensors, Inc. (Hawthorne, California) PIN-10DPI photodiode. Each scan consists of a user-defined discrete number of photodiode snapshot readings. The output of the reflectance camera is the average and standard deviation of all the individual diffuse reflectance snapshot readings acquired during a scan. Initially, a soot-damaged painting will have a small standard deviation that will increase as soot is removed. Cleaning will be considered completed when the change in standard deviation between consecutive measurements becomes negative.

A program written in Microsoft Visual C++, developed for operator interaction, controls the scanning process and data acquisition. The program requires an Intel-based PC with a Microsoft Windows 95, 98, or NT 4.0 operating system.

**For more information, visit the Electro-Physics Branch on the World Wide Web:**  
<http://www.grc.nasa.gov/WWW/epbranch/ephome.htm>

**Glenn contacts:**

Sharon K. Rutledge, (216) 433-2219,  
[Sharon.K.Rutledge@grc.nasa.gov](mailto:Sharon.K.Rutledge@grc.nasa.gov); and  
Bruce A. Banks, (216) 433-2308,  
[Bruce.A.Banks@grc.nasa.gov](mailto:Bruce.A.Banks@grc.nasa.gov)

**Dynacs Engineering Company, Inc., contacts:**

Edward A. Sechkar, (216) 433-2299,  
[Edward.A.Sechkar@grc.nasa.gov](mailto:Edward.A.Sechkar@grc.nasa.gov); and  
Thomas J. Stueber, (216) 433-2218,  
[Thomas.J.Stueber@grc.nasa.gov](mailto:Thomas.J.Stueber@grc.nasa.gov)

**Authors:**

Edward A. Sechkar, Thomas J. Stueber,  
Bruce A. Banks, and Sharon K. Rutledge

**Headquarters program office:**

OSS (ATMS)

**Programs/Projects:**

Art restoration, art conservation

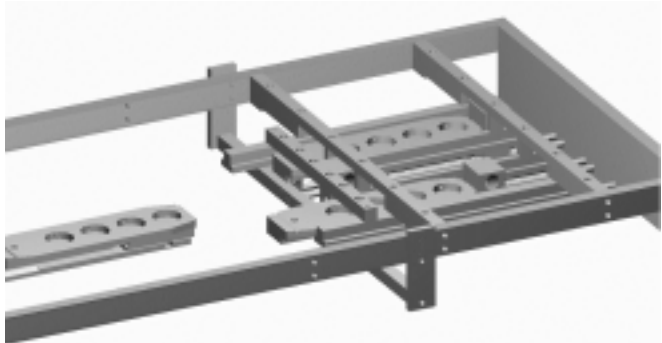
## Automated Multiple-Sample Tray Manipulation Designed and Fabricated for Atomic Oxygen Facility

Extensive improvements to increase testing capacity and flexibility and to automate the in situ Reflectance Measurement System (RMS) are in progress at the Electro-Physics Branch's Atomic Oxygen (AO) beam facility of the NASA Glenn Research Center at Lewis Field. These improvements will triple the system's capacity while placing a significant portion of the testing cycle under computer control for added reliability, repeatability, and ease of use.

The AO facility's electron-cyclotron resonance plasma source generates a low-energy AO beam with a total effective flux that can be set between  $1 \times 10^{15}$  and  $2 \times 10^{16}$  atoms/cm<sup>2</sup>/sec. Simultaneous vacuum ultraviolet radiation exposure is provided by deuterium lamps that yield radiation intensity levels of three to five equivalent Suns in the 115- to 200-nm range. Total hemispherical spectral reflectance of samples can be measured in the wavelength range from 250 to 2500 nm. A three-axis position-

ing system, composed of two linear stages and one rotary stage, is used to position a single sample tray, containing four samples, under the AO beam and to rotate the tray to extend it into the RMS.

Overall sample capacity is being tripled by the design and installation of a tray holder assembly that can hold up to three sample trays under the AO beam. The existing positioning system is being modified with an extension arm that can combine linear and rotary motions to pick any of the sample trays under the AO beam and bring it into the RMS. The sample tray can then be returned to the holder assembly for further exposure. In addition, the assembly has been designed so that two sample tray "ports" that are shielded from AO exposure can be added. This will allow a variety of exposure times to be used for different samples within the same test.



*Multiple sample trays in tray holder assembly.*

A movable sensor holder installed adjacent to each sample tray will provide for easy in situ characterization of the deuterium lamp performance. It can be positioned at any sample location for sample-specific vacuum ultraviolet radiation exposure levels.

The RMS makes use of a sliding stage containing two detectors and a sliding stage containing a reference material sample. These two stages were previously positioned with manual linear feedthroughs. With these feedthroughs, a stage could block the path of a sample tray that was being extended into the RMS. This system is being modified to include two motor-driven rotary feedthroughs connected to lead screw assemblies that translate the stages along linear bearing pathways, avoiding this potential problem.

A computer program is being developed to automate all sample tray pick-up and placement operations, RMS stage positioning, and any required data acquisition. System conditions will be monitored for quality and safety, and a graphical interface will show the real-time positions of all sample trays.

**For more information, visit the Electro-Physics Branch on the World Wide Web:**  
<http://www.grc.nasa.gov/WWW/epbranch/ephome.htm>

**Glenn contacts:**

Sharon K. Rutledge, (216) 433-2219, Sharon.K.Rutledge@grc.nasa.gov; Bruce A. Banks, (216) 433-2308, Bruce.A.Banks@grc.nasa.gov; and Joyce A. Dever, (216) 433-6294, Joyce.A.Dever@grc.nasa.gov

**Dynacs Engineering Company, Inc., contacts:**

Edward A. Sechkar, (216) 433-2299, Edward.A.Sechkar@grc.nasa.gov; and Thomas J. Stueber, (216) 433-2218, Thomas.J.Stueber@grc.nasa.gov

**Authors:**

Edward A. Sechkar, Thomas J. Stueber, Joyce A. Dever, Bruce A. Banks, and Sharon K. Rutledge

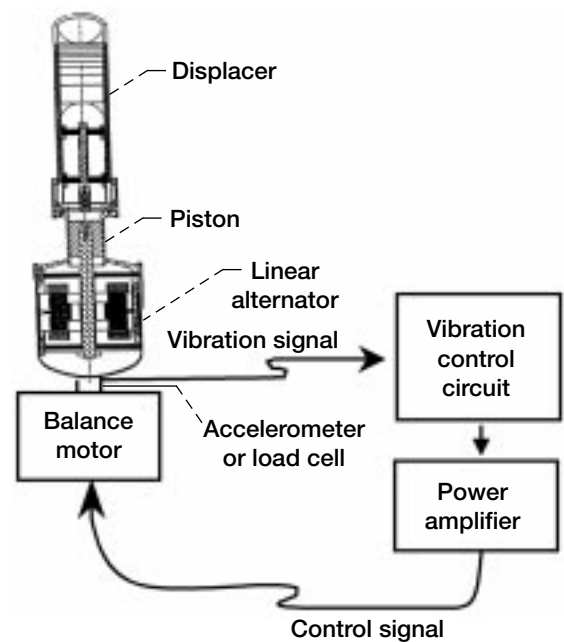
**Headquarters program office:**  
 OSS (ATMS)

**Programs/Projects:** Simulation of LEO atomic oxygen for accelerated exposure, materials testing for ISS and other LEO spacecraft

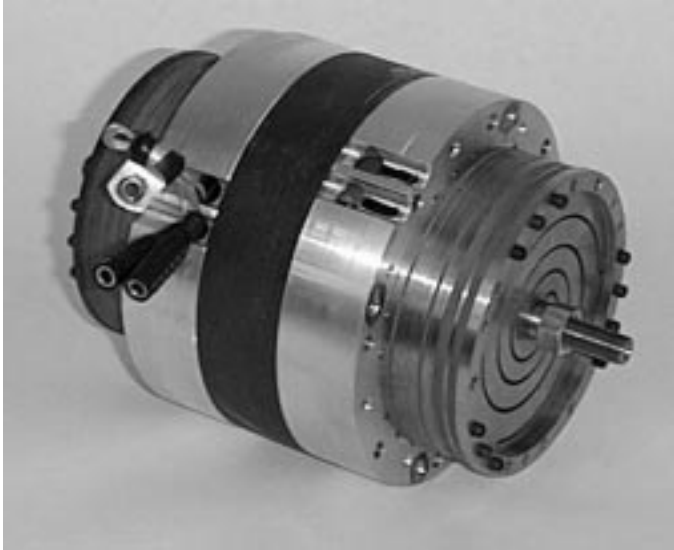
## Adaptive Vibration Reduction System Shown to Effectively Eliminate Vibrations for the Stirling Radioisotope Power System

Stirling Technology Company (STC), as part of a Small Business Innovation Research contract Phase II with the NASA Glenn Research Center at Lewis Field, is developing an Adaptive Vibration Reduction System (AVRS) that will effectively eliminate vibrations for the Stirling radioisotope power system. The AVRS will reduce vibration levels for two synchronized, opposed Stirling converters by a factor of 10 or more under normal operating conditions. Even more importantly, the AVRS will be adaptive and will be able to adjust to any changing converter conditions over the course of a mission.

The Stirling converter is being developed by NASA and the Department of Energy (DOE) as a high-efficiency option for a radioisotope power system to provide onboard electric power for NASA deep space missions. The high Stirling efficiency of over 25 percent for this application will reduce the required amount of isotope by more than a factor of 3 in comparison to the current radioisotope thermoelectric generators (RTG's). Stirling is the most developed converter option of the advanced power technologies under consideration.



*Adaptive vibration reduction system.*



*Balance motor for 350-We converters.*

The AVRS (see the illustration on the preceding page) uses an active balance system with feedback from a vibration signal and will cancel the fundamental vibration and up to 10 harmonics. A balance mass is driven by a separate linear motor; only one balance motor is needed for two opposed Stirling converters. A balance motor being used in the first AVRS testing is shown in the photo. A fast Fourier transform of the vibration signal is used to construct a compensation signal that is sent to the balance motor through a power amplifier. Both the amplitude and phase of each harmonic can be adjusted. Converter frequency must also be measured on a continual basis and factored into the control algorithm. The AVRS will adjust to any change in converter operating conditions, any converter degradation that may occur over a mission, and even to a converter failure, in the unlikely event that one occurs. The AVRS will first be demonstrated on two 350-We RG-350 converters and then on the DOE/STC 55-We converters being developed for the radioisotope power system.

Initial tests of the AVRS on the RG-350 converters have shown a 500-fold reduction in unbalanced vibrations under normal operating conditions with two synchronized converters in an opposed configuration. This compares to a fortyfold to fiftyfold reduction achieved when the converters are just synchronized, and these further reductions were accomplished with only 2 W of power dissipation. Testing was also done with a simulated failed converter, and a 50-fold vibration reduction was obtained with only 7 W of power dissipation. This power dissipation scales to less than 2 to 3 W for

a 55-We converter. For these initial tests, the AVRS balanced only the fundamental of the vibration signal (no harmonics). The full control algorithm is now being developed, and vibration levels should be decreased even further as the balancing is extended to include the harmonics of the vibration signal.

**Find out more on the World Wide Web:**

**Research at Stirling Technology Company:**

<http://www.stirlingtech.com>

**Research at Glenn:**

<http://www.grc.nasa.gov/WWW/tmsb/stirling.html>

**Bibliography**

Thieme, L.G.; Qiu, S.; and White, M.A.: Technology Development for a Stirling Radioisotope Power System for Deep Space Missions. NASA/TM-2000-209767 (Proceedings of the 34th Intersociety Energy Conversion Engineering Conference), 2000.

Thieme, L.G.; Qiu, S., and White, M.A.: Technology Development for a Stirling Radioisotope Power System. NASA/TM-2000-209791 (Proceedings of the Space Technology and Applications International Forum), 2000.

**Glenn contact:**

Lanny G. Thieme, (216) 433-6119, [Lanny.G.Thieme@grc.nasa.gov](mailto:Lanny.G.Thieme@grc.nasa.gov)

**Author:** Lanny G. Thieme

**Headquarters program office:** OSS

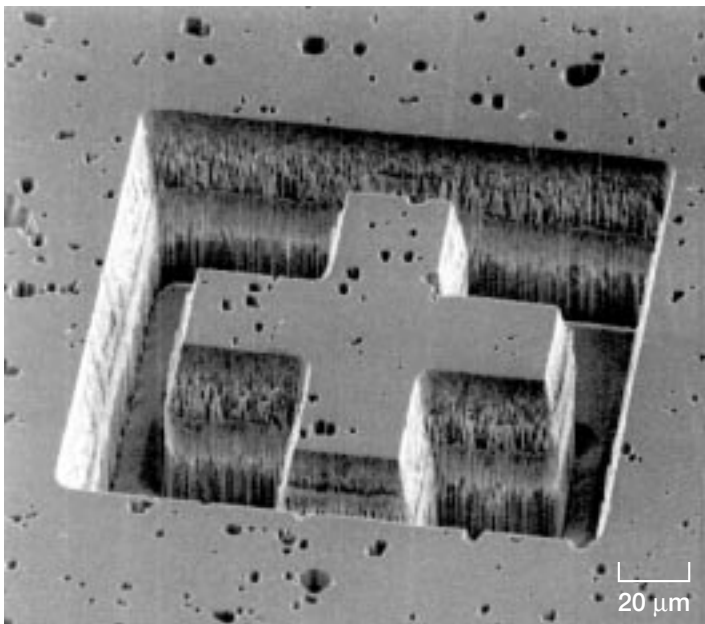
**Programs/Projects:** SBIR, AVRS, advanced radioisotope power

# Instrumentation and Controls

## Deep Etching Process Developed for the Fabrication of Silicon Carbide Microsystems

Silicon carbide (SiC), because of its superior electrical and mechanical properties at elevated temperatures, is a nearly ideal material for the microminiature sensors and actuators that are used in harsh environments where temperatures may reach 600 °C or greater. Deep etching using plasma methods is one of the key processes used to fabricate silicon microsystems for more benign environments, but SiC has proven to be a more difficult material to etch, and etch depths in SiC have been limited to several micrometers. Recently, the Sensors and Electronics Technology Branch at the NASA Glenn Research Center at Lewis Field developed a plasma etching process that was shown to be capable of etching SiC to a depth of 60  $\mu\text{m}$ .

Deep etching of SiC is achieved by inductive coupling of radiofrequency electrical energy to a sulfur hexafluoride ( $\text{SF}_6$ ) plasma to direct a high flux of energetic ions and reactive fluorine atoms to the SiC surface. The plasma etch is performed at a low pressure, 5 mtorr, which together with a high gas throughput, provides for rapid removal of the gaseous etch products. The lateral topology of the SiC microstructure is defined by a thin film of etch-resistant material, such as indium-tin-oxide, which is patterned using conventional photolithographic processes. Ions from the plasma bombard the exposed SiC surfaces and supply the energy needed to initiate a reaction between SiC and atomic fluorine. In the absence of ion bombardment, no reaction occurs, so surfaces perpendicular to the wafer surface (the etch sidewalls) are etched slowly, yielding the desired vertical sidewalls.



Scanning electron micrograph of 60- $\mu\text{m}$ -deep etch in SiC.

The figure shows a scanning electron micrograph of a 60- $\mu\text{m}$ -deep plasma etch of SiC. This etch was performed at a rate of 0.3  $\mu\text{m}/\text{min}$ , which is greater than the rates for previous processes that were demonstrated to be capable of only much shallower etches. The holes in the top surface are the result of pinholes in the indium-tin-oxide, which opened up as the initially 120-nm-thick mask was eroded to a thickness of less than 20 nm. Use of a thicker mask is expected to eliminate these holes. These preliminary results clearly demonstrate the feasibility of etching deep vertical-walled structures in SiC. This etch process will be used to fabricate a SiC pressure sensor for use at 500 °C.

Here, a 60- $\mu\text{m}$ -deep hole, approximately 1 mm in diameter, will be etched into an 80- $\mu\text{m}$ -thick piece of SiC to produce a 20- $\mu\text{m}$ -thick pressure-sensing diaphragm. Work is in progress to refine the etch process to increase the etch rate and reduce the roughness of the etch sidewalls, since smooth sidewalls will be required for other applications requiring deep etching, such as vertical structure high-voltage diodes.

**Find out more about this research on the World Wide Web:** <http://www.grc.nasa.gov/WWW/SiC/SiC.html>

**Glenn contact:**

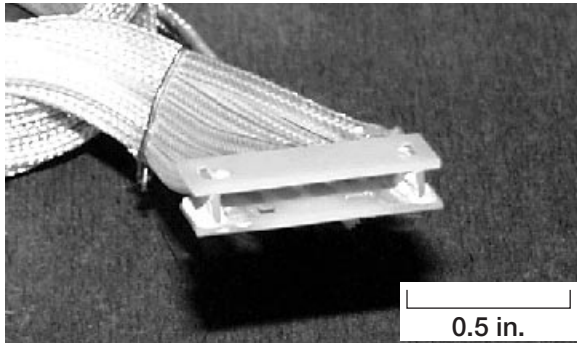
Dr. Glenn M. Beheim, (216) 433-3847,  
Glenn.M.Beheim@grc.nasa.gov

**Author:** Dr. Glenn M. Beheim

**Headquarters program office:**  
OAST, OSS

**Programs/Projects:** HITEMP, GMI

# Packaging Technology Developed for High-Temperature SiC Sensors and Electronics



*Prototype high-temperature electronic package (with test wires) composed of AlN substrate and Au thick-film metallization being developed for SiC sensors and electronic devices.*

A ceramic- and thick-film-materials-based prototype electronic package designed for silicon carbide (SiC) high-temperature sensors and electronics has been successfully tested at 500 °C in an oxygen-containing air environment for 500 hours. This package was designed, fabricated, assembled, and electronically evaluated at the NASA Glenn Research Center at Lewis Field with an in-house-fabricated SiC semiconductor test chip.

High-temperature electronics and sensors are necessary for harsh-environment space and aeronautical applications, such as space missions to the inner solar system or the emission control electronics and sensors in aeronautical engines. Single-crystal SiC has such excellent physical and chemical material properties that SiC-based semiconductor electronics can operate at temperatures over 600 °C, which is significantly higher than the limit for Si-based semiconductor devices. SiC semiconductor chips were recently demonstrated to be operable at temperatures as high as 600 °C, but only in the probe-station environment because suitable packaging technology for sensors and electronics at temperatures of 500 °C and beyond did not exist. Thus, packaging technology for SiC-based sensors and electronics is immediately needed for both application and commercialization of high-temperature SiC sensors and electronics.

In response to this need, researchers at Glenn designed, fabricated, and assembled a prototype electronic package for high-temperature electronics, sensors, and microelectromechanical systems (MEMS) using aluminum nitride (AlN) substrate and gold (Au) thick-film materials. This prototype package successfully survived a soak test at 500 °C in air for 500 hours. Packaging components tested included thick-film high-temperature metallization, internal wire bonds, external lead bonds, and a SiC diode chip die-attachment. Each test loop, which was composed of thick-film printed wire, wire bond, and lead bond was subjected to a 50-mA direct current for 250 hours at 500 °C.

As desired, when soaked at 500 °C with or without current load, the test loops exhibited low electrical resistance ( $\sim 0.3\Omega$ ). Also as expected, the electrical isolation impedance between printed wires that were not electrically joined by a wire bond remained high ( $>0.4G\Omega$ ) during and after the 500 °C soak. The attached SiC die (diode) showed low resistance ( $< 5\Omega/\text{mm}^2$ ) backside electrical contact, at both room temperature and 500 °C, through the die-attachment. These results indicate that the prototype package meets the initial design standards for low-power, long-term, high-temperature operation. This technology is being evaluated and developed further through statistical tests of each packaging element for longer lifetime and higher operation temperatures.

**Find out more about this research on the World Wide Web:** <http://www.grc.nasa.gov/WWW/sensors/>

**A.Y.T. Corporation contact:**

Dr. Liang-Yu Chen, (216) 433-6458, Liangyu.Chen@grc.nasa.gov

**Glenn contact:**

Dr. Jih-Fen Lei, (216) 433-3922, Jih-Fen.Lei@grc.nasa.gov

**Authors:** Dr. Liang-Yu Chen, Dr. Gary W. Hunter, Dr. Philip G. Neudeck, and Dr. Jih-Fen Lei

**Headquarters program office:**

OAST, OSS

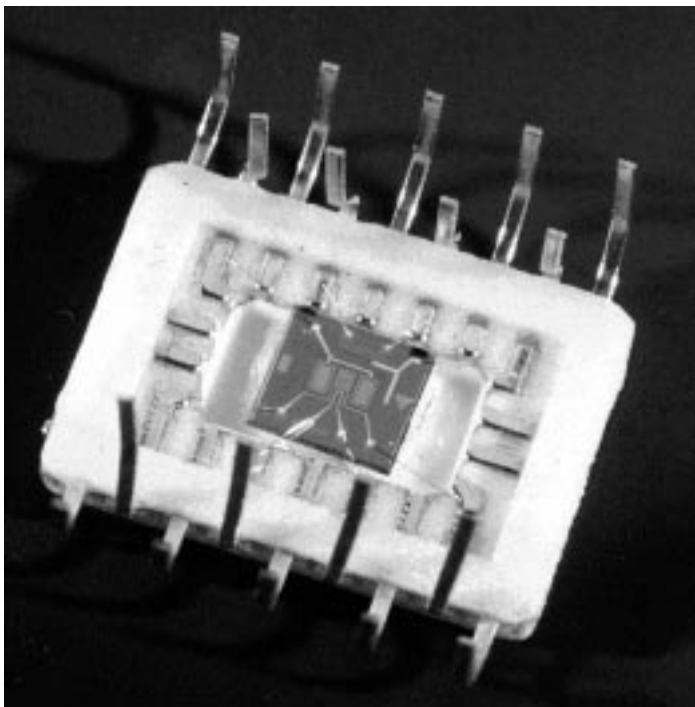
**Programs/Projects:** GMI, IT Base

## Hydrogen Sensors Demonstrated on the Shuttle

Microelectromechanical-systems- (MEMS-) based hydrogen sensor technology developed by the NASA Glenn Research Center at Lewis Field and Case Western Reserve University was demonstrated on shuttle missions STS-95 (Senator Glenn's mission) and STS-96. These smart sensors, commercialized by Makel Engineering Inc., were part of an "Integrated Vehicle Health Monitoring HEDS Technology Demonstration" series conducted at the NASA Kennedy Space Center. The experiments were designed to demonstrate the effect of technological upgrades on shuttle performance.

The hydrogen sensors were microfabricated for minimal size, weight, and power consumption. A temperature detector and heater were included on the sensor for temperature control. Two palladium chrome (PdCr) hydrogen detection devices were included in each sensor package: a Schottky diode for low concentrations and a resistor for high concentrations. These sensor designs allow operation in inert environments. "Smart" electronics developed by Makel Engineering were integrated with the sensors to control the sensor temperature and process the output of the various sensors.

This complete hydrogen detection system (two sensors on a chip with smart electronics) flew on STS-95 (launched October 1998) and STS-96 (launched May 1999). It was installed in the aft compartment of the shuttle and used to monitor the hydrogen concentration in that region.



*Microfabricated hydrogen sensor.*

Up to this time, a mass spectrometer had monitored the hydrogen concentration in the aft compartment before launch, and "grab" bottles had been used after launch. The inside of these bottles is at vacuum. During flight, the grab bottles are pyrotechnically opened for a brief period, and the gas in the aft compartment is captured in the bottle. Several of these bottles are opened at different times during takeoff, and their contents are used to determine the time profile of the gases in the aft chamber. However, this information is not available until after the flight.

On the launch pad, results from the new sensor technology paralleled the responses of the mass spectrometer with, in some cases, a quicker response time. In flight, data from the new sensors agreed with those derived from analyzing the contents of the grab bottles. Moreover, this microsensor can monitor the aft compartment continuously and, in principle, could monitor the health of the vehicle in real time during flight.

**Find out more about this research on the World Wide Web:**

<http://www.grc.nasa.gov/WWW/chemsensors/>

**Glenn contact:**

Dr. Gary W. Hunter, (216) 433-6459,  
Gary.W.Hunter@grc.nasa.gov

**Author:** Dr. Gary W. Hunter

**Team members:** Dr. Gary W. Hunter, Frank L. DeAngelo, Professor C.C. Liu, Q.H. Wu, Dr. D. Makel, and Greg Hall

**Headquarters program office:** OAST

**Programs/Projects:**

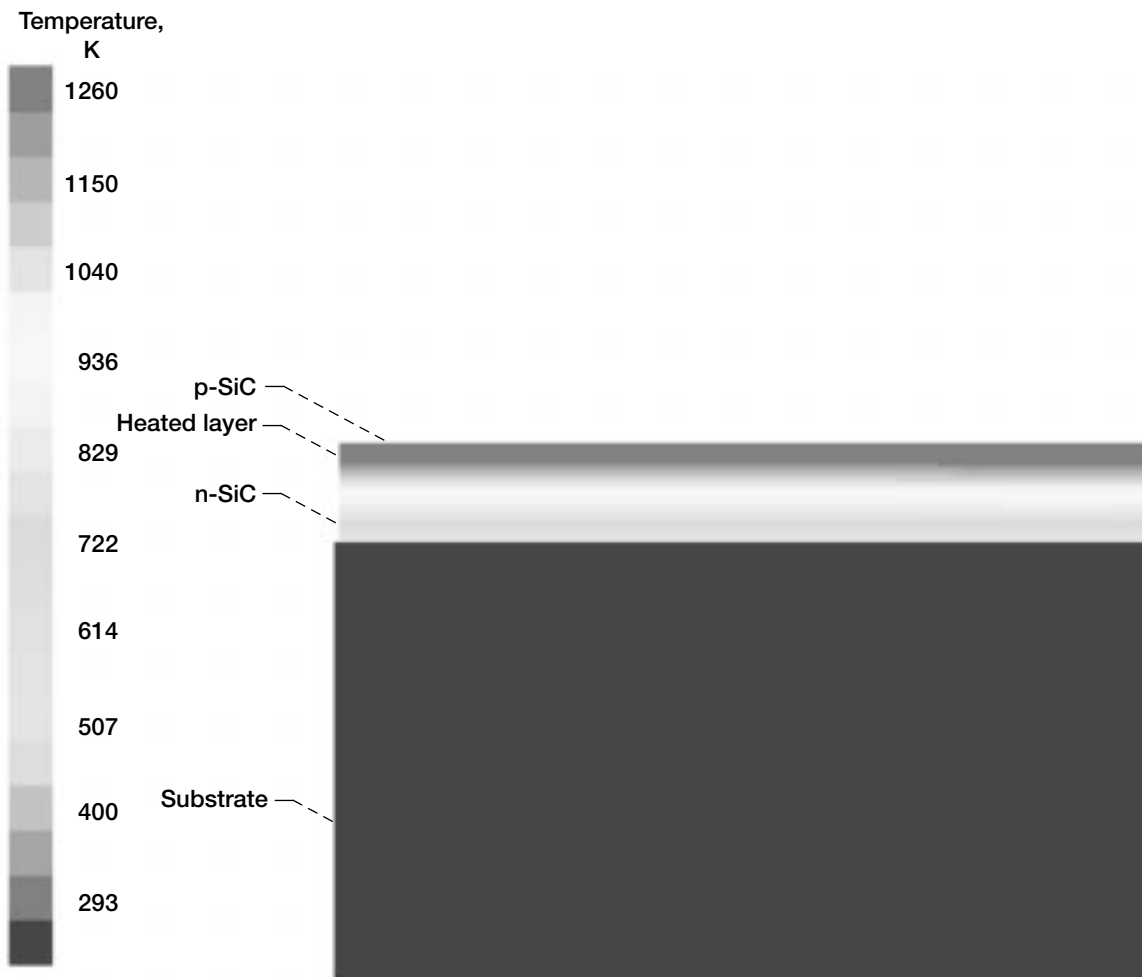
Shuttle Upgrade, HTD

# Temperature Distribution Within a Defect-Free Silicon Carbide Diode Predicted by a Computational Model

Most solid-state electronic devices—diodes, transistors, and integrated circuits—are based on silicon. Although this material works well for many applications, its properties limit its ability to function under extreme high-temperature or high-power operating conditions. Silicon carbide (SiC), with its desirable physical properties, could someday replace silicon for these types of applications. A major roadblock to realizing this potential is the quality of SiC material that can currently be produced. Semiconductors require very uniform, high-quality material, and commercially available SiC tends to suffer from defects in the crystalline structure that have largely been eliminated in silicon. In some power circuits, these defects can focus energy into an extremely small area, leading to overheating that can damage the device.

In an effort to better understand the way that these defects affect the electrical performance and reliability of an SiC device in a power circuit, the NASA Glenn Research Center at Lewis Field began an in-house three-

dimensional computational modeling effort. The goal is to predict the temperature distributions within a SiC diode structure subjected to the various transient overvoltage breakdown stresses that occur in power management circuits. A commercial computational fluid dynamics computer program (FLUENT—Fluent, Inc., Lebanon, New Hampshire) was used to build a model of a defect-free SiC diode and generate a computational mesh. A typical breakdown power density was applied over 0.5  $\mu$ sec in a heated layer at the junction



Temperature contours in a silicon carbide diode predicted by FLUENT 5.0.

between the p-type SiC and n-type SiC, and the temperature distribution throughout the diode was then calculated. The peak temperature extracted from the computational model agreed well (within 6 percent) with previous first-order calculations of the maximum expected temperature at the end of the breakdown pulse. This level of agreement is excellent for a model of this type and indicates that three-dimensional computational modeling can provide useful predictions for this class of problem.

The model is now being extended to include the effects of crystal defects. The model will provide unique insights into how high the temperature rises in the vicinity of the defects in a diode at various power densities and pulse durations. This information also will help researchers in understanding and designing SiC devices for safe and reliable operation in high-power circuits.

For more information, visit us on the World Wide Web: <http://www.grc.nasa.gov/WWW/SiC/SiC.html>

**Glenn contact:** Dr. Maria A. Kuczmariski, (216) 433-3651, [Maria.A.Kuczmariski@grc.nasa.gov](mailto:Maria.A.Kuczmariski@grc.nasa.gov); and Dr. Philip G. Neudeck, (216) 433-8902, [Philip.G.Neudeck@grc.nasa.gov](mailto:Philip.G.Neudeck@grc.nasa.gov)

**Author:** Dr. Maria A. Kuczmariski and Dr. Philip G. Neudeck

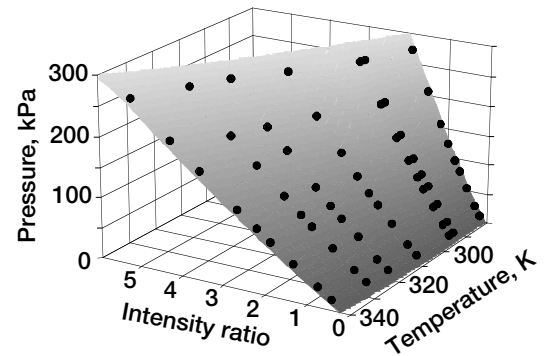
**Headquarters program office:** OAST

**Programs/Projects:** IT Base

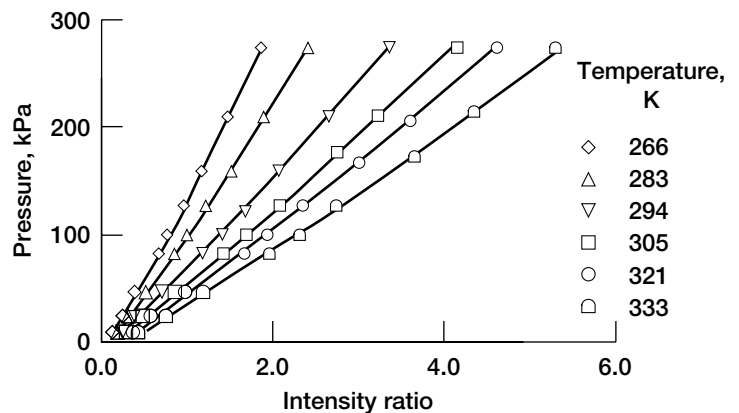
## Temperature Correction of Pressure-Sensitive Paints Simplified

Pressure-sensitive paint (PSP) has become a useful tool to augment conventional pressure taps in measuring the surface pressure distribution of aerodynamic components in wind tunnel testing. Although PSP offers the advantage of nonintrusive global mapping of the surface pressure, one prominent drawback to the accuracy of this technique is the inherent temperature sensitivity of PSP's luminescent intensity. Typical aerodynamic surface PSP tests rely on the coated surface to be both spatially and temporally isothermal, along with conventional instrumentation, to yield the highest accuracy pressure mappings. In some tests, however, spatial and temporal thermal gradients are generated by the nature of the test, as in a blowing jet impinging on a surface. In these cases, high accuracy and reliable data cannot be obtained unless the temperature variations on the painted surface are accounted for. A new temperature-correction technique was developed at the NASA Glenn Research Center at Lewis Field to collapse a "family" of PSP calibration curves to a single curve of intensity ratio versus pressure. This correction allows a streamlined procedure to be followed whether or not temperature information is used in the data reduction of the PSP.

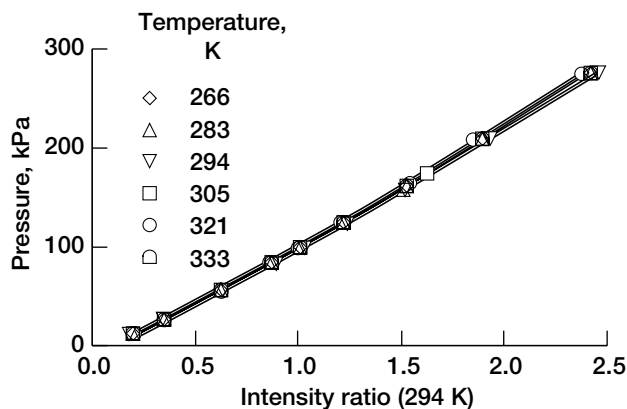
The old procedure for temperature correcting PSP images was to determine the intensity ratio and temperature at each pixel and then calculate the pressure by using the  $I_{REF}/I_{CAL} = f\{P, T\}$  calibration surface (top plot). The new simplified method goes one step further and assumes that, given the intensity ratio and temperature at each pixel, a corrected intensity ratio can be determined. The corrected intensity ratio is dependent on only temperature in the form of  $[I_{RATIO}]_{COR} = I_{RATIO}\{T\}$ ,



Calibration surface plot of PSP.



Calibration data shows temperature dependence of PSP.



*Temperature-corrected PSP: calibration data collapses to the reference temperature curve.*

since the intensity ratio is already pressure dependent. This correction collapses the family of curves in the bottom graph on the previous page to a single curve at the reference, as illustrated in the final graph.

The simplified temperature correction procedure streamlines the data reduction of PSP data by eliminating the need to use a three-dimensional lookup table for each pixel location. Once the corrected intensity ratio is computed, any number of traditional calibration techniques can be implemented to convert the normalized intensity images to pressure.

**Glenn contact:**

Timothy J. Bencic, (216) 433-5690,  
Timothy.J.Bencic@grc.nasa.gov

**Author:** Timothy J. Bencic

**Headquarters program office:** OAST

**Programs/Projects:** IT Base

## Surge Flow in a Centrifugal Compressor Measured by Digital Particle Image Velocimetry

A planar optical velocity measurement technique known as Particle Image Velocimetry (PIV) is being used to study transient events in compressors. In PIV, a pulsed laser light sheet is used to record the positions of particles entrained in a fluid at two instances in time across a planar region of the flow. Determining the recorded particle displacement between exposures yields an instantaneous velocity vector map across the illuminated plane. Detailed flow mappings obtained using PIV in high-speed rotating turbomachinery components are used to improve the accuracy of computational fluid dynamics (CFD) simulations, which in turn, are used to guide advances in state-of-the-art aircraft engine hardware designs.

Compressor stall is a catastrophic breakdown of the flow in a compressor that can lead to a loss of engine power, large pressure transients in the inlet and nacelle, and engine flameout. The distance on a performance map between the operating point of a compressor and its stall point is referred to as the stall margin. This margin must account for increased clearances within the compressor caused by throttle transients and component deterioration due to aging. Optimal engine designs tend toward minimal stall margins, since modifications to increase the stall margin typically result in heavier, less efficient, and less loaded compressors. However, if active or passive stall control is employed instead, stable operation over a wider range of flow conditions (improved stall margin) can be obtained with a minimal loss in performance.

Traditionally, dynamic pressure measurements have been employed to decipher the flow changes occurring during stall and surge events. These measurements yield vague indications of the kinematic changes in the flow field. The instantaneous flow-field capture capability of Digital Particle Image Velocimetry (DPIV) is better suited to the task of studying the change in flow conditions surrounding the development of stall precursors, stall cell propagation, and eventually, compressor surge. DPIV has been used at the NASA Glenn Research Center at Lewis Field to study the changes in the compressor flow field occurring during surge in a centrifugal compressor. The DPIV measurements show that flow reversal occurs in the diffuser during surge

and that forward flow is reestablished via a supersonic shock front that propagates down into the diffuser, as shown in the figure. These results are being used to understand the flow changes occurring during rotating stall that eventually lead to surge, and to optimize the stall control strategies that will be implemented in the compressor.

**Find out more about this research on the World Wide Web:**

<http://www.grc.nasa.gov/WWW/OptInstr/piv.html>

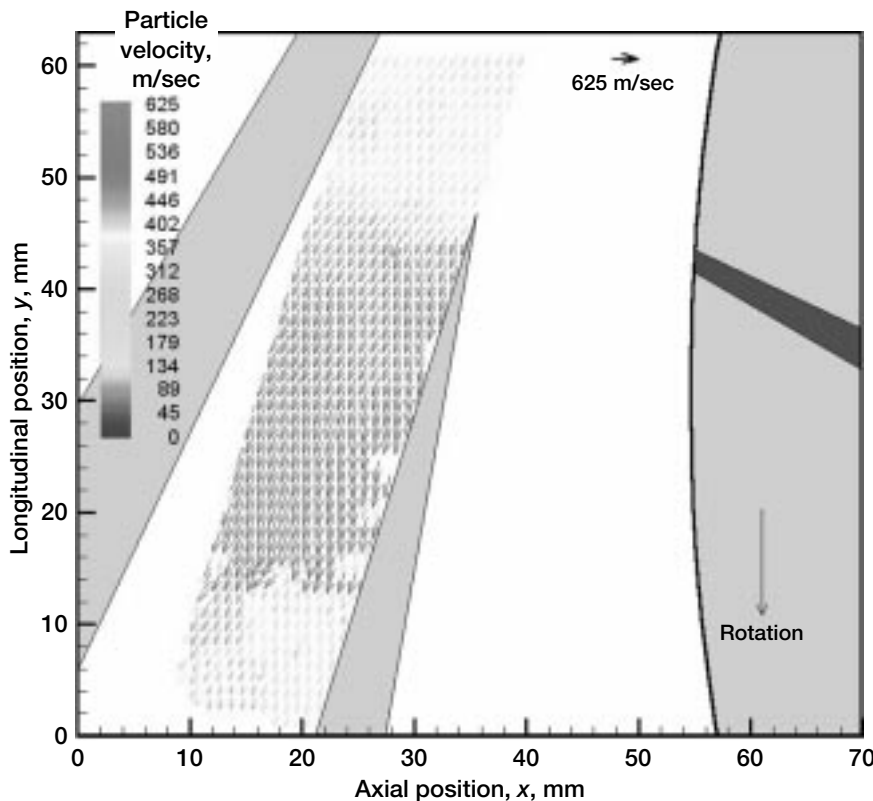
**Glenn contacts:**

Dr. Mark P. Wernet, (216) 433-3752, Mark.P.Wernet@grc.nasa.gov;  
 Gary J. Skoch, (216) 433-3396, Gary.J.Skoch@grc.nasa.gov; and  
 Michelle M. Bright, (216) 433-2304, Michelle.M.Bright@grc.nasa.gov

**Author:** Dr. Mark P. Wernet

**Headquarters program office:** OAST

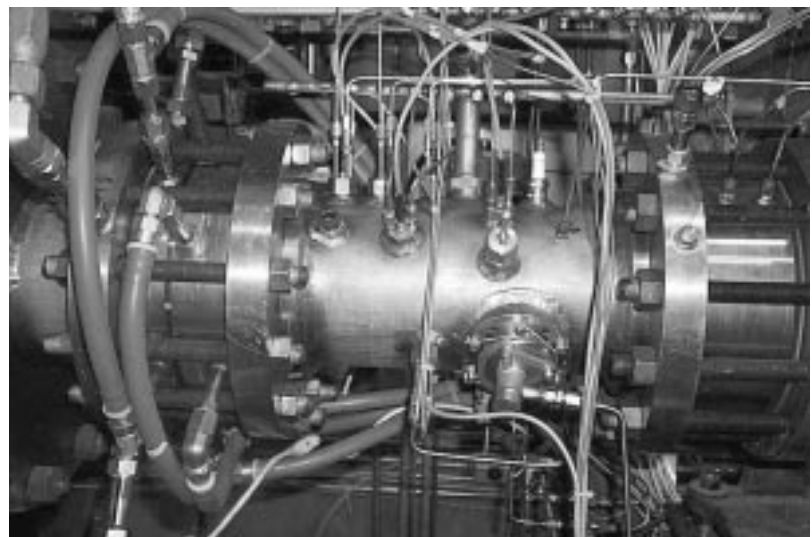
**Programs/Projects:** IITS, P&PM



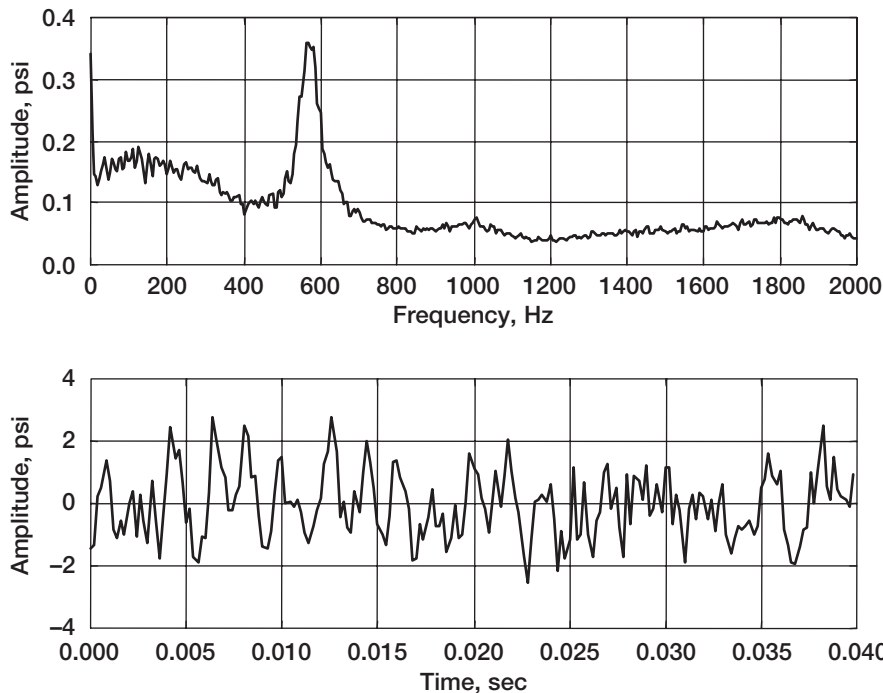
The instantaneous velocity field captured during compressor surge. The velocity vector magnitudes are coded by color. The position of the impeller is shown on the right, and the diffuser vanes are shown on the left. Velocity measurements are obtained in the region of the flow field illuminated by the laser light sheet.

## Engine-Scale Combustor Rig Designed, Fabricated, and Tested for Combustion Instability Control Research

Low-emission combustor designs are prone to combustor instabilities. Because active control of these instabilities may allow future combustors to meet both stringent emissions and performance requirements, an experimental combustor rig was developed for investigating methods of actively suppressing combustion instabilities. The experimental rig has features similar to a real engine combustor and exhibits instabilities representative of those in aircraft gas turbine engines. Experimental testing in the spring of 1999 demonstrated that the rig can be tuned to closely represent an instability observed in engine tests. Future plans are to develop and demonstrate combustion instability control using this experimental combustor rig.



Experimental combustor for stability and active control experiments.



*Experimental power spectral density and partial time trace of combustor internal pressure show 500-Hz thermoacoustic instability.*

The NASA Glenn Research Center at Lewis Field is leading the Combustion Instability Control program to investigate methods for actively suppressing combustion instabilities. Under this program, a single-nozzle, liquid-fueled research combustor rig was designed, fabricated, and tested (see the photo on the preceding page). The rig has many of the complexities of a real engine combustor, including an actual fuel nozzle and swirler, dilution cooling, and an effusion-cooled liner.

Prior to designing the experimental rig, a survey of aircraft engine combustion instability experience identified an instability observed in a prototype engine as a suitable candidate for replication. The frequency of the instability was 525 Hz, with an amplitude of approximately 1.5-psi peak-to-peak at a burner pressure of 200 psia. The single-nozzle experimental combustor rig was designed to preserve subcomponent lengths, cross-sectional area distribution, flow distribution, pressure-drop distribution, temperature distribution, and other factors previously found to be determinants of burner acoustic frequencies, mode shapes, gain, and damping.

Analytical models were used to predict the acoustic resonances of both the engine combustor and proposed experiment. The analysis confirmed that the test rig configuration and engine configuration had similar longitudinal

acoustic characteristics, increasing the likelihood that the engine instability would be replicated in the rig. Parametric analytical studies were performed to understand the influence of geometry and condition variations and to establish a combustion test plan. Cold-flow experiments verified that the design values of area and flow distributions were obtained. Combustion test results established the existence of a longitudinal combustion instability in the 500-Hz range with a measured amplitude approximating that observed in the engine (see the graphs). Modifications to the rig configuration during testing also showed the potential for injector independence.

The research combustor rig was developed in partnership with Pratt & Whitney of West Palm Beach, Florida, and United Technologies Research Center of East Hartford, Connecticut. Experimental testing of the combustor rig took place at United Technologies Research Center.

**Find out more about this research on the World Wide Web:**

<http://www.grc.nasa.gov/WWW/cdtb/projects/combustor/>

**Glenn contacts:**

John C. DeLaat, (216) 433-3744, [John.C.DeLaat@grc.nasa.gov](mailto:John.C.DeLaat@grc.nasa.gov); and Kevin J. Breisacher, (216) 433-7475, [Kevin.J.Breisacher@grc.nasa.gov](mailto:Kevin.J.Breisacher@grc.nasa.gov)

**Authors:**

John C. DeLaat and Kevin J. Breisacher

**Headquarters program office:** OAST

**Programs/Projects:** Propulsion Systems R&T Base Program, Turbomachinery and Combustion Technology Project

# Aerospike Engine Post-Test Diagnostic System Delivered to Rocketdyne

The NASA Glenn Research Center at Lewis Field, in cooperation with Rocketdyne, has designed, developed, and implemented an automated Post-Test Diagnostic System (PTDS) for the X-33 linear aerospike engine. The PTDS was developed to reduce analysis time and to increase the accuracy and repeatability of rocket engine ground test fire and flight data analysis. This diagnostic system provides a fast, consistent, first-pass data analysis, thereby aiding engineers who are responsible for detecting and diagnosing engine anomalies from sensor data. It uses analytical methods modeled after the analysis strategies used by engineers. Glenn delivered the first version of PTDS in September of 1998 to support testing of the engine's power pack assembly. The system was used to analyze all 17 power pack tests and assisted Rocketdyne engineers in troubleshooting both data acquisition and test article anomalies. The engine version of PTDS, which was delivered in June of 1999, will support all single-engine, dual-engine, and flight firings of the aerospike engine.

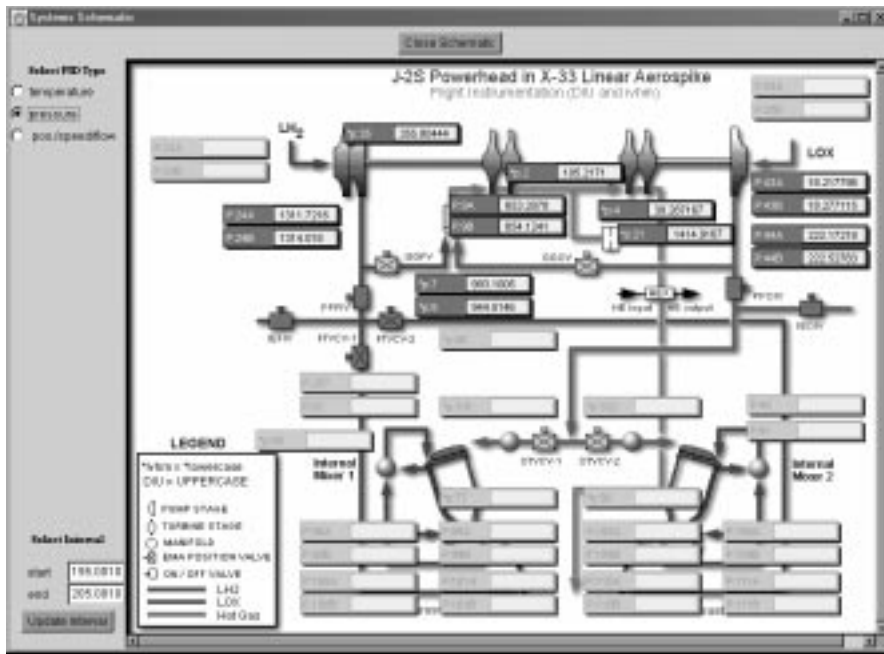
The aerospike engine PTDS has two primary components: the analysis system and the viewing system. The analysis system performs automated diagnosis and performance assessment of the sensors, valves, turbo-machinery, gas generator, thrust chamber assembly, nozzle, and facility thrust measurement system. Open-loop and closed-loop system-level models of the aerospike engine are employed for model-based fault detection. Detailed performance predictions are generated for each component, and data are statistically characterized during startup and shut-down transients and at key steady-state conditions. Finally, life tracking is performed on a test article basis.

The viewing system, which provides the essential interface to the data and the analysis results, is Web-based to promote platform independence. Data and results can be accessed through reports, annotated schematics, a sophisticated plotting tool, or an interactive statistics tool. The plotting tool, called WebPlot, and the statistics tool were provided to promote experimentation with the data and with the PTDS-generated performance predictions; such experimentation continues to facilitate an understanding of both the nominal and off-nominal behavior of aerospike engine subsystems. Users can actually expand the routine analysis performed by the aerospike engine PTDS through statistics interface requests.

The analysis and viewing system architectures designed for the aerospike engine PTDS emphasize modularity, extensibility, and reusability. The modular architecture accommodates both procedural and nonprocedural knowledge-based components, thereby permitting the inclusion of conventional algorithms as well as heuristic, model-based, and case-based analyses. Extensibility has been essential, since the PTDS has evolved concurrently with the engine system design. Although domain knowledge and limits are specific to this engine, many aspects of the analysis system such as the event-detection routines, statistical characterization, and sensor validation methodology have been and are being applied to other aerospace systems as well. Likewise, the statistics tool and WebPlot are generic and, in addition to aerospike data, have successfully handled data from



The Web-based viewing system allows users to access PTDS analysis results and data through reports, an interactive plotting tool called WebPlot, schematics, and an interactive statistics tool.



The schematic portion of the viewing system provides users with access to values for key test parameters during a user-specified time interval. Sensor failure information also is given.

the Space Shuttle Main Engine and from the Fastrac engine developed by NASA Marshall Space Flight Center. Current efforts are focused on preparing for the engine test and increasing the depth of the automated data analysis.

**Dynacs Engineering Company, Inc., contact:**

Claudia M. Meyer, (216) 977-7511, Claudia.M.Meyer@grc.nasa.gov

**Author:** Claudia M. Meyer

**Headquarters program office:** OAST

**Programs/Projects:** X-33, RLV, STR

## Communications Technology

### Internet Protocol Suite Enhanced for Satellite-Based Networks

Research conducted by the Satellite Networks and Architectures Branch of the NASA Glenn Research Center at Lewis Field as well as by GTE Internetworking has increased the performance of the standard Internet protocol efficiency over long-delay satellite channels (ref. 1). These protocol extensions will enable efficient operation of standard off-the-shelf networking software in NASA's network of space-based assets (e.g., the International Space Station and data-gathering satellites).

The work at Glenn focused on two areas. The first was the startup phase of a transfer between two computers. This period in a transfer has been shown to use the available network resources inefficiently. We experimented with several ways to improve the network utilization during this period (refs. 2 and 3). The second area was making the protocols estimate the available bandwidth of the network path so that the transfer could make better use of the available resources (ref. 4). These studies have shown that transfer times improve when the mechanisms developed at Glenn are used. Finally, Glenn funded GTE Internetworking to incorporate a "pacing" algorithm into the standard Internet protocols. This protocol

extension provides high performance over a long-delay-based network, while minimizing the impact of these transfers on shorter terrestrial network elements. A simulation study (ref. 5) showed that performance increased when pacing protocols were used instead of the standard protocols.

#### References

1. Allman, M.; Glover, D.; and Sanchez, L.: Enhancing TCP Over Satellite Channels Using Standard Mechanisms. RFC 2488, BCP 28, Jan. 1999. (Available online: <http://roland.grc.nasa.gov/~mallman/papers/rfc2488.txt>)

2. Allman, M.: TCP Byte Counting Refinements. ACM Computer Communication Review, vol. 29, no. 3, 1999. (Available online: <http://roland.grc.nasa.gov/~mallman/papers/bc-ccr.ps>)
3. Allman, M.; Floyd, S.; and Partridge, C.: Increasing TCP's Initial Window. RFC 2414, Sept. 1998. (Available online: <http://roland.grc.nasa.gov/~mallman/papers/rfc2414.txt>)
4. Allman, M.; Paxson, V.: On Estimating End-to-End Network Path Properties. ACM SIGCOMM, Cambridge, MA, Sept. 1999. (Available online: <http://roland.grc.nasa.gov/~mallman/papers/estimation.ps>)
5. Kulik, J.: A Simulation Study of Paced TCP. Proceedings of the Workshop on Satellite-Based Information Systems (WOSBIS), Dec. 1999.

General information about NASA Glenn's Internet protocol research can be found on the World Wide Web: <http://ctd.grc.nasa.gov/5610/5610.html>

**GTE Internetworking contact:**

Mark A. Allman, (216) 433-6586,  
Mark.A.Allman@grc.nasa.gov

**Glenn contact:**

William D. Ivancic, (216) 433-3494,  
William.D.Ivancic@grc.nasa.gov

**Author:** Mark A. Allman

**Headquarters program office:**

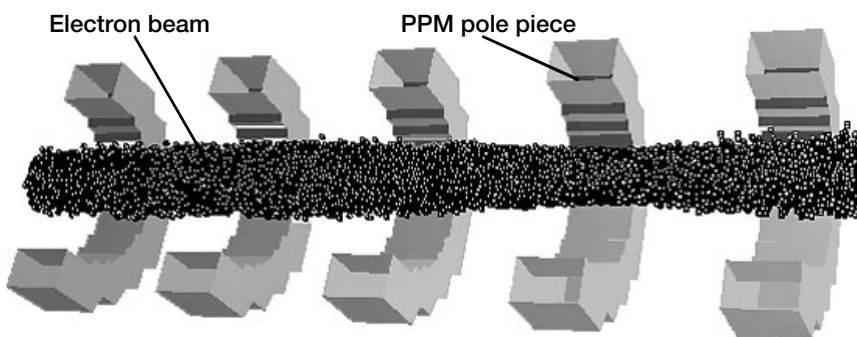
OSS (SCO)

**Programs/Projects:** R&T

## Three-Dimensional Electron Optics Model Developed for Traveling-Wave Tubes

A three-dimensional traveling-wave tube (TWT) electron beam optics model including periodic permanent magnet (PPM) focusing has been developed at the NASA Glenn Research Center at Lewis Field. This accurate model allows a TWT designer to develop a focusing structure while reducing the expensive and time-consuming task of building the TWT and hot-testing it (with the electron beam). In addition, the model allows, for the first time, an investigation of the effect on TWT operation of the important azimuthally asymmetric features of the focusing stack.

The TWT is a vacuum device that amplifies signals by transferring energy from an electron beam to a radiofrequency (RF) signal. A critically important component is the focusing structure, which keeps the electron beam from diverging and intercepting the RF slow-wave circuit. Such an interception can result in excessive circuit heating and decreased efficiency, whereas excessive growth in the beam diameter can lead to backward wave oscillations and premature saturation, indicating a serious reduction in tube performance. The most commonly used focusing structure is the PPM stack, which consists of a sequence of cylindrical iron pole pieces and opposite-polarity magnets.



*Three-dimensional cutaway of electron beam focused by a PPM stack (magnets and beam tunnel not shown).*

Typically, two-dimensional electron optics codes are used in the design of magnetic focusing devices. In general, these codes track the beam from the gun downstream by solving equations of motion for the electron beam in static-electric and magnetic fields in an azimuthally symmetric structure. Because these two-dimensional codes cannot adequately simulate a number of important effects, the simulation code MAFIA (solution of Maxwell's equations by the Finite-Integration-Algorithm) was used at Glenn to develop a three-dimensional electron optics model (refs. 1 and 2). First, a PPM stack was modeled in three dimensions. Then, the fields obtained using the magnetostatic solver were loaded into a particle-in-cell solver where the fully three-dimensional behavior of the beam was simulated in the magnetic focusing field. For the first time, the effects of azimuthally asymmetric designs and critical azimuthally asymmetric characteristics of the focusing stack (such as shunts, C-magnets, or magnet misalignment) on electron beam behavior have been investigated. The illustration shows a cutaway portion of a simulated electron beam focused by a PPM stack.

Although solid-state electronics have replaced vacuum devices in many areas, certain applications such as satellite communications and radar require frequencies and power in excess of what solid-state devices can provide. The phenomenal growth of satellite communications and planned NASA missions anticipating significantly higher data rates have created great demand for TWT amplifiers with greater efficiencies, frequencies, and power than existing designs. Accurate simulation tools such as the three-dimensional electron optics model are imperative if these demands are to be met with first-pass TWT designs satisfying system specifications.

**Find out more about this research on the World Wide Web:**  
<http://ctd.grc.nasa.gov/5620/5620.html>

#### References

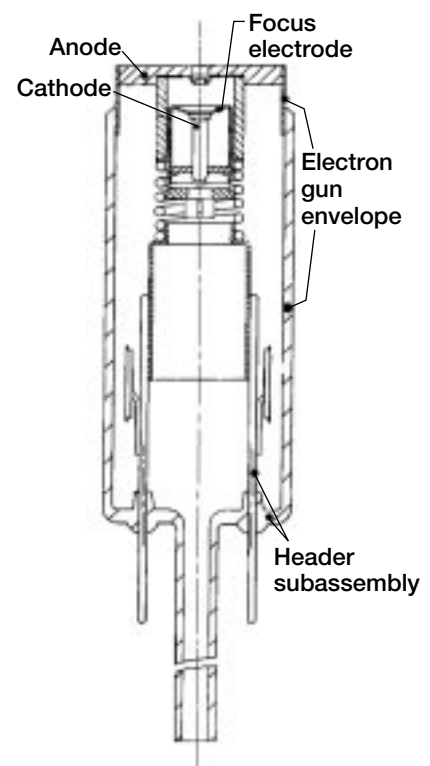
1. Weiland, T.: On the Numerical Solution of Maxwell's Equations and Applications in the Field of Accelerator Physics. Part. *Accel.*, vol. 15, 1984, pp. 245–292.
2. Weiland, T.: On the Unique Numerical Solution of Maxwellian Eigenvalue Problems in Three Dimensions. Part. *Accel.*, vol. 17, 1985, pp. 227–242.

## Modular Low-Heater-Power Cathode/Electron Gun Assembly for Microwave and Millimeter Wave Traveling Wave Tubes

A low-cost, low-mass, electrically efficient, modular cathode/electron gun assembly has been developed by FDE Inc. of Beaverton, Oregon, under a Small Business Innovation Research (SBIR) contract with the NASA Glenn Research Center at Lewis Field. This new assembly offers significant improvements in the design and manufacture of microwave and millimeter wave traveling-wave tubes (TWT's) used for radar and communications. It incorporates a novel, low-heater-power, reduced size and mass, high-performance barium-dispenser type thermionic cathode (ref. 1) and provides for easy integration of the cathode into a large variety of conventional TWT circuits. Among the applications are TWT's for Earth-orbiting communication satellites and for deep space communications, where future missions will require smaller spacecraft, higher data transfer rates (higher frequencies and radiofrequency output power), and greater electrical efficiency. A particularly important TWT application is in the microwave power module (a hybrid microwave/millimeter wave amplifier consisting of a low-noise solid-state driver, a small TWT, and an electronic power conditioner integrated into a single compact package), where electrical efficiency and thermal loading are critical factors and lower cost is needed for successful commercialization.

The design and fabrication are based on practices used in producing cathode ray tubes (CRT's), which is one of the most competitive and efficient manufacturing operations in the world today. The approach used in the design and manufacture of thermionic cathodes and electron guns for CRT's has been optimized for fully automated production, standardization of parts, and minimization of costs. It is applicable to the production of similar components for microwave tubes, with the additional benefits of low mass and significantly lower cathode heater power (less than half that of dispenser cathodes presently used in TWT's).

**Glenn contact:**  
Dr. Vernon O. Heinen, (216) 433-3245,  
[Vernon.O.Heinen@grc.nasa.gov](mailto:Vernon.O.Heinen@grc.nasa.gov)  
**Author:** Carol L. Kory  
**Headquarters program office:**  
OSS (ATMS)  
**Programs/Projects:** HRDD, CETDP



*Modular cathode/electron gun assembly.*

The modular cathode/electron gun assembly consists of four subassemblies—the cathode, the focus electrode, the header (including the electrical feedthroughs), and the gun envelope (including the anode)—a diagram of which is shown in the figure. The modular construction offers a number of significant advantages, including flexibility of design, interchangeability of parts, and a drop-in final assembly procedure for quick and accurate alignment. The gun can accommodate cathodes ranging in size from 0.050- to 0.250-in. in diameter and is applicable to TWT's over a broad range of sizes and operating parameters, requiring the substitution of only a few parts: that is, the cathode, focus electrode, and anode. The die-pressed cathode pellets can be made with either flat or concave (Pierce gun design) emitting surfaces. The gun can be either gridded (pulse operation) or ungridded (continuous operation). Important factors contributing to low cost are the greater use of CRT materials and parts, the standardization of processes (welding and mechanical capture), and tooling amenable to automated production. Examples are the use of simple shapes, drawn or stamped metal parts, and parts joined by welding or mechanical capture.

Feasibility was successfully demonstrated in the retrofit and testing of a commercial Ka-band (22-GHz) TWT. The modular cathode/electron gun assembly was computer modeled to replicate the performance of the original electron gun and fabricated largely from existing CRT parts. Significant test results included demonstration of low heater power (1.5-W, 1010 °C brightness temperature for a 0.085-in.-diameter cathode), mechanical ruggedness (100g shock and vibration tests in accordance with military specifications (MIL specs)), and a very fast warmup. The results of these tests indicate that the low-cost CRT manufacturing

approach can be used without sacrificing performance and reliability.

**Find out more on the World Wide Web:** <http://www.fdeassc.com>

**References**

1. Wintucky, E.G.: Novel Low-Cost, Low-Power Miniature Thermionic Cathode Developed for Microwave/Millimeter Wave Tube and Cathode Ray Tube Applications. NASA/TM-1999-208815, 1999, pp. 82-83. (Available online: <http://www.grc.nasa.gov/WWW/RT1998/5000/5620wintucky.html>)

**Glenn contact:**

Edwin G. Wintucky, (216) 433-3510, [Edwin.G.Wintucky@grc.nasa.gov](mailto:Edwin.G.Wintucky@grc.nasa.gov)

**FDE Inc. contact:**

Bernard K. Vancil, (503) 628-0703, [Bernie@fdeassc.com](mailto:Bernie@fdeassc.com)

**Author:** Edwin G. Wintucky

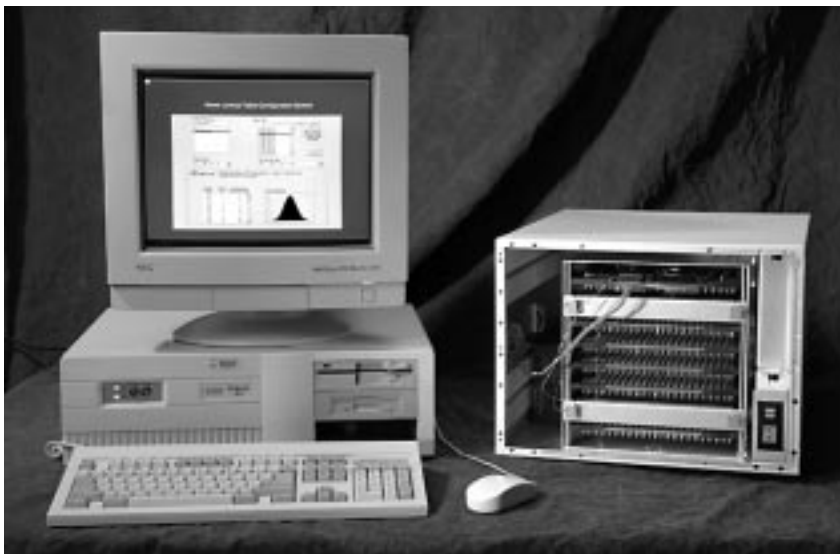
**Headquarters program office:** OSS (ATMS)

**Programs/Projects:** Space Communications

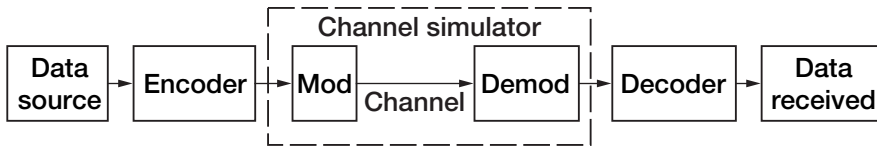
## Digital Channel Simulator Developed and Tested

The Digital Channel Simulator (DCS) is a real-time test set developed in-house by the NASA Glenn Research Center at Lewis Field that simulates the characteristics of the modulator, demodulator, and transmission

medium in a typical communications system to enable controlled laboratory testing of codec pairs. The DCS can support data rates up to 100 megasymbols per second (Msymbols/sec) with symbol sizes up to 10 bits and is compatible with both TTL (transistor transistor logic) and ECL (emitter coupled logic) interfaces. Because of its use of digital integrated circuits (IC's), the DCS offers the user accurate and repeatable testing while maintaining a simple reconfiguration of the modulation scheme and noise characteristics. The PC-based graphical user interface (GUI) assures user friendly operation for configuring, controlling, and monitoring the DCS and system during tests.

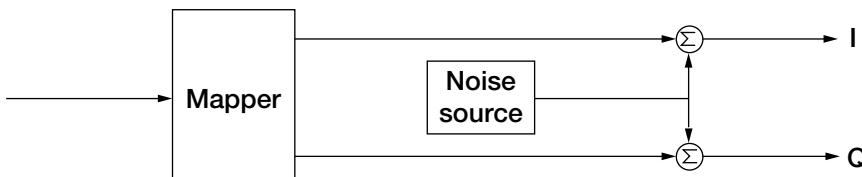


Digital Channel Simulator.

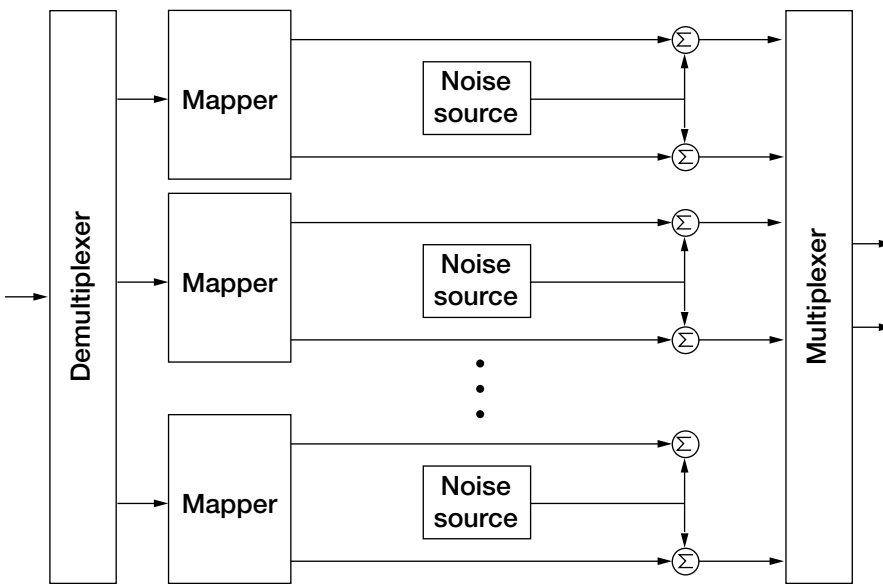


Typical communications system showing items simulated with DCS.

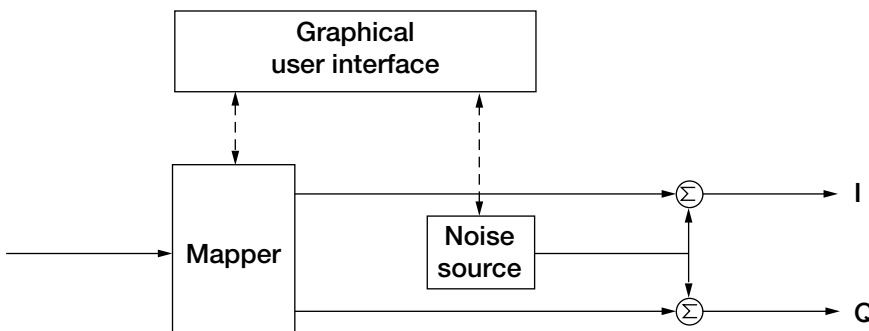
In a typical communications system, the modulator places a symbol in constellation space and puts it on a carrier to be sent to the demodulator. Because of noise on the channel, the I and Q position in constellation space cannot be recovered exactly, and the received coordinates shift.



DCS functional block diagram.



DCS block diagram.



Connections between graphical user interface and DCS.

To mimic this process in the laboratory, the DCS uses a mapper to place the symbol in constellation space. It simulates the shift in coordinates by digitally adding "noise" to the I and Q values.

The mapper and noise source are implemented in lookup tables. Modulation schemes and noise characteristics are set by the values loaded in these tables. The mapper also has a pass-through mode to facilitate modulator testing, allowing noise to be added to 8-bit I and Q values of modulated data without a second mapping.

To achieve high symbol rates, eight processing circuits are placed in parallel between an ECL demultiplexer and multiplexer.

A graphical user interface was developed to calculate, load, and verify the values for the lookup tables. This interface can also be used to debug and verify proper operation of the channel simulator or to control an experiment.

Operation of the DCS has been verified through three tests: a low-speed comprehensive system test, a high-speed (20 Msymbols/sec) test of the TTL interface, and a high-speed (100 Msymbols/sec) test of the ECL interface. The DCS is now ready for use by NASA and external customers.

**Glenn contact:**

Thomas P. Bizon, (216) 433-8121,  
Thomas.P.Bizon@grc.nasa.gov

**Author:** Thomas P. Bizon

**Headquarters program office:** OSS

**Programs/Projects:**

Space Communications

## ACTS High-Speed VSAT Demonstrated

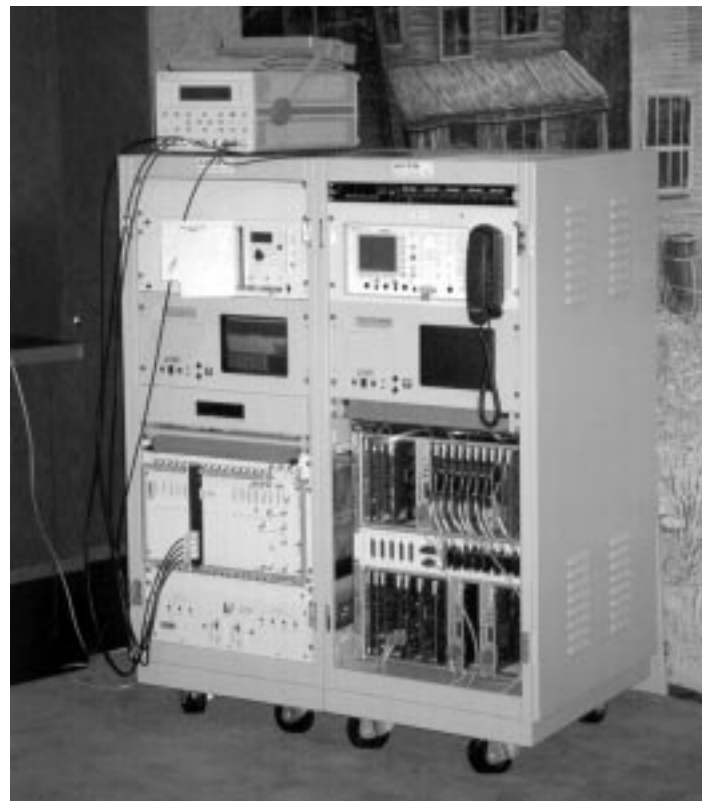
The Advanced Communication Technology Satellite (ACTS) developed by NASA has demonstrated the breakthrough technologies of Ka-band transmission, spot-beam antennas, and onboard processing. These technologies have enabled the development of very small and ultrasmall aperture terminals (VSAT's and USAT's), which have capabilities greater than have been possible with conventional satellite technologies.

The ACTS T1 VSAT operates at a burst rate of 27.5 Mbps, but the maximum user data rate is 1.792 Mbps. The throughput efficiency is slightly more than 6.5 percent. For an operational network, this level of overhead will greatly increase the cost of the user Earth stations, and that increased cost must be repeated thousands of times, which may ultimately reduce the market for such a system.

The ACTS High Speed VSAT (HS VSAT) is an effort at the NASA Glenn Research Center at Lewis Field to experimentally demonstrate the maximum user throughput data rate that can be achieved using the technologies developed and implemented on ACTS. This was done by operating the system uplinks as frequency division multiple access (FDMA), essentially assigning all available time division multiple access (TDMA) time slots to a single user on each of two uplink frequencies. Preliminary results show that, using a 1.2-m antenna in this mode, the High Speed VSAT can achieve between 22 and 24 Mbps of the 27.5 Mbps burst rate, for a throughput efficiency of 80 to 88 percent.

The High Speed VSAT is the result of an effort to improve the throughput efficiency of the ACTS VSAT by eliminating, in experimental scenarios, any uplink TDMA and devoting all the time slots in the frame to a single Earth station. Its design combines the individual channels in a single high-speed interface, rather than in multiple 64-kbps ports. Then, the channels are buffered and formatted to meet standard network protocols and data rates. The photos to the right show the outdoor and indoor units for a High Speed VSAT.

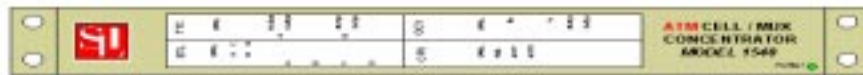
Development of the high-speed port involved the replication of the T1 VSAT circuit buffer cards, whose primary function is buffering data between the modem bus and the serial port connection. It also involved the definition of a high-speed port address in the address space, and implementation of the



*High Speed VSAT. Top: Outdoor unit. Bottom: Indoor unit.*

custom T1 VSAT address and data bus interfaces on the board. Initial experiments used a prototype high-speed interface; an improved high-speed interface has been developed to support further experimentation.

The new High Speed VSAT interface board for the ACTS satellite will enable services in the 25-Mbps range, thus increasing user throughput efficiency from 6.5 to over 80 percent. To maximize the number of services provided and accommodate the maximum number of users, the High Speed VSAT architecture includes a commercial asynchronous transfer mode (ATM) concentrator (the Cell Mux Concentrator) in addition to the high-speed board. This off-the-shelf device, diagrammed in the following figure, allows several high-data-rate interfaces while it does all the processing for ATM transmission.

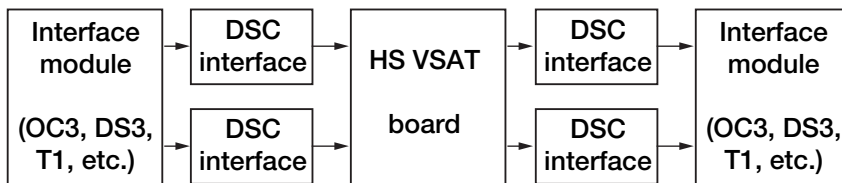


Off-the-shelf Cell Mux Concentrator for the High Speed VSAT.

The Cell Mux Concentrator (ref. 4) is a flexible, modular, scaleable, and cost-effective ATM cell multiplexer (Mux) that uses ATM cell bus architecture. It provides the system/network integrator with an ATM cell platform that operates on the "net edge" to concentrate both cell traffic (frame relay and ATM) and legacy (non-ATM) traffic. It supports both ATM cell and legacy data applications and networks, performs HEC (header error control) byte search functions, multiplexes and switches ATM cell traffic, provides synchronous interfaces for satellite and secure networks, and gives cost-effective access to ATM networks for legacy communications equipment and applications.

There are several applications for this interface (ref. 4), but the most interesting is the transmission of ATM/SONET through the satellite. This ATM concentrator allows a satellite transmission network to transport ATM cell-bearing traffic at user programmable rates in 8 kbps increments. This facilitates an "ATM anywhere" capability, whereby remote users can tap into ATM networks via satellite access. Users can program the device to gain access via any available or economical satellite segment.

By using the HS VSAT interface to the ATM programmable concentrator, any number of possible applications can be transmitted through ACTS. The ATM concentrator can be configured to process and format ATM cells from any of its interface modules and route them to the DSC interface module. The following figure shows a block diagram of the end-to-end user interface.



End-to-end user interface for the High Speed VSAT. (Data rates: OC3 = 155 Mbps, DS3 = 43 Mbps, T1 = 1.544 Mbps.)

This new flexible, scaleable interface will allow cost-effective access to ATM networks and the transmission of ATM cells at low speeds over commercial systems. It is expected to be fully operational by the fall of 1998. Experiments being planned include a telemedicine/telemammography demonstration, ATM over satellite, TCP/IP (Internet protocol) over satellite, video-conferencing and distance education, LAN to ATM networks, and a high-speed Internet demonstration. New experiments can be scheduled through the ACTS experiments office.

#### References

1. Campanella, S.J.: An Onboard Processing Beam Hopping Satellite. AIAA Ninth International Conference on Digital Satellite Communications, May 1992.
2. Dendy, R.P.: ACTS: Next Generation Satellite Technologies for Tomorrow's Communication Satellite Applications. National Engineering Consortium Annual Review of Communications, vol. 46, 1992, pp. 892-902.
3. O'Reilly, M.; Jirberg, R.; and Spisz, E.: LBR-2 Earth Stations for the ACTS Program. AIAA Paper 90-0838, 1990.
4. Information on ATM concentrator and modules, Aug. 1998. Online information: <http://www.slidata.com/m1500.htm>

#### Glenn contact:

Quang K. Tran, (216) 433-2723,  
Quang.K.Tran@grc.nasa.gov

**Author:** Quang K. Tran

**Headquarters program office:** OSS

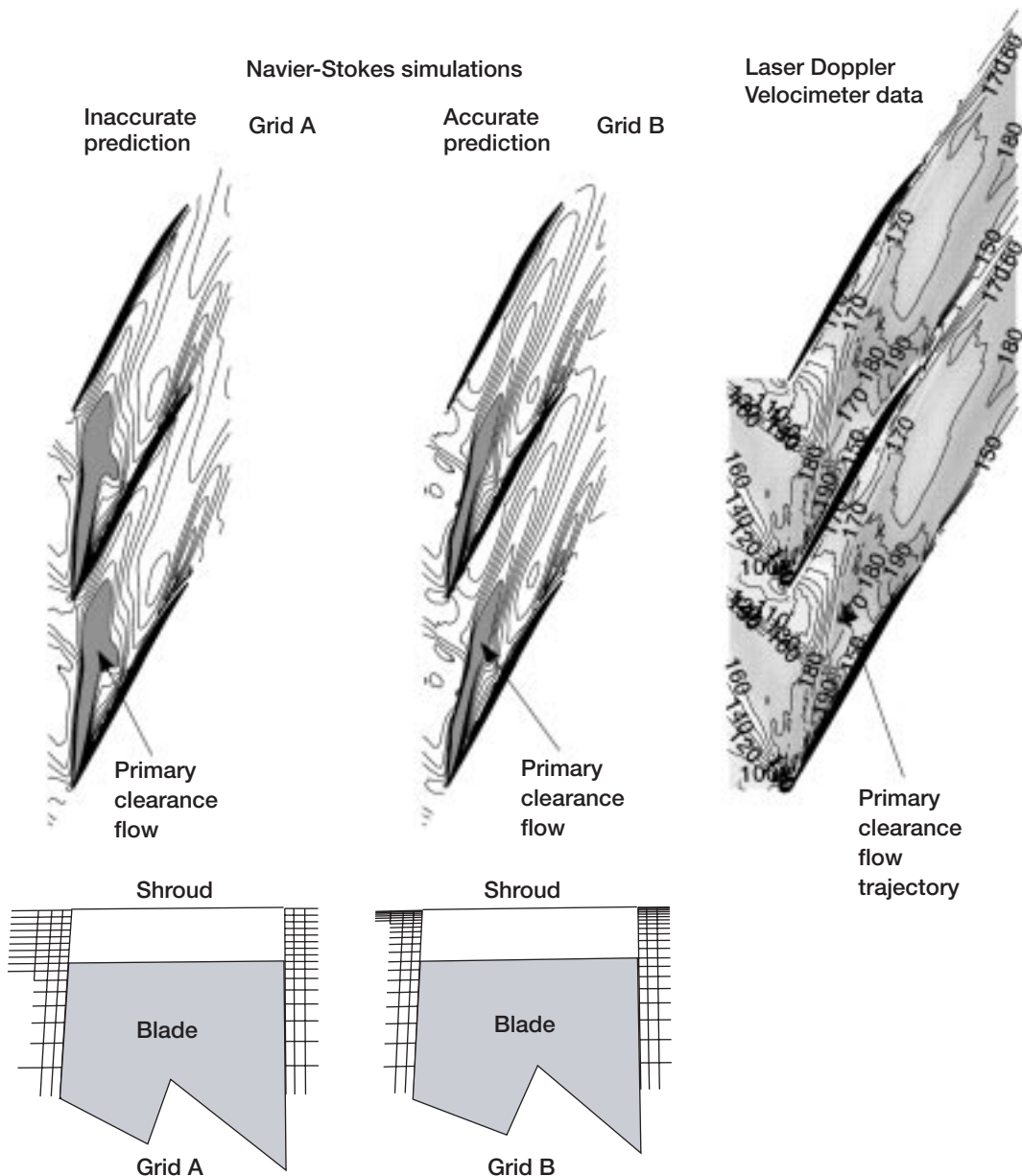
**Programs/Projects:** ACTS

# Turbomachinery and Propulsion Systems

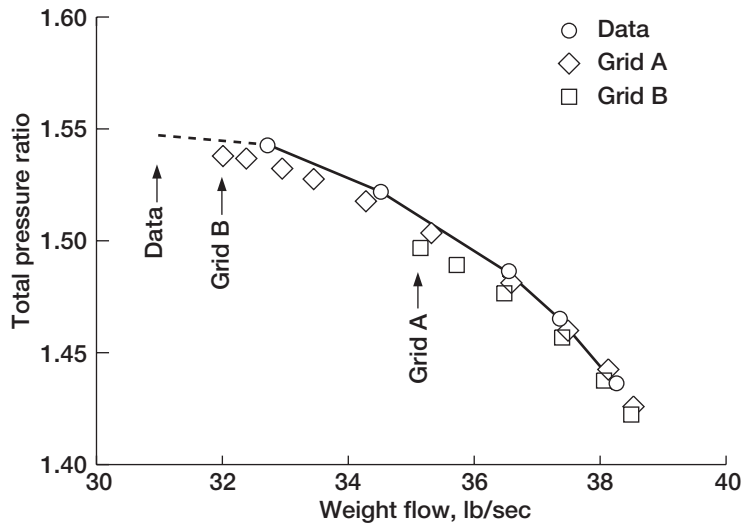
## Accuracy of Numerical Simulations of Tip Clearance Flow in Transonic Compressor Rotors Improved Dramatically

The tip clearance flows of transonic compressor rotors have a significant impact on rotor and stage performance. Although numerical simulations of these flows are quite sophisticated, they are seldom verified through rigorous comparisons of numerical and measured data because, in high-speed machines, measurements acquired in sufficient detail to be useful are rare. Researchers at the NASA Glenn Research Center at Lewis Field compared measured tip clearance flow details (e.g., trajectory and radial extent) of the NASA Rotor 35 with results obtained from a numerical

simulation. Previous investigations had focused on capturing the detailed development of the jetlike flow leaking through the clearance gap between the rotating blade tip and the stationary compressor shroud. However, we discovered that the simulation accuracy



Predicted and measured rotor tip clearance flow in the blade tip plane of the NASA 35.



Predicted and measured rotor operating range

depends primarily on capturing the detailed development of a wall-bounded shear layer formed by the relative motion between the leakage jet and the shroud.

The figure on the preceding page compares the Laser Doppler Velocimeter (LDV) measurements with the clearance flow on a plane at the blade tip as calculated with two different grids. We found that because the wall-bounded shear layer lies very close to the shroud it cannot be captured by standard grid topologies such as Grid A, which employs a uniformly spaced mesh with relatively few points in the clearance gap. In contrast, Grid B employs a stretched mesh to position points closer to the shroud wall with only a small increase in the total number of points in the clearance gap.

Differences in the predicted clearance flow result in significantly different rotor performance characteristics in the simulations. For example, the operating range for Rotor 35 (see the graph) will be greatly underestimated from a simulation using Grid A. Simulations using the improved

grid topology, Grid B, demonstrate dramatically better agreement with the data.

Additional rotor performance effects, a detailed explanation for the improved solution accuracy, and recommendations for a numerical simulation setup to obtain accurate results are discussed in reference 1.

#### References

1. Van Zante, D.E., et al.: Recommendations for Achieving Accurate Numerical Simulation of Tip Clearance Flows in Transonic Compressor Rotors. ASME Paper 99-GT-390, 1999.

#### Glenn contacts:

Dr. Dale E. Van Zante, (216) 433-3640, Dale.E.Vanzante@grc.nasa.gov;  
 Dr. Anthony J. Strazisar, (216) 433-5881, Anthony.J.Strazisar@grc.nasa.gov; and  
 Jerry R. Wood, (216) 433-5880, Jerry.R.Wood@grc.nasa.gov

#### U.S. Army Vehicle Technology Center

at Glenn contact: Dr. Michael D. Hathaway, (216) 433-6250, Michael.D.Hathaway@grc.nasa.gov

Authors: Dr. Dale E. Van Zante, Dr. Anthony J. Strazisar, Jerry R. Wood, Dr. Michael D. Hathaway, and Dr. Theodore H. Okiishi

Headquarters program office: OAST

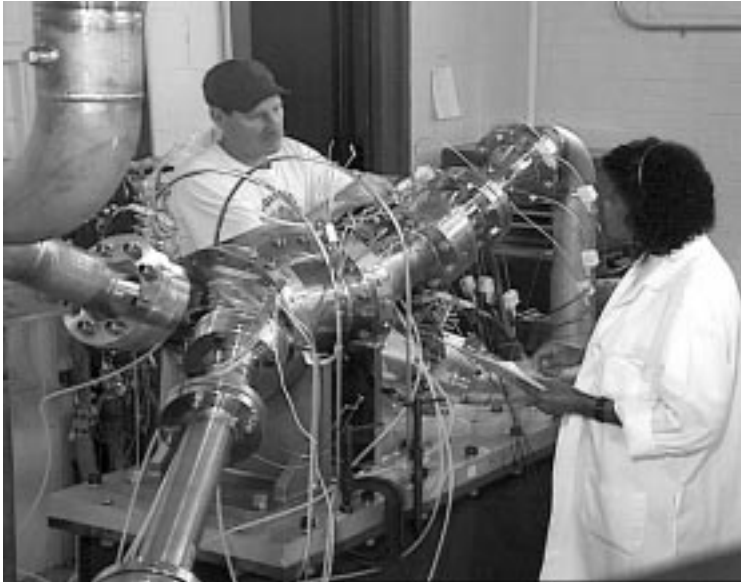
Programs/Projects: TCT

## Wave Rotor Technology Tested Successfully

The wave rotor is a turbomachinery component that accomplishes the compression and expansion processes of a high-pressure spool (i.e., a gas generator or gasifier) within a single component. It is self-cooling and aerodynamically compatible with the low corrected flow rates supplied by the compressors of modern, high-pressure-ratio turboshaft engines. A wave rotor can be embedded concentrically between the high-pressure compressor and high-pressure turbine to increase the overall pressure ratio of the gas turbine engine by a factor of three and increase the peak temperature by 25 percent, without increasing the temperatures of the rotating machinery components. These thermodynamic increases enhance gas turbine engine power and efficiency significantly. For example, the wave rotor is predicted to increase the specific power of the Rolls-Royce

Allison model 250 helicopter engine by 18 percent while reducing specific fuel consumption by 15 percent.

A four-port wave-rotor component (see the photo) that could be used to top future advanced gas turbine engines was successfully tested at the NASA Glenn Research Center at Lewis Field in this past year. This series of experiments established



*Four-port wave rotor test rig.*

the first operating map for a four-port throughflow wave rotor, marking a major milestone for Glenn's wave rotor project. The wave-rotor pressure ratio—a measure of performance—was found to be a function of corrected heat addition, corrected flow, and corrected rotor speed, in qualitative agreement with numerical predictions from in-house computational fluid dynamics (CFD) codes. The performance levels were lower than anticipated, and this has been attributed to augmented heat transfer between the rotor and the working fluid. The in-house CFD tool for wave-rotor design and analysis was improved and further validated with the on- and off-design data generated during the experiments. The wave-rotor operating map and the validated CFD tool are key to future wave rotor technology development.

Progress toward the planned demonstration of a four-port wave rotor within a small turboshaft engine was made in the past year under a contracted effort with Rolls-Royce Allison. Previous work included a preliminary design and general layout of the wave-rotor-topped engine, a detailed cycle analysis that established the predicted performance levels of the demonstrator engine, and a successful aerodynamic design of low-loss transition ducts for porting hot gases from the wave rotor to the high-pressure turbine. In the past year, the mechanical design of the rotor portion of the wave rotor was initiated. The work includes preliminary design and detailed heat transfer, stress, and structural dynamics analyses.

**Glenn contact:**

Dr. Gerard E. Welch, (216) 433-8003,  
Gerard.E.Welch@grc.nasa.gov

**Authors:** Dr. Gerard E. Welch, Dr. Jack Wilson, and Dr. Daniel E. Paxson

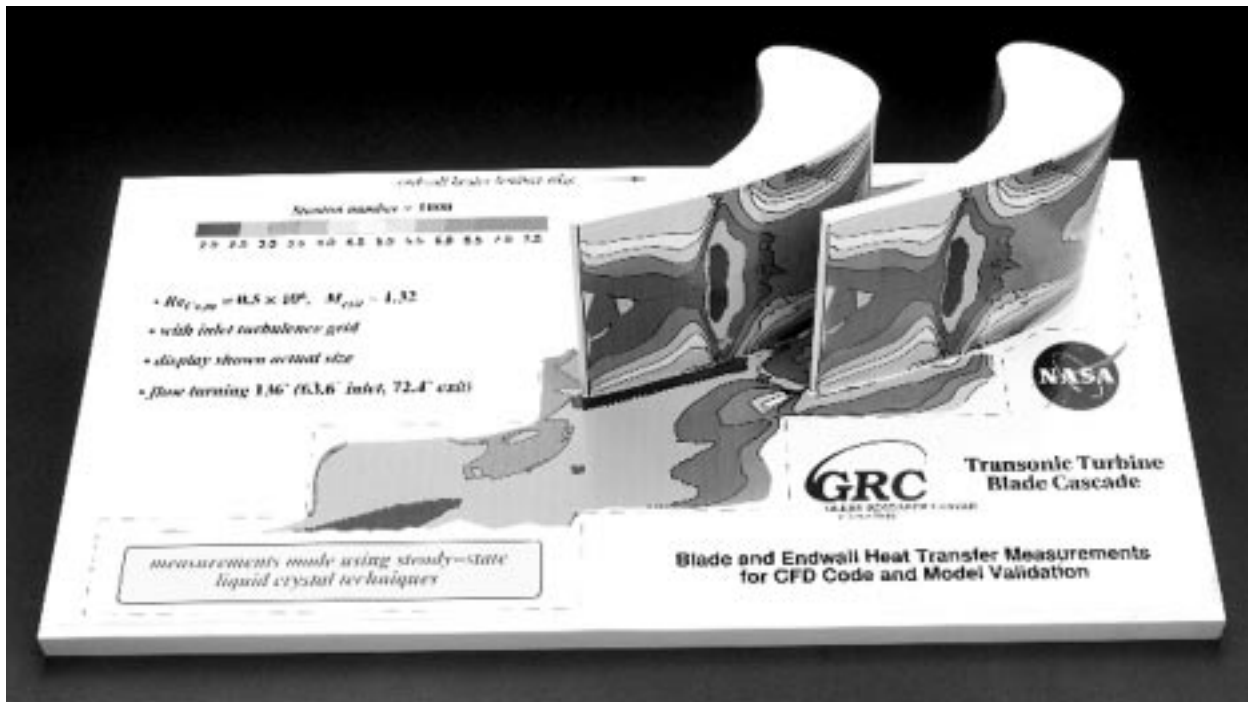
**Headquarters program office:** OAST

**Programs/Projects:** Propulsion R&T

## **Turbine Blade and Endwall Heat Transfer Measured in NASA Glenn's Transonic Turbine Blade Cascade**

Higher operating temperatures increase the efficiency of aircraft gas turbine engines, but can also degrade internal components. High-pressure turbine blades just downstream of the combustor are particularly susceptible to overheating. Computational fluid dynamics (CFD) computer programs can predict the flow around the blades so that potential hot spots can be identified and appropriate cooling schemes can be designed. Various blade and cooling schemes can be examined computationally before any hardware is built, thus saving time and effort. Often though, the accuracy of these programs has been found to be inadequate for predicting heat transfer. Code and model developers need highly detailed aerodynamic and heat transfer data to validate and improve their analyses. The Transonic Turbine Blade Cascade was built at the NASA Glenn Research Center at Lewis Field to help satisfy the need for this type of data.

The Transonic Turbine Blade Cascade facility can match engine conditions through pertinent flow parameters such as the Reynolds number, the Mach number, and the inlet turbulence levels. Future high-pressure turbines will eliminate blade rows by producing higher loading on a single stage. Single-stage turbines inherently have regions of supersonic flow and a high degree of flow turning, both of which are reproduced in the facility.



Display model of blade and endwall heat transfer measurements from the NASA Transonic Turbine Blade Cascade.

A long inlet section is used to build up thick inlet boundary layers. These boundary layers, combined with the high flow turning, result in highly three-dimensional flow in the blade passage, again representative of flow in an actual engine. The large scale, lower temperatures, and liquid-crystal temperature measurement technique allow for very detailed, full surface measurements to be obtained on the blades and endwalls. The generic, next-generation test blade was designed with a relatively large, blunt leading edge that reduced the peak heat transfer typically observed near the stagnation region. The full surface blade and endwall data obtained in the facility have been made available on compact disks for a variety of flow conditions.

#### Bibliography

Giel, P.W., et al.: Blade Heat Transfer Measurements and Predictions in a Transonic Turbine Cascade. ASME Paper 99-GT-125 (NASA/TM-1999-209296), 1999. (Available online: <http://gltrs.grc.nasa.gov/cgi-bin/GLTRS/browse.pl?/1999/TM-1999-209296.html>)

Giel, P.W., et al.: Endwall Heat Transfer Measurements in a Transonic Turbine Cascade. ASME J. Turbomach., vol. 120 (NASA/TM-1998-107387), Apr. 1998, pp. 305-313.

Giel, P.W., et al.: Three-Dimensional Flow Field Measurements in a Transonic Turbine Cascade. ASME Paper 96-GT-113 (NASA TM-107388), 1996.

These publications are available online (select "Publications," then refs. 52, 54, and 53, respectively): <http://www.grc.nasa.gov/WWW/TURBINE/Turbine.htm>

**Dynacs Engineering Co., Inc. contact:**  
 Dr. Paul W. Giel, (216) 977-1340,  
 Paul.W.Giel@grc.nasa.gov

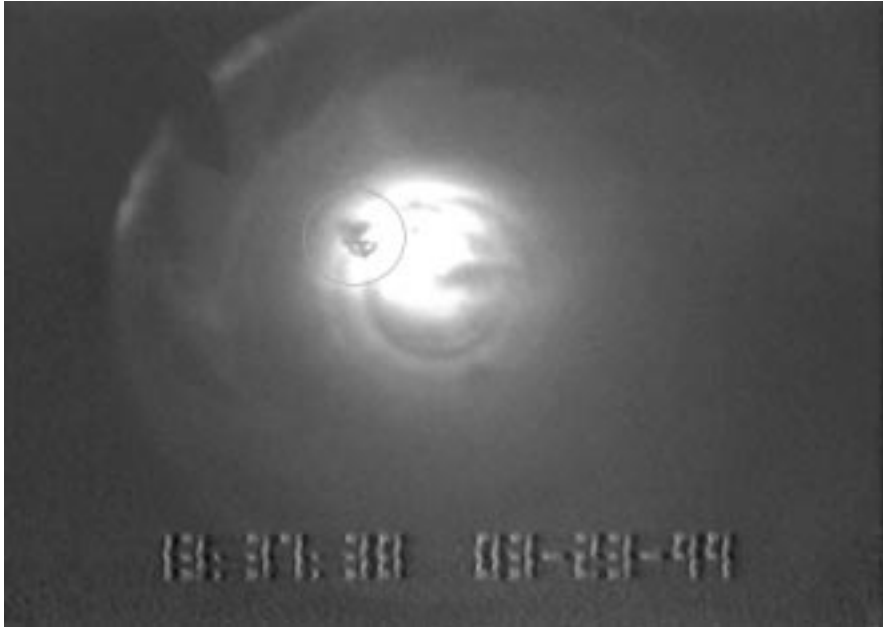
**Glenn contact:** Dr. Raymond E. Gaugler, (216) 433-5882,  
 Raymond.E.Gaugler@grc.nasa.gov

**Author:** Dr. Paul W. Giel

**Headquarters program office:** OAST

**Program/Projects:**  
 Propulsion Systems R&T

## Solid Hydrogen Formed for Atomic Propellants



*Solid hydrogen particles floating in liquid helium.*

Several experiments on the formation of solid hydrogen particles in liquid helium were recently conducted at the NASA Glenn Research Center at Lewis Field. The solid hydrogen experiments are the first step toward seeing these particles and determining their shape and size. The particles will ultimately store atoms of boron, carbon, or hydrogen, forming an atomic propellant. Atomic propellants will allow rocket vehicles to carry payloads many times heavier than possible with existing rockets or allow them to be much smaller and lighter.

Solid hydrogen particles are preferred for storing atoms. Hydrogen is generally an excellent fuel with a low molecular weight. Very low temperature hydrogen particles ( $T < 4$  K) can prevent the atoms from recombining, making it possible for their lifetime to be controlled. Also, particles that are less than 1 mm in diameter are preferred because they can flow easily into a pipe when suspended in liquid helium. The particles and atoms must remain at this low temperature until the fuel is introduced into the engine combustion (or recombination) chamber. Experiments were, therefore, planned to look at the particles and observe their formation and any changes while in liquid helium.

During the experiments, a small amount of liquid hydrogen was poured onto the surface of the liquid helium. The liquid helium was kept in a Dewar to keep it cool and was held at 3 to 4 K. The liquid hydrogen that flowed onto the surface was at 14 K, just above its freezing point. As the liquid hydrogen fell toward the helium surface, it began to freeze, and

particles formed immediately after hitting the helium surface. The figure shows a frame from the videotape of the experiment. The small particles were allowed to float on the helium surface for 20 to 60 minutes. Very quickly, they began to stick together, or agglomerate. In the final fuel application, the particles may be used to gel the liquid helium, as well as store the atoms. Gelling the helium would prevent the particles from sticking together. The particles also changed from clear crystals to cloudy crystals, indicating a transition from face-centered cubic (FCC) to hexagonal close-packed (HCP) molecule packing.

### **Fuels and Space Propellants Web**

**site:** <http://www.grc.nasa.gov/WWW/TU/launch/foctopsb.htm>

### **Bibliography**

Palaszewski, B.: Launch Vehicle Performance for Bipropellant Propulsion Using Atomic Propellants With Oxygen. AIAA Paper 99-2837, 1999.

Palaszewski, B.: Atomic Propellants for Aerospace Propulsion Systems: Solid Hydrogen Experiments and Vehicle Analyses. 1999 USAF High Energy Density Materials Contractors Conference, Cocoa Beach, FL, June 8-10, 1999.

Palaszewski, B.: Launch Vehicle Performance With Solid Particle Feed Systems for Atomic Propellants. AIAA Paper 98-3736, NASA/TM-1998-208498, 1998. (Available on line: <http://gltrs.grc.nasa.gov/cgi-bin/GLTRS/browse.pl?/1998/TM-1998-208498.html>)

### **Glenn contact:**

Bryan A. Palaszewski, (216) 977-7493, [Bryan.A.Palaszewski@grc.nasa.gov](mailto:Bryan.A.Palaszewski@grc.nasa.gov)

**Author:** Bryan A. Palaszewski

**Headquarters program office:** OAST

**Programs/Projects:** ASTP (STR)

# Atomic Rocket Vehicle Performance Improved

The NASA Glenn Research Center at Lewis Field conducted several analyses of atomic rocket propulsion systems (refs. 1 and 2). The atomic rocket engine performance and gross lift-off weight (GLOW) of several vehicle designs were used to describe the best atom loadings in rocket fuels. These best loadings will influence the vehicle dry mass, GLOW, and rocket pressurization system. Both monopropellant (fuel only with no oxidizer) and bipropellant (oxidizer and fuel) propulsion systems were assessed. The left graph provides the rocket's specific impulse  $I_{sp}$  for a type of atomic boron rocket: 22-wt % atomic boron. These  $I_{sp}$  values were computed with several helium loadings. The helium, added to the fuel mass, creates a gelled liquid to carry the atomic fuel to the rocket engine from its fuel tank. As the helium is added, the  $I_{sp}$  values are reduced, but not so much that the rocket vehicle becomes impractical.

The center graph illustrates the GLOW of rocket vehicles using the 22-wt % atomic boron propellants. The baseline rocket and payload weight for the comparison is an oxygen/hydrogen National Launch System (NLS) rocket taking 96,000 kg of payload to Earth orbit; the complete rocket and payload weighs 1,891,000 kg. For the atomic rockets, the helium addition has a strong influence on the GLOW. At an oxygen-to-fuel ratio  $O/F$  of 0.0, the rocket vehicle is too massive to be practical. At an  $O/F$  of 2.0, the mass of the 22-wt % atomic boron rocket GLOW decreased to a level comparable to the baseline oxygen/hydrogen NLS rocket GLOW. The right graph shows the GLOW for the 50-wt % atomic boron ( $O/F = 0.0$ ). It is very low in comparison to the baseline GLOW; atomic boron allows a 39-percent GLOW reduction. With 40-wt % He added, instead of having a mass that is about 61 percent of the NLS baseline vehicle GLOW, the rocket's GLOW is much greater than the baseline. However, at an  $O/F$  ratio of 0.5 or 1.0, even with the addition of helium, the GLOW is still significantly lower than the base-

line of 1,891,500 kg. The operating points for atomic rockets must be carefully selected; and these techniques illustrate the way to assess the best operating points.

## References

1. Palaszewski, B.: Launch Vehicle Performance for Bipropellant Propulsion Using Atomic Propellants With Oxygen. AIAA Paper 99-2837, 1999.
2. Palaszewski, B.: Atomic Propellants for Aerospace Propulsion Systems: Solid Hydrogen Experiments and Vehicle Analyses. Presented at the 1999 USAF High Energy Density Materials Contractors Conference, Cocoa Beach, FL, June 8-10, 1999.

## Fuels and Space Propellants Web

Site: <http://www.grc.nasa.gov/WWW/TU/launch/foctopsb.htm>

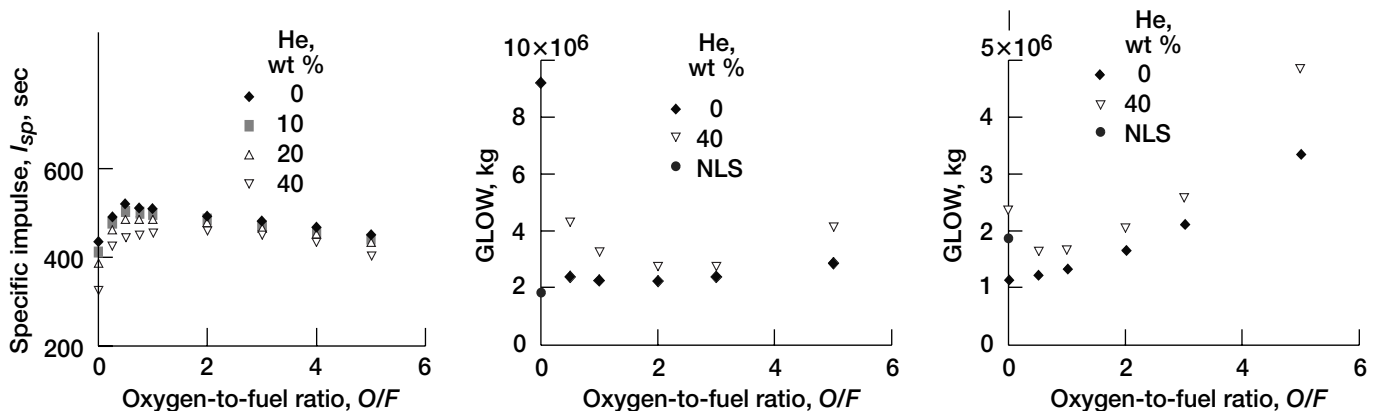
## Glenn contact:

Bryan A. Palaszewski, (216) 977-7493,  
Bryan.A.Palaszewski@grc.nasa.gov

Author: Bryan A. Palaszewski

Headquarters program office: OAST

Program supported: ASTP (STR)



Left: Atomic boron engine specific impulse; 22-wt % B. Center: Atomic boron GLOW; 22-wt % B. Right: Atomic boron GLOW; 50-wt % B.

## Extensive Testing Conducted for the Advanced Subsonics Technology Regional Engine Combustor Program

A substantial amount of testing was conducted in combustion facilities at the NASA Glenn Research Center at Lewis Field for the Advanced Subsonics Technology (AST) Regional Engine Program. Hardware was tested for three engine-manufacturing companies: General Electric, Rolls Royce-Allison, and AlliedSignal Aerospace. The hardware, which varied from single fuel-injector modules to three-cup sectors, was tested in Glenn's Engine Research Building CE5 test stands (Stand 1 and Stand 2) and in Glenn's large Advanced Subsonic Combustion Rig (ASCR). A three-cup sector was run in two separate test series for AlliedSignal in Stand 1 of CE5, and a three-cup sector for Rolls Royce-Allison in the ASCR, all at engine-operating conditions.

Measurement of pollutant emissions—NO<sub>x</sub>, CO, and unburned hydrocarbons—was the primary objective of the tests, along with a determination of combustion efficiency. The results have been used in the design of a full-annular combustor to be run at AlliedSignal. For Rolls Royce-Allison, single modules were run in Stand 1 for both pollutant emissions as well as laser measurement of the fuel spray by Phase Doppler Particle Analysis (PDPA) and location of the flame front by OH imaging. Also for Rolls Royce-Allison, an important milestone was reached with the successful test run of a three-cup sector in the ASCR in September. The test demonstrated that NO<sub>x</sub> emissions can be reduced by nearly 70 percent referred to the 1996

International Civil Aviation Organization (ICAO) Standards. For GE, single-fuel modules of a lean, direct injection (LDI) design by CFD Research Company (CFDRC) were run in Stand 2 of CE5, where emission and laser measurements were made. This capped a successful year that saw the timely completion of hardware testing for the three regional-engine AST contractors.

**Glenn contact:**

Paul F. Penko, (216) 433-5356,  
Paul.F.Penko@grc.nasa.gov

**Author:** Paul F. Penko

**Headquarters program office:** OAST

**Programs/Projects:**

Propulsion Systems R&T, AST

## Ice Accretions on Modern Airfoils Investigated

The Icing Branch at the NASA Glenn Research Center at Lewis Field initiated and conducted the Modern Airfoils Ice Accretions project to identify ice shapes and determine their effects on the aerodynamic performance of aircraft, particularly on lift and drag. Previous aircraft ice shape and performance documentation focused on a few, older airfoils. This permitted more basic studies of the ice accretion process to be undertaken. However, having established both a working data base of ice shapes and the capability to predict these shapes for basic airfoils, questions arose about how ice might accrete differently on airfoils more representative of those being designed and flown on various aircraft today. Similarly, information about how these ice shapes would affect aerodynamic performance was needed.

Three modern airfoils were selected for this project. One was representative of a commercial transport airfoil, one of a business jet airfoil, and one of a general aviation airfoil. Each was exposed to a range of icing conditions in Glenn's Icing Research Tunnel (IRT). All the ice shapes accreted on the models were recorded with tracings, photographs, and ice depth measurements. The following photograph shows one of the airfoils with ice accreted in the Icing Research Tunnel. Molds, which can be used to replicate ice shapes accurately, were made of selected ice shapes.

Researchers will use the resulting data base in designing ice protection for aircraft and in validating ice-accretion-prediction computer programs. Lift and drag measurements made of the iced airfoils will, in addition to providing information about the effects of various ice shapes on the aerodynamic performance of an airfoil, help validate computational fluid dynamics programs that predict aerodynamic performance.

To further investigate the ways that ice shapes affect the aerodynamic performance of modern airfoils, Glenn's Icing Branch conducted tests in the Low Turbulence Pressure Tunnel (LTPT) at the NASA



General aviation airfoil with ice accreted in the Icing Research Tunnel.

Langley Research Center. This wind tunnel's unique airflow characteristics allow aerodynamic performance measurements to be made over a wide range of operating conditions. Important scaling factors can be varied so that the aerodynamic performance is accurately simulated for larger airfoils, such as those used on full-scale aircraft. Castings of the ice shapes were made from selected molds. These castings were attached to the airfoil in the LTPT so that aerodynamic performance measurements could be made. The graph gives an example of the results of these tests.

The modern airfoil project is complete, and final reports will be published in January 2000. In addition, Glenn's Icing Branch is planning follow-on tests to investigate the aerodynamic performance of other iced airfoils. These tests are to include detailed flow-field measurements of both local and unsteady flows over iced airfoils.

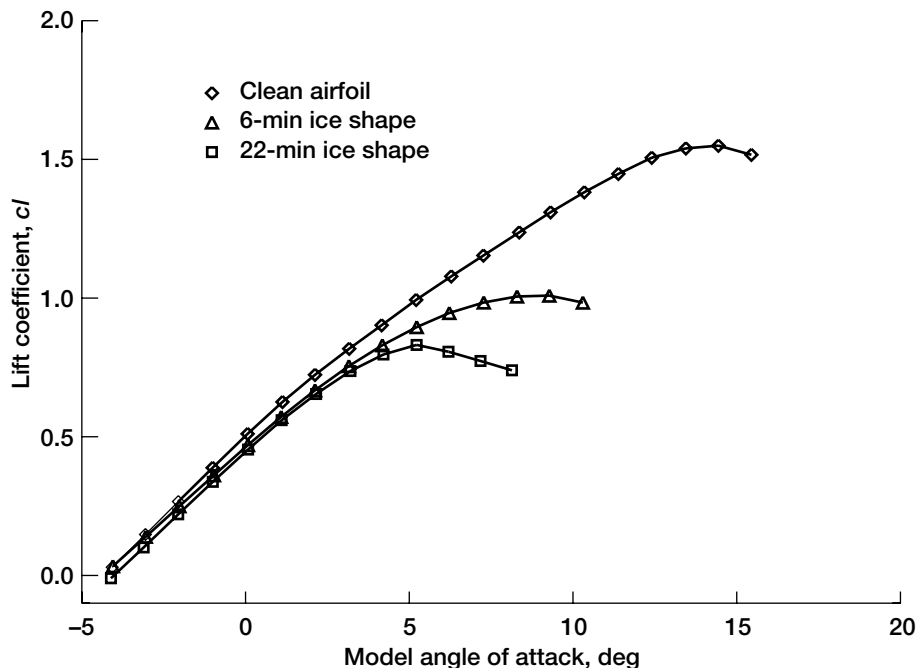
**Glenn contact:**

Harold E. Addy, Jr., (216) 977-7467,  
Harold.E.Addy@grc.nasa.gov

**Author:** Harold E. Addy, Jr.

**Headquarters program office:** OAST

**Programs/Programs:** AOS



Effect of ice shapes on airfoil lift characteristics.

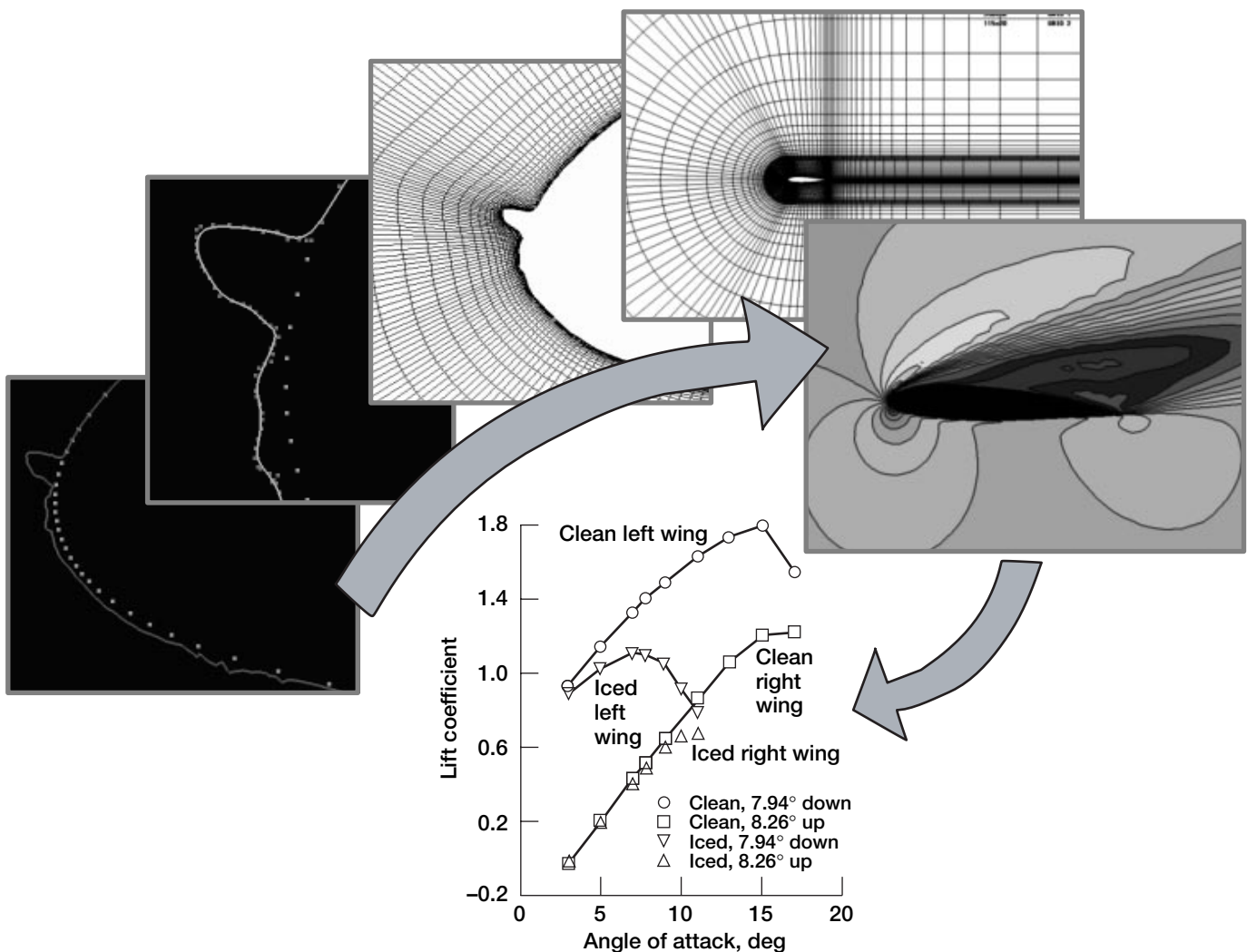
# Interactive Software System Developed to Study How Icing Affects Airfoil Performance (Phase 1 Results)

SmagglIce (Surface Modeling and Grid Generation for Iced Airfoils), which is being developed at the NASA Glenn Research Center at Lewis Field, is an interactive software system for data probing, boundary smoothing, domain decomposition, and structured grid generation and refinement. All these steps are required for aerodynamic performance prediction using structured, grid-based computational fluid dynamics (CFD), as illustrated in the following figure. SmagglIce provides the underlying computations to perform these functions, as well as a graphical user interface to control and interact with them, and graphics to display the results.

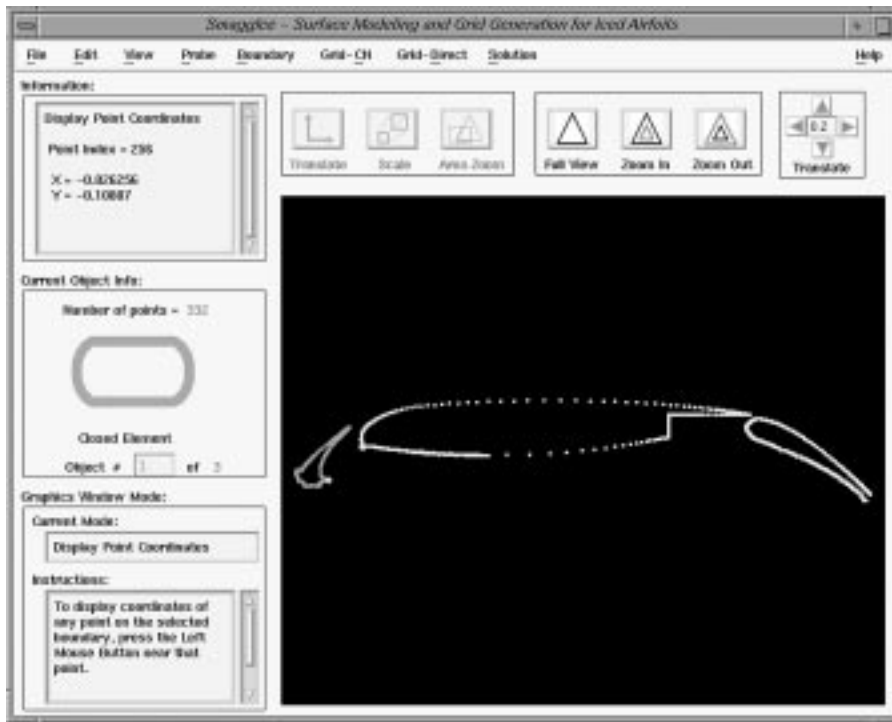
existing CFD tools to aircraft icing problems. SmagglIce has special features such as smoothing, explicit local and global control, and relevant grid topology to create the high-quality grids that are required for complicated ice shapes. With SmagglIce, CFD can be a robust tool for predicting the effects of icing on airfoil performance.

But why do we need SmagglIce? Can't we just use existing CFD tools to predict how icing will affect airfoil performance? Highly irregular ice shapes with sharp corners or segments with very high curvature present a considerable challenge in the grid-generation process. This increases the time and effort required by engineers and scientists when they try to apply

SmagglIce, a UNIX-based platform-independent software package, is being developed in planned phases that make it available to the aircraft



Process of predicting icing effects on airfoil performance.



SmagglIce main window.

icing community at the end of each phase. Phase 1 has been completed. The 1.0 Beta release became available in October 1999, and the 1.0 release will be available in February 2000. Phase 1 results contain two types of software tools: interactive ice shape probing and interactive ice shape control. SmagglIce's ice shape probing tools enable users to measure the physical characteristics of ice, and its ice shape control features allow users to examine input geometry data, to correct or modify any deficiencies of such data, and to systematically smooth the ice to a level that allows grids to be generated that are appropriate for accurate CFD analysis. The SmagglIce main window (see the screen capture) includes the Menu Bar, Information, Current Object Info, Graphics Window Mode, View Manipulations, and Graphics Drawing Area.

In Phase 2, the code will be extended to define and decompose domains, discretize perimeters, generate field grids, and check, control, and refine grid quality. In Phase 3, the SmagglIce code will be tied closely to a flow solver, and the whole process—from iced airfoil geometry to aerodynamic performance prediction—will be tested and demonstrated.

#### Bibliography

Baez, M.; Vickerman, M.; and Choo, Y.: SmagglIce User Guide SmagglIce Version 1.0. NASA/TM-2000-209793, 2000. (Available online: <http://gltrs.grc.nasa.gov/cgi-bin/GLTRS/browse.pl?/2000/TM-2000-209793.html>)

Vickerman, M.B., et al.: SmagglIce: Surface Modeling and Grid Generation for Iced Airfoils—Phase 1 Results. AIAA Paper 2000-0235 (NASA/TM-1999-209678), 2000. (Available online: <http://gltrs.grc.nasa.gov/cgi-bin/GLTRS/browse.pl?/1999/TM-1999-209678.html>)

#### Glenn contact:

Dr. Yung K. Choo, (216) 433-5868, Yung.K.Choo@grc.nasa.gov

**Authors:** Dr. Yung K. Choo and Mary B. Vickerman

**Headquarters program office:** OAST

#### Programs/Projects:

Aircraft Icing Effects, AOS

## Supercooled Large Droplet Icing Flight Research Program

During the past three winters, the NASA Glenn Research Center at Lewis Field conducted icing research flights throughout the Great Lakes region to measure the characteristics of a severe icing condition having Supercooled Large Droplets (SLD). SLD was implicated in the 1994 crash of the ATR-72 commuter aircraft. This accident focused attention on the safety hazard associated with SLD, and it led the Federal Aviation Administration (FAA) to identify the need for a better understanding of the atmospheric characteristics of this icing condition.

In response to this need, Glenn developed a cooperative icing flight research program with the FAA, the National Center for Atmospheric Research, and the Atmospheric Environment Service of Canada. The primary objectives were to (1) characterize the SLD icing condition in terms of important icing-related parameters (such as cloud droplet size, cloud

water content, and temperature), (2) develop and refine SLD icing weather forecast products, and (3) document and measure the effects of SLD ice accretions on aircraft performance.

SLD research flights were conducted with the NASA Glenn Twin Otter icing research aircraft during the winters of 1996-97, 1997-98, and 1998-99. National Center for Atmospheric Research meteorologists supported these flights by



*NASA Twin Otter icing research aircraft.*

providing SLD icing weather forecasts and in-flight guidance to the Twin Otter crew, enabling them to locate and safely fly into SLD icing conditions. Instrumentation onboard the Twin Otter was then used to sample SLD cloud characteristics, document the resultant SLD ice accretions, and measure their effect on aircraft performance. Ninety SLD icing research flights were conducted during the three winters, which resulted in a large SLD flight data base and the accomplishment of the program objectives:

- (1) SLD cloud characterization data were delivered to the FAA to develop a large droplet icing data base for regulatory examination that will provide the scientific basis for any changes and play a key role in the development of new atmospheric engineering standards of compliance.
- (2) SLD cloud characterization data were used by National Center for Atmospheric Research to develop improved SLD icing weather models. Feedback obtained from evaluating SLD forecast techniques from the 90 SLD flights facilitated the development of the National Center for Atmospheric Research's Integrated Icing Diagnostic Algorithm, which is being used by regional airlines to help pilots avoid SLD icing conditions.
- (3) NASA and the Atmospheric Environment Service sponsored an international SLD instrumentation test to compare the response of icing cloud instrumentation to SLD under controlled conditions. Results from this pioneering test quantified and intercompared instrument responses to SLD for the first time, and will lead to the development of improved SLD cloud instrumentation.
- (4) NASA and the Atmospheric Environment Service collaborated on the development of common methods for acquiring and analyzing SLD flight research data. These methods, which yielded high-quality SLD cloud characterization data, will form the basis for international acquisition and analysis standards.

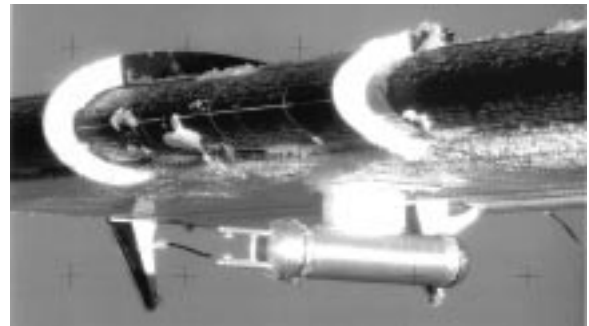
**Glenn contacts:**

Dean R. Miller, (216) 433-5349, Dean.R.Miller@grc.nasa.gov; and Thomas P. Ratvasky, (216) 433-3905, Thomas.P.Ratvasky@grc.nasa.gov

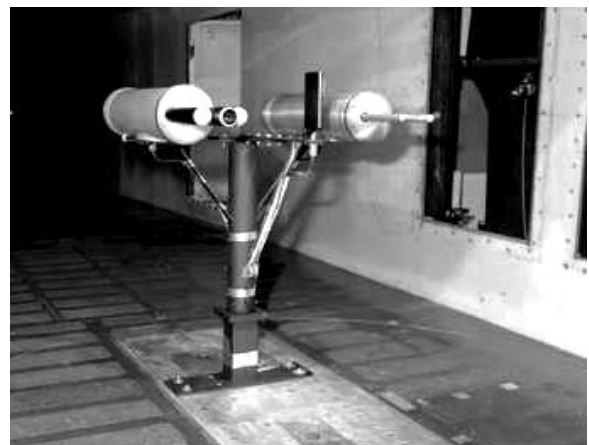
**Author:** Dean R. Miller

**Headquarters program office:** OAST

**Programs/Projects:** AOS



*Right wing of NASA Twin Otter showing SLD ice accretion and cloud-particle sizing probe.*



*Particle sizing probes in Glenn's Icing Research Tunnel during NASA/Atmospheric Environment Service international SLD instrumentation comparison test.*

# Software Released by LEWICE 2.0 Ice Accretion Software Development Project

Computational icing simulation methods are making the transition from the realm of research to commonplace use in design and certification. As such, standards of software management, design, validation, and documentation must be adjusted to accommodate the increased expectations of the user community with respect to accuracy, reliability, capability, and usability. With this in mind, in collaboration with Glenn's Engineering Design and Analysis Division, the Icing Branch of the NASA Glenn Research Center at Lewis Field began a software improvement project focused on the two-dimensional ice accretion simulation tool LEWICE. This project is serving as an introduction to the concepts of software management and is intended to serve as a pilot project for future icing simulation code development.

The LEWICE 2.0 Software Development Project consisted of two major elements: software management and software validation. The software management element consisted of identifying features of well-designed and well-managed software that are appropriate for an analytical prediction tool such as LEWICE and applying them to a revised version of the code. This element included tasks such as identification of software requirements, development and implementation of coding standards, and implementation of software revision control practices. With the application of these techniques, the LEWICE ice accretion code became a more stable and reliable software product. In addition, the lessons learned about software development and maintenance can be factored into future software projects at the outset.

The software validation activity was an integral part of our effort to make LEWICE a more accurate and reliable analysis tool. Because of the efforts taken to extensively validate this software, LEWICE 2.0 is more robust than previous releases and can reproduce results accurately across several computing platforms. It also differs from previous versions in the extensive quantitative comparisons of its results with a data base of ice shapes that were generated in Glenn's Icing Research Tunnel. The results of the shape comparisons were analyzed to determine the range of meteorological

conditions under which LEWICE 2.0 is within the repeatability found for ice shapes obtained from experiments. These comparisons show that the average variation of LEWICE 2.0 from experimental data is 7.2 percent, whereas the overall variability of the experimental data is 2.5 percent.

The LEWICE 2.0 Software Development Project resulted in the release, at the recent Icing Branch LEWICE Workshop, of a more useful and robust analysis tool than was previously available to the icing community. The lessons learned from this project will be applied to the Icing Branch's future software development efforts.

## Find out more about this work and other icing-related research on the World Wide Web:

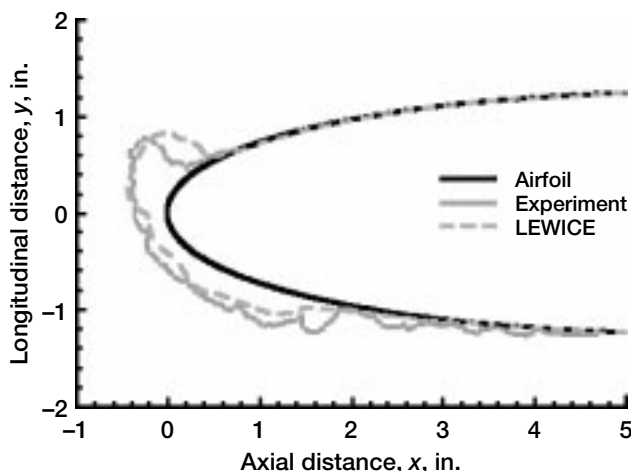
<http://icebox.grc.nasa.gov/>

### Bibliography

Levinson, L.H.; Potapczuk, M.G.; and Mellor, P.A.: Software Development Processes Applied to Computational Icing Simulation. NASA/TM-1999-208898 (AIAA Paper 99-0248), 1999. (Available online: <http://gltrs.grc.nasa.gov/cgi-bin/GLTRS/browse.pl?/1999/TM-1999-208898.html>)

Potapczuk, M.G.: A Review of NASA Lewis' Development Plans for Computational Simulation of Aircraft Icing. NASA/TM-1999-208904 (AIAA Paper 99-0243), 1999. (Available online: <http://gltrs.grc.nasa.gov/cgi-bin/GLTRS/browse.pl?/1999/TM-1999-208904.html>)

Wright, W.B.: A Summary of Validation Results for LEWICE 2.0. NASA/CR-1998-208687 (AIAA Paper 99-0249), 1998. (Available online: <http://gltrs.grc.nasa.gov/cgi-bin/GLTRS/browse.pl?/1999/CR-1999-208687.html>)



*LEWICE prediction compared with measured ice shape profile.*

**Glenn contact:**

Dr. Mark G. Potapczuk, (216) 433-3919, Mark.G.Potapczuk@grc.nasa.gov

**Dynacs Engineering Company, Inc., contact:**

William B. Wright, (216) 433-2161, William.B.Wright@grc.nasa.gov

**Author:** Dr. Mark G. Potapczuk

**Headquarters program office:** OAST

**Programs/Projects:** AOS

## Mt. Washington Icing Sensors Project (MWISP) Tests Technologies for Remote Sensing of Icing Conditions



*Radars used for MWISP field test.*

The Mt. Washington Icing Sensors Project (MWISP) was an intensive multi-agency field test of remote-sensing technologies and methods for in-flight icing detection. This field test was the first comprehensive examination of multiple remote-sensing technologies, and it included ground and airborne in situ measurements for comparison. The data gathered will allow the assessment of icing remote-sensing technologies leading toward the development of ground-based and airborne systems. These systems will provide flight crews with the information required for avoiding or exiting hazardous icing conditions.

MWISP took place on and around Mt. Washington, New Hampshire, during April 1999. The combination of persistent clouds with high liquid-water content and the opportunity for continuous in situ measurement provided by the Summit Observatory led to the selection of Mt. Washington. Field test participants included the NASA Glenn Research Center at Lewis Field, the Federal Aviation Administration (FAA), the National Oceanic and Atmospheric Administration's (NOAA) Environmental Technology Laboratory (ETL), the U.S. Army Cold Regions Research and Engineering Laboratory, the National Center for Atmospheric Research, the Canadian Defense Research Establishment Valcartier, universities, and private firms.

Technologies examined include

- Multiband radar differential attenuation techniques to detect liquid water—the NOAA ETL and University of Massachusetts X-, Ka-, and W-band radars were used for this activity.
- A multiband radar neural network technique to detect liquid water and classify droplet size—the NOAA ETL and University of Massachusetts X-, Ka-, and W-band radars were used for this activity.
- A multiple field of view lidar to detect liquid water and measure droplet size distributions—the Canadian Defense Research Establishment Valcartier lidar was used for this activity.
- Ground-based (up-looking) radiometric measurement of cloud liquid water and temperature—the NOAA ETL and Radiometrics, Corp., radiometers were used for this activity.
- Airborne (side-looking) radiometric measurement of cloud liquid water and temperature—the NOAA ETL Polarimetric Scanning Radiometer (PSR) was used for this activity.

In addition to the remote-sensing technologies examined, in situ measurements were made at the summit, aboard Glenn's Twin Otter Icing Research Aircraft, and on specially modified radiosondes (weather balloons).

The large quantity of data gathered at MWISP is currently being analyzed. A technology "down select" will follow the analysis, which in turn will lead to ground-based and airborne systems development and prototype testing in the user environment.

**Find out more about Glenn's icing research on the World Wide Web:**  
<http://icebox.grc.nasa.gov/>

**Glenn contact:**

Andrew L. Reehorst, (216) 433-3938,  
[Andrew.L.Reehorst@grc.nasa.gov](mailto:Andrew.L.Reehorst@grc.nasa.gov)

**Author:** Andrew L. Reehorst

**Headquarters program office:** OAST

**Programs/Projects:** AOS

## Aircraft Icing Educational and Training Videos Produced for Pilots



*Tailplane icing video.*

As a part of NASA's aviation safety mission, the Icing Branch of the NASA Glenn Research Center at Lewis Field is producing educational and training videos to help pilots recognize and recover from in-flight icing hazards. These videos are a result of experience gained from the NASA/FAA Tailplane Icing Program. The first educational video, "Tailplane Icing," was written and produced solely by NASA Glenn. The response following the September 1998 release has been overwhelming. Thus far, 700 copies have been distributed. A request soon came to produce more videos covering a wider range of topics. Released in November 1999 was "Icing for Regional and Corporate Pilots." This training video was cowritten by NASA, the Federal Aviation Administration (FAA), and the Air Line Pilots Association (ALPA). It is focused specifically on the pilots and aircraft most likely to encounter in-flight icing conditions. A video tailored specifically for general aviation pilots will be produced in the Fall of 2000 followed by an Icing Basics primer.

The motivation for the educational video "Tailplane Icing" (running time, 23 min) was to equip pilots with an understanding of ice-contaminated tailplane stall, the cause of at least 16 accidents and 139 fatalities. The

video discusses the role of the horizontal tailplane, illustrates the "paths to stall," and explains why the procedure for recovery from a tail stall is exactly opposite that for a wing stall and how to recognize the subtle tactile differences between the two.

The training video, "Icing for Regional and Corporate Pilots," is more comprehensive in scope. This 37-min video discusses ice protection systems, ice accretion physics, and the symptoms of ice accretion, the effects of ice on the aircraft in regards to both performance penalties and handling anomalies, recovery techniques, and finally, the phenomenon of supercooled large droplets (SLD's). It is available now.

**Find out more about these videos or order them free of charge:** <http://icebox.grc.nasa.gov/Education/Videos>

**Dynacs Engineering Co., Inc. contact:**  
Dr. Judith Foss Van Zante, (216) 433-3587, [Judith.VanZante@grc.nasa.gov](mailto:Judith.VanZante@grc.nasa.gov)

**Glenn contacts:**

Thomas P. Ratvasky, (216) 433-3905,  
[Thomas.P.Ratvasky@grc.nasa.gov](mailto:Thomas.P.Ratvasky@grc.nasa.gov); and  
William J. Rieke, (216) 433-2036,  
[William.J.Rieke@grc.nasa.gov](mailto:William.J.Rieke@grc.nasa.gov)

**Author:** Dr. Judith Foss Van Zante

**Headquarters program office:** OAST

**Programs/Projects:** AOS

## Inlet Unstart Propulsion Integration Wind Tunnel Test Program Completed for High-Speed Civil Transport

One of the propulsion system concepts to be considered for the High-Speed Civil Transport (HSCT) is an underwing, dual-propulsion, pod-per-wing installation. Adverse transient phenomena such as engine compressor stall and inlet unstart could severely degrade the performance of one of these propulsion pods. The subsequent loss of thrust and increased drag could cause aircraft stability and control problems that could lead to a catastrophic accident if countermeasures are not in place to anticipate and control these detrimental transient events. Aircraft system engineers must understand what happens during an engine compressor stall and inlet unstart so that they can design effective control systems to avoid and/or alleviate the effects of a propulsion pod engine compressor stall and inlet unstart.

The objective of the Inlet Unstart Propulsion Airframe Integration test program was to assess the underwing flow field of a High-Speed Civil Transport propulsion system during an engine compressor stall and subsequent inlet unstart. Experimental research testing was conducted in the 10- by 10-Foot Supersonic Wind Tunnel at the NASA Glenn Research Center at Lewis Field. The representative propulsion pod consisted of a two-dimensional, bifurcated inlet mated to a live turbojet engine. The propulsion pod was mounted below a large flat plate that acted as a wing simulator. Because of the plate's long length (nominally 10-ft wide by 18-ft long), realistic boundary layers could form at the inlet cowl plane.

Transient instrumentation was used to document the aerodynamic flow-field conditions during an unstart sequence. Acquiring these data was a significant technical challenge because a typical unstart sequence disrupts the local flow field for about only 50 msec. Flow surface information was acquired via static pressure taps installed in the wing simulator, and intrusive pressure probes were used to acquire flow-field information. These data were extensively analyzed to determine the impact of the unstart transient on the surrounding flow field.

This wind tunnel test program was a success, and for the first time, researchers acquired flow-field aerodynamic data during a supersonic propulsion system engine compressor stall and inlet unstart sequence. In addition to obtaining flow-field pressure data, Glenn researchers determined other properties such as the transient flow angle and Mach number. Data are still being reduced, and a comprehensive final report will be released during calendar year 2000.

**Glenn contact:**

A. Robert Porro, (216) 433-5921,  
Alvin.R.Porro@grc.nasa.gov

**Author:** A. Robert Porro

**Headquarters program office:** OAST

**Programs/Projects:** HSR



*View of test model and instrumentation installed in Glenn's 10- by 10- Foot Supersonic Wind Tunnel.*

# CFD Software for Aerospace Applications Available From the NPARC Alliance

The NPARC (National Program for Application-Oriented Research in CFD) Alliance is a formal partnership between the NASA Glenn Research Center at Lewis Field and the Air Force Arnold Engineering Development Center, with additional significant involvement by the Boeing Company's Phantom Works Group, whose mission is to provide an applications-oriented computational fluid dynamics (CFD) system primarily for aerospace flow simulation. The Alliance is committed to the long-range maintenance and improvement of this capability, with teams focused on user support, code development, and validation.

The principal product of the NPARC Alliance is the WIND code, a general-purpose, structured, multizone, compressible flow solver that can be used to analyze steady or unsteady flow for a wide range of geometric configurations and over a wide range of flow conditions. WIND can be run in serial mode on a variety of platforms, including personal computers, or in a fault-tolerant parallel-processing mode on a heterogeneous network of Unix workstations. Version 2.0 of WIND was released in April 1999. In addition to the WIND code itself, a variety of preprocessing and postprocessing tools are included for setting boundary conditions, examining computed results, and other functions.

The Alliance maintains extensive World Wide Web sites that contain code documentation and validation data. The documentation includes user manuals that describe the operation and use of the WIND code and its associated utilities, and developer reference material for those who are interested in modifying or extending the code. The validation site contains detailed examples showing the use of WIND for a variety of flows and geometries. It serves as an archive of analytical, experimental, and computational data suitable for CFD code validation.

The NPARC Alliance is continuing to expand and improve the software, with current efforts focused on enhancing WIND's chemistry capability, adding unstructured and hybrid grid technology, and developing a



*The NPARC Alliance, a partnership between NASA Glenn and the Arnold Engineering Development Center, is dedicated to the establishment of a national, application-oriented computational fluid dynamics system for aerospace flow simulation.*

global code framework for multidisciplinary analyses.

All NPARC Alliance software is available without charge to U.S.-owned companies, public and private universities, and government agencies (for use by U.S. citizens and resident aliens). Instructions for obtaining the code may be obtained from the NPARC Alliance home page, or from the NPARC Alliance User Support team. Since its initial release in February 1998, the WIND code has been acquired by over 130 different organizations.

**Additional information about the NPARC Alliance and the WIND code is available at the following World Wide Web sites:**

**NPARC Alliance:**  
<http://www.arnold.af.mil/nparc>

**WIND Documentation:**  
<http://www.grc.nasa.gov/www/wind/winddocs>

**WIND Validation:**  
<http://www.grc.nasa.gov/www/wind/valid>

**Glenn contacts:**  
Dr. Charles E. Towne, (216) 433-5851, Charles.E.Towne@grc.nasa.gov; and  
Nicholas J. Georgiadis, (216) 433-3958, Nicholas.J.Georgiadis@grc.nasa.gov

**AEDC contact:** NPARC Alliance User Support, (931) 454-7455, nparc-support@info.arnold.af.mil

**Author:** Dr. Charles E. Towne

**Headquarters program office:** OAST

**Programs/Projects:** HSR, AST, UEET, HPCC, Propulsion Systems R&T

**Special recognition:** An Honorable Mention was awarded to the NPARC Alliance Flowfield Simulation System in the 1999 NASA Software of the Year Competition.

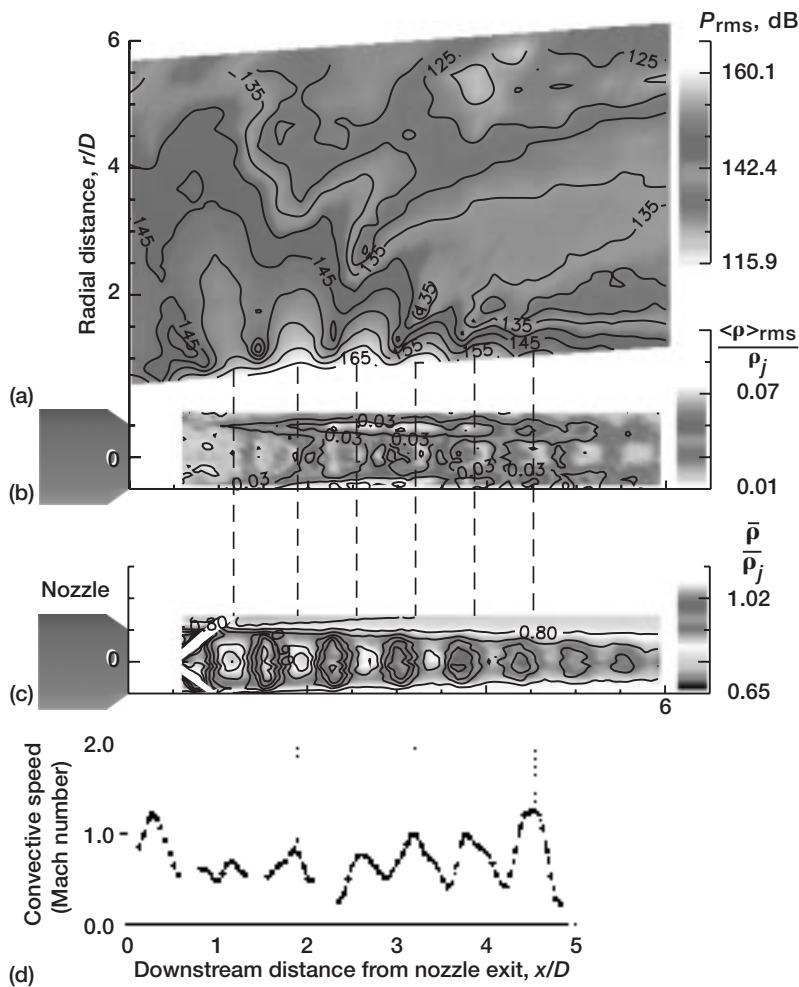
# Screech Noise Generation From Supersonic Underexpanded Jets Investigated

Many supersonic military aircraft and some of the modern civilian aircraft (such as the Boeing 777) produce shock-associated noise. This noise is generated from the jet engine plume when the engine nozzle is operated beyond the subsonic operation limit to gain additional thrust. At these underexpanded conditions, a series of shock waves appear in the plume. The turbulent vortices present in the jet interact with the shock waves and produce the additional shock-associated noise. Screech belongs to this noise category, where sound is generated in single or multiple pure tones. The high dynamic load associated with screech can damage the tailplane.

One purpose of this study at the NASA Glenn Research Center at Lewis Field was to provide an accurate data base for validating various computational fluid dynamics (CFD) codes. These codes will be used to predict the

frequency and amplitude of screech tones. A second purpose was to advance the fundamental physical understanding of how shock-turbulence interactions generate sound. Previously, experiments on shock-turbulence interaction were impossible to perform because no suitable technique was available. As one part of this program, an optical Rayleigh-scattering measurement technique was devised to overcome this difficulty.

Rayleigh-scattering measurements provided the flow information for this figure (parts (b), (c), and (d)), and the acoustic information (part (a)) is from a microphone. Since screech appeared as a single tone for the 2.39 nozzle pressure ratio (Mach 1.19) jet, a phase-averaging process was employed for data acquisition. The time-averaged air density plot (part (c)) shows the periodic shock waves present in the plume. The red-yellow regions (dark circular regions) have higher densities from shock compression, and the blue-green regions (the rest of part (c)) correspond to the lower density in the expansion regions. Part (b) shows the strength of turbulence fluctuation as measured through root-mean-square density fluctuations. Once again, the red-yellow zones (darker areas) represent high fluctuation. Note that the turbulent fluctuations are modulated as they pass over the periodic shock train. Part (d) shows the speed variation of the turbulent vortices. The actual speed is divided by the speed of the ambient sound to arrive at the convective Mach number values. Clearly, the vortices go through a periodic acceleration and deceleration. Part (a) shows the sound pressure fluctuation measured in



Mechanism for screech noise generation from a 2.39 nozzle pressure ratio (Mach 1.19) supersonic jet produced from a circular choked nozzle. (a) Root-mean-square noise pressure fluctuation. (b) Normalized air density fluctuation. (c) Normalized, time-averaged air density. (d) Convective speed of turbulent vortices. This figure is shown in color in the online version of this article (<http://www.grc.nasa.gov/WWW/RT1999/5000/5860panda.html>).

the jet vicinity. Close to the jet boundary, the yellow to orange pattern (bottom left of part (a)) shows a series of peaks and valleys from which the rest of the sound field appears to radiate. The peaks are identified as the sound sources. Finally, the vertical chain lines link all the parts. The sound sources are located in the regions of the jet where the turbulent vortices are fastest and have the strongest fluctuations. Further analyses showed that the spacing between the sound sources follows an interference scale that is somewhat different from the shock spacing. This length scale was used to develop an exact screech frequency formulation (refs. 1 and 2).

**Find out more about this research on the World Wide Web:**

<http://www.grc.nasa.gov/WWW/jp>

**References**

1. Panda, J.; and Seasholtz, R.G.: Measurement of Shock Structure and Shock-Vortex Interaction in Underexpanded Jets Using Rayleigh Scattering. *Phys. Fluids*, vol. 11, issue 12, Dec. 1999, pp. 3761–3777.

2. Panda, J.: An Experimental Investigation of Screech Noise Generation. *J. Fluid Mech.*, vol. 378, 1999, pp. 71–96.

**Modern Technologies Corp. contact:**

Jayanta Panda, (216) 433–8891,  
Jayanta.Panda@grc.nasa.gov

**Glenn contact:** Dr. Richard G. Seasholtz, (216) 433–3754,  
Richard.G.Seasholtz@grc.nasa.gov.

**Authors:** Jayanta Panda and  
Dr. Richard G. Seasholtz

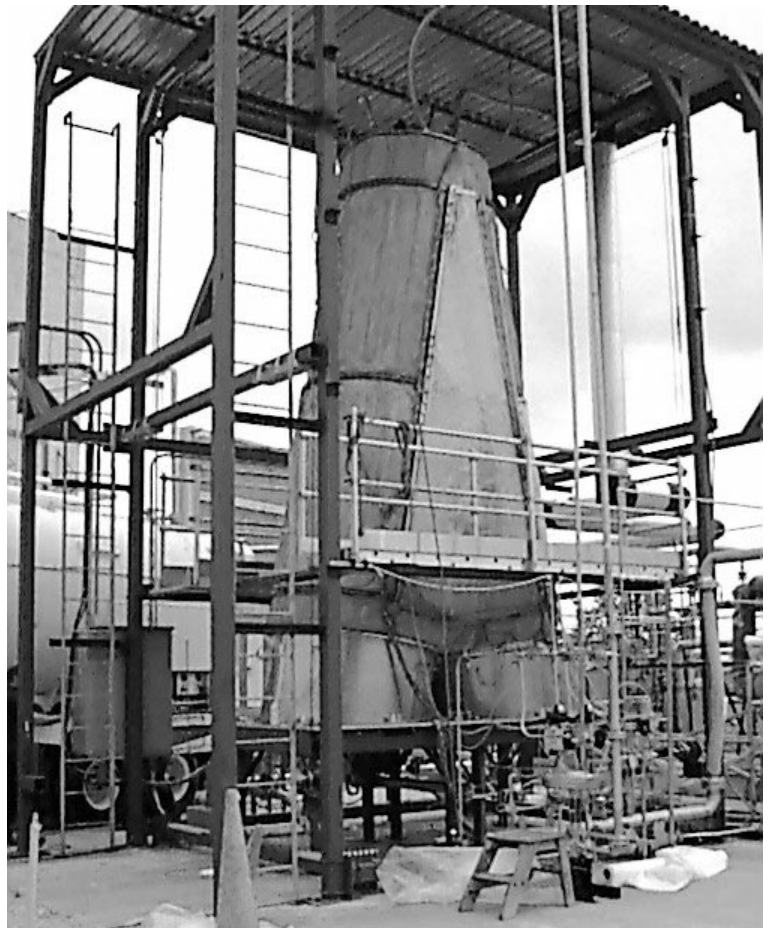
**Headquarters program office:** OAST

**Programs/Projects:** FQE, ASCOT, IITS

## Propellant Densification Ground Testing Conducted for Launch Vehicles

The NASA Glenn Research Center at Lewis Field has taken the lead in the development of practical densified cryogenic propellants for launch vehicle applications. The technology of subcooling cryogenic propellants below their normal boiling point to produce a denser fluid is one of the key process technologies necessary to meet the challenge of single-stage-to-orbit and reusable launch vehicles. Densified propellants are critical to lowering launch costs because they enable more propellant to be packed into a given unit volume, thus improving the performance by reducing the overall size and weight of the launch vehicle. This two-pronged research and test program has evolved into (1) conducting tank loading tests using densified liquid hydrogen and (2) developing two large-scale propellant densification systems that will be performance tested next year at Glenn.

The propellant-loading test program was undertaken at Glenn in coordination with Lockheed Martin Michoud Space Systems. In this testing, the liquid hydrogen recirculation and densification process was simulated, and the thermal stratification of the densified propellant was recorded throughout the tank. The test article was a flight-weight tank constructed from composite materials similar to those to be used on the X-33 launch vehicle. The tank geometry as designed by Lockheed Martin had two cylindrical



*A composite dual-lobe X-33 prototype test tank is configured for propellant loading and recirculation testing with high-density 27 °R liquid hydrogen.*



*Inside the NASA Glenn hangar, a team of engineers and technicians put the final touches on a 1000-ft<sup>2</sup> liquid oxygen propellant densification unit that promises to reduce the cost of access to space.*

cal lobes with a center septum. Liquid hydrogen flow rate, pressure data, and temperature data plotted over time were collected while the subscale tank was filled with 27 °R (15 K) densified liquid hydrogen propellant. This testing has validated mathematical models and demonstrated the readiness of densified propellant technology for near-term use. It marks the first time that such a process has been carried out with a multiple-lobe, flight-similar tank.

Glenn researchers have also been working on providing a process and critical test data for the continuous production of densified liquid hydrogen (LH<sub>2</sub>) and densified liquid oxygen (LO<sub>2</sub>). Each densification production process uses a high-efficiency, subatmospheric boiling bath heat exchanger to cool the working fluid. A near triple-point hydrogen boiling bath is used to condition and subcool hydrogen to 27 °R (15 K), and a nitrogen boiling bath is used to cool the liquid oxygen to 120 °R (66.7 K). Multistage centrifugal compressors operating at cryogenic inlet conditions maintain the heat exchanger bath vapor pressure below 1 atm. The LO<sub>2</sub> propellant densification unit shown in the photograph has a 30 lb/sec capacity, whereas the LH<sub>2</sub> unit was designed to process 8 lb/sec of propellant. Each densification unit will be transported to Glenn's South Forty area after all fabrication work is completed sometime late next year. There the LO<sub>2</sub> and LH<sub>2</sub> densifier performance tests will be conducted with another larger Lockheed Martin tank designated the Structural Test Article (STA). This liquid oxygen tank is a full-scale, flight-weight, prototype aluminum tank designed for the X-33. It has a capacity of 20,000 gallons of LO<sub>2</sub>. The tank loading and recirculation testing planned for next year with STA will provide the data necessary for full-scale development of propellant densification technology.

#### **Bibliography**

Greene, W.D.; Knowles, T.E.; and Tomsik, T.M.: Propellant Densification for Launch Vehicles: Simulation and Testing 1999. AIAA Paper 99-2335, 1999.

Greene, W.D.; and Vaughan, D.A.: Simulation and Testing of In-Tank Propellant Densification for Launch Vehicles. AIAA Paper 98-3688, 1998.

Tomsik, T.M.: Performance Tests of a Liquid Hydrogen Propellant Densification Ground Support System for the X33/RLV. AIAA Paper 97-2976 (NASA TM-107469), 1997.

Lak, T.; Lozano, M.; and Tomsik, T.M.: Advancement in Cryogenic Propulsion System Performance Through Propellant Densification. AIAA Paper 96-3123, 1996.

#### **Glenn contact:**

Thomas M. Tomsik, (216) 977-7519, Thomas.M.Tomsik@grc.nasa.gov

**Author:** Thomas M. Tomsik

**Headquarters program office:** OAST

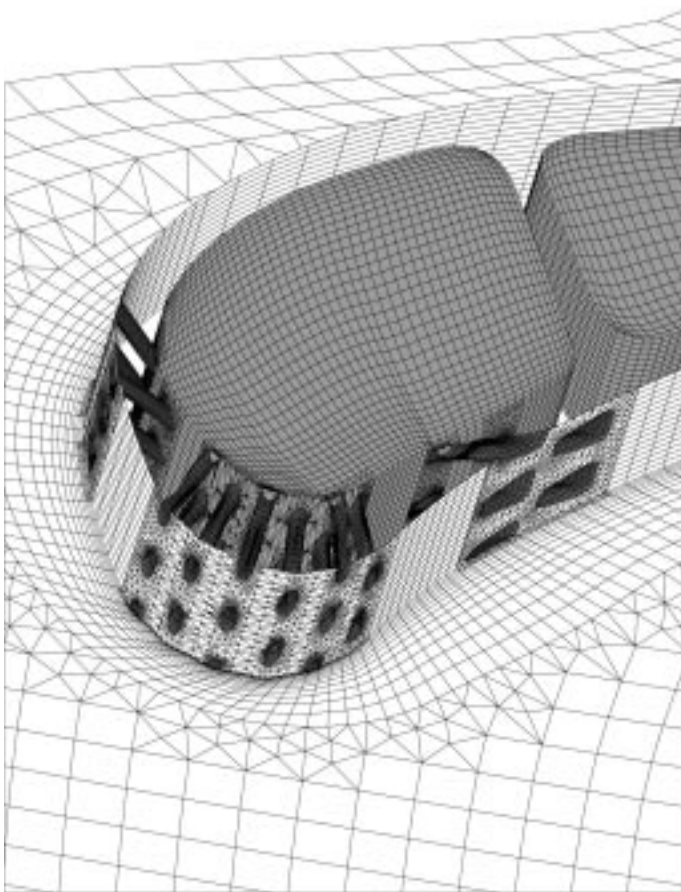
#### **Programs/Projects:**

Affordable Access to Space, X-33, RLV, Space-Liner 100, ASTP

# DRAGON Grid: A Three-Dimensional Hybrid Grid Generation Code Developed

Because grid generation can consume 70 percent of the total analysis time for a typical three-dimensional viscous flow simulation for a practical engineering device, payoffs from research and development could reduce costs and increase throughputs considerably. In this study, researchers at the NASA Glenn Research Center at Lewis Field developed a new hybrid grid approach with the advantages of flexibility, high-quality grids suitable for an accurate resolution of viscous regions, and a low memory requirement. These advantages will, in turn, reduce analysis time and increase accuracy. They result from an innovative combination of structured and unstructured grids to represent the geometry and the computation domain.

The present approach makes use of the respective strengths of both the structured and unstructured grid methods, while minimizing their weaknesses. First, the Chimera grid generates high-quality, mostly orthogonal meshes around individual components. This process is flexible and can be done easily. Normally, these individual grids are required to overlap each other so that the solution on one grid can communicate with another.



*Cut-through view of the DRAGON grid in the leading-edge region of a film-cooled turbine vane, showing the internal plenums and coolant holes inside the vane.*

However, when this communication is carried out via a nonconservative interpolation procedure, a spurious solution can result. Current research is aimed at entirely eliminating this undesired interpolation by directly replacing arbitrary grid overlapping with a nonstructured grid called a DRAGON grid, which uses the same set of conservation laws over the entire region, thus ensuring conservation everywhere.

The figure shows the DRAGON grid for a typical film-cooled turbine vane with 33 holes and 3 plenum compartments. There are structured grids around each geometrical entity and unstructured grids connecting them. In fiscal year 1999, Glenn researchers developed and tested the three-dimensional DRAGON grid-generation tools (ref. 1). A flow solver suitable for the DRAGON grid has been developed, and a series of validation tests are underway.

## **Find out more about this research on the World Wide Web:**

<http://www.grc.nasa.gov/WWW/DragonGrid/>

## **Reference**

1. Zheng, Y.; Liou, M.-S.; and Civinskas, K.C.: Development of Three-Dimensional DRAGON Grid Technology. NASA/TM-1999-209458, 1999. (Available online: <http://gltrs.grc.nasa.gov/cgi-bin/GLTRS/browse.pl?1999/TM-1999-209458.html>)

## **Glenn contact:**

Dr. Meng-Sing Liou, (216) 433-5855, [Meng-Sing.Liou@grc.nasa.gov](mailto:Meng-Sing.Liou@grc.nasa.gov)

**Author:** Dr. Meng-Sing Liou

**Headquarters program office:** OAST

**Programs/Projects:**  
Propulsion Systems R&T

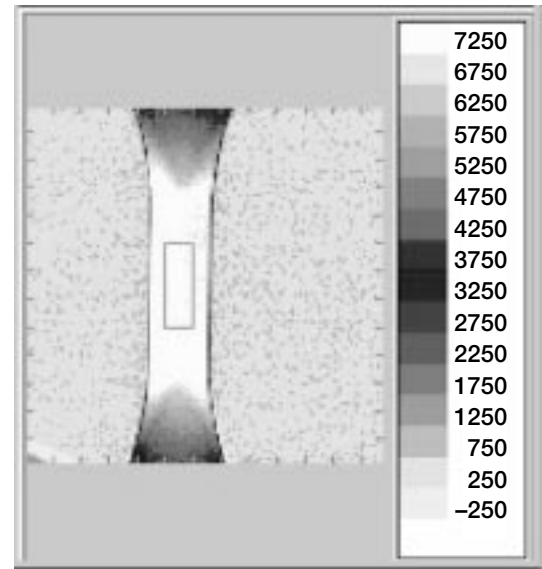
# Structures and Acoustics

## Thermoelastic Stress Analysis: An NDE Tool for the Residual Stress Assessment of Metallic Alloys

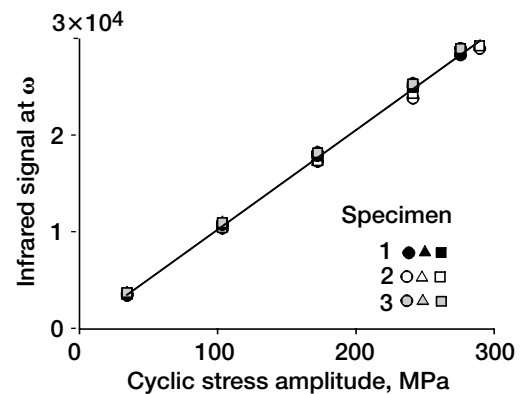
During manufacturing, certain propulsion components that will be used in a cyclic fatigue environment are fabricated to contain compressive residual stresses on their surfaces because these stresses inhibit the nucleation of cracks. Overloads and elevated-temperature excursions cause the induced residual stresses to dissipate while the component is still in service, lowering its resistance to crack initiation. Research at the NASA Glenn Research Center at Lewis Field has focused on employing the Thermoelastic Stress Analysis technique (TSA, also recognized as SPATE: Stress Pattern Analysis by Thermal Emission) as a tool for monitoring the residual stress state of propulsion components.

TSA is based on the fact that materials experience small temperature changes when they are compressed or expanded. When a structure is cyclically loaded (i.e., cyclically compressed and expanded), the resulting surface-temperature profile correlates to the stress state of the structure's surface. The surface-temperature variations resulting from a cyclic load are measured with an infrared camera. Traditionally, the temperature amplitude of a TSA signal has been theoretically defined to be linearly dependent on the cyclic stress amplitude. As a result, the temperature amplitude resulting from an applied cyclic stress was assumed to be independent of the cyclic mean stress.

Recent studies established that the temperature response also depends on the cyclic mean stress or static stress. A study by the authors (ref. 1) showed that static stresses significantly influenced the TSA results for titanium- and nickel-based alloys. A more indepth analysis, which involved analyzing multiple harmonics of the temperature response, was also conducted (ref. 2). This research showed that the thermoelastic response of a structure subjected to a pure sinusoidal mechanical load with frequency  $\omega$  produced a TSA signal with frequency components at the primary frequency,  $\omega$ , as well as at the second harmonic,  $2\omega$ . The first harmonic of the thermal response is a function of the cyclic stress amplitude and the mean stress, whereas the second harmonic is a function of the square of the stress amplitude. By obtaining the TSA amplitudes of the first and second harmonics, we are now able to obtain the stress amplitude and the mean stress at a given point on a structure subjected to a cyclic load simultaneously. The rather complex analysis of the temperature response involved obtaining the first and second harmonic amplitudes for 16,384 infrared detectors (in a 128 by 128 focal plane array). In addition, comparisons were made between the experimental data and theoretical predictions that were based on a revised theory that takes into account the mean stress effect. Good agreement was achieved.



Typical infrared test image for a dogbone TIMETAL 21S specimen. The rectangular box within the specimen indicates the area where the average signal was obtained. The scale displays the dimensionless digital values of the infrared camera signal corresponding to the cyclic temperature amplitude.



First harmonic ( $\omega$ ) infrared signal output at various stress amplitudes ( $\sigma_m = 0$ ) for TIMETAL 21S. Indicated is the linear relationship of the TSA signal to the cyclic stress amplitude for a fixed mean stress. Mean stress variations would affect the data by changing the slope of the line.

Since confidence was achieved concerning reliable TSA measurements of the mean stress effect (i.e., the static stress), research can focus on the application of the method to residual stress assessment. Such measurements will assist researchers in the characterization of materials in the laboratory as well as in the in situ monitoring of the current residual stress state in actual structural components during fabrication and service.

#### References

1. Gyekenyesi, A.L.; and Baaklini G.Y.: Thermoelastic Stress Analysis: The Mean Stress Effect in Metallic Alloys. NASA/TM-1999-209376, 1999. (Available online: [http:// gltrs.grc.nasa.gov/cgi-bin/GLTRS/browse.pl?/1999/TM-1999-209376.html](http://gltrs.grc.nasa.gov/cgi-bin/GLTRS/browse.pl?/1999/TM-1999-209376.html))
2. Gyekenyesi, A.L.; and Baaklini G.Y.: Quantifying Residual Stresses by Means of Thermoelastic Stress Analysis. SPIE: Conference on the NDE of Aging Materials and Composites, Newport Beach, CA, March 5-9, 2000.

#### Ohio Aerospace Institute contact:

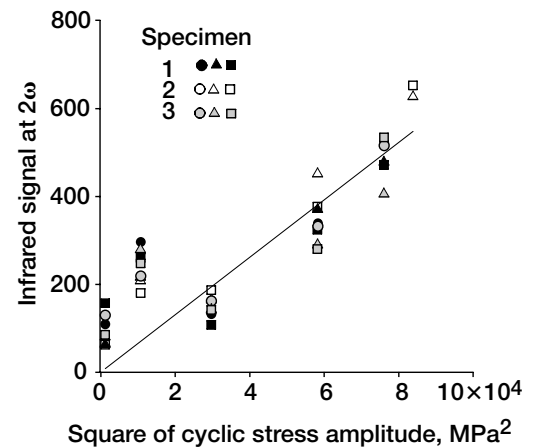
Dr. Andrew L. Gyekenyesi, (216) 433-8155,  
Andrew.L.Gyekenyesi@grc.nasa.gov

**Glenn contact:** Dr. George Y. Baaklini, (216) 433-6016,  
George.Y.Baaklini@grc.nasa.gov

**Authors:** Dr. Andrew L. Gyekenyesi and Dr. George Y. Baaklini

**Headquarters program office:** OAST

**Program/Project:** AvSP



*Second harmonic ( $2\omega$ ) infrared signal output at various stress amplitudes ( $\sigma_m = 0$ ). Indicated is the linear relationship of the TSA signal to the square of the cyclic stress amplitude. The second harmonic TSA response is independent of the cyclic mean stresses.*

## Composite Flywheels Assessed Analytically by NDE and FEA

As an alternative to expensive and short-lived lead-acid batteries, composite flywheels are being developed to provide an uninterruptible power supply for advanced aerospace and industrial applications. Flywheels can help prevent irregularities in voltage caused by power spikes, sags, surges, burnout, and blackouts. Other applications include load-leveling systems for wind and solar power facilities, where energy output fluctuates with weather. Advanced composite materials are being considered for these components because they are significantly lighter than typical metallic alloys and have high specific strength and stiffness. However, much more research is needed before these materials can be fully utilized, because there is insufficient data concerning their fatigue characteristics and non-linear behavior, especially at elevated temperatures.

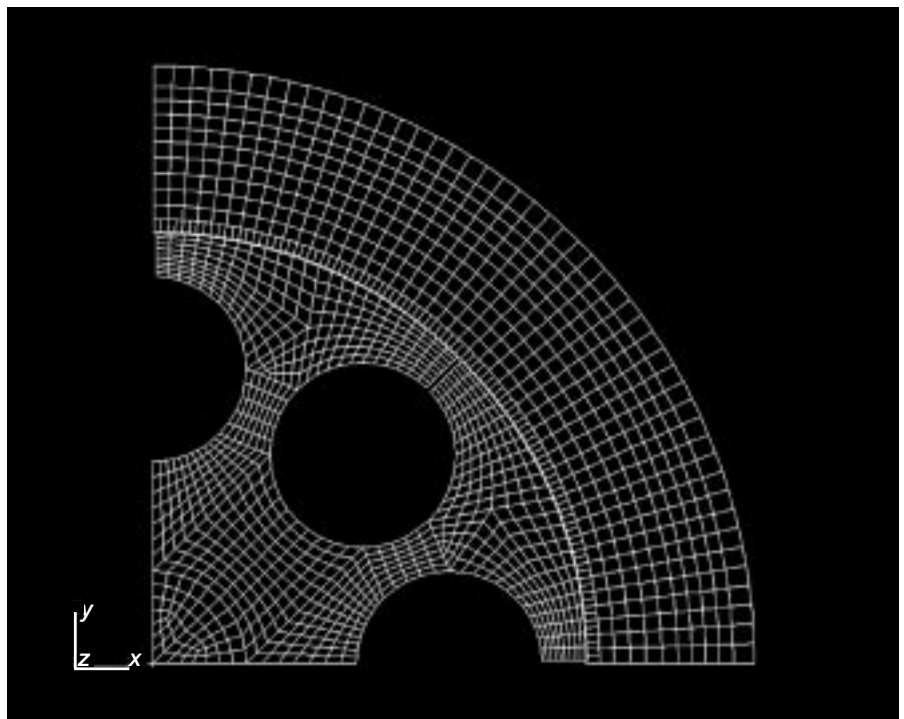
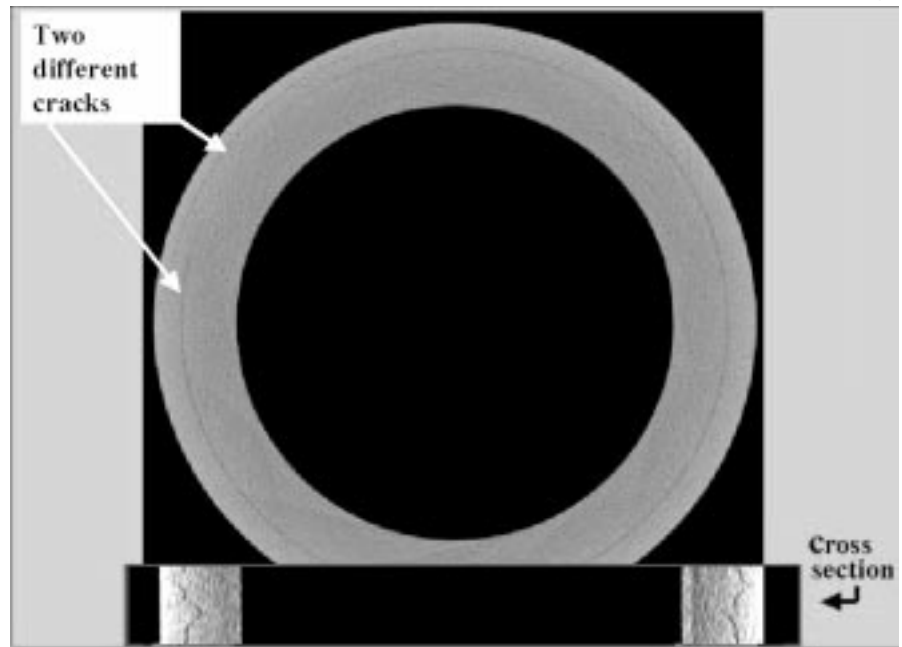
Moreover, these advanced types of structural composites pose greater challenges for nondestructive evaluation (NDE) techniques than are encountered with typical monolithic engineering metals (refs. 1 and 2). This is particularly true for ceramic polymer and metal matrix composites, where structural properties are tailored during the processing stages. In fully densified components, NDE techniques must detect and characterize various types of discrete defects like cracks, voids, and other overt discontinuities. It is also important to detect and characterize microstructural and diffuse flaw conditions that govern overall strength, fracture toughness, impact resistance, and resistance to thermal-mechanical-chemical degrada-

tion. These diffuse flaw states can reduce reliability and diminish service life just as much as discrete flaws (ref. 3).

In addition, the processing of innovative high-temperature materials requires the concurrent development of innovative NDE technologies. Sanders and Baaklini (ref. 4) demonstrated that the nondestructive characterization of materials and proper feedback help optimize the processing procedures. Applying American Society for Testing and Materials (ASTM) standards in nondestructive quality inspection assures the reliability of selected materials. Vary (ref. 5) suggested that new NDE standards and methodologies should mature simultaneously with advancements in materials development.

Current efforts involving the NDE group at the NASA Glenn Research Center at Lewis Field are focused on evaluating many important structural components, including the flywheel system. It has been shown that, with proper motor-generator and rotor design, flywheels have potentially higher efficiencies and longer lifetimes than other power systems, especially those made of fiber-reinforced polymer composite materials (ref. 6). However, the challenge of designing high-energy flywheel systems that can withstand the stresses caused by high rotational speeds is still considerable. At certain centrifugal loads, steel or titanium flywheels have shattered and been destroyed, which has increased interest in investigating the use of composite materials for future flywheels.

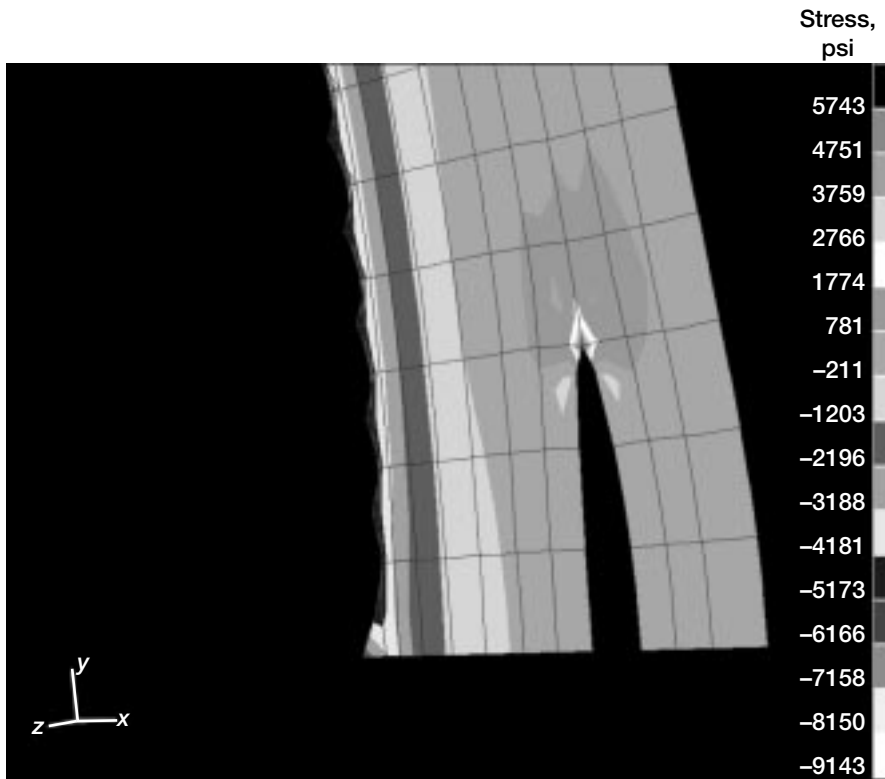
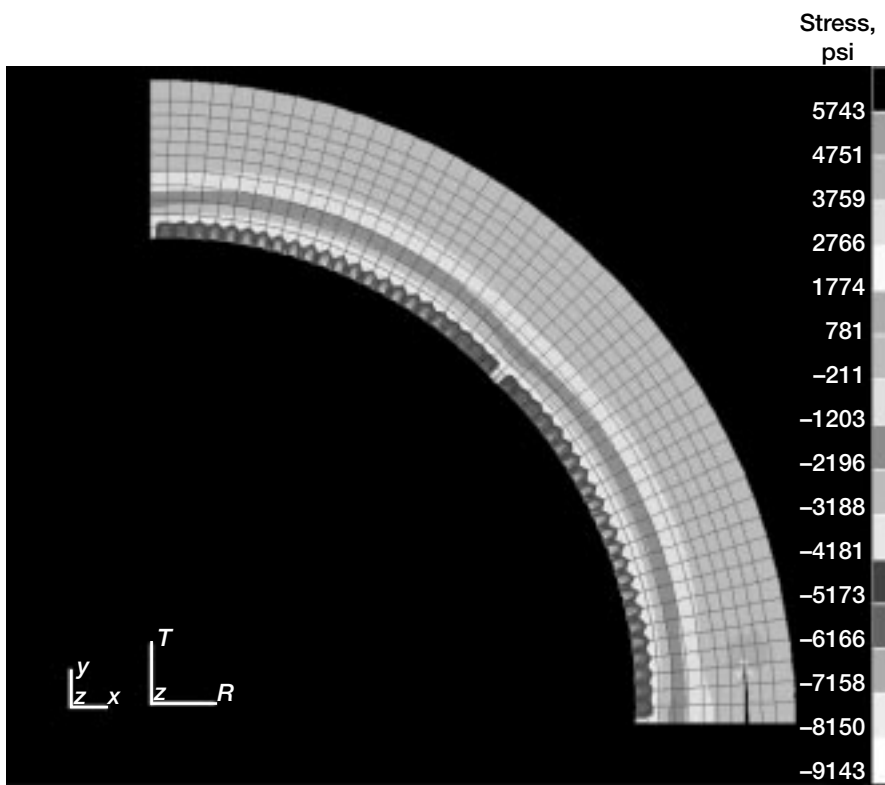
Glenn's in-house analytical and experimental capabilities are being applied to analyze data produced by computed tomography (CT) scans to help assess the damage and defects of high-temperature structural composite materials. Finite element analysis (FEA) has been used extensively to model the effects of static and dynamic loading on aerospace propulsion components. This technique allows the use of complicated loading schemes by breaking the complex part geometry into many smaller, geometrically simple elements. In-house and commercial software packages are being used to construct three-dimensional models of images from CT scan slices. For example, Velocity<sup>2</sup> (image processing and three-dimensional reconstruction visualization software, ref. 7) is being used to construct the three-dimensional model and subsequently to generate a stereolithography file that will be suitable for computer-aided design applications. Tools developed in-house are being used to convert Velocity<sup>2</sup>



Top: CT cross section of a tested flywheel and cross section from a limited three-dimensional data set. Bottom: Finite element model of rotor-hub assembly.

stereolithography files to solid, three-dimensional FEA meshes. The entire process that outlines the link between the data extracted via NDE and FEA will be published soon.

The figures presented in this article represent typical NDE–FEA results. The top figure shows a computed tomography (CT) scan for a polymer matrix composite rotor. It illustrates the defects due to centrifugal loading extracted by the CT scan in the rotor (spun at 34,000 rpm); two cracks



Top: Fracture mechanics analysis, radial stress distribution. Bottom: Fracture mechanics analysis, radial stress distribution, and closer view of crack propagation.

along the circumferential direction are clearly shown. In addition, a cross-sectional view of the crack that is parallel to the axis of rotation of the rotor is shown at the bottom of the top figure on the preceding page. The bottom figure on the preceding page is the FEA model of the rotor-hub assembly.

The figures to the left represent the FEA results obtained via fracture mechanic analyses; radial stress distribution is presented. Crack propagation is also documented in these figures. Stress levels due to the applied loading are noted. Tensile stresses at the crack tip reached nearly 6 ksi while the region where the rim contacts the hub remained compressive as anticipated. It can be concluded from the data that the finite element fracture mechanics closely simulated the CT scan findings. Furthermore, this work has established the preliminary grounds for an NDE-FEA-Fracture Mechanics interface methodology that can be used for the structural analysis of composite rotors.

#### References

1. Achenbach, J.D.; and Rajapakse, Y., eds.: Solid Mechanics Research and Qualitative Non-Destructive Evaluation, Martinus Nijhoff Publishers, Dordrecht, The Netherlands, 1987.
2. Vary, A.; and Snyder, J., eds.: Proceedings of the Nondestructive Testing of High-Performance Ceramics Conference, The American Ceramics Society, Westerville, OH, 1987.
3. Vary, A.; and Klima, S.J.: Nondestructive Techniques for Characterizing Mechanical Properties of Structural Materials—An Overview. ASME Paper 86-GT-75, 1986.
4. Sanders, W.A.; and Baaklini, G.Y.: Correlation of Processing and Sintering Variables With the Strength and Radiography of Silicon Nitride. Adv. Ceram. Mater., vol. 3, no. 1, 1988, pp. 88-94.

- Vary, A.: NDE Standards for High Temperature Materials. NASA TM-103761, 1991.
- Ashley, S.: Flywheels Put a New Spin on Electric Vehicles. Mech. Eng., vol. 115, Oct. 1993, pp. 44-51.
- Velocity<sup>2</sup> Technical Reference Manual Version 2.1, Velocity™ from 3D Imaging to 3D Reality. IMAGE3, LLC, South Salt Lake City, UT, 1996-1999.

**Glenn contact:**

Ali Abdul-Aziz, (216) 433-6729,  
Ali.Abdul-Aziz@grc.nasa.gov

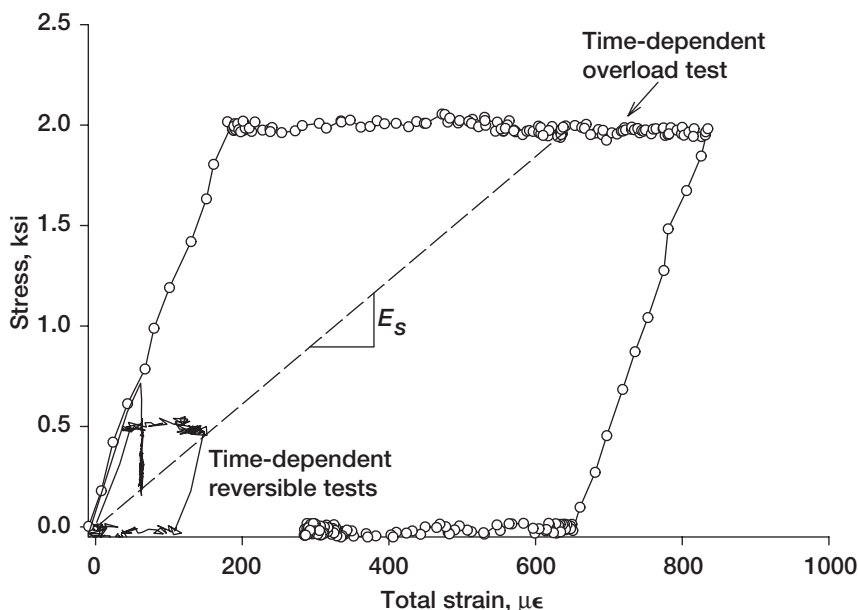
**Authors:** Ali Abdul-Aziz and  
Dr. George Y. Baaklini

**Headquarters program office:** OAST

**Programs/Projects:** Base Aeronautics  
& Space, HITEMP, ACESE

## Time-Dependent Reversible-Irreversible Deformation Threshold Determined Explicitly by Experimental Technique

Structural materials for the design of advanced aeropropulsion components are usually subject to loading under elevated temperatures, where a material's viscosity (resistance to flow) is greatly reduced in comparison to its viscosity under low-temperature conditions. As a result, the propensity for the material to exhibit time-dependent deformation is significantly enhanced, even when loading is limited to a quasi-linear stress-strain regime as an effort to avoid permanent (irreversible) nonlinear deformation. An understanding and assessment of such time-dependent effects in the context of combined reversible and irreversible deformation is critical to the development of constitutive models that can accurately predict the general hereditary behavior of material deformation. To this end, researchers at the NASA Glenn Research Center at Lewis Field developed a unique experimental technique that identifies the existence of and explicitly determines a threshold stress  $\kappa$ , below which the time-dependent material deformation is wholly reversible, and above which irreversible deformation is incurred.



*Time-dependent deformation tests provide explicit determination of the reversible-irreversible threshold stress ( $\kappa = \sigma_{\text{applied}} - \epsilon_{\text{IR}} E_s$ ) by using viscoelastic subtraction for a titanium alloy at 650 °C.*

This technique is unique in the sense that it allows, for the first time, an objective, explicit, experimental measurement of  $\kappa$ . The underlying concept for the experiment is based on the assumption that the material's time-dependent reversible response is invariable, even in the presence of irreversible deformation. The first step is to conduct a test (preferably two) where the time-dependent deformation response is wholly reversible. Shown in the figure are two such tests on the titanium alloy TIMETAL 21S at 650 °C; one is a creep test (constant stress hold) at 0.5 ksi, and the other is a stress relaxation test (constant strain hold) at 60  $\mu\epsilon$ .

Both tests exhibit shutdown of the time-dependent response, which is generally best seen in a time-based plot. For example, after approximately 5 hours of creep at 0.5 ksi, the creep strain rate went to zero (i.e., all creep shut down), and it remained in that state for 7 more hours. Upon unloading to zero stress subsequent to 12 hours of stress hold, the data revealed that the creep strain was fully recovered in time. The viscoelastic creep shut down at a strain of approximately 140  $\mu\epsilon$ . The stress relaxation test behaved in a similar way, terminating at approximately 0.23 ksi with subsequent full strain recovery observed. The stress-strain

slope  $E_s$  determined by the termination point(s) represents the time-independent stiffness at 650 °C and is indicative of an infinite limit stress for the spring within the standard solid viscoelastic model (see ref. 1).

The value of  $\kappa$  is determined by loading a sample beyond  $\kappa$  (well into the irreversible range) and holding the load long enough to allow the viscoelastic (time-dependent reversible) response to be fully exhausted. This is termed the "overload" test in the figure. The minimum hold time for this test should correspond to the shutdown time required for the viscoelastic tests. Subsequent to this hold period, where the accumulated creep strain results from both time-dependent reversible and irreversible behavior, the specimen is unloaded and given sufficient time to allow for full recovery of the time-dependent reversible strains. From this data, the excess equilibrium stress corresponding to the irreversible portion of the induced strain is calculated ( $\sigma_{\chi e} = \epsilon^{IR} E_s$ ) and then simply subtracted from the stress level at which the test is performed to obtain  $\kappa$  ( $\kappa = \sigma_{\text{applied}} - \sigma_{\chi e}$ ). This value effectively represents the upper bound of the viscoelastic regime and, thereby, represents the threshold of irreversible behavior. Appropriately, this technique has been termed "viscoelastic subtraction." Values of  $\kappa$  obtained from the viscoelastic subtraction technique were initially verified with more tedious, so-called probing experiments designed to establish the threshold of yield and extremely slow-rate proportional limit tests (ref. 2).

## References

1. Saleeb, A.F.; and Arnold, S.M.: A General Reversible Hereditary Constitutive Model: Part I—Theoretical Developments. NASA TM-107493, 1997.
2. Arnold, S.M.; Saleeb, A.F.; and Castelli, M.G.: A General Reversible Hereditary Constitutive Model: Part II—Application to a Titanium Alloy. NASA TM-107494, 1997.

## Glenn contact:

Dr. Steven M. Arnold, (216) 433-3334, Steven.M.Arnold@grc.nasa.gov

**Authors:** Michael G. Castelli and Dr. Steven M. Arnold

**Headquarters program office:** OAST

**Programs/Projects:** HITEMP

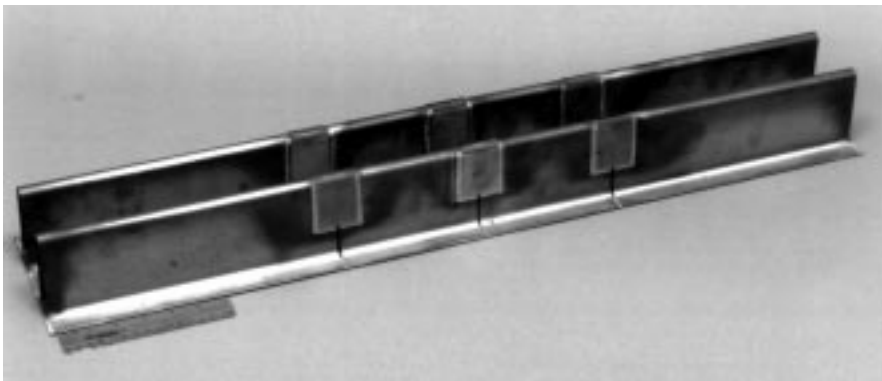
## Benchmark Testing of the Largest Titanium Aluminide Sheet Subelement Conducted

To evaluate wrought titanium aluminide ( $\gamma$ TiAl) as a viable candidate material for the High-Speed Civil Transport (HSCT) exhaust nozzle, an international team led by the NASA Glenn Research Center at Lewis Field successfully fabricated and tested the largest  $\gamma$ TiAl sheet structure ever manufactured. The  $\gamma$ TiAl sheet structure, a 56-percent subscale divergent flap subelement, was fabricated for benchmark testing in three-point bending. Overall, the subelement was 84-cm (33-in.) long by 13-cm (5-in.) wide by 8-cm (3-in.) deep. Incorporated into the subelement were features that might be used in the fabrication of a full-scale divergent flap. These features include the use of (1)  $\gamma$ TiAl shear clips to join together sections of

corrugations, (2) multiple  $\gamma$ TiAl face sheets, (3) double hot-formed  $\gamma$ TiAl corrugations, and (4) brazed joints.

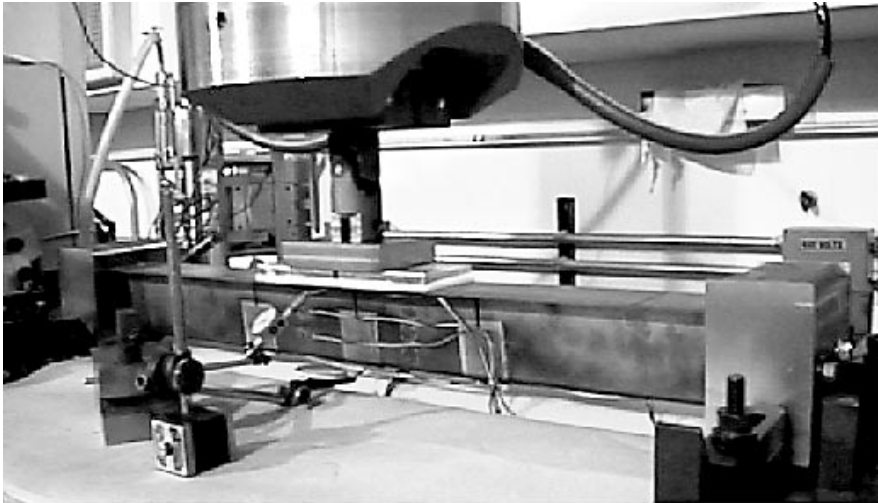
The structural integrity of the  $\gamma$ TiAl sheet subelement was evaluated by conducting a room-temperature three-point static bend test. The maximum beam deflection was approximately 2 mm (0.075 in.) at 340 kg (750 lb). Subelement failure occurred shortly after reaching 385 kg (850 lb). This is 93-percent higher than the predicted failure load.

The subelement failed at the center shear clip edge within the stress concentration area. Pretest finite element analysis (FEA) results accurately predicted the measured corrugation strains and stresses. Corrugation stresses were within 4 percent of predicted stresses. The pretest FEA results illustrated that



*Double corrugated titanium aluminide divergent flap subelement.*

### Research and Technology



*Benchmark test of titanium aluminide subelement (load at 340 kg).*

the tools and methodology to design components with this new material were in hand. Posttest FEA using a failure load of 850 lb (385 kg) showed that the stress at the failure location was 520 MPa (75 ksi). Since this is within 5 percent of the  $\gamma$ -sheet's ultimate tensile strength of 550 MPa (80 ksi), it proved that the fabrication process of hot-forming and brazing did not affect the material's structural capability.

This successful effort showed the tremendous potential of the  $\gamma$ TiAl sheet for advanced aerospace propulsion systems. Present interests in this material technology include a metallic thermal protection system for the VentureStar (Lockheed Martin Corporation) program, hot ducts and acoustic tiles for the Joint Strike Fighter program, and nozzle elements in the F119 propulsion system program.

**Glenn contacts:**

Dr. Paul A. Bartolotta, (216) 433-3338, Paul.A.Bartolotta@grc.nasa.gov; and David L. Krause, (216) 433-5465, David.L.Krause@grc.nasa.gov

**Authors:** Dr. Paul A. Bartolotta and David L. Krause

**Headquarters program office:** OAST

**Programs/Projects:** HSR, VentureStar, JSF, F119 propulsion system

## Titanium Aluminide Technologies Successfully Transferred From HSR Program to RLV VentureStar Program

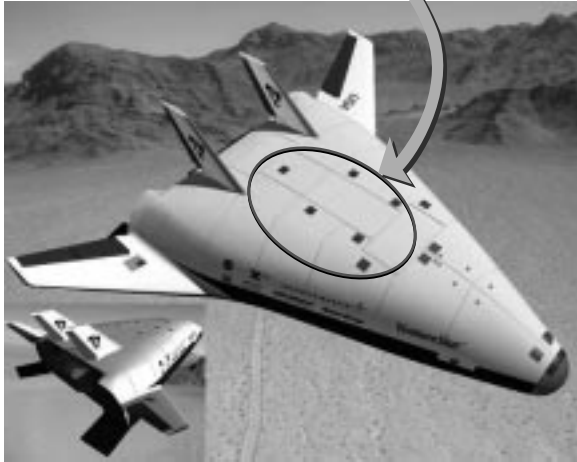
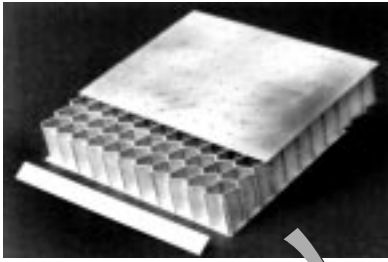
Through a cost-share contract, BFGoodrich Aerostructures group successfully fabricated three titanium aluminide ( $\gamma$ TiAl) truss core structures using technologies pioneered in the High-Speed Research (HSR) program at the NASA Glenn Research Center at Lewis Field. The truss core subelement is approximately 60-cm (24-in.) long by 14-cm (5.5-in.) wide by 6-cm (2.5-in.) deep. To fabricate this subelement, BFGoodrich first obtained  $\gamma$ TiAl sheets from Plansee (Austria) which produced the sheets using techniques developed collaboratively by Glenn, Pratt & Whitney, and Plansee. This new  $\gamma$ TiAl production technology has significantly lowered the cost of  $\gamma$ TiAl sheet (~75-percent decrease) and has made the production of larger  $\gamma$ TiAl sheets possible (~60-percent increase).

BFGoodrich then hot-formed the  $\gamma$ TiAl sheets into "hat" sections (individual internal stiffeners of the truss core that are shaped like the Greek letter omega) using a production hot press at near production rates as established by the HSR program. The  $\gamma$ TiAl hat sections and  $\gamma$ TiAl face sheets were then joined using HSR brazing technologies to produce the final truss core structure. NDE methods indicated that the truss core structures were sound, with over 98-percent coverage of all brazed joints.

The significance of this program is twofold. First, it demonstrated that HSR  $\gamma$ TiAl sheet fabrication technologies could be transferred



*Titanium aluminide truss core subelement manufactured by BFGoodrich Aerostructures group using HSR technologies.*



*VentureStar reusable launch vehicle, showing where the titanium aluminide metallic thermal protection system will be used.*

from the laboratory into the production house environment. Second, it was a vehicle to transfer the HSR  $\gamma$ TiAl fabrication technologies to the Reusable Launch Vehicle (RLV)/VentureStar (Lockheed Martin Corporation) program and other space transportation programs. According to BFGoodrich, this transfer has significantly aided their efforts in developing a metallic  $\gamma$ TiAl thermal protection system for the RLV/VentureStar program. This technology transfer is a prime example of the synergy between technologies developed for aeronautic applications enabling space transportation programs to meet their goals.

**Glenn contact:**

Dr. Paul A. Bartolotta, (216) 433-3338,  
Paul.A.Bartolotta@grc.nasa.gov

**Author:** Dr. Paul A. Bartolotta

**Headquarters program office:** OAST

**Programs/Projects:** HSR, VentureStar

## Test Standard Developed for Determining the Life Prediction Parameters of Advanced Structural Ceramics at Elevated Temperatures

The process of slow crack growth often limits the service life of structural ceramic components. Therefore, it is important to develop a test methodology for accurately determining the life prediction parameters required for component life prediction. In addition, this methodology should be useful in determining the influences of component processing variables and composition on the slow crack growth and strength behavior of newly developed or existing materials, thus allowing component processing to be tailored and optimized to specific needs.

In 1998, the authors initiated the development of a test method to determine the life prediction parameters of advanced structural ceramics at elevated temperatures. Performed at the NASA Glenn Research Center at Lewis Field, the work was done for the C28 Advanced Ceramics Committee of the American Society for Testing and Materials (ASTM). The draft standard written by the authors is going through the required balloting process. We expect it to be established in 2000 as a new ASTM test method, "Standard Test Method for Determining of Slow Crack Growth Parameters of Advanced Ceramics by Constant Stress-Rate Flexural Testing at Elevated Temperatures," and to be published in the year 2000 Annual Book of ASTM Standards, Vol. 15.01.

Briefly, the test method utilizes constant stress-rate testing to determine strengths as a function of the applied stress rate at elevated temperatures. The merit of this method lies in its simplicity: strengths are measured in a routine manner at four or more applied stress rates through the application of constant displacement or loading rates. The slow crack growth parameters necessary for life prediction are then determined from a simple relationship between the strength and the stress rate.

Glenn has maintained an active leadership role in the standardization of slow crack growth testing of

advanced ceramics within ASTM. The authors also wrote a companion ambient-temperature standard, ASTM C 1368–97, “Standard Test Method for Determination of Slow Crack Growth Parameters of Advanced Ceramics at Ambient Temperature,” which has been used by related industry, academia, and government agencies. In addition, Glenn has been actively involved with several international standardization organizations such as the Versailles Project on Advanced Materials and Standards (VAMAS) and the International Energy Agency. In 1988, for example, Glenn participated in a VAMAS round robin on fracture toughness of ceramics, using the Single-Edge-V-Notched Beam method.

**Glenn contacts:**

Dr. Sung R. Choi, (216) 433–8366, Sung.R.Choi@grc.nasa.gov; and Dr. John P. Gyekenyesi, (216) 433–3210, John.P.Gyekenyesi@grc.nasa.gov

**Authors:** Dr. Sung R. Choi and Dr. John P. Gyekenyesi

**Headquarters program office:** OAST

**Programs/Projects:** HITEMP, P&PM

## Nonlinearity and Strain-Rate Dependence in the Deformation Response of Polymer Matrix Composites Modeled

There has been no accurate procedure for modeling the high-speed impact of composite materials, but such an analytical capability will be required in designing reliable lightweight engine-containment systems. The majority of the models in use assume a linear elastic material response that does not vary with strain rate. However, for containment systems, polymer matrix composites incorporating ductile polymers are likely to be used. For such a material, the deformation response is likely to be nonlinear and to vary with strain rate. An analytical model has been developed at the NASA Glenn Research Center at Lewis Field that incorporates both of these features.

A set of constitutive equations that was originally developed to analyze the viscoplastic deformation of metals (Ramaswamy-Stouffer equations) was modified to simulate the nonlinear, rate-dependent deformation of polymers. Specifically, the effects of hydrostatic stresses on the inelastic response, which can be significant in polymers, were accounted for by a modification of the definition of the effective stress. The constitutive equations were then incorporated into a composite micromechanics model based on the mechanics of materials theory. This theory predicts the deformation response of a composite material from the properties and behavior

of the individual constituents. In this manner, the nonlinear, rate-dependent deformation response of a polymer matrix composite can be predicted.

In the figure, the tensile deformation response of a representative composite material that could be used in a fan-containment application is predicted. The predicted results compare favorably with experimentally obtained values. Currently, the deformation model is being implemented into a transient, dynamic finite element code. High-strain-rate data, which are required for the model, are also being obtained. The high-strain-rate data and the deformation model will be used to simulate ballistic impact tests that will be conducted in Glenn’s Structures and Acoustics Division Ballistic Impact Facility.

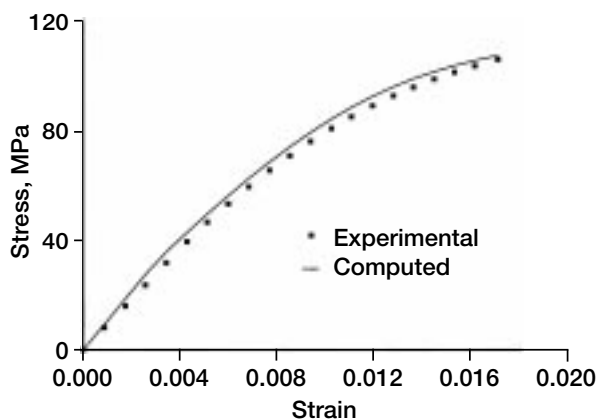
**Glenn contacts:**

Robert K. Goldberg, (216) 433–3330, Robert.K.Goldberg@grc.nasa.gov; and Dr. J. Michael Pereira, (216) 433–6738, J.M.Pereira@grc.nasa.gov

**Authors:** Robert K. Goldberg

**Headquarters program office:** OAST

**Programs/Projects:** Ultrasafe



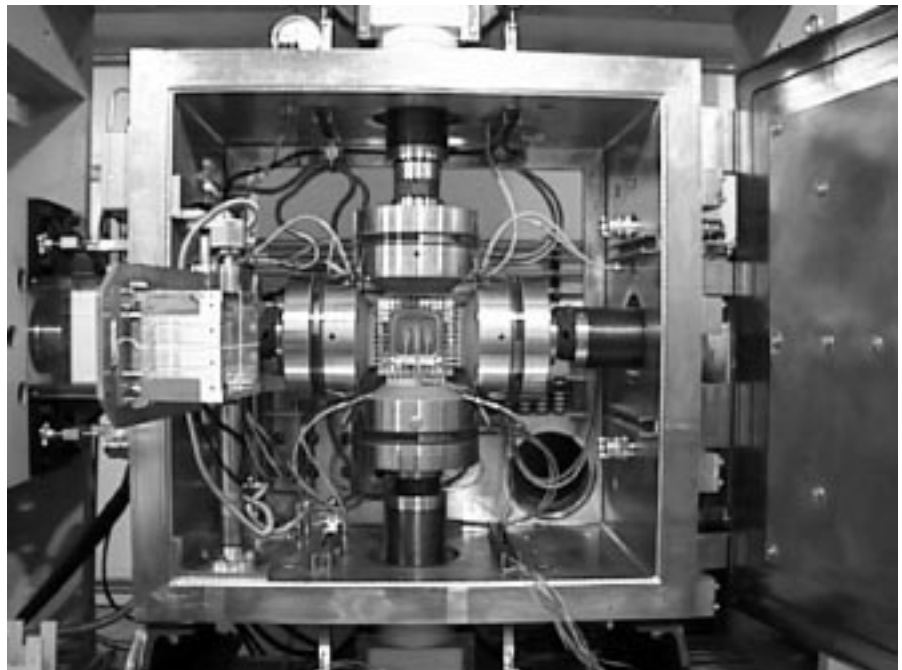
Model prediction for [45°] IM7/977–2 laminate compared with experimental results.

# Strain Measurement System Developed for Biaxially Loaded Cruciform Specimens

Components of mechanical equipment under load are routinely subjected to multiaxial states of stress at elevated temperatures. In addition, many construction materials exhibit anisotropic properties. For these conditions, in-plane biaxial testing of cruciform (cross-shaped) specimens is important for deriving mechanical properties used in design and life prediction.

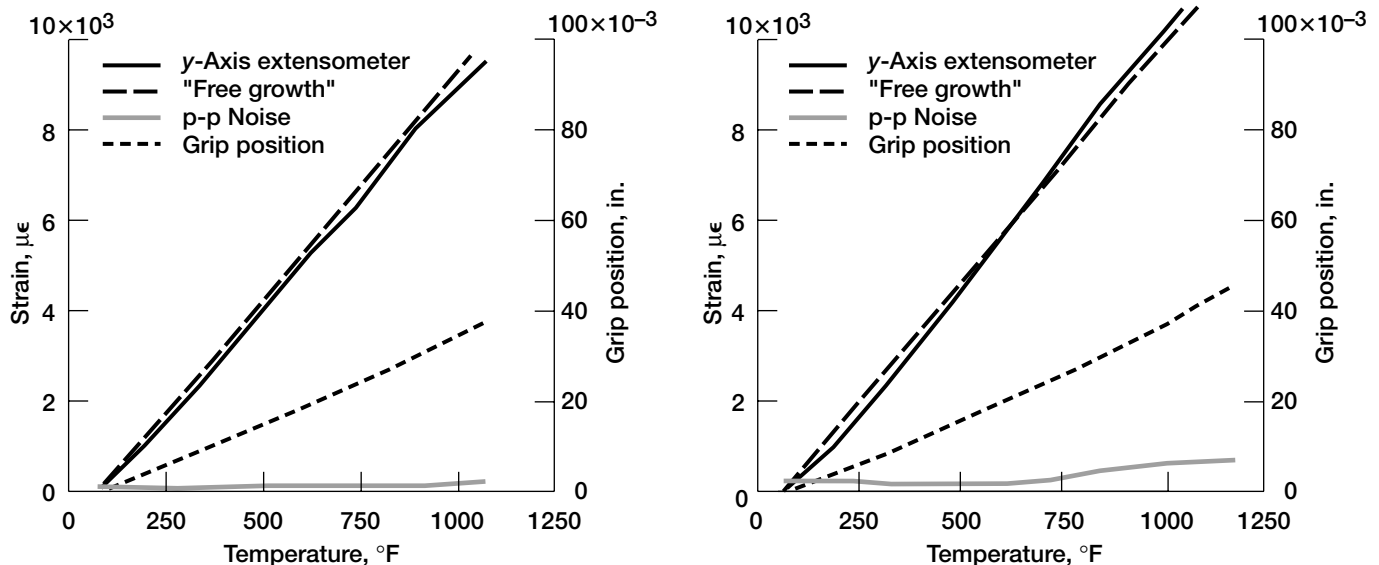
Accurate strain measurement during biaxial testing is critical. It permits calculating specimen test area stresses under various loading conditions. Real-time measurement permits observation of deformation behavior under biaxial loading conditions. In addition, continuous electronic measurement is used in the closed-loop test control for strain-controlled experiments and in all test types for sensing test-termination strain limits.

A new extensometer system developed at the NASA Glenn Research



*In-plane biaxial load frame with cruciform specimen.*

Center at Lewis Field measures test area strains along two orthogonal axes in flat cruciform specimens. This system incorporates standard axial contact extensometers to provide a cost-effective high-precision instrument. The device was validated for use by extensive testing of a stainless steel specimen, with specimen temperatures ranging from room temperature to



*Extensometer operation for free thermal growth of AISI<sup>1</sup> Type 304 specimen. Left: x-direction. Right: y-direction.*

<sup>1</sup>American Iron and Steel Institute (<http://www.steel.org>).

1100 °F. In-plane loading conditions included several static biaxial load ratios, plus cyclic loadings of various waveform shapes, frequencies, magnitudes, and durations. The extensometer system measurements were compared with strain gauge data at room temperature and with calculated strain values for elevated-temperature measurements. All testing was performed in house in Glenn's Benchmark Test Facility in-plane biaxial load frame.

A summary of the verification testing results follows: (1) the new extensometer system was calibrated with a maximum error of 0.8 percent; (2) the room-temperature correlation with strain gauge data yielded an average variation of 58 microstrain; (3) operation under cyclic conditions resulted in tracking errors of less than 3 percent; (4) elevated-temperature results compared accurately with theoretical predictions; and (5) long-duration testing proved to be stable.

This strain measurement system was developed to test advanced materials for the Advanced High Temperature Engine Materials Analysis Program (HITEMP) and the High-Speed Civil Transport propulsion system (HSR/EPM<sup>2</sup>). The candidate materials would be used in turbine engine components that are under highly multiaxial states of stress. Although monolithic,

the mechanical properties of these cast materials exhibit directionality because of large grain sizes. The extensometer system could be used for the future testing of other high-temperature materials, including polymer and ceramic matrix composite materials.

**Glenn contacts:**

David L. Krause, (216) 433-5465, David.L.Krause@grc.nasa.gov; and Dr. Paul A. Bartolotta, (216) 433-3338, Paul.A.Bartolotta@grc.nasa.gov

**Author:** David L. Krause

**Headquarters program office:** OAST

**Programs/projects:** HSR, EPM, HITEMP

---

<sup>2</sup><http://www.grc.nasa.gov/WWW/HSR/HSR.html>

## Damage Resistance of Titanium Aluminide Evaluated

As part of the aviation safety goal to reduce the aircraft accident rate, NASA has undertaken studies to develop durable engine component materials. One of these materials,  $\gamma$ -TiAl, has superior high-temperature material properties. Its low density provides improved specific strength and creep resistance in comparison to currently used titanium alloys. However, this intermetallic is inherently brittle, and long life durability is a potential problem. Of particular concern is the material's sensitivity to defects, which may form during the manufacturing process or in service. To determine the sensitivity of TiAl to defects, a team consisting of GE Aircraft Engines, Precision Cast Parts, and NASA was formed. The work at the NASA Glenn Research Center at Lewis Field has concentrated on the fatigue response to specimens containing defects.

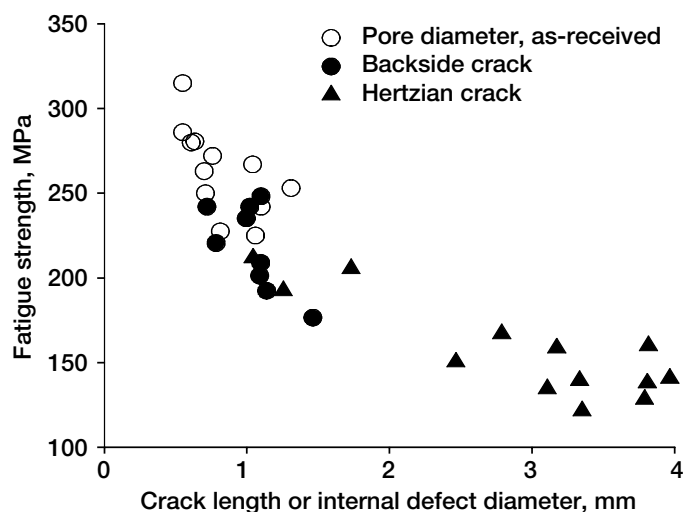
The overall objective of this work is to determine the influence of defects on the high cycle fatigue life of TiAl-simulated low-pressure turbine blades. Two types of defects have been introduced into the specimens: cracking from impact damage and casting porosity. For both types of defects, the cast-to-size fatigue specimens were fatigue tested at 650 °C and 100 Hz until failure.

Impacting the specimens yielded two forms of cracks, dependent on the impact energy. At a high energy, hertzian cracks were dominant and often led to material being removed from the edge of the specimen. At lower impact energies, cracks formed on the backside of the specimen perpendicular to the specimen axis. Both types of cracks are described in reference 1.

Additional specimens, which were originally rejected because of nondestructive evaluation (NDE) indications, were fatigue tested to study the degradation in fatigue life due to the presence of the casting defects.

Before testing, these specimens were reexamined using microfocus x-ray and computed tomography (ref. 2). Microfocus x-ray was successful in identifying 90 percent of the casting defects that caused failure and improved the detection capabilities over conventional radiography. Computed tomography, a time-consuming method, was only performed on two samples. This method gave cross-sectional information about the defects, which could be used to estimate the subsequent fatigue life.

Defect size played a large role in determining the critical fatigue loads. Increasing the defect size, regardless of whether the flaws resulted from casting porosity or from impact cracks, led to a decrease in the fatigue strength. Some of the severest impacts reduced the fatigue strength by almost a factor of three. The larger casting defects only reduced the fatigue strength by a maximum of 35 percent.



*Decline in fatigue strength with increasing defect size.*

This information on the effects of defects in  $\gamma$ -TiAl will be used in several ways. First, it will help set accept-reject limits for castings at the foundry, and in some cases, depending on part cost and defect location, may indicate when casting repairs should be made. Second, it will help develop a damage-tolerant design and life-determination approach for  $\gamma$ , to make sure that  $\gamma$ -TiAl parts will have the necessary robustness to provide a long life in engine service. Third, it will help establish field inspection and repair limits for parts that develop damage in service.

## References

1. Draper, S.L.; Pereira, J.M.; and Nathal, M.V.: Impact Resistance of  $\gamma$ -Ti-48Al-2Nb-2Cr. NASA CP-10192, Vol. II, HITEMP Review 1997, paper no. 25, pp. 1-13. (Available from NASA Glenn's Subsonic Systems Office.)
2. Lerch, B.A., et al.: Effect of Defects on the Fatigue Life of  $\gamma$ -TiAl. NASA/CP-1999-208915, Vol. II, HITEMP Review 1999, paper no. 30, pp. 1-11. (Available from NASA Glenn's Subsonic Systems Office.)

## Glenn contact:

Dr. Bradley A. Lerch, (216) 433-5522, Bradley.A.Lerch@grc.nasa.gov

**Authors:** Dr. Bradley A. Lerch, Susan L. Draper, Dr. George Y. Baaklini, Dr. J. Michael Pereira, and Curt Austin

**Headquarters program office:** OAST

**Programs/Projects:** Aeronautics Base R&T, Ultrasafe, HITEMP, AITP

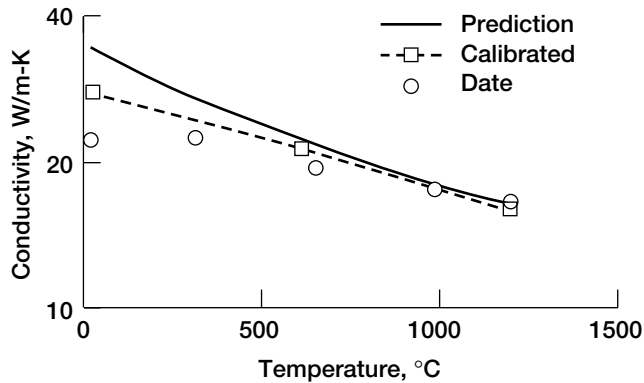
## CEMCAN Software Enhanced for Predicting the Properties of Woven Ceramic Matrix Composites

Major advancements are needed in current high-temperature materials to meet the requirements of future space and aeropropulsion structural components. Ceramic matrix composites (CMC's) are one class of materials that are being evaluated as candidate materials for many high-temperature applications. For example, combustor liners made of these materials can withstand very high temperatures. Furthermore, they can be operated uncooled, thereby improving engine performance as well as meeting or exceeding emission requirements. Past efforts to improve the performance of CMC's focused primarily on improving the properties of the fiber, interfacial coatings, and matrix constituents as individual phases. Design and analysis tools must take into consideration the complex geometries, microstructures, and fabrication processes involved in these composites and must allow the composite properties to be tailored for optimum performance. Major accomplishments during the past year include the development and inclusion of woven CMC micromechanics methodology into the CEMCAN (Ceramic Matrix Composites Analyzer) computer code.

Woven composite analysis, which is based on micromechanics techniques, is applicable to generalized two-dimensional woven architectures. The technique can account for the complex microstructure of these composites (i.e., the distribution and the volume fraction of the multiple constituent

phases that these advanced composites are now employing). Such an analysis tool is useful for preliminary screening of new candidate materials and to help material developers perform tradeoff studies by evaluating different fiber architectures, constituents, and their volume fractions.

The code enables one to calibrate a consistent set of constituent properties as a function of temperature with the aid of experimentally measured data. Such properties, though hard to find, are quite useful in computational design and analysis. With the aid of this code, the properties of an advanced five-harness SiC/SiC



Through-the-thickness thermal conductivity. Constituents: F-34.<sup>1</sup>

composite were predicted as a function of temperature. However, we realized that there were still some issues regarding the constituent properties at high temperatures and the confidence that can be put in these properties. The composite property predictions were compared with measured data available from the High-Speed Research (HSR) program to create calibrated constituent properties as a function of temperature. This information is very useful for material developers and design engineers. Such analytical tools can be used to predict the complete set of material properties needed by design engineers, whereas only a handful of them can be measured experimentally. In the figure, the through-the-thickness thermal conductivity of an advanced SiC/SiC composite is shown as a function of temperature. The predictions are shown for the initially assumed constituent properties as well as for the calibrated set of constituent properties with the measured data.

### Bibliography

Murthy, P.L.N.; Mital, S.K.; and DiCarlo, J.A.: Characterizing the Properties of a Woven SiC/SiC Composite Using W-CEMCAN Computer Code. NASA/TM-1999-209173, 1999. (Available online: <http://gltrs.grc.nasa.gov/cgi-bin/GLTRS/browse.pl?/1999/TM-1999-209173.html>)

Mital, S.K., et al.: Micromechanics-Based Modeling of Thermal and Mechanical Properties of an Advanced SiC/SiC Composite Material. NASA TM-206295, 1998. (Available from Glenn's HSR or UEET Project Office.)

**Glenn contact:** Dr. Pappu L.N. Murthy, (216) 433-3332, Pappu.L.Murthy@grc.nasa.gov

**University of Toledo contact:** Subodh K. Mital, (216) 433-3261, Subodh.K.Mital@grc.nasa.gov

### Authors:

Dr. Pappu L.N. Murthy, Subodh K. Mital, and Dr. James A. DiCarlo

**Headquarters program office:** OAST

**Programs/Projects:** HSR, EPM

<sup>1</sup>A set of constituents that leads to an overall fiber volume ratio of 34 vol % in the resulting composite.

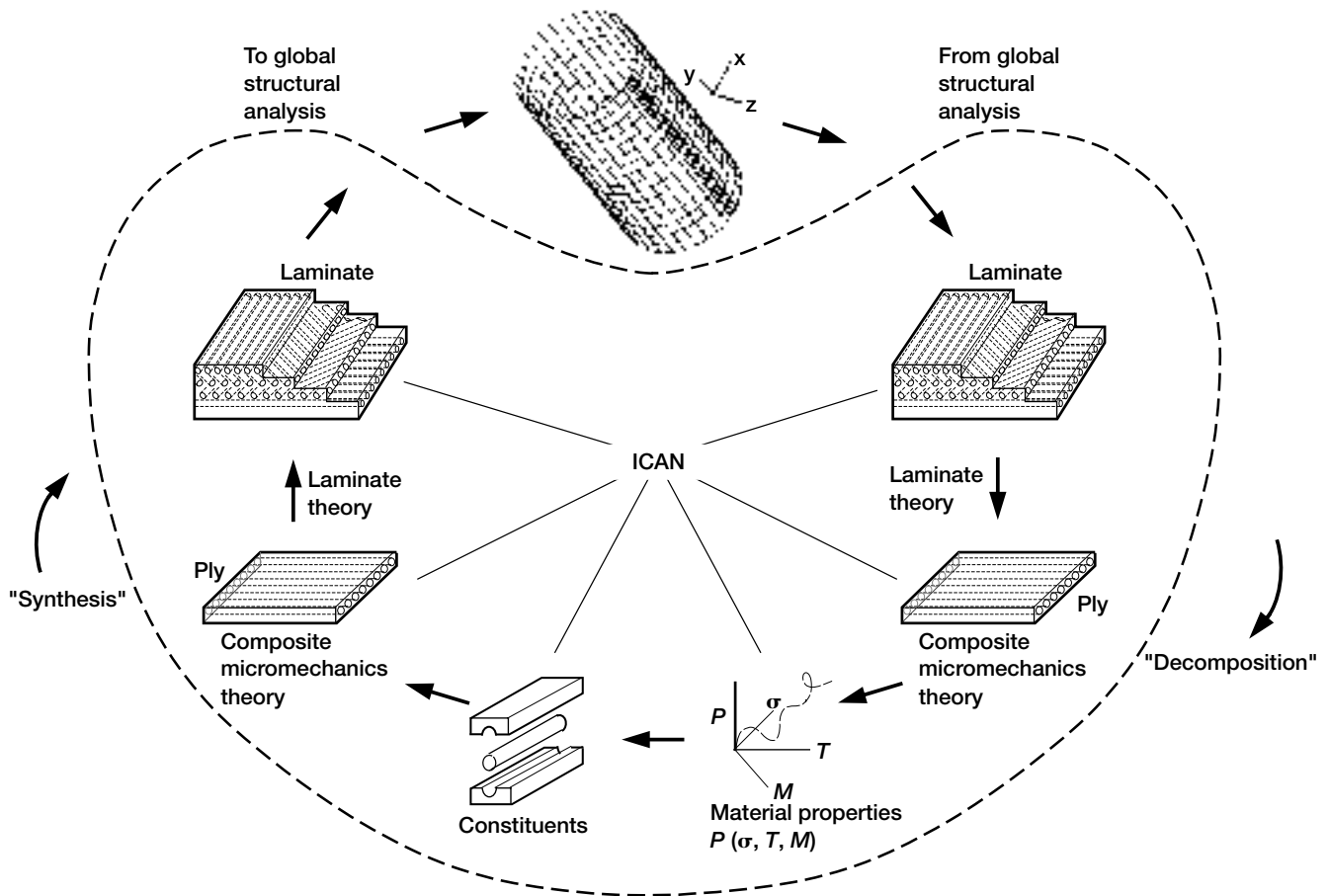
## GENOA-PFA: Progressive Fracture in Composites Simulated Computationally

GENOA-PFA is a commercial version of the Composite Durability Structural Analysis (CODSTRAN) computer program that simulates the progression of damage ultimately leading to fracture in polymer-matrix-composite (PMC) material structures under various loading and environmental conditions. GENOA-PFA offers several capabilities not available in other programs developed for this purpose, making it preferable for use in analyzing the durability and damage tolerance of complex PMC structures in which the fiber reinforcements occur in two- and three-dimensional weaves and braids.

GENOA-PFA implements a progressive-fracture methodology based on the idea that a structure fails when flaws that may initially be small (even microscopic) grow and/or coalesce to a critical dimension where the structure no longer has an adequate safety margin to avoid catastrophic global fracture. Damage is considered to progress through five stages: (1) initiation, (2) growth, (3) accumulation (coalescence of propagating flaws), (4) stable propagation (up to the critical dimension), and (5) unstable or very rapid propagation (beyond the critical dimension) to catastrophic

failure. The computational simulation of progressive failure involves formal procedures for identifying the five different stages of damage and for relating the amount of damage at each stage to the overall behavior of the deteriorating structure.

In GENOA-PFA, mathematical modeling of the composite physical behavior involves an integration of simulations at multiple, hierarchical scales ranging from the macroscopic (lamina, laminate, and structure) to the microscopic (fiber, matrix, and fiber/matrix interface),



Simulation of composite damage and fracture propagation via CODSTRAN (where  $M$  is moisture;  $P$ , property;  $T$ , temperature; and  $\sigma$ , stress).

as shown in this figure. The code includes algorithms to simulate the progression of damage from various source defects, including (1) through-the-thickness cracks and (2) voids with edge, pocket, internal, or mixed-mode delaminations.

Some of the salient features of the GENOA-PFA software follow:

- (1) Inclusion of the material's nonlinearities through periodic updates of the stiffness and inclusion of geometric nonlinearities through Lagrangian updating
- (2) Simulation of the initiation and growth of cracks and of the ultimate failure of the composite under static, cyclic, creep, and impact loads
- (3) Identification of the fractional contributions of various possible composite failure modes involved in critical damage events, and determination of the sensitivities of failure modes to such design parameters as fiber volume fractions, ply thicknesses, fiber orientations, and adhesive bond thicknesses.

#### Bibliography

Chamis, C.C.; Murthy, P.L.N.; and Minnetyan, L.: Progressive Fracture of Polymer Matrix Composite Structures. Theoret. Appl. Fracture Mech., vol. 25, no. 1, 1996, pp. 1-15.

GENOA Progressive Failure Analysis Program: Computational Simulation of Three-Dimensional Fiber Reinforced Composites. Volume 1—Theoretical Manual, Prepared by Dade Huang, Alpha STAR Corporation, Long Beach, CA, Sept. 1998.

GENOA: Progressive Failure Analysis Module for 2D/3D Laminate/Woven/Braided/Stitched Polymer Matrix Composites, USER's Manual, Version 7.0, Alpha STAR Corporation, Long Beach, CA, Jan. 1999.

**Glenn contacts:** Dr. Pappu L.N. Murthy, (216) 433-3332, Pappu.L.Murthy@grc.nasa.gov; and Dr. Christos C. Chamis, (216) 433-3252, Christos.C.Chamis@grc.nasa.gov

**Author:** Dr. Pappu L.N. Murthy

**Headquarters program office:** OAST

**Programs/Projects:** Base R&T

**Special recognition:**

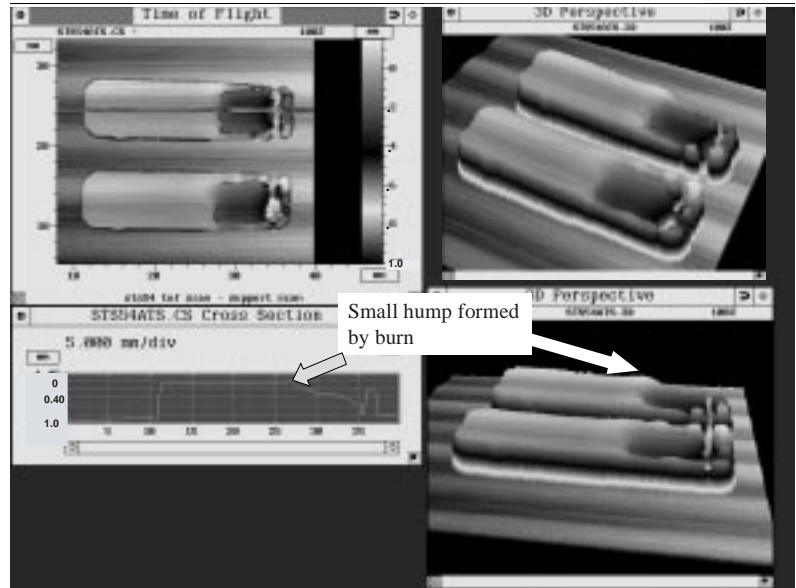
1999 Software of the Year award

## New Technology—Large-Area Three-Dimensional Surface Profiling Using Only Focused Air-Coupled Ultrasound—Given 1999 R&D 100 Award

Surface topography, which significantly affects the performance of many industrial components, is normally measured with diamond-tip profilometry over small areas or with optical scattering methods over larger areas. To develop air-coupled surface profilometry, the NASA Glenn Research Center at Lewis Field initiated a Space Act Agreement with Sonix, Inc., through two Glenn programs, the Advanced High Temperature Engine Materials Program (HITEMP) and COMMTECH. The work resulted in quantitative surface topography profiles obtained using only high-frequency, focused ultrasonic pulses in air. The method is nondestructive, noninvasive, and noncontact, and it does not require light-reflective surfaces. Air surface profiling may be desirable when diamond-tip or laser-based methods are impractical, such as over large areas, when a significant depth range is required, or for curved surfaces. When the configuration is optimized, the method is reasonably rapid and all the quantitative analysis facilities are online, including two- and three-dimensional visualization, extreme value filtering (for faulty data), and leveling.

The method is simple and reproducible because it relies mainly on the knowledge of and the constancy of the velocity of sound through air. When the air transducer is scanned across the surface, it sends pulses to the sample surface, where they are reflected back along the same path as the incident wave. (We recommend an air transducer with a ~1-MHz nominal center frequency to generate the air pulses.) Time-of-flight images of the sample surface are acquired and converted to depth and surface profile images using the simple relation  $d = V(t/2)$ , where  $d$  is the distance,  $t$  is the time of flight, and  $V$  is the velocity of sound in air.

The system can resolve surface depression variations as small as 25  $\mu\text{m}$  with 400- $\mu\text{m}$  lateral resolution, is useable over a 1.4-mm vertical depth range, and can profile large areas limited only by the scan limits of the particular ultrasonic system. (The best-case depth resolution is 0.25- $\mu\text{m}$ , which may be achievable with improved isolation from air currents and vibrations—both external vibrations and those due to motor or bridge assembly movement.) Results are shown for several proof-of-concept samples: plastic samples burned in microgravity on the STS-54 space shuttle mission and a partially coated, cylindrical ceramic composite sample. When compared with diamond-tip profiles and measurements from micrometers, the topographical representations for all the samples are impressive. Funding for this work came from the NASA HITEMP and COMMTECH programs and from Sonix, Inc.



*Air surface profiles for Burned Space Experiment samples. Left: Two-dimensional view and line profile across one scan line of top sample. Right: Three-dimensional views.*

### Find out more about this research on the World Wide Web:

<http://www.grc.nasa.gov/WWW/LPB/research/nde/rnd100.html>

### Bibliography

Roth, D.J., et al.: 3-D Surface Depression Profiling Using High-Frequency Focused Air-Coupled Ultrasonic Pulses. NASA/TM-1999-209053, 1999. (Available online: <http://gltrs.grc.nasa.gov/cgi-bin/GLTRS/browse.pl?/1999/TM-1999-209053.html>)

### Glenn contact:

Dr. Don J. Roth, (216) 433-6017,  
Don.J.Roth@grc.nasa.gov

### Authors:

Dr. Don J. Roth, Harold E. Kautz,  
Dr. Phillip B. Abel, Mike F. Whalen,  
J. Lynne Hendricks, and James R. Bodis

### Headquarters program office: OAST

**Programs/Projects:** HITEMP,  
COMMTECH, Space Act Agreement

### Special recognition:

1999 R&D 100 Award

# Propulsion Aeroelastic Analysis Developed for Flutter and Forced Response

The NASA Glenn Research Center at Lewis Field develops new technologies to increase the fuel efficiency of aircraft engines, improve the safety of engine operation, reduce emissions, and reduce engine noise. With the development of new designs for fans, compressors, and turbines to achieve these goals, the basic aeroelastic requirements are that there should be no flutter (self-excited vibrations) or high resonant blade stresses (due to forced response) in the operating regime. Therefore, an accurate prediction and analysis capability is required to verify the aeroelastic soundness of the designs. Such a three-dimensional viscous propulsion aeroelastic analysis capability has been developed at Glenn with support from the Advanced Subsonic Technology (AST) program.

This newly developed aeroelastic analysis capability is based on TURBO, a three-dimensional unsteady aerodynamic Reynolds-averaged Navier-Stokes turbomachinery code developed previously under a grant from Glenn. TURBO can model the viscous flow effects that play an important role in certain aeroelastic problems—such as flutter with flow separation, flutter at high loading conditions near the stall line (stall flutter), flutter in the presence of shock and boundary-layer interaction, and forced response due to wakes and shock impingement. In aeroelastic analysis, the structural dynamics representation of the blades is based on normal modes. A finite-element analysis code is used to calculate these in-vacuum vibration modes and the associated natural frequencies.

In an aeroelastic analysis using the TURBO code, flutter and forced response are modeled as being uncoupled. To calculate if a blade row will flutter, one prescribes the motion of the blade to be a harmonic vibration in a specified in-vacuum normal mode. An aeroelastic analysis pre-processor is used to generate the displacement field required for the analysis. The work done by aerodynamic forces on the vibrating blade during a cycle of vibration is calculated. If this work is positive, the blade is dynamically unstable, since it will extract energy from the flow, leading to an increase in the blade's oscillation amplitude. The forced-response excitations on a blade row are calculated by modeling the flow through two adjacent blade rows using the TURBO code. The blades are assumed to be rigid. As an option, a single blade row can be modeled with the upstream blade row influence represented by a time-varying disturbance (gust) at the inlet boundary. The unsteady forces on a blade row from such analyses are used in a structural analysis along with the blade structural dynamics characteristics and aerodynamic damping associated with blade vibration to calculate the resulting dynamic stresses on the blade.

As part of the verification and validation of the aeroelastic analysis capability in TURBO, flutter and forced-response calculations were performed in collaboration with engine companies for various standard configurations and industry configurations. The aeroelastic analysis capability in the TURBO code will allow engine manufacturers to reduce design cycle times by allowing new blade designs to be verified for aeroelastic soundness before they are built and tested. With this prediction capability, it will be possible to build thinner, lighter, and faster rotating blades without encountering aeroelastic problems like stall flutter and high-cycle fatigue due to forced vibrations.

**Glenn contacts:**

Milind A. Bakhle, (216) 433-6037,  
Milind.A.Bakhle@grc.nasa.gov;  
Rakesh Srivastava, (216) 433-6045,  
Rakesh.Srivastava@grc.nasa.gov; and  
George L. Stefko, (216) 433-3920,  
George.L.Stefko@grc.nasa.gov

**Authors:** Milind A. Bakhle

**Headquarters program office:** OAST

**Programs/Projects:** AST

# Optical Measurements of Axial and Tangential Steady-State Blade Deflections Obtained Simultaneously

Case-mounted fiber-optic sensors have been used by aircraft engine manufacturers mainly to monitor blade vibration in fans and compressors. The simplest probe arrangement is a spot probe where, typically, a center fiber transmits laser light, and the outer fibers collect the reflected light from the blade tips and transmit it to a photodetector. Because the spot of incident light is fixed in space, whereas the blade deflects dynamically, the reflected light will originate from slightly different portions of the blade tip under different operating conditions. Unless corrections are developed to compensate for this effect, some error in vibratory tangential amplitude will occur. For monitoring vibrations, this error is usually not critical.

However, when steady-state blade deflections are being measured, it is very important to fix the spot on the blade tip at a particular location because the operating speed blade deflections are evaluated against a low-speed reference run. The change in speed usually implies a significant change in the blade orientation and possibly its shape brought about by the aerodynamic and centrifugal loading.

It is most convenient to select the blade's leading and trailing edges as the fixed points for which deflections will be evaluated. To capture the blade edges at various speeds, the light probe must be movable. This was achieved by mounting the probe in an eccentric hole in a bushing that fit the fan case in the region that overlapped the path of the blade edge. The probe was actuated to search for a blade edge while all the blades were viewed on an oscilloscope. The blade edge was considered to be captured when a pulse associated with a particular blade was significantly reduced in magnitude but was clearly distinguishable from the background noise level. By tracing the axial position of either blade edge, one could extend the deflection measurement to two dimensions: axial and tangential. These blade deflection measurements were obtained during a wind tunnel test of a fan prototype.

As shown in this photograph of the servomotor-actuator assembly, the cylindrical enclosure that accommodates the eccentrically positioned optical probe was open on one side to provide an exit path for the fiber-optic cable. The 180° opening in the housing was oriented such that its base (along the diameter) was parallel to the fan rotor axis. Thus, when the motor was actuated, the probe moved over a semicircular path, maximizing the extent of the motion in the axial direction. The two noncontacting limit switches (not shown in the photograph) restricted the extent of rotation to 180°. The servomotor had a resolution of 4000 counts per revolution and was controlled remotely by a computer.

## Bibliography

Kurkov, A.P.; and Dhadwal, H.S.: Simultaneous Optical Measurements of Axial and Tangential Steady-State Blade Deflections. NASA/TM-1999-209051, March 1999. (Available online: <http://gltrs.grc.nasa.gov/cgi-bin/GLTRS/browse.pl?/1999/TM-1999-209051.html>)



*Probe-actuator/motor assembly.*

## Glenn contact:

Dr. Anatole P. Kurkov, (216) 433-5695, Anatole.P.Kurkov@grc.nasa.gov

**Authors:** Dr. Anatole P. Kurkov and Dr. Harbans S. Dhadwal

**Headquarters program office:** OAST

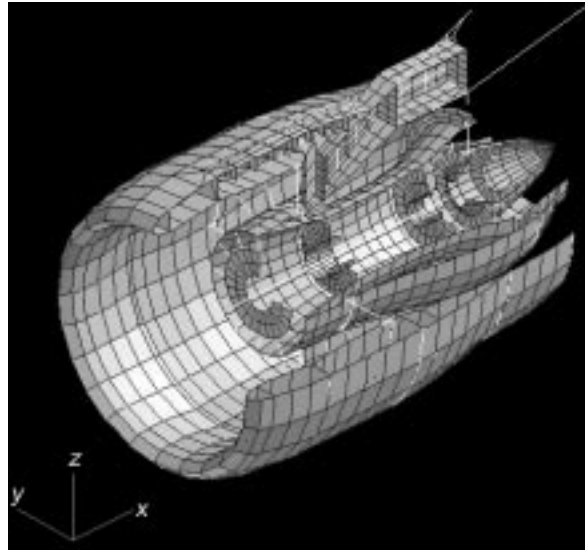
**Programs/Projects:** AST (Noise)

# Structural Simulations of Engine-Airframe Systems Being Improved

The current environment for designing engine and engine-airframe structural systems requires extensive efforts to prepare and integrate models, generate analysis results, and postprocess data. Despite these efforts, the accuracy of the simulations is inadequate, leading to less than optimal designs, costly testing and redesigns, and most important, significant uncertainties in safety factors. The goal of this project is to develop improved tools for structural simulations of engine-airframe systems. To develop these new tools, the NASA Glenn Research Center at Lewis Field has teamed with GE Aircraft Engines, Pratt & Whitney, and Boeing Commercial Aircraft. Boeing brings a wealth of large-scale, complex, structural systems analysis experiences and capabilities to the team, while GE and Pratt & Whitney bring aircraft-engine-specific structural expertise.

The tools that the team is creating are being used to assess a multitude of structurally related problems. The primary problem being addressed is the accurate simulation of a blade-out event and the subsequent windmilling of the engine. Reliable simulations of the loss of a blade are required to ensure structural integrity during flight as well as to guarantee successful blade-out certification testing. Simulation of the windmilling that occurs after blade-out is critical to avoiding excessive vibration levels, which may damage the aircraft and endanger passengers. In addition to blade-out and windmilling, the structural simulation tools are being used to determine structural response during regular aircraft operations and under loadings resulting from flight maneuvers. The loads generated by these analyses are critical for the teams designing several airplane components, including the engine, nacelle, strut, and wing.

The approach being used for the system simulation is to first develop a detailed high-fidelity simulation to capture the structural loads resulting from blade loss, and then use these loads in an overall system model that includes complete structural models of both the engines and airframe. The detailed simulation includes the time-dependent trajectory of the lost blade and its interactions with the containment structure, whereas the system simulation includes the lost blade loadings and the interactions between the rotating turbomachinery and the remainder of the aircraft's structural components. General-purpose finite-element structural analysis codes are being used to accomplish this task, and provisions are being



*Engine-wing structural system model.*

added to include transient effects from the blade loss and rotational effects resulting from the engine's turbomachinery. The figure depicts the generic structural model that was constructed to demonstrate and validate the tools that are being developed under this project.

**Glenn contacts:**

Dr. Charles Lawrence, (216) 433-6048, Charles.Lawrence@grc.nasa.gov; and Dr. Kelly S. Carney, (216) 433-2386, Kelly.S.Carney@grc.nasa.gov

**Author:** Dr. Charles Lawrence

**Headquarters program office:** OAST

**Programs/Projects:**

Propulsion Systems R&T

## Curved Thermopiezoelectric Shell Structures Modeled by Finite Element Analysis

"Smart" structures composed of piezoelectric materials may significantly improve the performance of aeropropulsion systems through a variety of vibration, noise, and shape-control applications. The development of analytical models for piezoelectric smart structures is an ongoing, in-house activity at the NASA Glenn Research Center at Lewis Field focused toward the experimental characterization of these materials.

Research efforts have been directed toward developing analytical models that account for the coupled mechanical, electrical, and thermal response of piezoelectric composite materials. Current work revolves around implementing thermal effects into a curvilinear-shell finite element code. This enhances capabilities to analyze curved structures and to account for coupling effects arising from thermal effects and the curved geometry.

The current analytical model implements a unique mixed multifield laminate theory to improve computational efficiency without sacrificing accuracy. The mechanics can model both the sensory and active behavior of piezoelectric composite shell structures. Finite element equations are being implemented for an eight-node curvilinear shell element, and numerical studies are being conducted to demonstrate capabilities to model the response of curved piezoelectric composite structures (see the figure).

### Bibliography

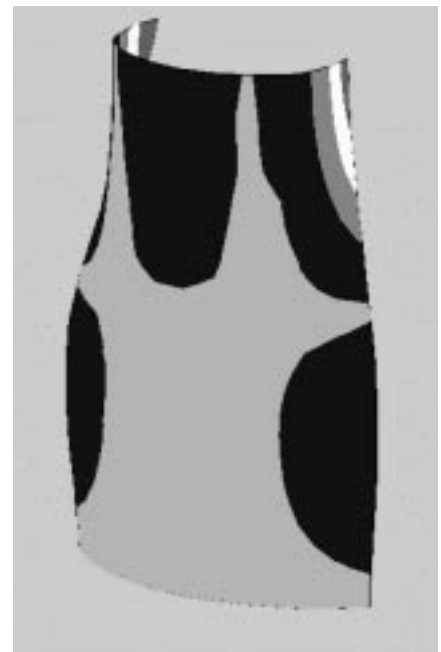
Lee, H.-J.; and Saravanos, D.A.: A Mixed Multi-Field Finite Element Formulation for Thermopiezoelectric Composite Shells. *Smart Structures and Materials 1999: Mathematics and Control in Smart Structures*. V.V. Varadan, ed., SPIE Proceedings, vol. 3667, Bellingham, WA, 1999, pp. 449–460.

**Glenn contact:** Ho-Jun Lee, (216) 433–3316, Ho-Jun.Lee@grc.nasa.gov

**Author:** Ho-Jun Lee

**Headquarters program office:** OAST

**Programs/Projects:** HITEMP



*Response of a curved piezoelectric composite shell under thermal loading.*

## Novel Vibration Damping of Ceramic Matrix Composite Turbine Blades Developed for RLV Applications

The Reusable Launch Vehicle (RLV) represents the next generation of space transportation for the U.S. space program. The goal for this vehicle is to lower launch costs by an order of magnitude from \$10,000/lb to \$1,000/lb. Such a large cost reduction will require a highly efficient operation, which naturally will require highly efficient engines. The RS–2200 Linear Aero-spike Engine is being considered as the main powerplant for the RLV. Strong, lightweight, temperature-resistant ceramic matrix composite (CMC) materials such as C/SiC are critical to the development of the RS–2200. Preliminary engine designs subject turbopump components to extremely high frequency dynamic excitation, and ceramic matrix composite materials are typically lightly damped, making them vulnerable to high-cycle fatigue.

The combination of low damping and high-frequency excitation creates the need for enhanced damping. Thus, the goal of this project has been to develop well-damped C/SiC turbine components for use in the RLV.

Foster-Miller and Boeing Rocketdyne have been using an innovative, low-cost process to develop

light, strong, highly damped turbopump components for the RS–2200 under NASA’s Small Business Innovation Research (SBIR) program. The NASA Glenn Research Center at Lewis Field is managing this work. The process combines three-dimensionally braided fiber reinforcement with a pre-ceramic polymer. The three-dimensional reinforcement significantly improves the structure over conventional two-dimensional laminates, including high through-the-thickness strength and stiffness.

Phase I of the project successfully applied the Foster-Miller pre-ceramic polymer infiltration and pyrolysis (PIP) process to the manufacture of dynamic specimens representative of engine components. An important aspect of the program has been the development of the manufacturing process. Results show that the three-dimensionally braided carbon-fiber reinforcement provides good processability and good mechanical stiffness and strength in comparison to materials produced with competing processes as shown in the graphs.

The RS–2200 turbopump turbine blades are susceptible to high-frequency vibration with motion dominated by leading- and trailing-edge motion. The most effective approach to controlling these vibrations is by increasing internal damping. Baseline C/SiC damping appears to decrease as a function of frequency and is too small, less than 0.2 percent for the turbine applications. Phase I results show that fiber architecture has little effect on damping. Previous research indicates that incorporating highly damped materials in the form of particulate fillers and coatings increases damping substantially. Several materials were identified that could be added to the base material to enhance damping, in particular, compounds containing boron. BN has a critical damping value as high as 2 percent.

The next step of this work will include end-to-end component development, encompassing process development and refinement, structural design, and structural dynamic testing. Damping materials will be incorporated into the material in the form of coatings and particulates, and the polymer infiltration and pyrolysis manufacturing will be modified to optimize mechanical behavior. The physical and mechanical properties of these materials will be completely characterized as a function of temperature and of microcracking caused by sustained centrifugal loads.

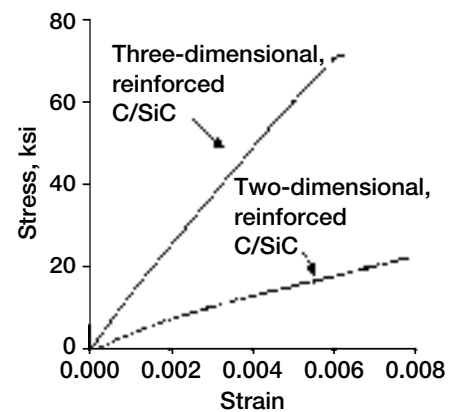
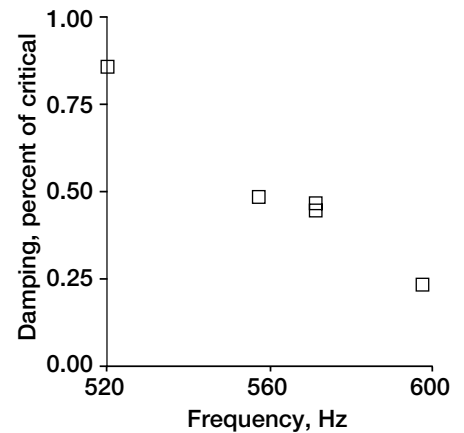
Foster-Miller and Boeing Rocketdyne will use these properties to design and manufacture insertable blades for the RS–2200 turbopump. The blades will be dynamically tested under simulated environmental and operational engine conditions.

**Bibliography**

Bishop, J.E.; and Kinra, V.K.: Some Improvement in the Flexural Damping Measurement Technique. *M<sup>3</sup>D: Mechanics and Mechanisms of Material Damping*. ASTM STP 1169, V.K. Kinra and A. Wolfenden, eds., ASTM, Philadelphia, PA, 1992, pp. 457–470.

Brockmeyer, J.W.; and Schnittgrund, G.D.: Fiber-Reinforced Ceramic Composites for Earth-to-Orbit Rocket Engine Turbines. NASA CR–185264, 1990.

Effinger, M.R.; Koenig, J.R.; and Halbig, M.C.: C/SiC Mechanical and Thermal Design Data for a Turbopump Blisk. *Proceedings of the Composites, Materials and Structures Conference*, Cocoa Beach, FL, Jan. 1997.



Top: Dynamic characterization.  
Bottom: Static characterization.

Genge, G.G., et al.: Development of a Ceramic Matrix Composite Integrally Bladed Disk for Use in the SIMPLEX Turbopump. The 1996 JANNAF Propulsion Meeting, Vol. 2, 1996, pp. 587–598.

Ting, J.M.; and Crawley, E.F.: Characterization of Damping of Materials and Structures From Nanostrain Levels to One Thousand Microstrain. *AIAA J.*, vol. 30, no. 7, 1992, pp. 1856–1863.

**Glenn contact:**

Dr. James B. Min, (216) 433–2587, James.B.Min@grc.nasa.gov

**Author:** Dr. James B. Min

**Headquarters program office:** OAST

**Programs/Projects:** Propulsion Systems R&T, HITEMP, ASTP, SBIR

# Cascade Optimization Strategy With Neural Network and Regression Approximations Demonstrated on a Preliminary Aircraft Engine Design

A preliminary aircraft engine design methodology is being developed that utilizes a cascade optimization strategy together with neural network and regression approximation methods. The cascade strategy employs different optimization algorithms in a specified sequence. The neural network and regression methods are used to approximate solutions obtained from the NASA Engine Performance Program (NEPP), which implements engine thermodynamic cycle and performance analysis models. The new methodology is proving to be more robust and computationally efficient than the conventional optimization approach of using a single optimization algorithm with direct reanalysis. The methodology has been demonstrated on a preliminary design problem for a novel subsonic turbofan engine concept that incorporates a wave rotor as a cycle-topping device. Computations of maximum thrust were obtained for a specific design point in the engine mission profile. The results (depicted in the figure) show a significant improvement in the maximum thrust obtained using the new methodology

in comparison to benchmark solutions obtained using NEPP in a manual design mode.

**Glenn contact:**

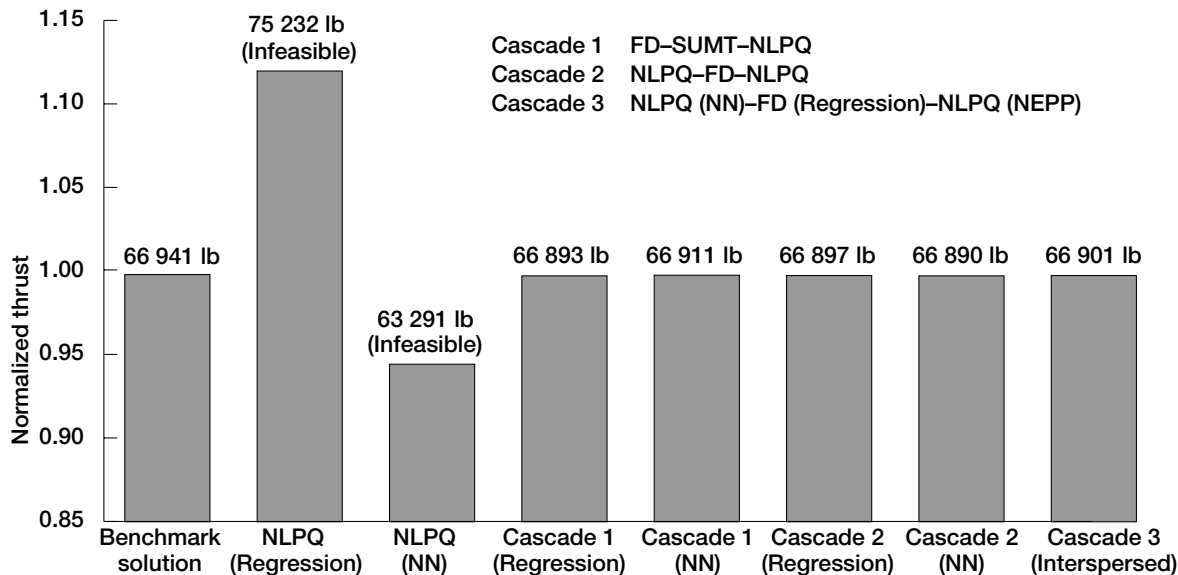
Dale A. Hopkins, (216) 433-3260,  
Dale.A.Hopkins@grc.nasa.gov

**Authors:** Dale A. Hopkins and  
Dr. Surya N. Patnaik

**Headquarters program office:** OAST

**Programs/Projects:**

Propulsion System R&T



Optimum thrust for a subsonic wave-rotor-topped engine for the sixth operating point.

Optimization method	Description
Benchmark solution	Average thrust obtained using 10 different initial designs.
NLPQ (Regression)	Thrust obtained using NLPQ and regression approximation.
NLPQ (NN)	Thrust obtained using the quadratic programming algorithm (NLPQ) and the neural network (NN) approximation.
Cascade 1 <sup>a</sup> (Regression)	Thrust obtained using the Cascade 1 strategy and the regression approximation.
Cascade 1 <sup>a</sup> (NN)	Thrust obtained using the Cascade 1 strategy and the neural network approximation.
Cascade 2 (Regression)	Thrust obtained using the Cascade 2 strategy and the regression approximation.
Cascade 2 (NN)	Thrust obtained using the Cascade 2 strategy (NLPQ-FD-NLPQ) and the neural network approximation.
Cascade 3 (Interspersed)	Thrust obtained using the interspersed cascade strategy (NLPQ with NN, FD with regression, and NLPQ with the NASA Engine Performance Program (NEPP) reanalysis).

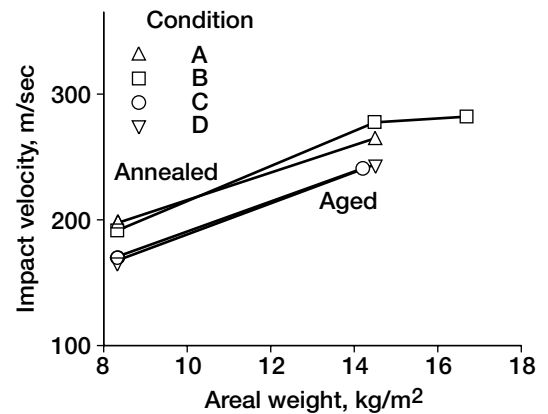
<sup>a</sup>The Cascade 1 strategy uses three algorithms: the Method of Feasible Directions (FD) followed by the Sequential Unconstrained Minimization Technique (SUMT) and the quadratic programming algorithm (NLPQ).

# Effects of Various Heat Treatments on the Ballistic Impact Properties of Inconel 718 Investigated

Uncontained failures of aircraft engine fan blades are serious events that can cause equipment damage and loss of life. Federal Aviation Administration (FAA) certification requires that all engines demonstrate the ability to contain a released fan blade with the engine running at full power. However, increased protection generally comes at the expense of weight. Proper choice of materials is therefore imperative to an optimized design. The process of choosing a good casing material is done primarily through trial and error. This costly procedure could be minimized if there was a better understanding of the relationships among static material properties, impact properties, and failure mechanisms. This work is part of a program being conducted at the NASA Glenn Research Center at Lewis Field to study these relationships. Ballistic impact tests were conducted on flat, square sheets of Inconel 718 that had been subjected to different heat treatments. Two heat treatments and the as-received condition were studied. In addition, results were compared with those from an earlier study involving a fourth heat treatment. The heat treatments were selected on the basis of their effects on the static tensile properties of the material.

The impact specimens used in this study were 17.8-cm square panels that were centered and clamped over a 15.2-cm square hole in a 1.27-cm-thick steel plate. Three nominal plate thickness dimensions were studied, 1.0, 1.8, and 2.0 mm. For each thickness, all the specimens were taken from the same sheet of material. The projectile was a Ti-6Al-4V cylinder with a length of 25.4 mm, a diameter of 12.7 mm, and a mass ranging from 14.05 to 14.20 g. The projectiles were accelerated toward the specimens at normal incidence using a gas gun with a 2-m-long, 12.7-mm inner-diameter barrel. The ballistic limit for each heat treatment condition and thickness was determined by conducting a number of impact tests that bracketed as closely as possible the velocity required to penetrate the specimen.

We found that both the static and impact properties as well as the failure mechanisms of Inconel 718 can be changed significantly by varying the heat treatment. Under the conditions used in this study, softer annealed material performed dramatically better in ballistic impact tests than harder annealed and aged material (see the figure). Micrographs indicated highly localized areas of large shear deformation in impacted aged specimens. In the annealed material, the deformation was not as localized. Future studies will attempt to determine what specific material properties have the greatest influence on impact properties.



*Ballistic limit of Inconel 718 as a function of areal weight and heat treatment.*

#### Glenn contacts:

Dr. J. Michael Pereira, (216) 433-6738, J.M.Pereira@grc.nasa.gov; and  
Dr. Bradley A. Lerch, (216) 433-5522, Bradley.A.Lerch@grc.nasa.gov

#### Authors:

Dr. J. Michael Pereira and  
Dr. Bradley A. Lerch

**Headquarters program office:** OAST

**Programs/Projects:** HSCT

## Failure Accommodation Tested in Magnetic Suspension Systems for Rotating Machinery



*Fault-tolerant magnetic bearing rig.*

The NASA Glenn Research Center at Lewis Field and Texas A&M University are developing techniques for accommodating certain types of failures in magnetic suspension systems used in rotating machinery. In recent years, magnetic bearings have become a viable alternative to rolling element bearings for many applications. For example, industrial machinery such as machine tool spindles and turbomolecular pumps can today be bought off the shelf with magnetically supported rotating components. Nova Gas Transmission Ltd. has large gas compressors in Canada that have been running flawlessly for years on magnetic bearings.

To help mature this technology and quiet concerns over the reliability of magnetic bearings, NASA researchers have been investigating ways of making the bearing system tolerant to faults. Since the potential benefits from an oil-free, actively controlled bearing system are so attractive, research that is focused on assuring system reliability and safety is justifiable. With support from the Fast Quiet Engine program, Glenn's Structural Mechanics and Dynamics Branch is working to demonstrate fault-tolerant magnetic suspension systems targeted for aerospace engine applications. The Flywheel Energy Storage Program is also helping to fund this research.

The fault-tolerant magnetic suspension facility in Glenn's Engine Research Building, test cell SW18, was completed in fiscal year 1999. The test rig has two eight-pole heteropolar magnetic bearings that suspend the rotor radially. Each pole is individually controlled with its own pulse-width-

modulated amplifier. Opening the circuit between the pulse-width-modulated amplifier and the coil simulates coil failures. Turning off the amplifier supply power simulates amplifier failures. All possible combinations of failures can be realized by flipping switches on the facility control panel.

In fiscal year 1999, Glenn researchers tested unique solutions to 22 different combinations of single and multiple coil failures on a single bearing at zero speed. In all cases, levitation of the rotor was achievable. In addition, levitation with only three of the eight coils operational was demonstrated. A test case where every other coil in the outboard bearing was unpowered behaved satisfactorily to 3000 rpm. In fiscal year 2000, we plan to develop a controller that can detect any combination of failures and accommodate it without loss of levitation.

**Glenn contact:**

Andy J. Provenza, (216) 433-6025,  
Andrew.J.Provenza@grc.nasa.gov

**Ohio Aerospace Institute contact:**

Ralph H. Jansen, (216) 433-6038,  
Ralph.H.Jansen@grc.nasa.gov

**Texas A&M University contact:**

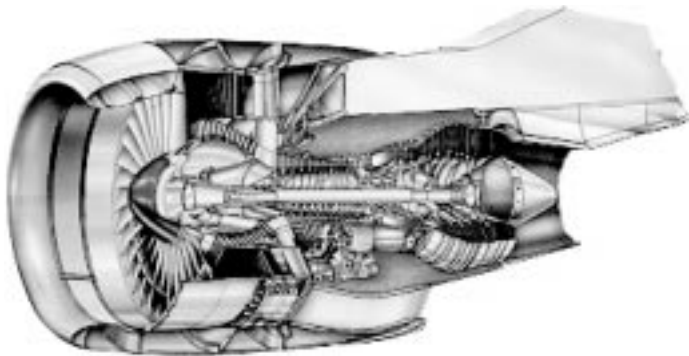
Dr. Alan Palazzolo, (409) 845-5280,  
abp8849@acs.tamu.edu

**Author:** Andy J. Provenza

**Headquarters program office:** OAST

**Programs/Projects:** FQE, Flywheel Energy Storage Program

# Acoustics and Thrust of Separate Flow Exhaust Nozzles With Mixing Devices Investigated for High Bypass Ratio Engines



*Typical installed separate-flow exhaust nozzle system.*

The jet noise from modern turbofan engines is a major contributor to the overall noise from commercial aircraft. Many of these engines use separate nozzles for exhausting core and fan streams. The illustration shows a typical exhaust nozzle system for a bypass ratio of about 5. As a part of NASA's Advanced Subsonic Technology (AST) program, the NASA Glenn Research Center at Lewis Field led an experimental investigation using model-scale nozzles in Glenn's Aero-Acoustic Propulsion Laboratory. The goal of the investigation was to develop technology for reducing the jet noise by 3 EPNdB.<sup>1</sup> Teams of engineers from Glenn, the NASA Langley Research Center, Pratt & Whitney, United Technologies Research Corporation, the Boeing Company, GE Aircraft Engines, Allison Engine Company, and Aero Systems Engineering contributed to the planning and implementation of the test.

New nozzles were designed to reduce the fully expanded jet velocity by mixing (1) core flow with fan flow only, (2) fan flow with ambient flow

only, or (3) both flows simultaneously. Depending on the type of mixing attempted, these designs fell into two broad categories: tabs and chevrons. Tabs are severe protrusions into the flow at the nozzle exit plane. Chevrons are also protrusions, but of much less severity than tabs. The aggressive mixing produced by the tabs greatly reduced low-frequency noise, but with the penalty of tab-induced high-frequency noise. Chevrons, which provided a more balanced approach to mixing, reduced low-frequency noise without significant chevron-induced high-frequency noise. Other nozzle designs attempted to shield the core flow by using a scarf fan nozzle and an offset fan nozzle.

A total of 54 exhaust nozzle systems were tested, including various combinations of nozzle designs within each category (tabs and chevrons) for each flow (core and fan). An extensive data base was generated on far-field acoustics,

<sup>1</sup>Effective perceived noise in decibels.



*Left: Chevrons on both nozzles. Right: Chevrons on fan nozzle and tabs on core nozzle.*

plume Schlieren images, exhaust plume pressures and temperatures, plume infrared signatures, jet noise source locations measured by one- and two-dimensional phased arrays, and thrust performance at a simulated cruise Mach of 0.8.

Several exhaust nozzle systems reduced jet noise by more than 2.5 EPNdB, calculated for a 1500-ft level flyover, without significant thrust loss either at takeoff or at cruise. The photos on the preceding page show two of the best exhaust nozzle systems.

Because of increasingly stringent restrictions near airports, the noise of an aircraft, much like its range and payload capability, has become a competitive factor. This investigation has generated great interest because of its timeliness and application to current exhaust nozzle systems. We expect

the resultant technologies to be incorporated in future turbofan engines.

**Glenn contacts:**

Naseem H. Saiyed, (216) 433-6736, Naseem.Saiyed@grc.nasa.gov; and Dr. James E. Bridges, (216) 433-2693, James.E.Bridges@grc.nasa.gov

**Author:** Naseem H. Saiyed

**Headquarters program office:** OAST

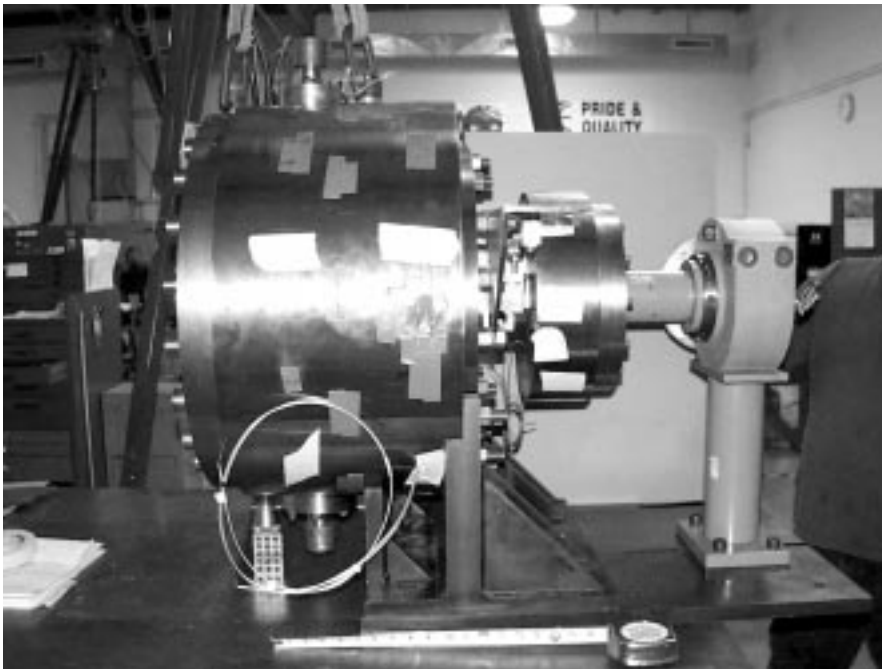
**Program/Projects:**

AST (Noise Reduction)

## New High-Temperature Turbine Seal Rig Fabricated

Current NASA program goals for aircraft engines and vehicle performance include reducing direct operating costs for commercial aircraft by 3 percent in large engines and 5 percent in regional engines, reducing engine fuel burn up to 10 percent, and reducing engine oxides of nitrogen emissions by more than 50 percent. Significant advancements in current gas turbine engines and engine components, such as seals, are required to meet these goals. Specifically, advanced seals have been identified as critical in meeting engine goals for specific fuel consumption, thrust-to-weight ratio, emissions, durability, and operating costs.

In a direct effort to address and make progress toward these goals, researchers at the NASA Glenn Research Center at Lewis Field have developed a unique high-temperature, high-speed engine seal test rig to evaluate seals under the temperature, speed, and pressure conditions anticipated for next generation turbine engines. This new seal test rig has capabilities beyond those of any existing seal rigs. It can test air seals (i.e., labyrinth, brush, and new seal concepts) at temperatures of up to 1500 °F and pressures up to 100 psid (even higher pressures are possible at lower temperatures), and at all surface speeds anticipated in future NASA (Ultra Efficient Engine Technology, UEET and Integrated High-Performance Turbine Engine Technology, IHPTET) engine programs. In addition, seals can be tested offset from the rotor centerline, in the rotor runout condition,<sup>1</sup> and with simulated mission profiles. Support for this new rig was provided by NASA Glenn, the U.S. Air Force, and the U.S. Army.



*High-Temperature Seal Rig fabrication complete.*

<sup>1</sup>With the rotor outer diameter eccentric to the rotor inner diameter.

The turbine seal test facility is planned to be installed at Glenn by October of 2000. Installation will include upgrading airflow systems, heating systems, instrumentation and measurement systems, and data acquisition systems. The operational envelope of the test rig will be verified through its full operating capabilities prior to actual seal tests.

**For more information about turbine seal work at Glenn, please visit the following web pages:**

<http://www.grc.nasa.gov/WWW/5900/5950/>  
<http://www.grc.nasa.gov/WWW/TurbineSeal/TurbineSeal.html>

**Bibliography**

Steinetz, B.M.; Hendricks, R.C.; and Munson, J.: Advanced Seal Technology Role in Meeting Next Generation Turbine Engine Goals. NASA/TM-1998-206961, 1998. (Available online: <http://gltrs.grc.nasa.gov/cgi-bin/GLTRS/browse.pl?/1999/TM-1999-206961.html>)

**U.S. Army Research Laboratory at Glenn contact:**

Irebert R. Delgado, (216) 433-3935, [Irebert.R.Delgado@grc.nasa.gov](mailto:Irebert.R.Delgado@grc.nasa.gov)

**Glenn contacts:**

Margaret P. Proctor, (216) 977-7526, [Margaret.P.Proctor@grc.nasa.gov](mailto:Margaret.P.Proctor@grc.nasa.gov); and Dr. Bruce M. Steinetz, (216) 433-3302, [Bruce.M.Steinetz@grc.nasa.gov](mailto:Bruce.M.Steinetz@grc.nasa.gov)

**Author:** Irebert R. Delgado

**Headquarters program office:** OAST

**Programs/Projects:**

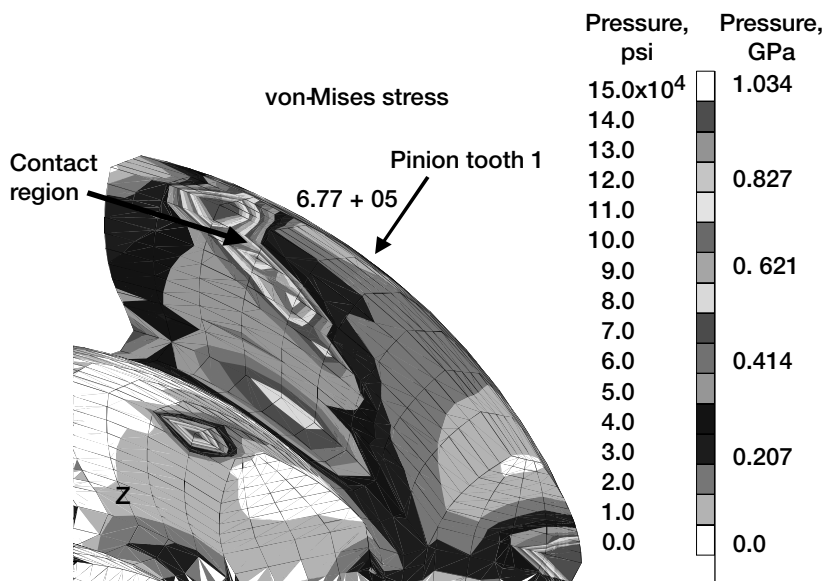
UEET, IHPTET, HITEMP, HSR, FQE

## Experimental and Analytical Determinations of Spiral Bevel Gear-Tooth Bending Stress Compared

Spiral bevel gears are currently used in all main-rotor drive systems for rotorcraft produced in the United States. Applications such as these need spiral bevel gears to turn the corner from the horizontal gas turbine engine to the vertical rotor shaft. These gears must typically operate at extremely high rotational speeds and carry high power levels. With these difficult operating conditions, an improved analytical capability is paramount to increasing aircraft safety and reliability. Also, literature on the analysis and testing of spiral bevel gears has been very sparse in comparison to that for parallel axis gears. This is due to the complex geometry of this type of gear and to the specialized test equipment necessary to test these components.

To develop an analytical model of spiral bevel gears, researchers use differential geometry methods to model the manufacturing kinematics. A three-dimensional spiral bevel gear modeling method was developed that uses finite elements for the structural analysis. This method was used to analyze the three-dimensional contact pattern between the test pinion and gear used in the Spiral Bevel Gear Test Facility at the NASA Glenn Research Center at Lewis Field. Results of this analysis are illustrated in the preceding figure. The development of the analytical method was a joint endeavor between NASA Glenn, the U.S. Army Research Laboratory, and the University of North Dakota.

To validate the predictions made by the newly developed numerical method, experimental tests were conducted on Glenn's Spiral Bevel Gear Test Facility. The following figure shows the instrumented spiral bevel pinion that was used in the test. The instrumented spiral bevel gears were tested from static to high rotational speeds (14,400 rpm) at various levels of load (up to 539 kW (720 hp)).



*Example of stress output produced by the model.*

### Research and Technology

Results from the experiments were compared with those produced analytically by the newly developed model. As seen in the final figure, the experimental and analytical results are in good agreement with each other. In addition, both sets of results indicate that the peak gear-tooth bending stresses occur in the fillet radius near the midface of the tooth.

**Find out more about this research on the World Wide Web:** <http://www.grc.nasa.gov/WWW/5900/5950/>

#### Bibliography

Handschuh, R.F.; and Bibel, G.D.: Comparison of Experimental and Analytical Tooth Bending Stress of Aerospace Spiral Bevel Gears. NASA/TM-1999-208903, 1999. (Available online: <http://gltrs.grc.nasa.gov/cgi-bin/GLTRS/browse.pl?/1999/TM-1999-208903.html>)

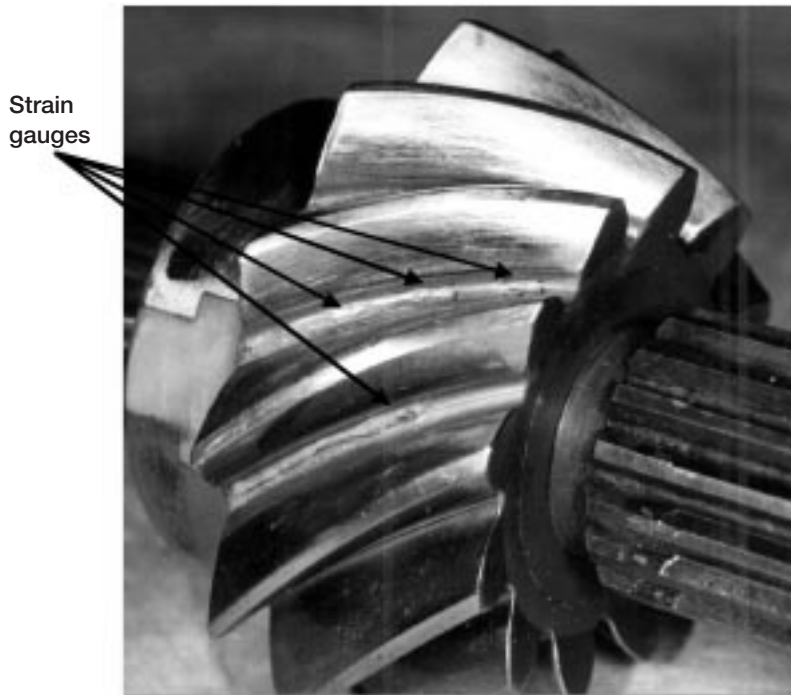
Bibel, G.D.; and Handschuh, R.F.: Meshing of a Spiral Bevel Gearset With 3-D Finite Element Analysis, NASA TM-107336, 1996.

**Glenn/U.S. Army Research Laboratory contact:** Dr. Robert F. Handschuh, (216) 433-3969, [Robert.F.Handschuh@grc.nasa.gov](mailto:Robert.F.Handschuh@grc.nasa.gov)

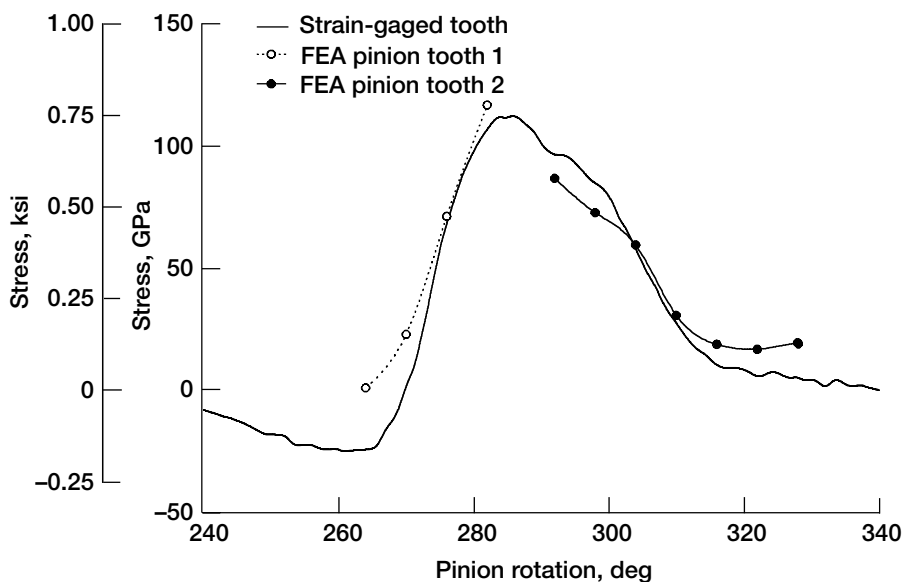
**Author:** Dr. Robert F. Handschuh

**Headquarters program office:** OAST

**Programs/Projects:**  
Rotorcraft Base Program



*Instrumented spiral bevel pinion used in the tests.*

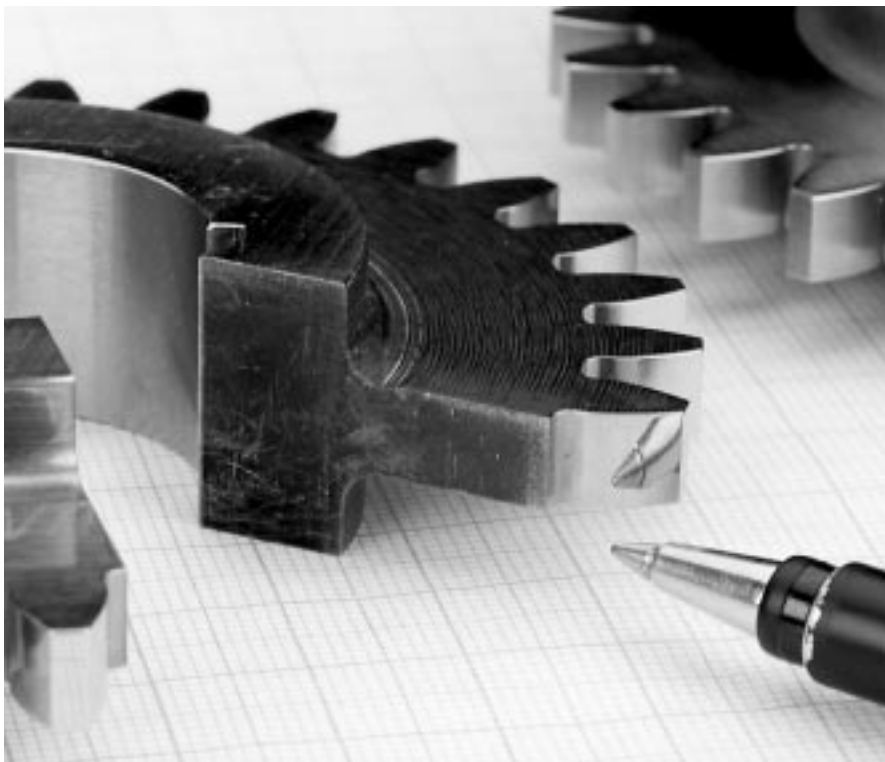


*Comparison of experimental and analytical stresses at the pinion midface at 14,400 rpm and 539 kW (720 hp).*

# Gear Durability Shown To Be Improved by Superfinishing

Gears, bearings, and similar mechanical elements transmit loads through contacting surfaces. At the NASA Glenn Research Center at Lewis Field, we postulated that the fatigue lives of gears could be improved by providing smoother tooth surfaces. A superfinishing process was applied to a set of conventionally ground, aerospace-quality gears. This process produced a highly polished, mirrorlike surface as shown in the following photograph. The surface fatigue lives of both superfinished and conventionally ground gears were measured by experiments. The superfinished gears survived about four times longer than the conventionally ground gears.

These superfinished gears were produced from conventionally ground, aerospace-quality gears whose geometry had been inspected. The gears were superfinished by placing them in a vibrating bath consisting of water, detergent, abrasive powder, and small pieces of zinc. Upon removal from the bath, the surfaces were highly polished, as depicted in the following photograph. The gears were again inspected, and dimensional measurements made before and after the superfinishing operation were compared. Superfinishing removed the peaks of the grinding marks and left a much smoother surface. Profile and spacing checks proved that the overall gear tooth shape was not affected in any harmful way. Super-finishing uniformly removed approximately 2.5  $\mu\text{m}$  from each surface. See reference 1 for a complete report.



*Highly polished surface of a superfinished gear.*

Superfinished 28-tooth, 8-pitch gears made from AISI 9310 steel were tested at Glenn at a hertzian contact stress of 1.71 GPa (248 ksi) for 300 million cycles or until surface failure occurred on any one tooth as illustrated in the photograph on the next page. The fatigue data, shown on Weibull coordinates in the graph, were analyzed using the method of reference 2. The lives shown are the lives of gear pairs in terms of stress cycles or revolutions. The lives of the superfinished gears were about four times longer than those of conventionally ground gears. The confidence number that the 10 percent life of the superfinished gears is greater than the 10 percent life of the conventionally ground gears is more than 90 percent, a statistically significant result.

This work was done as a partnership between NASA, the U.S. Army (Army Research Laboratory and The Army European Research Office), and the University of Wales.

#### **Find out more about this research on the World Wide Web:**

<http://www.grc.nasa.gov/WWW/5900/5950/>

#### **References**

1. Snidle, R.W.; Evans, H.P.; and Alanou, M.P.: The Effect of Superfinishing on Gear Tooth Profile. Report AD-A327916, June 1997. Available from the Defense Technical Information Center (DTIC, <http://www.dtic.mil/>) or the National Technical Information Service (NTIS, <http://www.ntis.gov/>), or the Center for AeroSpace Information (<http://www.sti.nasa.gov/rselect/FAQ.html#docorder>).
2. Johnson, L.G.: The Statistical Treatment of Fatigue Experiments. Elsevier Pub. Co., New York, NY, 1964.

**U.S. Army Research Laboratory at**

**Glenn contact:**

Timothy L. Krantz, (216) 433-3580,  
Timothy.L.Krantz@grc.nasa.gov

**Glenn contact:**

James J. Zakrajsek, (216) 433-3968,  
James.J.Zakrajsek@grc.nasa.gov

**Author:** Timothy L. Krantz

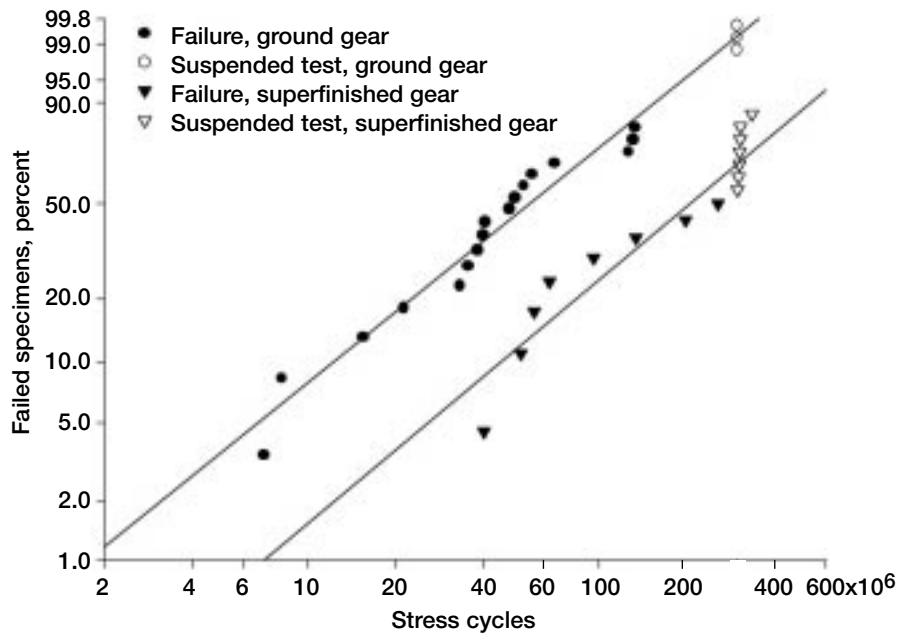
**Headquarters program office:** OAST

**Programs/Projects:**

Rotorcraft Base Program

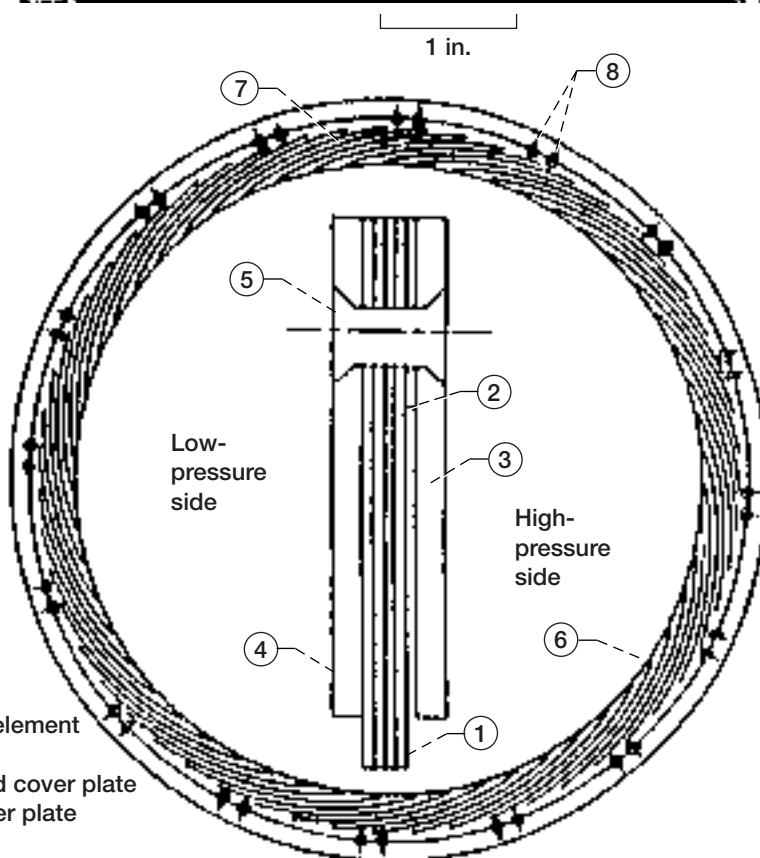
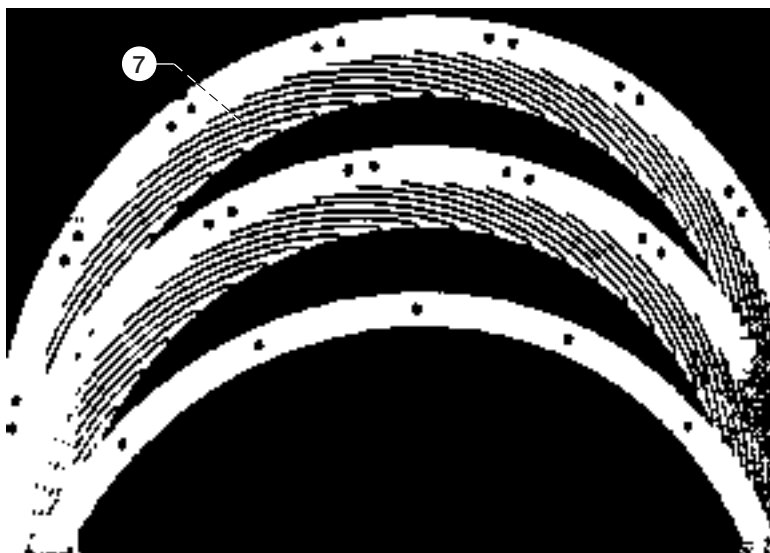


Typical surface fatigue failure.



Weibull plot of gear fatigue experiments.

# Pressure-Balanced, Low-Hysteresis Finger Seal Developed and Tested



- 1. Finger element
- 2. Spacer
- 3. Forward cover plate
- 4. Aft cover plate
- 5. Rivet
- 6. Finger contact pad
- 7. Finger
- 8. Indexing and rivet holes

*Baseline finger seal and its nomenclature.*

The "finger seal" is a revolutionary new technology in air-to-air sealing for secondary flow control and gas path sealing in gas turbine engines. Although this seal was developed for gas turbines, it can be used in any machinery where a high-pressure air cavity has to be sealed from a low-pressure air cavity, for both static and rotating applications. Recently patented (ref. 1) by AlliedSignal Engines, the finger seal has demonstrated considerably less air leakage than a conventional labyrinth seal, and it costs considerably less than a brush seal.

The availability of a long-life, low-leakage finger seal has many benefits for propulsion gas turbine engines. The most direct benefit would be to replace labyrinth seals at locations where very high pressures drop directly to the ambient pressure, typically main engine and thrust balance seals. This could save 1 to 2 percent of the engine flow, directly reducing specific fuel consumption by 0.7 to 1.4 percent and operating costs by 0.35 to 0.7 percent. Finger seals are made by photoetching finger shapes around the inner diameter of thin metal laminate rings, stacking the laminates so that the fingers of one laminate overlap the fingers of the adjacent laminates, sandwiching the stack of laminates between two sideplates, and riveting the whole stack together. Some final machining is required. The cost to produce finger seals is estimated to be 40 to 50 percent of the cost to produce brush seals.

A low-hysteresis finger seal designed by AlliedSignal Engines under a NASA contract was successfully developed and tested in a turbine seal rig at the NASA Glenn Research Center at Lewis Field. Finger seal air leakage measured 20 to 70 percent less than for a typical four-knife labyrinth seal with a 0.005-in. radial clearance. Finger seal operation was demonstrated at two extreme turbine operating conditions: (1) a tip speed of 778 ft/sec, a pressure differential of 60 psi, and an operating temperature of 1000 °F, and (2) a tip speed of 945 ft/sec, a pressure differential of 80 psi, and an operating temperature of 800 °F. A total of 13 finger seal configurations were tested to achieve the low-hysteresis design. The best design is a pressure-balanced finger seal with higher stiffness fingers. This design demonstrated very low hysteresis in repeated rig testing. The low-hysteresis seal design has undergone extensive rig testing to assess its hysteresis, leakage performance, and life capabilities. On the basis of this extensive testing, we have determined that the finger seal is ready for testing in an engine (see ref. 2 for more details).

**For more information about turbine seal work at Glenn, refer to our Web pages:**

**Mechanical Components Branch:** <http://www.grc.nasa.gov/WWW/5900/5950/>

**Turbine Seals:** <http://www.grc.nasa.gov/WWW/TurbineSeal/TurbineSeal.html>

## References

1. Johnson, M.D.; and Medlin, E.G.: Laminated Finger Seal With Logarithmic Curvature. U.S. Patent 5,108,116, Apr. 1992.
2. Arora, G.K., et al.: Pressure Balanced, Low Hysteresis, Finger Seal Test Results. NASA/TM-1999-209191, 1999. (Available online: <http://gltrs.grc.nasa.gov/cgi-bin/GLTRS/browse.pl?/1999/TM-1999-209191.html>)

## Glenn contacts:

Margaret P. Proctor, (216) 977-7526, [Margaret.P.Proctor@grc.nasa.gov](mailto:Margaret.P.Proctor@grc.nasa.gov); and Dr. Bruce M. Steinetz, (216) 433-3302, [Bruce.M.Steinetz@grc.nasa.gov](mailto:Bruce.M.Steinetz@grc.nasa.gov)

**Author:** Margaret P. Proctor

**Headquarters program office:** OAST

**Programs/Projects:** AST

## Thermal Barriers Developed for Solid Rocket Motor Nozzle Joints

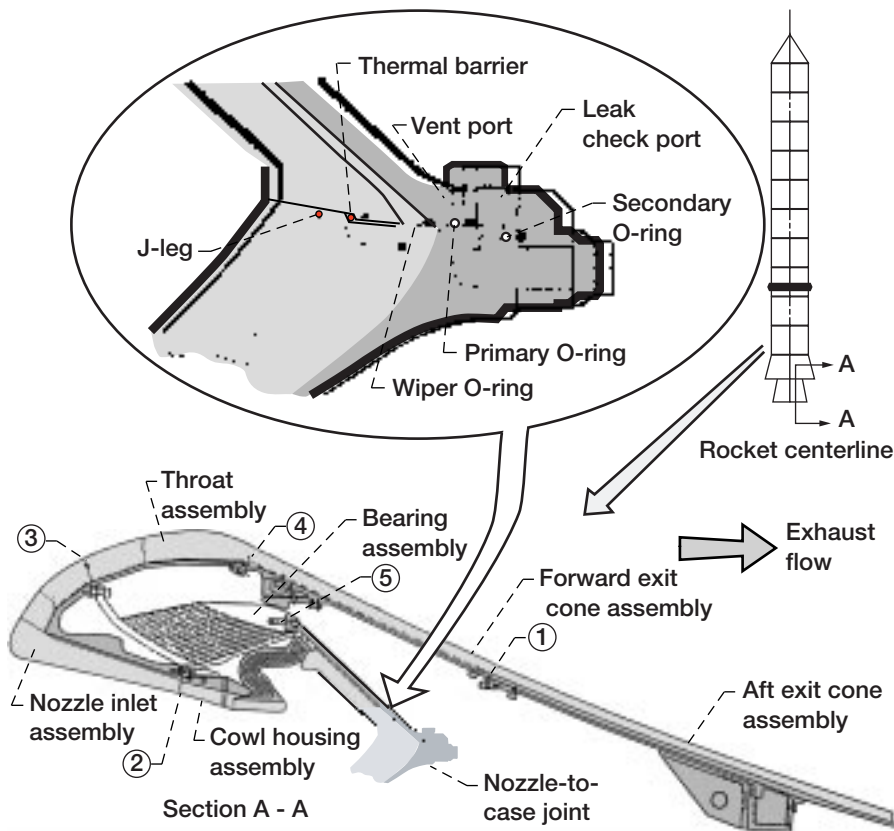
Space shuttle solid rocket motor case assembly joints are sealed with conventional O-ring seals that are shielded from 5500 °F combustion gases by thick layers of insulation and by special joint-fill compounds that fill assembly splitlines in the insulation. On a number of occasions, NASA has observed hot gas penetration through defects in the joint-fill compound of several of the rocket nozzle assembly joints. In the current nozzle-to-case joint, NASA has observed penetration of hot combustion gases through the joint-fill compound to the inboard wiper O-ring in one out of seven motors. Although this condition does not threaten motor safety, evidence of hot gas penetration to the wiper O-ring results in extensive reviews before resuming flight. The solid rocket motor manufacturer (Thiokol) approached the NASA Glenn Research Center at Lewis Field about the possibility of applying Glenn's braided fiber preform seal as a thermal barrier to protect the O-ring seals. Glenn and Thiokol are working to improve the nozzle-to-case joint design by implementing a more reliable J-leg design and by using a braided carbon fiber thermal barrier that would resist any hot gases that the J-leg does not block. The proposed new seal arrangement is shown in the illustration on the next page. This illustration also shows joints 1 through 5, which are other sites where the thermal barrier could be used.

The thermal resistance of Glenn's braided carbon fiber thermal barriers was assessed by exposing them to burn tests at temperatures representative of the rocket thermal environment. The thermal barriers were placed in the hottest part of the flame of an oxyacetylene torch at 5500 °F, and the amount of time needed to completely cut through them was measured. Thermal barrier designs with diameters of 0.20 and 0.26 in. resisted the flame for over 6 minutes before they were completely cut through, more

than three times longer than the burn time for the shuttle's solid rocket motors.

A test fixture was developed that allows the temperature drop to be measured across and along a thermal barrier when the barrier is in a compressed state and subjected to rocket-simulating narrow jets of hot gas at upstream temperatures of 3000 °F (see the photograph on the next page). Tests performed on the 0.20- and 0.26-in.-diameter thermal barriers showed that they are excellent insulators, causing temperature drops of 2500 to 2800 °F through their diameters. Gas temperatures measured only one seal diameter downstream from the thermal barrier were within the Viton<sup>1</sup> O-ring temperature limit of 600 °F. The test fixture also measured the jet-spreading feature of the rope seal. Results

<sup>1</sup>Viton is a registered trademark of DuPont.



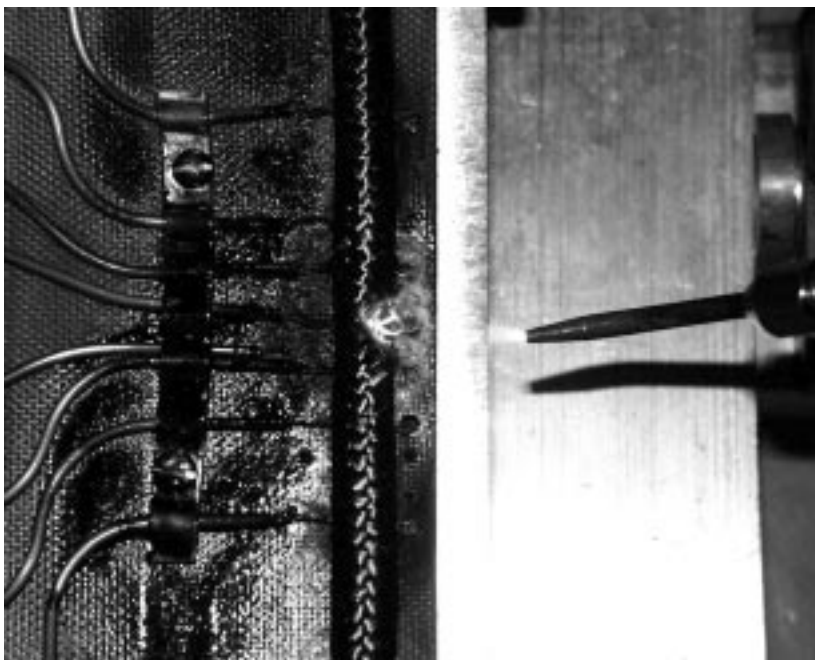
Potential shuttle solid-rocket-motor nozzle joint locations (circled numbers) for thermal barrier. Top: Enlarged view of nozzle-to-case joint showing J-leg, wiper, primary and secondary O-rings, leak check port, and proposed thermal barrier location. Bottom: Overall nozzle cross section (half view).

show that the 0.082-in. hot incoming jet was spread over a wide section of the braid (>1 in.), as measured by multiple cold-side thermocouples.

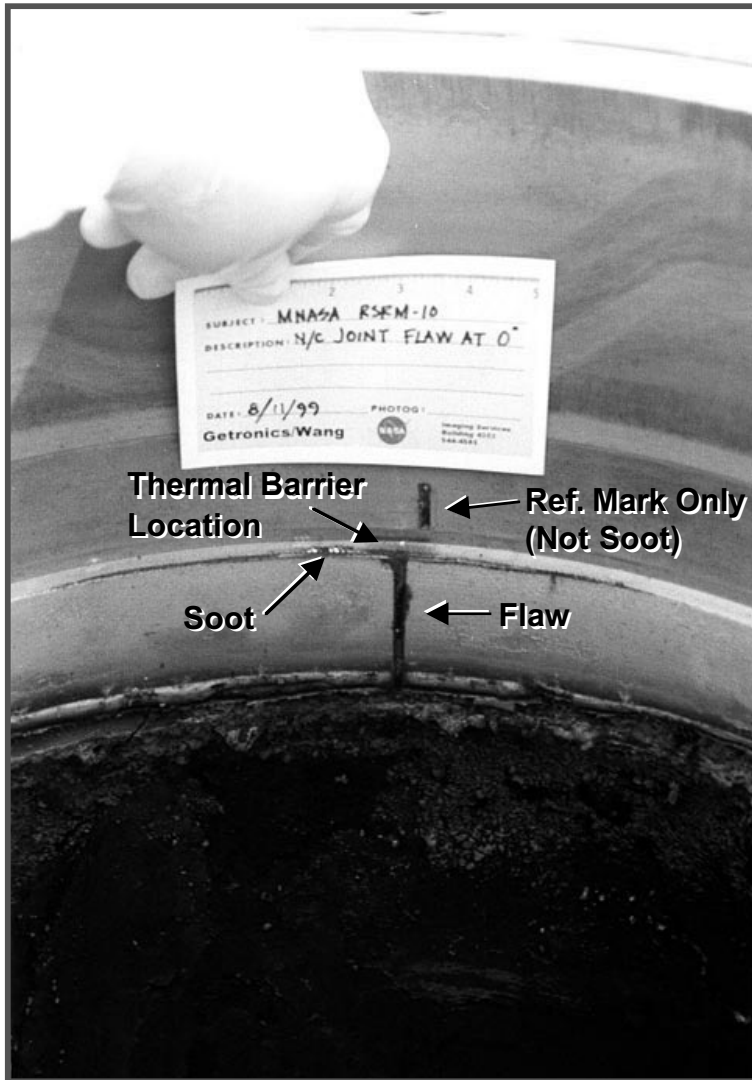
To simulate a rocket environment, Thiokol performed subscale rocket "char" motor tests in which the 0.26-in-diameter thermal barrier was subjected to hot gas at 3200 °F for an 11-sec rocket firing, simulating the maximum downstream joint-cavity fill time. The thermal barrier reduced the incoming hot gas temperature by 2200 °F in an intentionally oversized gap defect, spread the incoming jet flow, and blocked hot slag, thereby offering protection to the downstream O-rings. These results were consistent with those from the temperature-drop tests performed at Glenn.

A Glenn-developed braided carbon fiber thermal barrier was successfully evaluated at NASA Marshall in an MNASA-10 rocket, a one-fifth-scale version of the reusable solid rocket motor (RSRM) used to launch the space shuttle. The specimen was tested in the redesigned nozzle-to-case joint configuration. During the 29-sec rocket firing, an intentional flaw in the nozzle insulation allowed hot combustion gases to reach the thermal barrier as evidenced by soot observed on hardware upstream of the thermal barrier 5 in. on each side of the flaw (see the final photo). Posttest inspection revealed no soot downstream of the thermal barrier and no damage or erosion to either the thermal barrier or to downstream O-rings that the thermal barrier is designed to protect.

The Glenn-developed carbon thermal barrier is the primary candidate being considered by Thiokol for the space shuttle RSRM nozzle-to-case joint redesign to prevent Viton O-ring damage. Thiokol is continu-



Temperature-drop fixture showing a flame on the thermal barrier.



NASA Glenn thermal barrier feasibility proven in MNASA-10 RSRM.  
(Specimen was removed from the nozzle-to-case joint for this photo.)

ing to perform qualification tests of the Glenn-developed thermal barrier for the nozzle-to-case joint and has expressed interest in using the thermal barrier in joints 1 through 5 of the solid rocket motor nozzle. Thiokol is planning to perform full-scale RSRM static tests using the thermal barrier in January 2001 (no joint defect) and in May 2002 (with joint defect) to qualify the new design for its first shuttle flight in September 2002.

### Bibliography

Steinetz, B.M.; and Dunlap, P.H., Jr.: Development of Thermal Barriers for Solid Rocket Motor Nozzle Joints. NASA/TM-1999-209278 (AIAA Paper 99-2823), 1999. (Available online: <http://gltrs.grc.nasa.gov/cgi-bin/GLTRS/browse.pl?/1999/TM-1999-209278.html>)

### Find out more about this research on the World Wide Web:

<http://www.grc.nasa.gov/WWW/5900/5950/>

[http://www.grc.nasa.gov/WWW/TU/InventYr/1996Inv\\_Yr.htm](http://www.grc.nasa.gov/WWW/TU/InventYr/1996Inv_Yr.htm)

### Glenn contacts:

Dr. Bruce M. Steinetz, (216) 433-3302, [Bruce.M.Steinetz@grc.nasa.gov](mailto:Bruce.M.Steinetz@grc.nasa.gov); and Patrick H. Dunlap, Jr., (216) 433-6374, [Patrick.H.Dunlap@grc.nasa.gov](mailto:Patrick.H.Dunlap@grc.nasa.gov)

**Authors:** Dr. Bruce M. Steinetz and Patrick H. Dunlap, Jr.

**Headquarters program office:** OAST

**Programs/Projects:** HITEMP, STR

### Special recognition:

1996 NASA Invention of the Year awarded to the fiber preform seal, precursor to the thermal barrier

# Space



# Space Communications

## Seven Years of ACTS Technology Verification Experiments Reviewed

The Advanced Communications Technology Satellite (ACTS) was designed to achieve a 99.5-percent system availability rate and signals with less than one error in  $10^7$  bits throughout the continental United States. To accomplish such a high rate of system availability, ACTS uses multiple narrow hopping beams and very small aperture terminal (VSAT) technology. In addition, ACTS uses an adaptive rain fade compensation protocol to reduce the negative effects of propagation on the system.

To enhance knowledge on how propagation and system variances affect system availability, researchers at the NASA Glenn Research Center at Lewis Field performed technology verification experiments over a 7-year period (from September 1993 to the present). These experiments include T1VSAT System Availability, Statistical Rain Fade Compensation Characterization, Statistical Characterization of Ka-Band Propagation Effects on Communication Link Performance, and Multibeam Antenna Performance.

### **T1VSAT System Availability Experiment**

Using a performance index such as system fade availability, the T1VSAT System Availability Experiment focused on analyzing the effects of Ka-band system variances and propagation on the performance of seven T1VSAT's that were located in different rain zones. A main objective was to determine the overall availability of the selected T1VSAT's within the various rain zones. It was determined that the amount of rainfall is not necessarily a factor in determining outage; however, the type of rainfall is a large determinant. In addition to rainfall, other factors that contributed to outages included hardware and software anomalies (10 percent). After modifications were made to the T1VSAT and to operational procedures, T1VSAT availability increased by 3 percent.

### **Statistical Rain Fade Compensation Characterization Experiment**

The ACTS adaptive rain-fade compensation protocol was developed to ensure a T1VSAT bit error rate of  $<5 \times 10^{-7}$  for 99.5 percent of the time that the T1VSAT is operational. The protocol is adaptive, has decision-making capabilities, and is implemented to maintain T1VSAT performance during periods when the signal weakens as a result of fade or system effects. As shown by 1 year of collected data, system availability increased by 1.5 percent in an International Telecommunications Union Radiowave (ITU-R) medium rain zone. The protocol was considered to be more than adequate for all rain zones within the continental U.S. in which terminals were used for short amounts of time (less than 1 month).

### **Statistical Characterization of Ka-Band Propagation Effects on Communication Link Performance Experiment**

This experiment, which took place over a 5-year period at seven U.S. sites, focused on the effects of rain attenuation at Ka-band frequencies. As the dominant cause for signal impairment, rain attenuation is a function of frequency, elevation angle, rain intensity, raindrop size distribution, and raindrop temperature. Fades of 20 dB or larger were observed at least 0.1 percent of the time in subtropical rain zones and 0.01 percent of the

time in a dry rain zone. The effect of clouds was found to be around 2 dB for all rain zones.

### **Wet Antenna Experiment**

Selecting a subtropical rain zone (Cocoa, Florida) and using a tipping bucket rain gauge to collect rainfall data over a 10-month period, Glenn's researchers conducted the Wet Antenna Experiment to analyze the contribution that a wet feed and wet reflector antenna have on the signal path losses at Ka-band frequencies. The receiving signal strength was measured, and a small weather station was operated next to the T1VSAT terminals. The results indicated that feed wetness was the main contributor to system losses, with reflector wetness having less effect. The reflector losses were a result of scattering due to raindrop size at the reflector surface, which distorted the surface and reduced antenna gain significantly. Another observation showed that the cumulative fade distribution with a wet antenna was 3 to 5 dB worse than with a dry antenna.

### **Multibeam Antenna Performance Experiment**

A key technology on ACTS is the multibeam antenna system, which has 3 fixed and 47 rapidly reconfigurable spot beams operating at Ka-band frequencies. One of the most significant aspects of the system design is the accurate estimation of antenna performance degradation. Over a 7-year period, test measurements indicated that the multibeam antenna system operated well within the expected performance range. Thermal and mechanical disturbances affected

performance, but could be easily corrected in future designs. Thermal distortions were periodic, which makes it possible to predict and compensate for the impact of these effects on system performance. Other design anomalies were recorded, and can be corrected in future designs of this type of satellite system.

The 7 years of valuable research conducted on the ACTS system will enable designers to tailor a satellite system to provide quality system availability at relatively low cost. Using the ACTS rain fade compensation proved that coding gain can be extremely effective in combating rain fade. Continuing research is being performed on rain fade compensation to allow inexpensive Ka-band system implementation.

**Additional information can be obtained at the Technology Verification Experiments page of the ACTS web site:**

<http://acts.grc.nasa.gov/about/experiments/technology/>

## Advanced Communications Technology Satellite (ACTS) Used for Inclined Orbit Operations

The Advanced Communications Technology Satellite (ACTS) is operated by the NASA Glenn Research Center at Lewis Field 24 hours a day, 7 days a week. ACTS, which was launched in September 1993, is in its 7th year of operations, far exceeding the system's planned 2 years of operations and 4 years of designed mission life. After 5 successful years of operating as a geostationary satellite, the spacecraft's North-South stationkeeping was discontinued in August 1998. The system is now operating in an inclined orbit that increases at a rate of 0.8°/yr. With only scarce fuel remaining, operating in this mode extends the usage of the still totally functional payload. Although tracking systems are now needed on the experimenter Earth stations, experiment operations have continued with very little disruption. This is the only known geosynchronous Ka-band (30/20 GHz) spot-beam satellite operating in an inclined orbit.

The project began its transition from geostationary operations to inclined operations in August 1998. This did not interrupt operations and was transparent to the experimenters on the system. For the space segment, new daily procedures were implemented to maintain the pointing of the system's narrow 0.3° spot beams while the spacecraft drifts in the North-South direction. For the ground segment, modifications were designed, developed, and fielded for the three classes of experimenter Earth stations.

With the next generation of commercial satellite systems still being developed, ACTS remains the only operational testbed for Ka-band geosynchronous satellite communications over the Western hemisphere. Since inclined orbit operations began, the ACTS experiments program has supported 43 investigations by industry, Government, and academic organizations, as well as four demonstrations. The project's goals for inclined-orbit operations now reflect a narrower focus in the types of experiments that will be done. In these days of "faster, better, cheaper," NASA is seeking to gain greater relevance to the agency's mission from these experiments. One area that is of much interest both to NASA and

**Glenn contact:**

Dr. Roberto J. Acosta, (216) 433-6640,  
Roberto.J.Acosta@grc.nasa.gov

**Authors:**

Dr. Roberto J. Acosta, Sandra K. Johnson, Kathleen M. McEntee, William Gauntner, and Walber Feliciano

**Headquarters program office:** OSF

**Programs/Projects:** SOMO, TDRSS H,I,J, ISS, Deep Space Network, space shuttle, direct distribution systems, commercial Ka-band systems

the commercial world is the investigation of protocol issues related to the interoperability of satellites with terrestrial networks, such as Transmission Control Protocol/Internet Protocol (TCP/IP) and Asynchronous Transfer Mode (ATM) over wideband satellites. Other experiment areas of interest are supporting the U.S. Government and NASA as they begin using commercial space assets to meet their communications needs, evaluating issues related to operating a spot-beam satellite in inclined orbit, and evaluating new Ka-band hardware that requires a satellite link. ACTS is now in its last year of operations. Operations are planned through June 2000, when after 81 months of operations, this very successful spacecraft will be superorbited and made inert.

**Glenn contact:**

Robert A. Bauer, (216) 433-3431,  
Robert.A.Bauer@grc.nasa.gov

**Author:** Robert A. Bauer

**Headquarters program office:** OSF

**Programs/Projects:** JSC SOMO (Technology Activities Project)

# Satellite Broadcast of Graphical Weather Data Flight Tested

NASA Glenn Research Center at Lewis Field's aviation Weather Information Communications (WINCOMM) and NASA Langley Research Center's Aviation Weather Information (AWIN) projects collaborated in a flight test and evaluation of a worldwide weather data-link capability using satellites. This successful flight testing moves NASA closer to its goal of developing advanced communications and information technologies to enable high-quality and timely dissemination of aviation weather information to all relevant users on the aviation information network.

Recognized as a major contributing factor in aviation accidents and incidents, weather contributes directly or indirectly to nearly 80 percent of fatal general aviation (small private aircraft) accidents. In 1997, the Aeronautics Safety Investment Strategy Team's weather team produced a prioritized list of investment areas under weather accident prevention. Weather data dissemination is the most critical and highest ranked priority on the list. NASA's Aviation Safety Program founded the Aviation Weather Information initiative to focus efforts on significantly reducing the number of weather-related aviation fatalities. Access to accurate and timely weather data could contribute to a major reduction of weather-related incidents and accidents. However, a cost-effective solution has eluded most general aviation pilots because of the high cost of onboard weather radar equipment.

Rockwell Collins, through a contract with NASA and in cooperation with WorldSpace Corporation, successfully completed ground and flight testing of a receiver and antenna in Johannesburg, South Africa. This NASA/Rockwell Collins project is an evaluation of worldwide weather data-link capability using transmissions from the Satellite Digital Audio Radio Services (S-DARS) AfriStar satellite. Owned and operated by WorldSpace, AfriStar is a geostationary satellite that broadcasts commercial digital audio services to stationary and mobile platforms. S-DARS satellites are the most powerful communications satellites produced to date, allowing users to receive signals using simple, low-cost patch antennas instead of more expensive, beam-steered antenna arrays.

Engineers connected an inexpensive, commercially available radio receiver to a laptop computer and an antenna designed and built by Rockwell Collins, enabling them to receive WorldSpace signals from the AfriStar satellite during flight tests. WorldSpace broadcast their composite color graphical weather data files, which were multiplexed with normal audio streams, to the flat patch antenna mounted on a single-engine aircraft. The aircraft was equipped with a modified commercial S-DARS receiver, a Global Positioning Satellite (GPS) receiver, and a laptop computer with color display. Continuous data reception occurred during normal aircraft maneuvers performed throughout takeoff, cruise, and landing operations. In addition, engineers monitored receiver power levels during steep turns and banks. In most instances, the receiver was able to maintain acceptable



*Rockwell Collins patch antenna mounted on the fuselage of a Cessna-172 aircraft.*

power levels during all phases of flight and to obtain weather data with little or no error.

With the successful completion of ground and flight testing of a receiver and antenna in Johannesburg, South Africa, the team has started to prepare for experiments using high-speed aircraft in areas of the world with limited access to timely weather data. NASA plans to provide a more advanced antenna design and consultation support. This successful test of real-time aviation-related weather data is a positive step toward solving communications-specific issues associated with the dissemination of weather data directly to the cockpit.

**Glenn contacts:**

Robert J. Kerczewski, (216) 433-3434,  
Robert.J.Kerczewski@grc.nasa.gov;  
and Konstantinos S. Martzaklis,  
(216) 433-8966,  
Konstantinos.S.Martzaklis@grc.nasa.gov

**Author:** Paul G. Mallasch

**Headquarters program office:** OAST

**Programs/Projects:**

AvSP, WINCOMM, AWIN

# Proposal Drafted for Allocating Space-to-Space Frequencies in the GPS Spectrum Bands

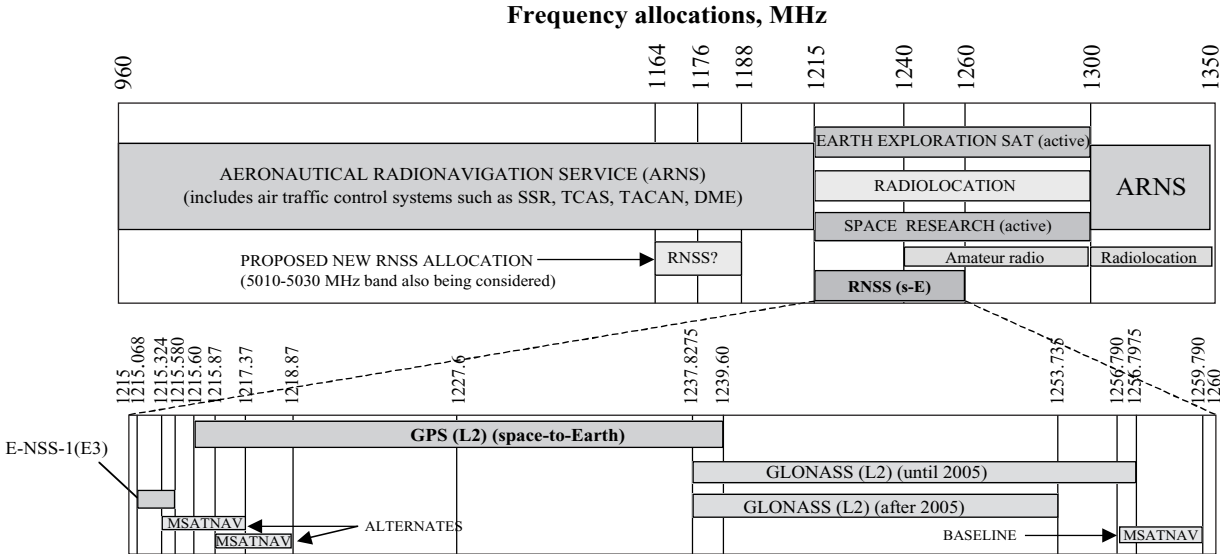
Radionavigation Satellite Service (RNSS) systems such as the U.S. Global Positioning System (GPS) and the Russian Global Navigation Satellite System (GLONASS) are primarily being used today in the space-to-Earth direction (i.e., from GPS satellite to Earth user) for a broad range of applications such as geological surveying; aircraft, automobile, and maritime navigation; hiking and mountain climbing; and precision farming and mining. However, these navigation systems are being used increasingly in space.

Beginning with the launch of the TOPEX/Poseidon remote-sensing mission in 1992, over 90 GPS receivers have flown onboard spacecraft for such applications as real-time spacecraft navigation, three-axis attitude control, precise time synchronization, precision orbit determination, and atmospheric profiling. In addition to use onboard many science spacecraft, GPS has been used or is planned to be used onboard the shuttles, the International Space Station, the International Space Station Emergency Crew Return Vehicle, and many commercial satellite systems such as Orbcomm, Globalstar, and Teledesic.

From a frequency spectrum standpoint, however, one important difference between the space and terrestrial uses of GPS is that it is being used in space with no interference protection. This is because there is no frequency allocation for the space-to-space use of GPS (i.e., from GPS satellite to user spacecraft) in the International Telecommunications Union (ITU) regulatory table of frequency allocations. If another space-based or ground-based

radio system interferes with a spaceborne GPS user, the spaceborne user presently has no recourse other than to accept the interference. Consequently, for the past year and a half, the NASA Glenn Research Center at Lewis Field and other Government agencies have been working within ITU toward obtaining a GPS space-to-space allocation at the next World Radio Conference in the year 2000 (WRC-2000).

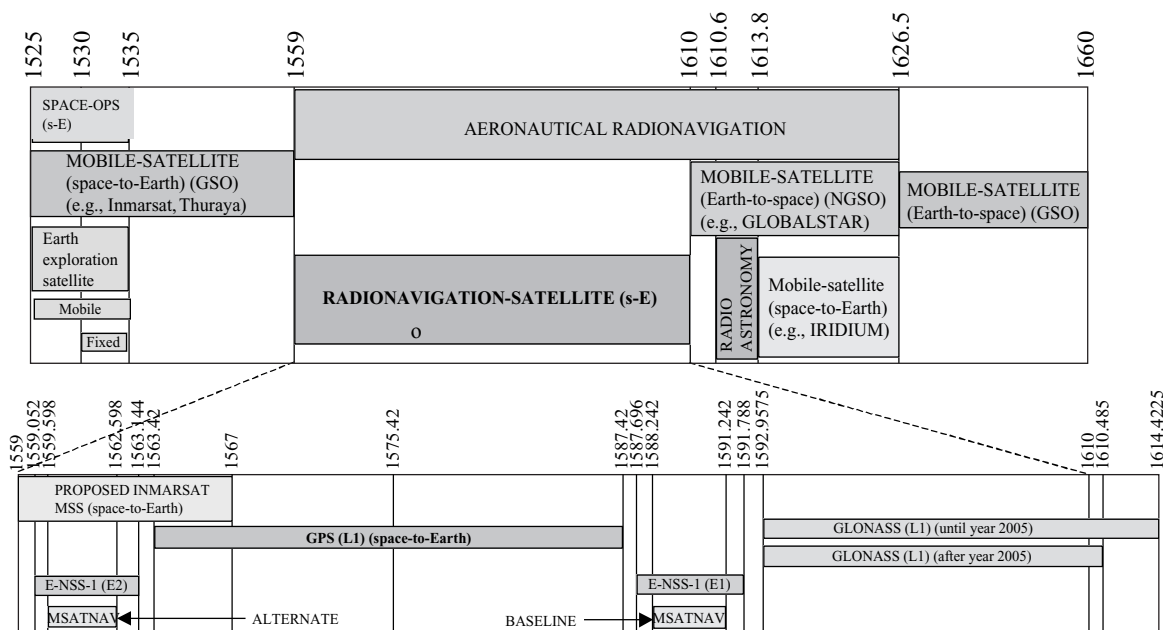
Numerous interference studies have been conducted in support of a primary space-to-space allocation in the 1215- to 1260-MHz and 1559- to 1610-MHz RNSS bands. Most of these studies and analyses were performed by Glenn and submitted as U.S. input documents to the international Working Party 8D meetings in Geneva, Switzerland. In the structure of the ITU, Working



KEY ITU-RR FOOTNOTES:  
 S5.330 also allocates the 1215 to 1300 MHz band to the fixed and mobile services on a primary basis in 34 countries. (WRC-97)  
 S5.332 states that in the band 1215 to 1300 MHz, active spaceborne sensors in the EES and SR services shall not cause harmful interference to or claim protection from the radionavigation-satellite service or radiolocation service.

Frequency allocations in the radio spectrum including the 1215- to 1260-MHz frequency band.

## Frequency allocations, MHz



### KEY ITU-RR FOOTNOTES:

S5.359 allocates the 1550 to 1645.5 MHz band (and the 1646.5 to 1660 MHz band) to the fixed service on a primary basis in 44 countries.

### Frequency allocations in the radio spectrum including the 1559- to 1610-MHz frequency band.

Party 8D is responsible for frequency spectrum issues in the RNSS and the mobile satellite service (MSS). The full texts of the studies are available from the ITU web site (<http://www.itu.org>) under Working Party 8D contributions.

Note that because spaceborne RNSS receivers operate in a receive-only mode with navigation signals already being broadcast toward the Earth, the addition of a space-to-space allocation will not result in interference with other systems. A space-based RNSS receiver, however, could experience interference from systems of other services, including intraservice interference from other RNSS systems. The interference scenarios examined in the studies can be inferred from the frequency allocation charts. In these charts, services labeled in all capital letters (e.g., "ARNSS") have primary status, whereas those labeled with sentence-style capitalization (e.g., "Amateur radio") have secondary status (i.e., a service with secondary status cannot claim interference protection from or cause harmful interference to a service with primary status).

The chart on the preceding page shows the ITU frequency allocations in the 960- to 1350-MHz range. Within this range, RNSS has a primary allocation in the space-to-Earth direction in the 1215- to 1260-MHz band. Active sensors (e.g., synthetic aperture radars) in the Earth exploration satellite (EES) service and space research (SR) service along with the radiolocation service also have primary status in the band. In addition, by footnote S5.330, fixed and mobile services also have primary status in some 34 countries. Interservice interference analyses to assess the sensitivity of space-based RNSS receivers to transmitters in these services were therefore conducted for all these cases.

The bottom portion of the first chart is an expanded view of the 1215- to 1260-MHz RNSS band showing the frequency plans for the current GPS and GLONASS systems as well as plans for some proposed European navigation satellite systems. These include the 48-satellite E-NSS-1 system from the European Space Agency, the 36-satellite MSATNAV system from the French space agency, and the 64-satellite LSATNAV system also from France. (Although not shown in the chart, LSATNAV is planned to have the same frequency plan as MSATNAV.) Europe has also proposed the Galileo system, which is still being defined. Note that navigation signals transmitted from the satellites of one RNSS system (e.g., MSATNAV) can potentially interfere with spaceborne receivers of a different RNSS system (e.g., GPS). Therefore, intraservice interference studies also were performed to evaluate this scenario.

The second chart shows the frequency allocations in the 1525- to 1660-MHz range. Within this range, RNSS has a primary allocation in the space-to-Earth direction in the 1559- to 1610-MHz band. Note also that the Aeronautical Radionavigation Service (ARNS) also has primary status in the band. In addition, by footnote S5.359, fixed service has primary status in some 44 countries. Thus, interservice interference analyses were performed to evaluate the sensitivity of space-based RNSS receivers to transmitters in these two services.

The bottom portion of the second chart is an expanded view of the 1559- to 1610-MHz RNSS band showing the frequency plans for GPS and GLONASS and the proposed E-NSS-1 and MSATNAV systems. As in the 1215- to 1260-MHz band, intraservice interference analyses were performed to evaluate potential interference between various RNSS systems.

The second chart also shows an allocation for mobile satellite service downlinks from geostationary orbit (GSO) satellites immediately below 1559 MHz, an allocation for mobile satellite service uplinks to nongeostationary orbit (NGSO) satellites immediately above 1610 MHz, and another (secondary) allocation for MSS downlinks from NGSO satellites in the 1613.8- to 1626.5-MHz band. An allocation for mobile satellite service uplinks to GSO satellites also exists in the 1626.5- to 1660-MHz band. There is concern among some administrations that mobile satellite service systems using these bands could be restricted if their out-of-band emissions cause excessive interference to RNSS space receivers. A number of out-of-band interference analyses were therefore conducted, although not all were completed in time to be submitted to the Working Party 8D meeting last April.

Collectively, the studies show that RNSS spaceborne receivers can operate satisfactorily in the current interference environment. From the results of these studies, a draft Conference Preparatory Meeting text for the World Radio Conference in the year 2000 has been written and approved for the space-to-space issue. NASA is optimistic that this will provide the basis for a GPS space allocation at the World Radio Conference and, hence, protect future space-to-space GPS users from interference.

**Find out more about this research on the World Wide Web:**

<http://www.itu.org>

**Glenn contact:**

Rodney L. Spence, (216) 433-3464,  
Rodney.Spence@grc.nasa.gov

**Author:** Rodney L. Spence

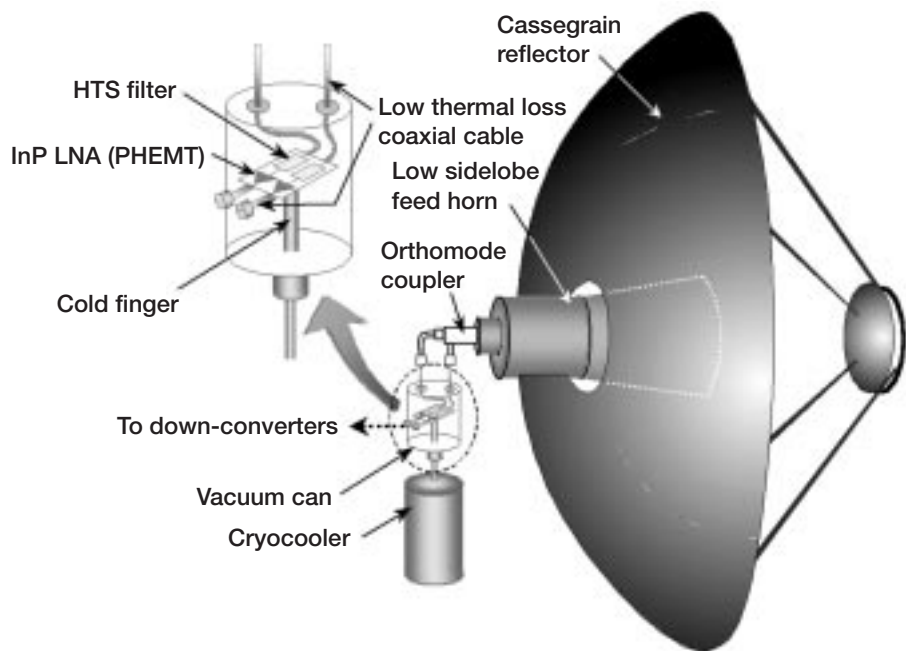
**Headquarters program office:**  
OSF, OSS

**Programs/Projects:**  
GPS, RNSS, Space Communications

## Low-Cost Tracking Ground Terminal Designed To Use Cryogenically Cooled Electronics

A computer-controlled, tracking ground terminal will be assembled at the NASA Glenn Research Center at Lewis Field to receive signals transmitted by the Glenn's Direct Data Distribution (D<sup>3</sup>) payload planned for a shuttle flight in low Earth orbit. The terminal will enable direct data reception of up to two 622-megabits-per-second (Mbps) beams from the space-based, K-band (19.05-GHz) transmitting array at an end-user bit error rate of up to 10<sup>-12</sup>. The ground terminal will include a 0.9-m-diameter receive-only Cassegrain reflector antenna with a corrugated feed horn incorporating a dual circularly polarized, K-band feed assembly mounted on a multiaxis, gimbaled tracking pedestal as well as electronics to receive the downlink signals. The tracking system will acquire and automatically track the shuttle through the sky for all elevations greater than 20° above the horizon. The receiving electronics for the ground terminal consist of a six-pole microstrip bandpass filter, a three-stage monolithic microwave integrated circuit (MMIC) amplifier, and a Stirling cycle cryocooler (1 W at 80 K). The Stirling cycle cryocooler cools the front end of the receiver, also known as the low-noise amplifier (LNA), to about 77 K. Cryocooling the LNA significantly increases receiver performance, which is necessary so that it can use the antenna, which has an aperture of only 0.9 m. The drawing on the next page illustrates the cryo-terminal.

A three-stage indium-phosphide (InP) MMIC low-noise amplifier (LNA) was designed to provide the flexibility for both broadband operation and high gain. Source feedback was used in the first-stage device to provide good noise match and input voltage standing wave ratio (VSWR) match simultaneously. The advantages of an InP High Electron Mobility Transistor (HEMT) over gallium arsenide (GaAs) devices include higher gain, lower power consumption, and a lower noise figure, especially at cryogenic temperatures. The MMIC LNA is fully monolithic and has exhibited good reliability with median time to failure of 10<sup>8</sup> hours. The LNA gives a noise figure of



*Cryogenic receiver terminal for the Direct Data Distribution project. (HTS, high-temperature superconducting; PHEMT, Pseudomorphic High Electron Mobility Transistor.)*

1.1 dB with 33 dB gain at 20 GHz at room temperature. From 17 to 22 GHz, input and output return losses greater than 10 dB can be achieved with an MMIC amplifier. Under normal operation, the amplifier can take input power up to 20 dBm without any degradation. When biased for minimum noise at 19.0 GHz, the minimum noise at 299 K was 1.6 dB with an associated gain of 27 dB. At 82 K, the minimum noise was within the measurement uncertainty of the system, estimated at 0.2 dB, and the associated gain was 27 dB.

## Feasibility Activities Completed for the Direct Data Distribution (D<sup>3</sup>) Experiment

The Direct Data Distribution (D<sup>3</sup>) project being designed at the NASA Glenn Research Center at Lewis Field will demonstrate a high-performance communications system that transmits information at up to 1.2 gigabits per second (Gbps) from an advanced technology payload carried by the space shuttles in low Earth orbit to small (0.9-m) autonomously tracking terminals on the Earth. The flight communications package features a solid-state, phased-array antenna operating in the commercial K-band frequency that electronically steers two independently controlled downlink beams toward low-cost tracking ground terminals. The array enables agile, vibration-free beam steering at reduced size and weight with increased reliability over traditional mechanically steered reflectors. The flight experiment will also demonstrate efficient digital modulation technology that allows transmission of substantially increased amounts of latency-tolerant data (up to 72 Gb of data per minute of contact time) with very high quality ( $10^{-11}$  bit error rate). D<sup>3</sup> enables transmission from low-Earth-orbit science spacecraft, the shuttles, or the International Space Station directly to NASA field

centers and principle investigator sites, or directly into the commercial terrestrial telecommunications network for remote distribution and archive. The ground terminal features a cryocooled receiver for ultralow noise and a reduced antenna aperture as well as openloop tracking for unattended operations. The D<sup>3</sup> technology validation and service demonstration will help to facilitate NASA's transition from using Government-owned communications assets to using commercially provided services.

### Glenn contacts:

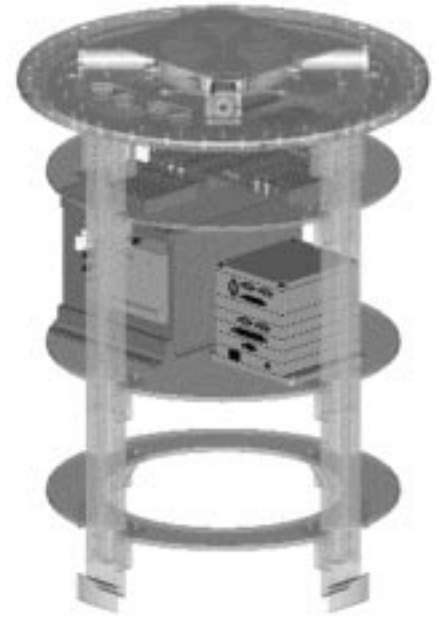
Lawrence W. Wald, (216) 433-5219, Lawrence.W.Wald@grc.nasa.gov; Robert R. Romanofsky, (216) 433-3507, Robert.R.Romanofsky@grc.nasa.gov; and Joseph D. Warner, (216) 433-3677, Joseph.D.Warner@grc.nasa.gov

**Authors:** Lawrence W. Wald, Robert R. Romanofsky, and Joseph D. Warner

**Headquarters program office:** OSS

**Programs/Projects:** D<sup>3</sup>, CETDP (HRDD)

The hardware for D<sup>3</sup> will incorporate advanced technology components developed under the High Rate Data Delivery Thrust Area of the NASA Cross-Enterprise Technology Development Program (CETDP) in Glenn's Communications Technology Division. Components for the flight segment will include the electrically steerable phased-array antenna being built by the Raytheon Systems Corporation, which uses monolithic microwave integrated circuit (MMIC) technology operating at 19.05-gigahertz (GHz), and the digital encoder-modulator chipset, which uses four-channel orthogonal frequency division multiplexing (OFDM). The encoder-modulator will use a chipset developed by SICOM, Inc., which is both bandwidth and power efficient. Components for the ground segment will include a low-cost, open-loop tracking ground terminal incorporating a cryoreceiver to minimize terminal size without compromising receiver capability. The D<sup>3</sup> project team is currently negotiating the final arrangements for the experiment's shuttle flight, which is tentatively planned for the fourth quarter of calendar year 2002. D<sup>3</sup> is a work area under the Advanced Communications campaign within the Space Operations Technology Project of the Space Operations Management Office at the NASA Johnson Space Center.



*Preliminary layout of the Direct Data Distribution experiment in a NASA Goddard Space Flight Center Hitchhiker-G canister.*

In fiscal year 1999, the D<sup>3</sup> team, composed of both civil servants and Dynacs Engineering Company, Inc., personnel, completed several feasibility activities. The initial thermal and structural designs of the flight payload were developed for the NASA Goddard Space Flight Center Hitchhiker-G carrier. The preliminary structural layout is shown in the illustration. In addition, the team has been working on mechanical, electrical, and safety integration issues with Raytheon, the developer of the array. The results of the tracking feasibility study indicated the requirements for the size of the ground terminal antenna, desirable locations, and contact times. The initial design for the orthogonal frequency division multiplexing modulator board was completed, and a local vendor was contracted to fabricate and populate the breadboard version of the board.

**Glenn contact:**

Lawrence W. Wald, (216) 433-5219,  
Lawrence.W.Wald@grc.nasa.gov

**Author:** Lawrence W. Wald

**Headquarters program office:** OSS

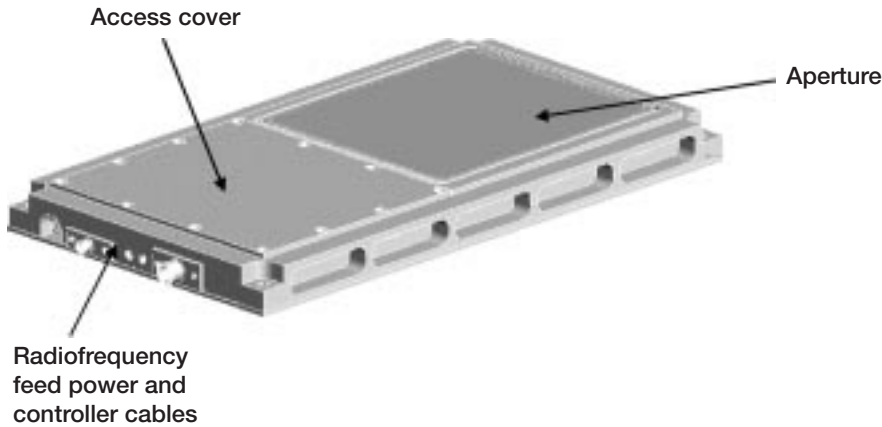
**Programs/Projects:** D<sup>3</sup>, CETDP (HRDD)

## Antennas Designed for Advanced Communications for the Air Traffic Management (AC/ATM) Project

The goal of the Advanced Communications for Air Traffic Management (AC/ATM) Project at the NASA Glenn Research Center at Lewis Field is to enable a communications infrastructure that provides the capacity, efficiency, and flexibility necessary to realize a mature free-flight environment. The technical thrust of the AC/ATM Project is targeted at the design, development, integration, test, and demonstration of enabling technologies for global broadband aeronautical communications. Since Ku-band facilities and equipment are readily available, one of the near-term demonstrations involves a link through a Ku-band communications satellite.

Two conformally mounted antennas will support the initial AC/ATM communications links. Both of these are steered electronically through

monolithic microwave integrated circuit (MMIC) amplifiers and phase shifters. This link will be asymmetrical with the downlink to the aircraft (mobile vehicle) at a throughput rate of >1.5 megabits per second (Mbps), whereas the throughput rate of the uplink from the aircraft will be >100 kilobits per second (kbps). The data on the downlink can be narrow-band, wide-band, or a combination of



*Boeing 254-element Ka-band phased-array transmitting antenna.*

both, depending on the requirements of the experiment. The AC/ATM project is purchasing a phased-array Ku-band transmitting antenna for the uplink from the test vehicle. Many Ku-band receiving antennas have been built, and one will be borrowed for a short time to perform the initial experiments at the NASA Glenn Research Center at Lewis Field.

The Ku-band transmitting antenna is a 254-element MMIC phased-array antenna being built by Boeing Phantom Works. Each element can radiate 100 mW. The antenna is approximately 43-cm high by 24-cm wide by 3.3-cm thick. It can be steered beyond 60° from broadside. The beamwidth varies from 6° at broadside to 12° at 60°, which is typical of phased-array antennas. When the antenna is steered to 60°, the beamwidth will illuminate approximately five satellites on the orbital arc. Spread spectrum techniques will be employed to keep the power impinging on the adjacent satellites below their noise floor so that no interference results. This antenna is power limited. If the antenna elements (currently 254) are increased by a factor of 4 (1024) or 16 (4096), the gain will increase and the beamwidth will decrease in proportion. For the latter two antenna sizes, the power must be “backed off” to prevent interference with the neighboring satellites. The receiving antenna, which is approximately 90-cm high, 60-cm wide, and 3.5-cm thick, is composed of 1500 phased-array elements.

The system phased-array controller can control both a 1500-element receiving antenna and a 500-element transmitting antenna. For ground

testing, this controller will allow manual beam pointing and polarization alignment. For normal operation, the system can be connected to the receiving antenna and the navigation system for real-time autonomous track operation. This will be accomplished by first pointing both antennas at the satellite using information from the aircraft data bus. Then, the system phased-array controller will electronically adjust the antenna pointing of the receiving antenna to find the peak signal. After the peak signal has been found, the beam of the transmitting antenna will be pointed to the same steering angles as the receiving antenna. For initial ground testing without an aircraft, the ARINC 429 data bus (ARINC Inc., Annapolis, Maryland) will be simulated by a gyro system purchased for the follow-on to the Monolithic Microwave Integrated Circuit (MMIC) Arrays for Satellite Communication on the Move (MASCOM) Project. MASCOM utilized the Advanced Communications Technology Satellite (ACTS) with a pair of Ka-band experimental phased-array antennas.

**Glenn contact:**

Robert J. Zakrajsek, (216) 433-3487,  
Robert.J.Zakrajsek@grc.nasa.gov

**Author:** Robert J. Zakrajsek

**Headquarters program office:** OAST

**Programs/Projects:** AC/ATM

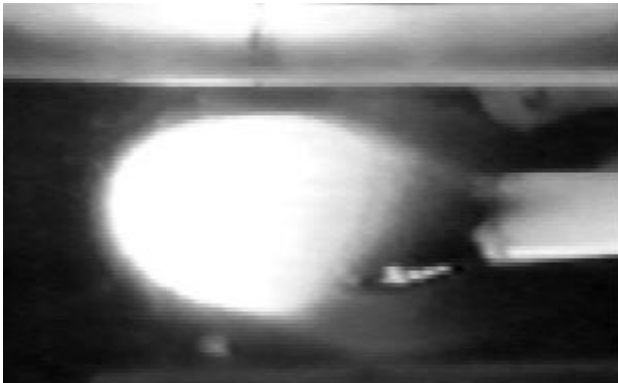
# Microgravity Science

## Burning Plastics Investigated in Space for Unique U.S./Russian Cooperative Project

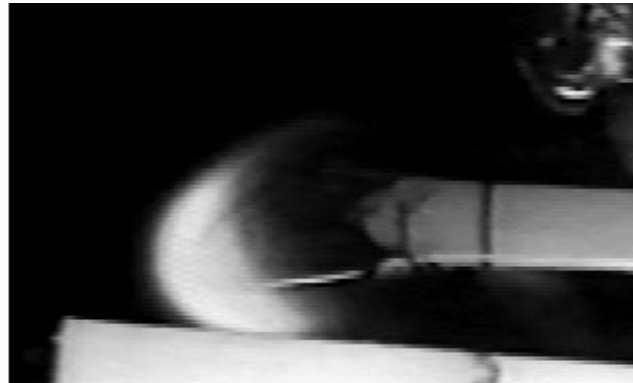
It is well known that fires in the low-gravity environment of Earth-orbiting spacecraft are different from fires on Earth. The flames lack the familiar upward plume, which is the result of gravitational buoyancy. These flames, however, are strongly influenced by minor airflow currents. A recent study conducted in low gravity (microgravity) on the Russian orbital station Mir used burning plastic rods mounted in a small chamber with a controllable fan to expose the flame to airflows of different velocities. In this unique project, a Russian scientific agency, the Keldysh Research Center, furnished the apparatus and directed the Mir tests, while the NASA Glenn Research Center at Lewis Field provided the test materials and the project management. Reference testing and calibrations in ground laboratories were conducted jointly by researchers at Keldysh and at the NASA Johnson Space Center's White Sands Test Facility.

Multiple samples of three different plastics were burned in the tests: Delrin, a common material for valve bodies; PMMA, a plastic "glass"; and polyethylene, a familiar material for containers and films. Each burned with a

unique spherical or egg-shaped flame that spread over the rod. The effect of varying the airflow was dramatic. At the highest airflow attainable in the combustion chamber, nearly 10 cm/sec (a typical ventilation breeze), the flames were bright and strong. As airflow velocity decreased, the flames became shorter but wider. In addition, the flames became less bright, and for PMMA and polyethylene, they showed two colors, a bright part decreasing in volume and a nearly invisible remainder (see the photographs).



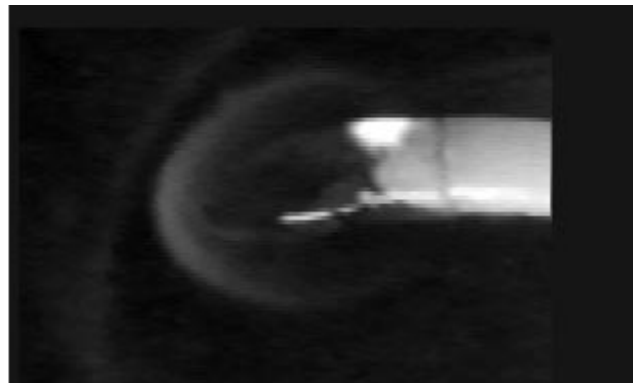
(a)



(b)



(c)



(d)

*Changes in flame appearance with airflow velocity for burning polyethylene rods in microgravity. Airflow and flame spread are from left to right in the photographs. (a) Air velocity, 8.5 cm/sec. (b) Air velocity, 4.0 cm/sec. (c) Air velocity, 2.0 cm/sec. (d) Air velocity, 1.0 cm/sec.*

Finally, at a very low velocity, the flames extinguished. For the plastics tested, this minimum velocity was very low, around 0.3 to 0.5 cm/sec. This finding confirms that at least a slight airflow is required to maintain a flame in microgravity for these types of materials.

The results of the project are significant for spacecraft fire safety. Of course, the plastics studied are flammable, and their use is limited on spacecraft. Because they are so common and difficult to replace, however, some quantities of these materials will be present in cabins, even on the International Space Station. The encouraging result is that the practice of shutting off ventilation or cooling airflows upon a fire indication or alarm will very likely extinguish small fires. On the other hand, if the shutoff is slow, fires may persist for some time under the stimulation of low airflows. The Mir tests also showed that the nearly invisible flames observed under low airflows are still hot and, therefore, could ignite nearby objects.

#### Bibliography

Ivanov, A.V., et al.: Preliminary Results of the Third Test Series of Nonmetal Material Flammability Evaluation in SKOROST Apparatus on the Space Station Mir. Kurt Sacksteder, compiler, Fifth International Microgravity Combustion Workshop. NASA/CP-1999-208917, 1999, pp. 47-50. (Available online: <http://gltrs.grc.nasa.gov/cgi-bin/GLTRS/browse.pl?/1999/CP-1999-208917.html>)

Ivanov, A.V., et al.: Experimental Verification of Material Flammability in Space. NASA/CR-1999-209405, Nov. 1999. (Available online: <http://gltrs.grc.nasa.gov/cgi-bin/GLTRS/browse.pl?/1999/CR-1999-209405.html>)

#### Glenn contact:

Robert Friedman, (216) 433-5697,  
fax (216) 977-7065,  
[Robert.Friedman@grc.nasa.gov](mailto:Robert.Friedman@grc.nasa.gov)

**Author:** Robert Friedman

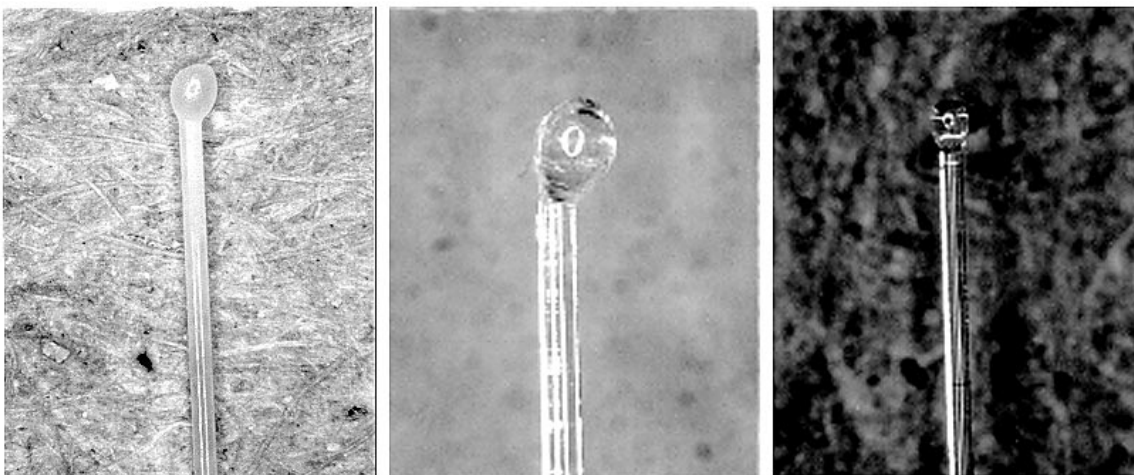
**Headquarters program office:** OLMSA

**Programs/Projects:**  
Microgravity Science

## Novel High Gas-Temperature Calibration System Demonstrated

Accurate measurement of high gas temperatures, typically above 1300 K, has always presented challenges to researchers. Thermocouples often perturb the local gas flow and temperature field; they provide indirect information; and at high temperatures, they require large corrections so that actual gas temperatures can be determined. The physical and chemical stability of thermocouples to withstand the thermal loads and reactive environments prevailing at high temperatures naturally limits their life and

maximum use temperature. Optical systems have their own drawbacks since accurate results depend on well-characterized emissivity, optical thickness, and gas composition information. These properties are rarely well known, especially in



Microscope photographs (30×) of molten fiber tips after resolidification. Left: Alumina/yttrium aluminum garnet (YAG) eutectic; melting point, 2095 K. Center: YAG; melting point, 2200 K. Right: Alumina; melting point, 2320 K.

high-temperature, chemically reacting environments. In addition, optical systems usually require independent calibrations, which often involve the use of thermocouples, and hence, suffer from their aforementioned limitations.

A new technique developed by researchers at the NASA Glenn Research Center at Lewis Field exploits an abrupt increase in the emittance of optically thin materials at their unique melting temperatures for a direct determination of gas temperature. Pure metallic-oxide fibers, varying in diameter from 60 to 400  $\mu\text{m}$ , have been used in measurements over a temperature range of 2050 to 2700 K. The accuracy and reproducibility of the technique is estimated to be  $\pm 15$  K: that is, within the uncertainty in the melting points of the materials. Other fiber materials with different, but unique, melting points could be used to extend the technique over a larger temperature range.

The technique has been demonstrated in hydrogen-air and hydrogen-oxygen flames stabilized on a flat-flame burner. Flame temperatures were varied by adjusting reactant flow rates. Fibers were inserted horizontally, along the fiber axis, into a cross-stream of up-flowing gases at temperatures lower than the gas melting points. Fiber tips were placed at the edge of the uniform-temperature zone of the flame. The flame temperature was increased toward the melting-point temperature by increments controllable to less than 4 K. Small fiber diameters and large length-to-diameter ratios assured rapid thermal equilibration with the surrounding hot gases and minimal conductive heat loss. When the fiber tip melted, a molten droplet was formed and then swept away by the gas stream. Consequently, the fiber was typically shortened by 1 mm. A small, resolidified drop remained on the fiber tip, as shown in the photographs, providing physical evidence of actual melting.

The reactant flow rates at which the fibers reproducibly reached their melting points in the experiments were also found to be independent of fiber diameters. The calculated emittance values of the fibers, based on published absorption coefficient data of the fiber materials, were around 0.01 at a few degrees below the fibers' melting points. These findings indicate that radiative cooling of the fibers was negligible prior to melting, allowing direct measurement of gas temperature without a radiative correction.

The technique lends itself to gas-temperature measurement under relatively few discrete conditions. Hence, it could most effectively be utilized to calibrate other gas-temperature-measurement devices, improving their accuracy especially at higher temperatures where their reliability becomes increasingly questionable. The technique was applied to assess the accuracy of gas-temperature measurements inferred from thermocouples, and it confirmed that such measurements are typically accompanied by uncertainties larger than 100 K (see the graph). It was also used to calibrate an infrared camera to measure gas temperatures using the band-ratio method.

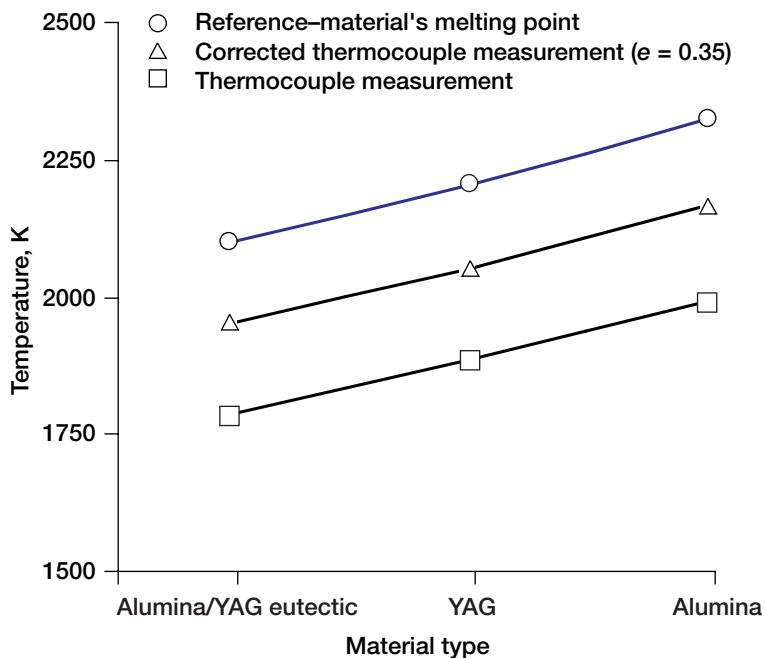
**Glenn contact:**

Suleyman A. Gokoglu, (216) 433-5499,  
Suleyman.A.Gokoglu@grc.nasa.gov

**Authors:** Suleyman A. Gokoglu and  
Donald Schultz

**Headquarters program office:** OLMSA

**Programs/Projects:**  
Microgravity Science



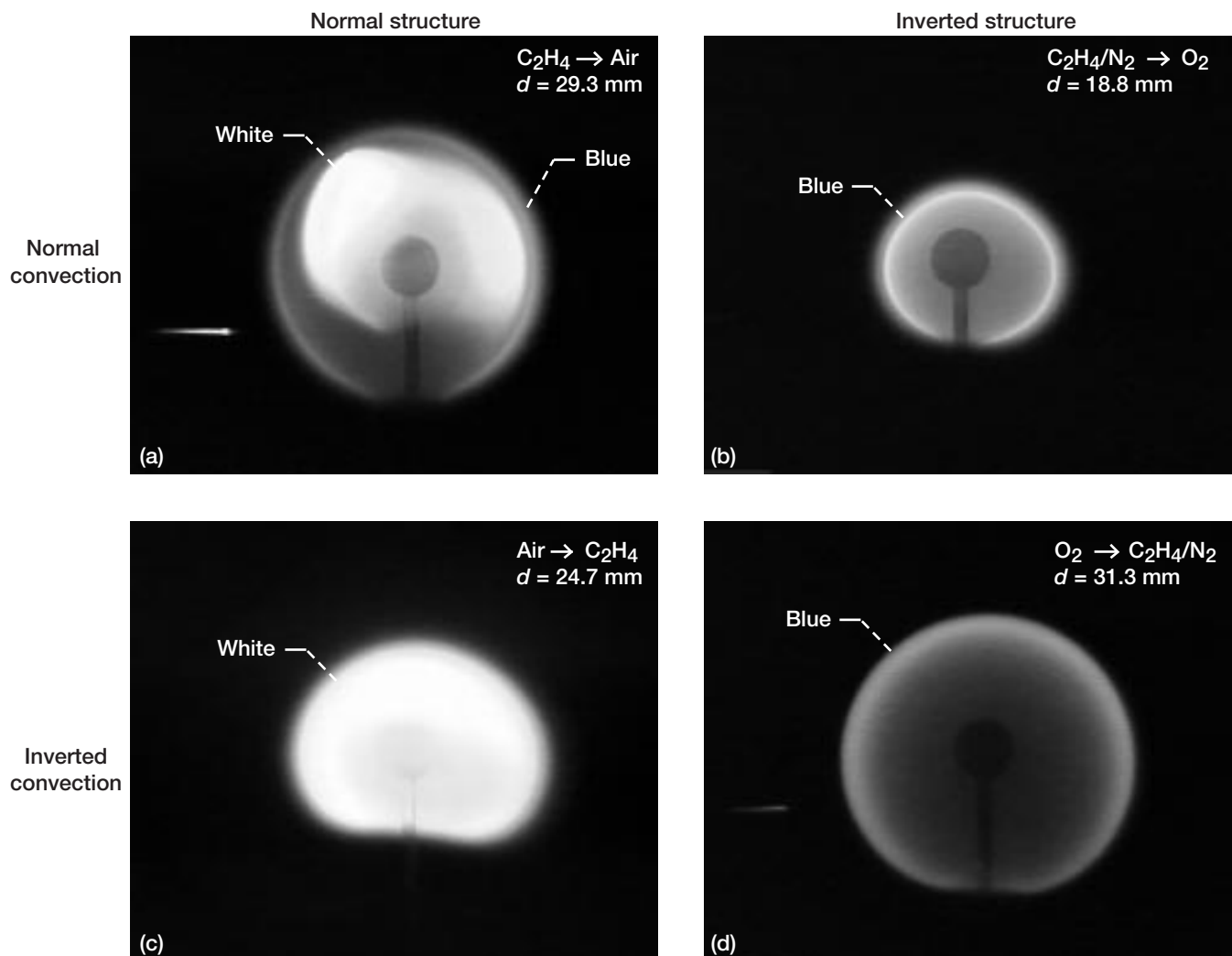
Gas temperatures measured and inferred from thermocouples versus "reference" melting-point measurements for alumina/yttrium aluminum garnet (YAG) eutectic, YAG, and alumina. (The symbol  $e$  refers to the emissivity.)

# Flame Design—A Novel Approach Developed to Produce Clean, Efficient Diffusion Flames

Soot formation and flame extinction are vital concerns in the combustion of fossil fuels. In particular, soot is responsible for pollutant emissions, and extinction can cause inefficient or unstable burning. Normal-gravity experiments have demonstrated that flames can be designed to improve both characteristics by redirecting some or all of the nitrogen from the oxidizer into the fuel. Such nitrogen exchange can produce permanently blue flames, which are soot free under all possible flame conditions. Furthermore, this approach can lead to stronger, extinction-resistant flames.

Past investigations of nitrogen exchange were unable to identify the physical mechanisms responsible for its benefits because these mechanisms

cannot be isolated when normal-gravity flames are studied. In contrast, the Diffusion Flame Extinction and Soot Inception (DESI) experiment considers spherical flames, where nearly perfect spherical symmetry affords new levels of control. Because of buoyancy, spherical flames cannot be created in Earth's gravity.



Images of four representative flames. (a) Ethylene ( $C_2H_4$ ) burning in air; diameter 29.3 mm. (b) Diluted ethylene ( $C_2H_4/N_2$ ) burning in oxygen; diameter, 18.8 mm. (c) Air issuing into ethylene ( $C_2H_4$ ); diameter, 24.7 mm. (d) Oxygen issuing into diluted ethylene ( $C_2H_4/N_2$ ); diameter, 31.3 mm. The scale is revealed by the 6.4-mm spherical burner. Color images are available at <http://mesun4.wustl.edu/ME/lacer/soot.html> and in the online version of this article (<http://www.grc.nasa.gov/WWW/RT1999/6711stocker.html>).

DESI was conceived by principal investigator Professor R.L. Axelbaum of Washington University in St. Louis. Tests to date have utilized the 2.2-Second Drop Tower at the NASA Glenn Research Center at Lewis Field. The experiment is slated for testing aboard the International Space Station in a few years.

Two mechanisms have been proposed to explain the connection between nitrogen exchange and permanently blue flames. These are the structure (chemical effects) and hydrodynamics (flow direction and speed). In normal-gravity flames, the structure and hydrodynamics are coupled, since nitrogen exchange simultaneously modifies both. Spherical microgravity flames, on the other hand, allow independent control of these factors. Specifically, structure can be modified via nitrogen exchange, and flow direction can be reversed by swapping the ambient and burner-feed gases. In DESI, these variations can be accomplished without changing the theoretical flame temperature.

Images of four flames observed in the 2.2-Second Drop Tower are shown here. The flames surround the burner (barely visible), which is a 6-mm porous steel sphere to which gas is supplied through a 2-mm tube. As is typical for hydrocarbon-fueled flames, yellow regions indicate the presence of glowing soot, and the reaction zones are bright blue. These four flames burn ethylene ( $C_2H_4$ ) at a rate of 1.5 mg/sec in a still ambient at a pressure of 1 atm. Several salient features of these flames are summarized in the table. In these flames, structure has a defining influence on soot production, with soot suppressed entirely when nitrogen is supplied with the fuel. Convection direction has a smaller influence, suppressing soot when convection is directed toward the oxidizer. These observations contribute significantly to the understanding of permanently blue diffusion flames.

Because of the inherent transient nature of 2-sec tests, preparations are underway to repeat these tests in Glenn's 5-sec facility. Nevertheless, burn times of 2 min will ultimately be required to obtain steady flames and limit conditions. Thus, if approved, DESI will be conducted aboard the International Space Station. We envision that such tests will yield fully steady flames and will measure sooting and extinction limits, temperatures, soot

## Cool Flames and Autoignition: Thermal-Ignition Theory of Combustion Experimentally Validated in Microgravity

At temperatures as low as 120 °C, fuel-air mixtures react chemically and produce very weak flames called cool flames. Unlike conventional flames—which generate large amounts of heat, carbon dioxide, and water—cool flames generate very little heat (e.g., a temperature rise of only 10 °C), carbon dioxide, and water. At low temperatures, the fuel and oxygen molecules have little energy and, therefore, do not react vigorously. The reaction never proceeds to complete combustion; rather, the molecules break down and recombine to produce a variety of stable chemical compounds including alcohols, acids, peroxides, aldehydes, and carbon monoxide. The weak temperature rise is produced by the breaking and reforming of the chemical bonds.

SUMMARY OF THE FOUR  
REPRESENTATIVE FLAMES

Flame	Structure	Flow direction	Soot
(a)	Normal	Normal	Present
(b)	Inverted	Normal	Absent
(c)	Normal	Inverted	Present
(d)	Inverted	Inverted	Absent

concentrations and morphology, and radiative emissions. The tests will continue to exploit a class of flames that cannot be observed in Earth's gravity.

### Find out more about this research on the World Wide Web:

<http://mesun4.wustl.edu/ME/lacer/soot.html>

### National Center for Microgravity Research contact:

Dr. Peter B. Sunderland, (216) 433-8087, [Peter.B.Sunderland@grc.nasa.gov](mailto:Peter.B.Sunderland@grc.nasa.gov)

### Glenn contacts:

Dennis P. Stocker, (216) 433-2166, [Dennis.P.Stocker@grc.nasa.gov](mailto:Dennis.P.Stocker@grc.nasa.gov);  
Jeffrey A. Jones, (216) 433-2870, [Jeffrey.A.Jones@grc.nasa.gov](mailto:Jeffrey.A.Jones@grc.nasa.gov); and  
Dr. David L. Urban, (216) 433-2835, [David.L.Urban@grc.nasa.gov](mailto:David.L.Urban@grc.nasa.gov)

**Authors:** Professor Richard L. Axelbaum, Dr. David L. Urban, Dr. Peter B. Sunderland, and Professor Beei-Huan Chao

**Headquarters program office:** OLMSA

### Programs/Projects:

HEDS, Microgravity Science

Cool flames were accidentally discovered in 1817 by Sir Humphry Davy, who noticed that he did not burn his fingers and could not ignite a match in a cool flame. While cool flames were a curiosity at first, they gained widespread attention when Sir Davy noticed that they could spontaneously develop into hot conventional flames. Moreover, an external

ignition source such as a spark, hot wire, or hot surface was unnecessary for ignition if the temperature, pressure, and mixture composition were within certain limits.

Understanding cool flames and autoignition is important for engineers and designers to mitigate potential combustion hazards. Cool flames are also responsible for engine knock—the undesirable, erratic, and noisy combustion process that occurs in low-octane fuels. Physically, the crankshaft rotates, the pistons compress the unburned fuel-air mixture, and the gases heat as they are compressed. If the rate at which the heat is liberated by the chemical reactions exceeds the rate at which the heat is lost through heat transport, the temperature of the gas increases and slow reactions ensue. As the temperature continues to increase, cool flames develop and the mixture autoignites. Note that cool flames and autoignitions are not always undesirable. Diesel engines, for example, rely on the compressed fuel-air mixture to autoignite so that the engine can operate without spark plugs.

The objective of this study at the NASA Glenn Research Center at Lewis Field is to hone our understanding of spontaneous chemical reactions and determine the various factors that influence when, where, and how cool flames and autoignitions develop. These factors include the molecular structure of the fuel, the pressure and temperature of the mixture, and the various ways in which heat can be lost—through conduction, convection, or radiation. Generally, radiation heat transfer is weak at low temperatures, and most of the heat is lost through convection or conduction.

Current mathematical models neglect convective heat transport because it introduces nonlinear complexities into the formulation. However, analyses that have been formulated to include conductive heat transport must be tested against experiments to confirm (or refute) their predictions.

Unfortunately, performing such experiments on Earth is not simple. When the heat liberated by the chemical reactions locally heats the gas, it generates convection, since hot (less dense) gas rises and cold (more dense) gas falls. This self-generated convective flow then alters the transport of heat. In effect, it is a “Catch-22,” since the heat liberated by the chemical reactions generates convection, but convection is difficult to incorporate into the mathematical formulation.

The best way to eliminate the effects of convection is to study these reactions at reduced gravity, where hot gas doesn't rise and cold gas doesn't fall. This is precisely why these reactions are currently being studied in NASA's reduced-gravity facilities (drop towers and aircraft) and are planned to be studied on space-based microgravity platforms.

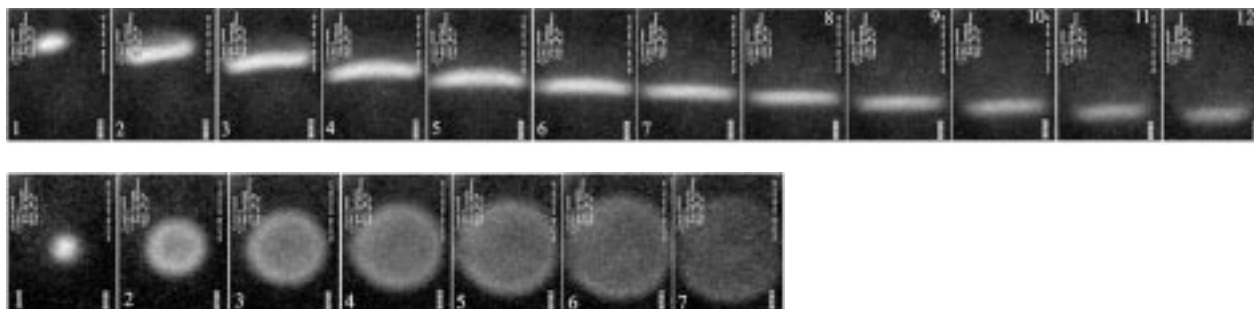
During fiscal year 1999, experiments were conducted using a variety of fuels (hydrocarbons, carbon monoxide, hydrogen, and natural gas) mixed with air at different temperatures and pressures, both in the laboratory and aboard NASA's KC-135 reduced-gravity aircraft. The hardware and crew are shown in the photograph.



*Cool flame experiment aboard NASA's KC-135 reduced-gravity aircraft.*

It is readily observed that on Earth (1g), the heat generated during the early stages of the chemical reaction rises to the top of the vessel. When the temperature exceeds a critical value, a cool flame develops. This is shown in the top portion of the following figure. At reduced-gravity ( $10^{-2}$  g) aboard the KC-135, heat does not rise or fall but accumulates in the center of the flask. A spherically propagating cool flame ensues as shown in the bottom portion of this figure.

Interestingly, we also learned that cool flames and autoignitions do not occur at the same temperature and pressure at Earth's gravity and reduced gravity. Generally, they occur at lower temperatures and pressures in reduced-gravity environments, since the gas does not readily cool in the absence of buoyant convection. In other words, fuel-air mixtures that do not autoignite on Earth may ignite in



Premixture, 50%  $n\text{-C}_4\text{H}_{10}$ -50%  $\text{O}_2$  (in volume percent); 4-in. inner diameter spherical vessel; vessel temperature, 300 °C; initial pressure, 3.2 psia; elapsed time between adjacent frames, 1/30 sec. Top: 1g (Earth's gravity). Bottom:  $10^{-2}g$  (reduced gravity).

reduced gravity, making a space-based atmosphere potentially more susceptible to autoignition.

Ongoing work in this area is actively being conducted at Glenn. Current plans include additional tests with the same fuels as well as with the commercial fuels used in aircraft and spacecraft.

**National Center for Microgravity Research contact:**

Dr. Ming-Shin Wu (Project Scientist), (216) 433-3781, Ming-Shin.Wu@grc.nasa.gov

**Glenn contacts:**

Richard M. Chapek, (216) 433-2025, Richard.M.Chapek@grc.nasa.gov; and  
Donna L. Neville, (216) 433-5243, Donna.L.Neville@grc.nasa.gov

**Authors:**

Dr. Howard Pearlman (Principal Investigator) and Richard M. Chapek

**Headquarters program office:** OLMSA

**Programs/Projects:**

Microgravity Science

**Special recognitions:**

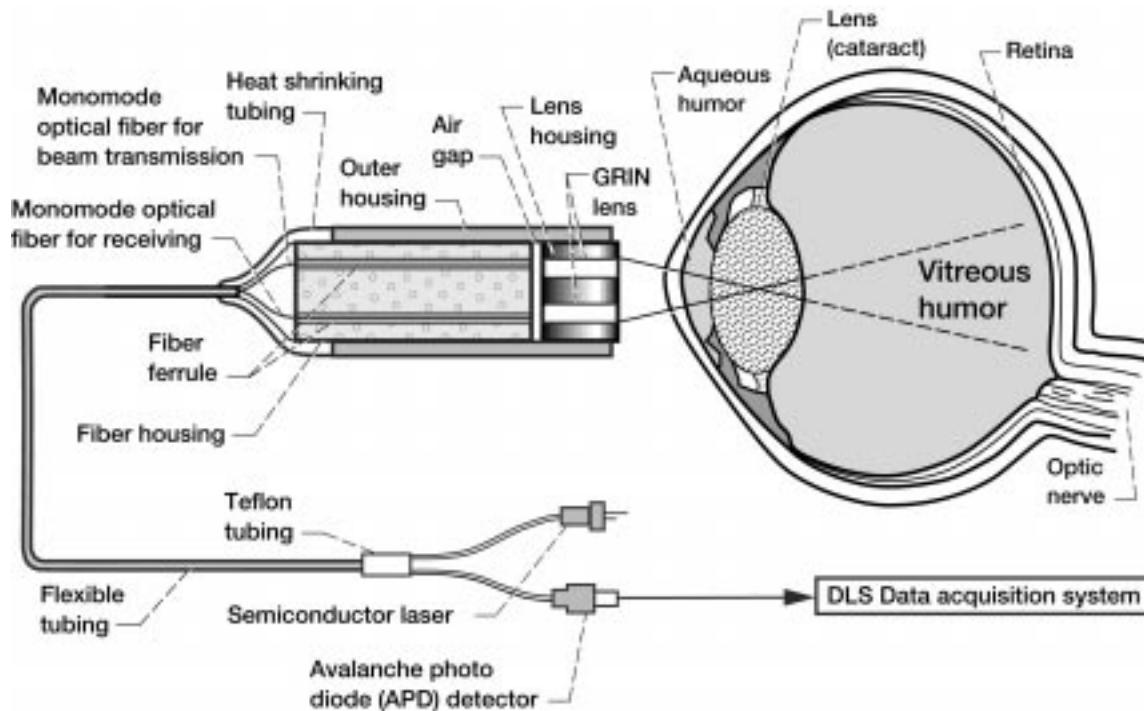
Presidential Early Career Award for Scientists and Engineers (PECASE)  
Award for Cool Flames (presented at the White House to Dr. Howard Pearlman). Craftsmanship Award for Cool Flames (presented to Richard M. Chapek).

## Fiber-Optic Imaging Probe Developed for Space Used to Detect Diabetes Through the Eye

Approximately 16 million Americans have diabetes mellitus, which can severely impair eyesight by causing cataracts, diabetic retinopathy, and glaucoma. Cataracts are 1.6 times more common in people with diabetes than in those without diabetes, and cataract extraction is the only surgical treatment. In many cases, diabetes-related ocular pathologies go undiagnosed until visual function is compromised. This ongoing pilot project seeks to study the progression of diabetes in a unique animal model by monitoring changes in the lens with a safe, sensitive, dynamic light-scattering probe.

Dynamic light scattering (DLS), has the potential to diagnose cataracts at the molecular level. Recently, a new DLS fiber-optic probe was developed at the NASA Glenn Research Center at Lewis Field for noncontact, accurate, and extremely sensitive particle-sizing measurements in fluid dispersions and suspensions (ref. 1). This compact, portable, and rugged probe is free of optical alignment, offers point-and-shoot operation for various online field applications and challenging environments, and yet is extremely flexible in regards to sample container sizes, materials, and shapes. No external vibration isolation and no index matching are required. It can measure

particles as small as 1 nm and as large as few micrometers in a wide concentration range from very dilute (waterlike) dispersions to very turbid (milklike) suspensions. It is safe and fast to use, since it only requires very low laser power (10 nW to 3 mW) with very short data acquisition times (2 to 10 sec). The new DLS probe has been applied to characterize protein solutions and protein crystallization processes in NASA's flight hardware (ref. 2), but it can be quickly adapted to the various state-of-the-art ophthalmic instruments (e.g., the slit-lamp and Scheimpflug imaging) presently in use at the National Eye Institute of the National Institutes

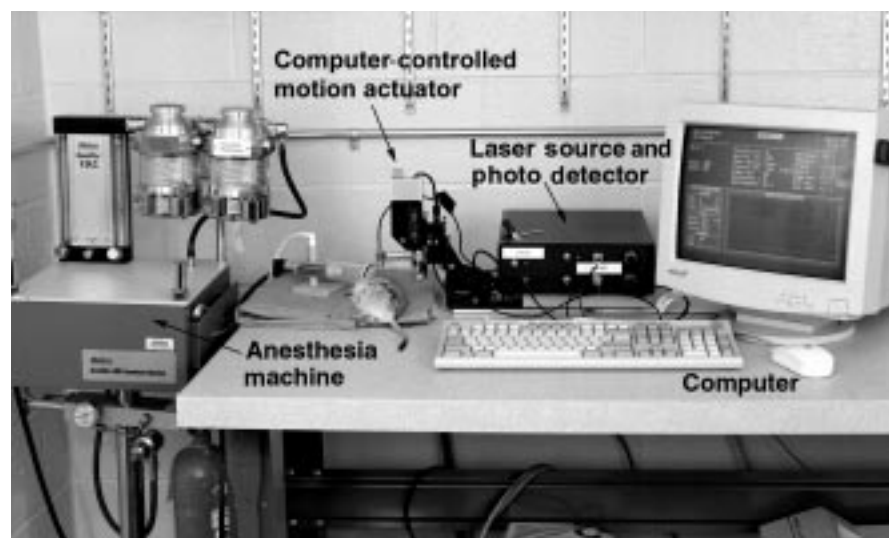


*Dynamic light scattering (DLS) probe.*

of Health. This modification advances the cataract diagnostic process from mere visual and photographic observations to molecular level investigations (ref. 3). Detection of lens changes may enable the early identification of diabetes in the many millions of people worldwide, including 8 million Americans, who have undiagnosed diabetes. DLS also detects and quantifies the early changes associated with diabetes in the vitreous (ref. 4) (the fluid that occupies 80 percent of the volume of the eye).

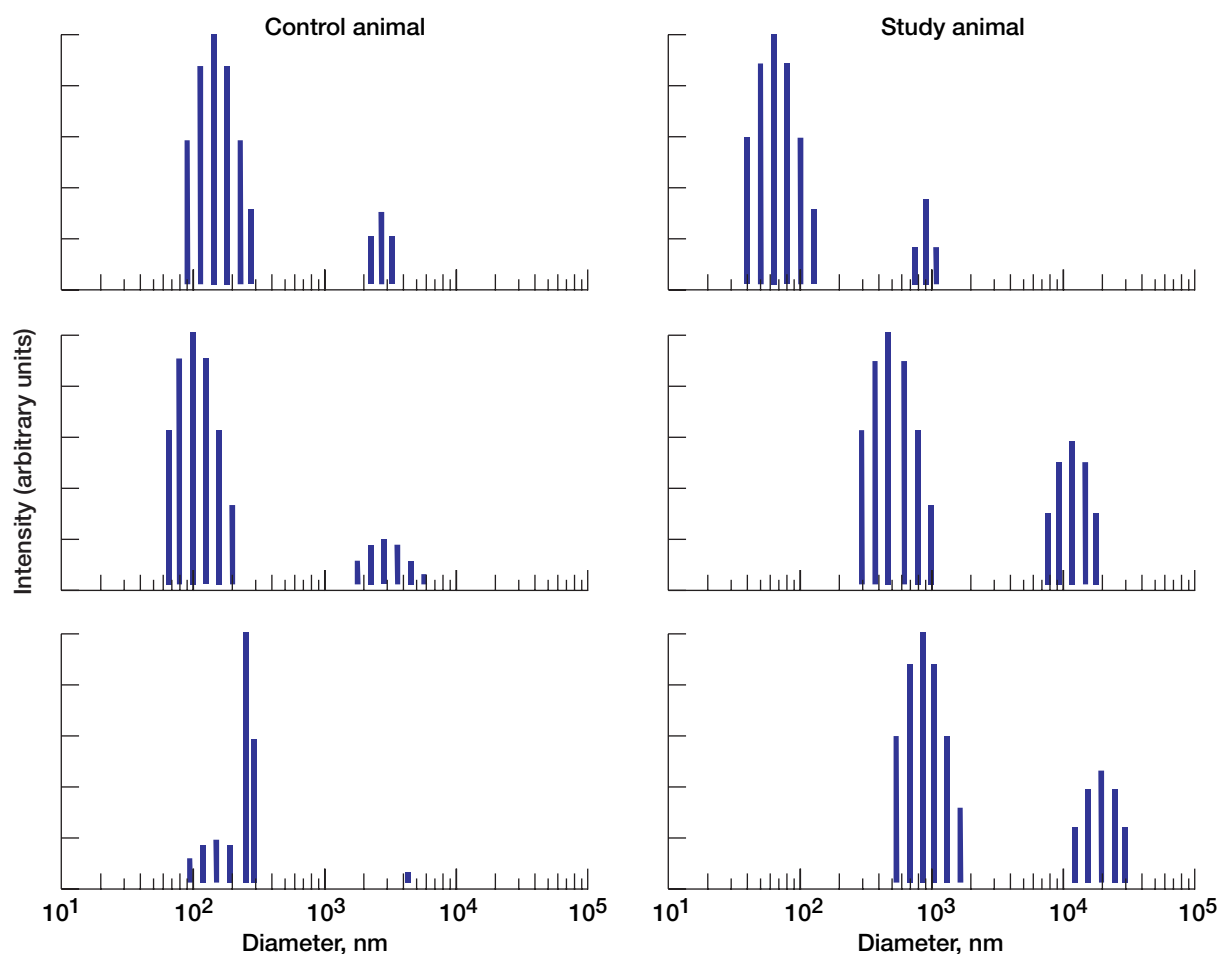
Desert rodents, commonly called sand rats, are being used in a Food and Drug Administration study with the DLS probe. This animal is unique in

that it develops diabetes in a manner similar to humans. Typical results are shown as histograms of protein size distribution in the eye lens for a control animal and a diabetic animal over a 3-month period. The DLS probe can discern subtle and diffusive changes in the lenses, specifically the shift in the size of the proteins, which increases during the initial stages of diabetes in these animals. Our preliminary results also demonstrate that there are subtle changes in the lenses of diabetic sand rats when the rats are kept on a diabetogenic diet (one that will produce diabetes) for 2 months. The minor changes over time seen in the control animals are attributed to age and instrument conditions and are considered to be insignificant.



*Experimental setup at the Food and Drug Administration for diagnosing diabetes through the eyes of sand rats.*

The DLS probe is proving to be a practical, noninvasive diagnostic tool that is useful for the early detection of ocular pathologies and for understanding the mechanism of cataract formation (ref. 5). In the long term, it may be possible to use DLS data obtained from the eye to



Macromolecular size distribution ( $\alpha$  crystalline protein) in the eye lens of a sand rat on a normal (control) diet (left) and a diabetogenic diet (right). Top: Baseline—All animals on the control (normal) diet. Center: 30 days after initiation of diabetogenic diet. Bottom: 60 days after initiation of diabetogenic diet.

predict diabetic status. In addition, a noninvasive diagnostic method of molecular evaluation would enable repeat measurements to gauge response to therapy. The NASA probe seems to hold particular promise for ocular diagnostic work.

#### References

1. Ansari, R.R.; and Suh, K.I.: Dynamic Light Scattering Particle-Size Measurements in Turbid Media. Proceedings of Coherence Domain Optical Methods in Biomedical Science and Clinical Applications II, vol. 3251, SPIE, Bellingham, WA, 1998, pp. 146–156.
2. Ansari, R.R., et al.: Fiber Optic Probe for Monitoring Protein Aggregation, Nucleation, and Crystallization. J. Crystal Growth, vol. 168, no. 1–4, 1996, pp. 216–226.
3. Ansari, R.R.; and Datiles, M.B.: Use of Dynamic Light Scattering and Scheimpflug Imaging for the Early Detection of Cataracts. Diabetes Technology & Therapeutics, vol. 1, no. 2, 1999, pp. 159–168.
4. Sebag, J., et al.: Dynamic Light Scattering of Diabetic Vitreopathy. J. Diabetes Technology & Therapeutics, vol. 1, no. 2, 1999, pp. 169–176.
5. Betelheim, F.A., et al.: The Mode of Chaperoning of Dithiothreitol-Denatured  $\alpha$ -Lactalbumin by  $\alpha$ -Crystallin. Biochemical and Biophysical Research Communications, vol. 261, no. 2, 1999, pp. 292–297.

#### National Center for Microgravity Research (at Glenn) contact:

Dr. Rafat R. Ansari, (216) 433–5008, Rafat.R.Ansari@grc.nasa.gov

#### Authors:

Dr. Rafat R. Ansari, Dr. Michelle V. Chenault, Dr. Manuel B. Datiles III, Dr. J. Sebag, and Dr. Kwang I. Suh

#### Headquarters program office:

OLMSA (under NASA–NIH and NASA–FDA Interagency Agreements)

#### Programs/Projects:

Microgravity Science

#### Special recognition:

NASA Public Service Medal 1999

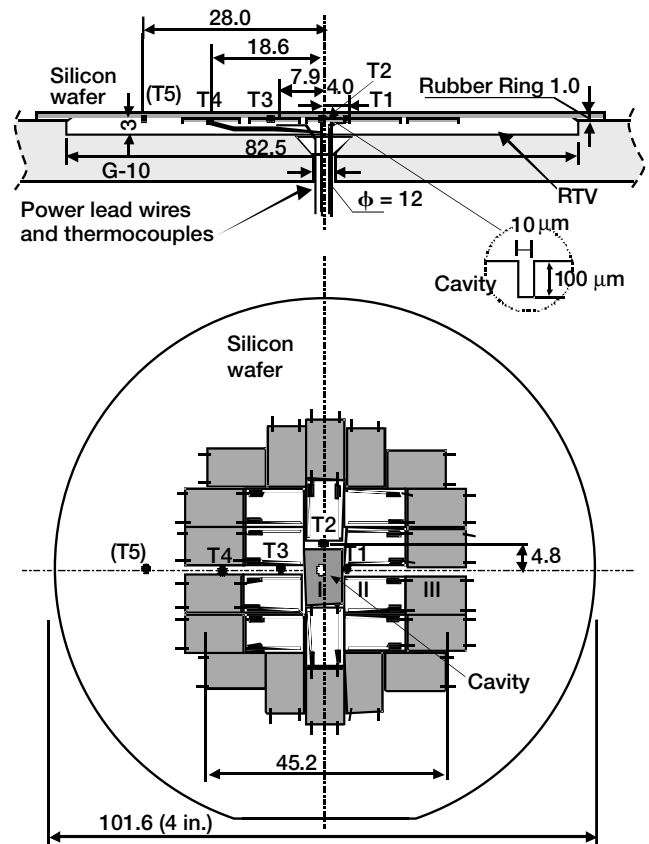
# Nucleate Boiling Heat Transfer Studied Under Reduced-Gravity Conditions

Boiling is known to be a very efficient mode of heat transfer, and as such, it is employed in component cooling and in various energy-conversion systems. In space, boiling heat transfer may be used in thermal management, fluid handling and control, power systems, and on-orbit storage and supply systems for cryogenic propellants and life-support fluids. Recent interest in the exploration of Mars and other planets and in the concept of in situ resource utilization on the Martian and Lunar surfaces highlights the need to understand how gravity levels varying from the Earth's gravity to microgravity ( $1g \geq g/g_e \geq 10^{-6}g$ ) affect boiling heat transfer.

Because of the complex nature of the boiling process, no generalized prediction or procedure has been developed to describe the boiling heat transfer coefficient, particularly at reduced gravity levels. Over the last three decades, a limited number of experimental studies performed in short- and long-duration low-gravity environments provided valuable insights into the boiling phenomena. However, these studies produced nonconclusive findings and often yielded contradictory data that could not provide sufficient understanding of the phenomena so that models or correlations could be developed. Recently, Professor Vijay K. Dhir of the University of California at Los Angeles proposed a novel building-block approach to investigate the boiling phenomena in low-gravity to microgravity environments (see ref. 1

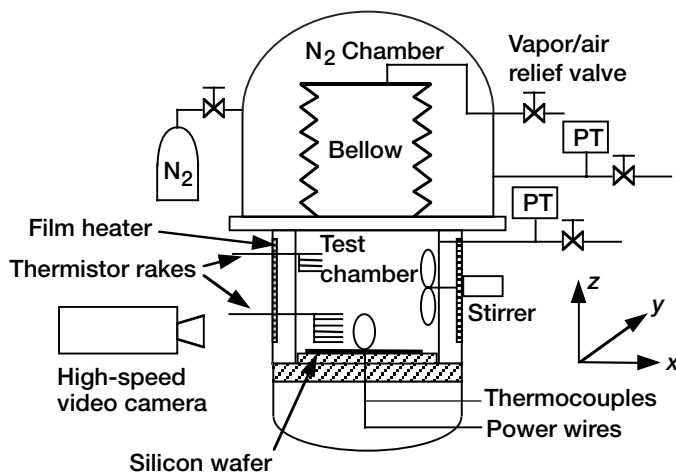
and Dhir, V.K.; and Hasan, M.M.: Science Requirement Document for a Mechanistic Study of Nucleate Boiling Heat Transfer Under Microgravity Conditions. Unpublished document, NASA Glenn Research Center, Cleveland, Ohio, 1999). This approach experimentally investigates the complete process of bubble inception, growth, and departure for single bubbles formed at a well-defined and controllable nucleation site.

Principal investigator Professor Vijay K. Dhir, with support from researchers from the NASA Glenn Research Center at Lewis Field, is performing a series of pool boiling experiments in the low-gravity environments of the KC-135

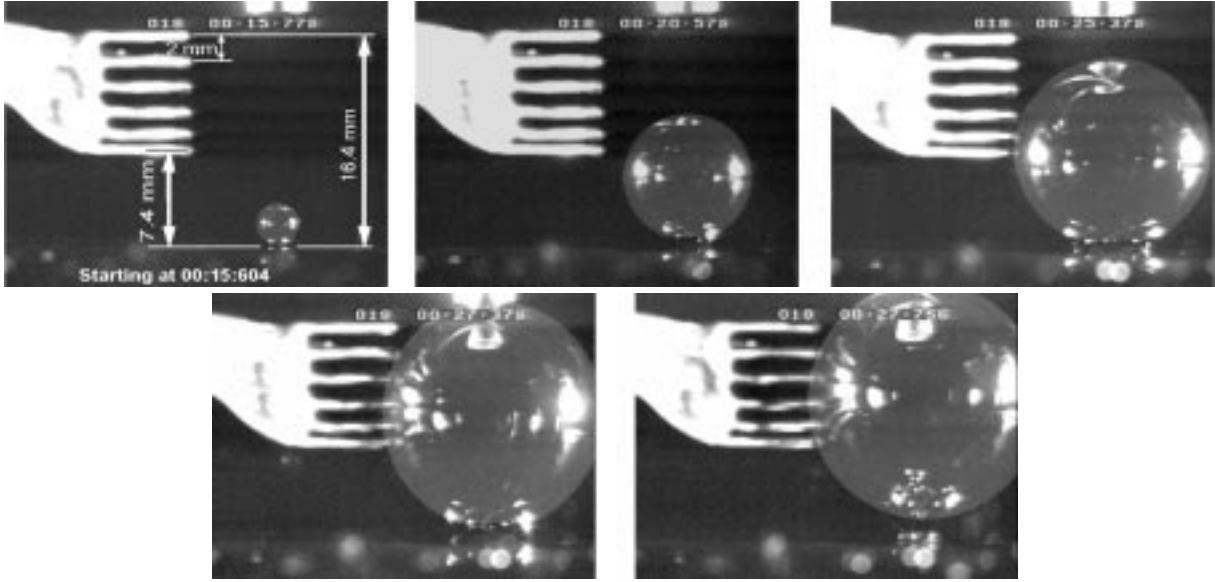


Configuration of silicon wafer heater. (Dimensions in millimeters unless marked otherwise.)

PT Pressure transducer



Experimental setup.



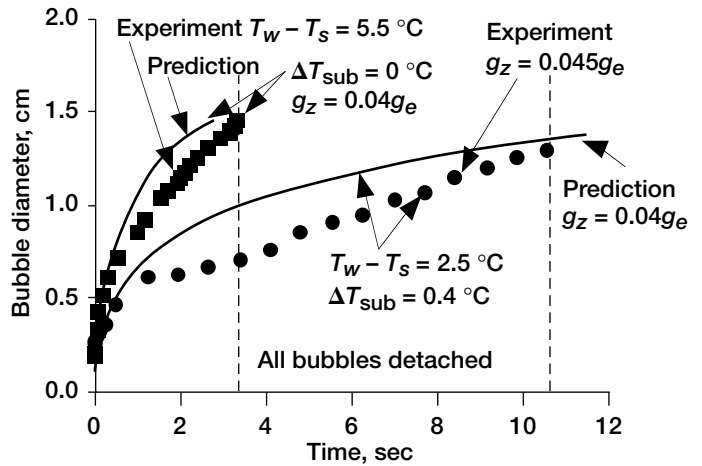
Selected pictures of a single bubble during a growth-departure cycle inception of nucleation.

microgravity aircraft's parabolic flight to investigate the inception, growth, departure, and merger of bubbles from single- and multiple-nucleation sites as a function of the wall superheat and the liquid subcooling. Silicon wafers with single and multiple cavities of known characteristics are being used as test surfaces. Water and PF5060 (an inert liquid) were chosen as test liquids so that the role of surface wettability and the magnitude of the effect of interfacial tension on boiling in reduced gravity can be investigated.

On the opposite page, the left drawing shows a schematic of the KC-135 apparatus, and the right drawing shows the location of the heaters and thermocouples on the silicon wafer. To date, we have obtained data on the growth and departure of bubbles from a single nucleation site in the low gravity environments of the KC-135 as a function of the wall superheat from 2.5 to 8 °C and of the liquid subcooling of less than 1 °C. The top figure (on this page) shows selected pictures of a complete cycle of bubble growth with nucleation occurring at the designed cavity, and the graph compares the measured bubble diameter with the prediction of the numerical solution. The experimental findings are described in detail in reference 2.

**References**

1. Dhir, V.K.: Investigation of Mechanisms Associated With Nucleate Boiling Under Microgravity Conditions. Proceedings of the Third Microgravity Fluid Physics Conference. NASA CP-3338, 1996, pp. 153-158.
2. Qiu, D., et al.: Single and Multibubble Dynamics During Nucleate Boiling Under Microgravity Conditions. Microgravity Fluid Physics and Heat Transfer, United Engineering Foundation, Inc., New York, NY, Sept. 19-24, 1999.



Comparisons of measured bubble diameter and numerical prediction in saturated water and in subcooled water at low gravity. Time,  $t$ , 0 sec; wall superheat,  $\Delta T_{sub}$ , 0.3 °C; wall temperature minus the saturated liquid temperature,  $T_w - T_s$ , 4.2 °C; Earth's gravitational acceleration in the z-direction,  $g_z \approx 0.02 g/g_e$  (where  $g_e$  is Earth's normal gravitational acceleration).

**Glenn contacts:**

Dr. David F. Chao, (216) 433-8320, David.F.Chao@grc.nasa.gov; and Dr. Mohammad M. Hasan, (216) 977-7494, Mohammad.Hasan@grc.nasa.gov

**Authors:** Dr. David F. Chao and Dr. Mohammad M. Hasan

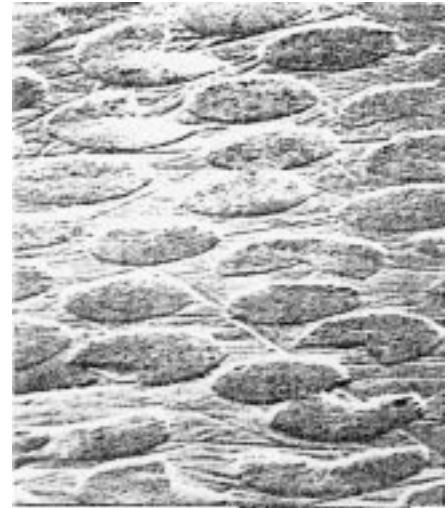
**Headquarters program office:** OLMSA

**Programs/Projects:** Microgravity Science

# Boiling on Microconfigured Composite Surfaces Enhanced

Boiling heat transfer is one of the key technologies for the two-phase active thermal-control system used on space platforms, as well as for the dynamic power systems aboard the International Space Station. Because it is an effective heat transfer mode, boiling is integral to many space applications, such as heat exchangers and other cooling devices. Nucleate boiling near the critical heat flux (CHF) can transport very large thermal loads with a much smaller device and much lower pumping power than for single-phase heat exchangers. However, boiling performance sharply deteriorates in a reduced-gravity environment, and operation in the CHF regime is somewhat perilous because of the risk of burnout to the device surface.

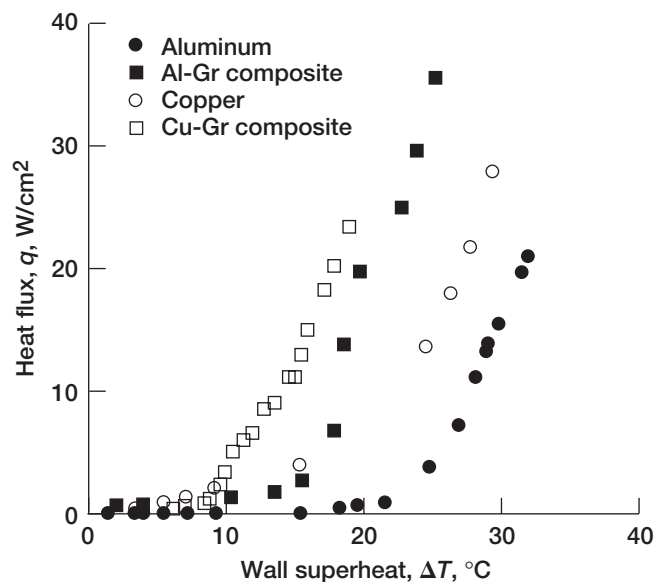
New materials called microconfigured metal-graphite composites can enhance boiling. The photomicrograph shows the microconfiguration ( $\times 3000$ ) of the copper-graphite (Cu-Gr) surface as viewed by scanning electronic microscope. The graphite fiber tips appear as plateaus with rugged surfaces embedded in the copper matrix. It has been experimentally demonstrated that this type of material manifests excellent boiling heat transfer performance characteristics and an increased CHF. Non-isothermal surfaces were less sensitive to variations of wall superheat in the CHF regime (ref. 1). Because of the great difference in conductivity between the copper base and the graphite fiber, the composite surfaces have a nonisothermal surface characteristic and, therefore, will have a much larger "safe" operating region in the CHF regime. In addition, the thermocapillary forces induced by the temperature differences between the fiber tips and the metal matrix play an important role in bubble detachment, and may not be adversely affected in a reduced-gravity environment. All these factors indicate that microconfigured composites may improve the reliability and economy (dominant factors in all space applications) of various thermal components found on spacecraft during future missions.



Cu-Gr composite surface.

More experimental study of the boiling heat transfer performance of metal-graphite composite surfaces is being conducted, including the CHF of pentane and the entire nucleate boiling regime of water on Cu-Gr and Al-Gr composite surfaces. The new experimental data will be used to recheck and improve the mathematical model.

The current experiment was conceived by Dr. Nengli Zhang of the Ohio Aerospace Institute. Experimental studies were conducted of the nucleate boiling heat transfer of pentane on metal-graphite composite surfaces with a fiber volume concentration of 50 vol %, including copper-graphite (Cu-Gr) and aluminum-graphite (Al-Gr) composite surfaces. The nucleate boiling heat transfer performance of metal-graphite surfaces is obviously much better than that of pure metal surfaces, as shown in the graph. In this figure, superheat  $\Delta T$  is equal to the difference between the wall temperature and the saturation temperature of the working fluid (here, pentane), and  $q$  is heat flux transferred from the wall to the working fluid. On the basis of the experimental results and according to the two-tier configuration and mathematical model proposed by Zhang et al. (ref. 2), a correlation for the heat transfer performance in the nucleate boiling regime was derived.



Performance of nucleate boiling heat transfer.

## References

1. Yang, W.J.; and Zhang, N.: Boiling Performance on Nonisothermal Surfaces. Proceedings of the Engineering Foundation Conference on Pool and External Flow Boiling, ASME, New York, NY, 1992, pp. 119–124.
2. Zhang, N.; Yang, W.J.; and Yang, G.W.: Two-Tier Model for Nucleate Pool Boiling on Microconfigured Composite Surfaces. Int. Comm. J. Heat Mass Trans., vol. 19, no. 6, 1992, pp. 767–779.

## Glenn contact:

Dr. David F. Chao, (216) 433–8320,  
David.F.Chao@grc.nasa.gov

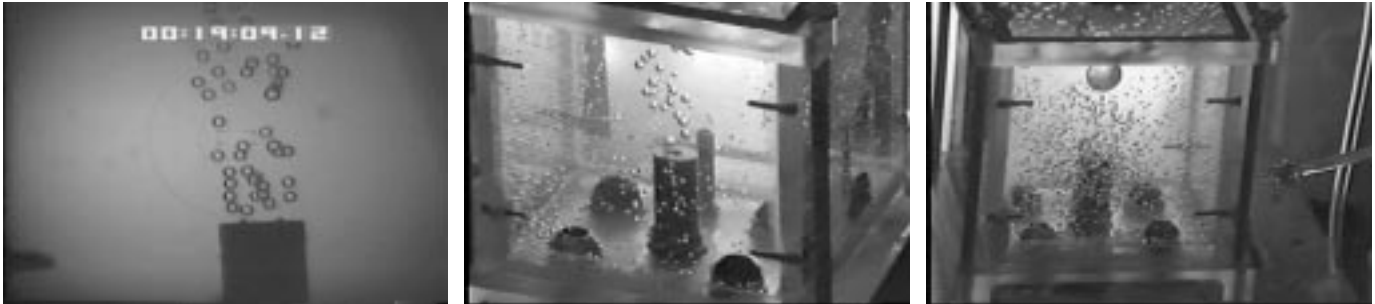
**Author:** Dr. David F. Chao

**Headquarters program office:** OLMSA

**Programs/Projects:**

Microgravity Science

## Bubbly Suspension Generated in Low Gravity

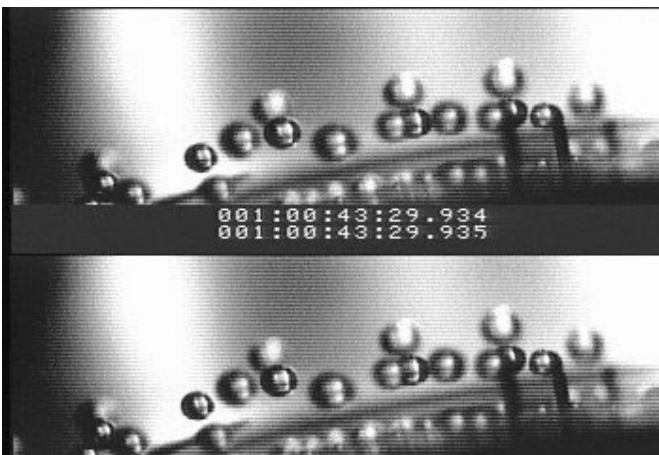


*Spinning bubbler concept. Left: Two-dimensional side view. Center and Right: Three-dimensional views.*

Bubbly suspensions are crucial for mass and heat transport processes on Earth and in space. These processes are relevant to pharmaceutical, chemical, nuclear, and petroleum industries on Earth. They are also relevant to life support, in situ resource utilization, and propulsion processes for long-duration space missions such as the Human Exploration and Development of Space program. Understanding the behavior of the suspension in low gravity is crucial because of factors such as bubble segregation, which could result in coalescence and affect heat and mass transport. Professors A. Sangani and D. Koch, principal investigators in the Microgravity Fluid Physics Program managed by the NASA Glenn Research Center at Lewis Field, are studying the physics of bubbly suspension. They plan to shear a bubbly suspension in a couette cell in microgravity to study bubble segregation and compare the bubble distribution in the couette gap with the

one predicted by the suspension-averaged equations of motion. Prior to the Requirement Definition Review of this flight experiment, a technology for generating a bubbly suspension in microgravity has to be established, tested, and verified.

Generation of bubbly suspensions of uniform bubble diameter (standard deviation <10 percent) in space is a difficult task because bubbles do not detach as easily as



*Stationary bubblers concept in a couette cell. Left: Two-dimensional top view. Right: Three-dimensional view.*

on Earth. Under microgravity, the buoyancy force is not present to detach the bubbles as they are formed from nozzles. One way to detach the bubbles is to apply an external force on them. As suggested by Kim et al. (ref. 1), the drag force produced by a liquid flowing in a cross-flow or co-flow configuration with respect to the nozzle direction will detach the bubbles as they are being formed.

Two flow loops were designed and built to test different concepts for creating a suspension in low gravity. In the first, bubbles were generated in a cubic test chamber, and in the second, in a couette cell. Both loops were totally contained and did not require any additional air or water during the low-gravity experiments. All bubbly-suspension-generation experiments were performed on NASA's DC-9 and KC-135 low-gravity aircraft. Two bubbler concepts were explored. The first was a spinning bubbler that uses the relative velocity of the nozzle spin to detach the bubbles. The top photographs on the preceding page show two- and three-dimensional views of this concept, which was tested in the first flow loop. The second was a stationary bubbler placed in a couette shear flow. The drag force created by the moving fluid causes the bubbles to detach. The bottom photographs show the stationary bubblers as indexed in the couette cell shear flow.

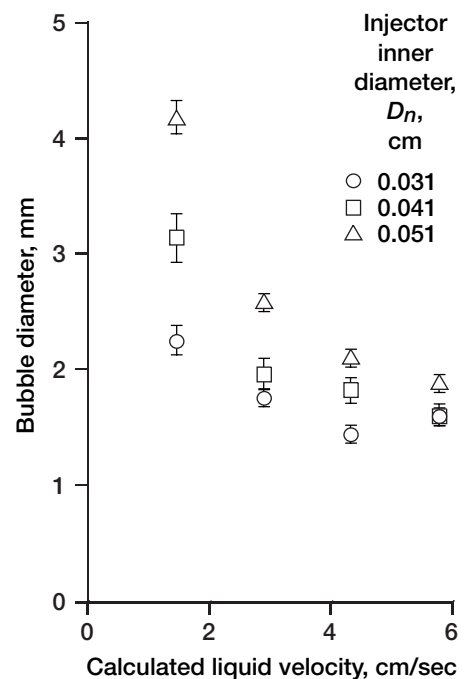
The latest results from the stationary bubbler are shown in the graph, where the bubble diameter at detachment is plotted as a function of the local fluid velocity (ref. 2). As the liquid velocity is increased, the bubble diameter decreases because of the reduction in the time to detachment. This, in turn, is due to the higher drag force applied on the bubble. Similar trends were shown for the spinning bubbler. Both concepts are promising for generating uniform suspensions. Future efforts are planned to focus on the stationary bubbler concept integrated in the couette cell.

**References**

1. Kim, I.; Kamotani, Y.; and Ostrach, S.: Modeling Bubble and Drop Formation in Flowing Liquids in Microgravity. *AIChEJ*, vol. 40, no. 1, 1994, pp. 19–28.
2. Nahra, H.K.; and Hoffmann, M.: Generation of Bubbly Suspension in Low Gravity. AIAA Paper 2000–0854, 38th AIAA Aerospace Sciences Meeting and Exhibit, Reno, NV, 2000.

**Glenn contacts:**

Henry K. Nahra, (216) 433–5385, Henry.K.Nahra@grc.nasa.gov; and  
 Monica I. Hoffmann, (216) 433–6765, Monica.I.Hoffmann@grc.nasa.gov



*Latest results from the stationary bubbler concept. Bubble diameter is plotted as a function of the liquid velocity. The distance of the bubbler tip from the stationary inner wall and into the couette gap is 0.25 cm; the gas flow rate is 16 cm<sup>3</sup>/min.*

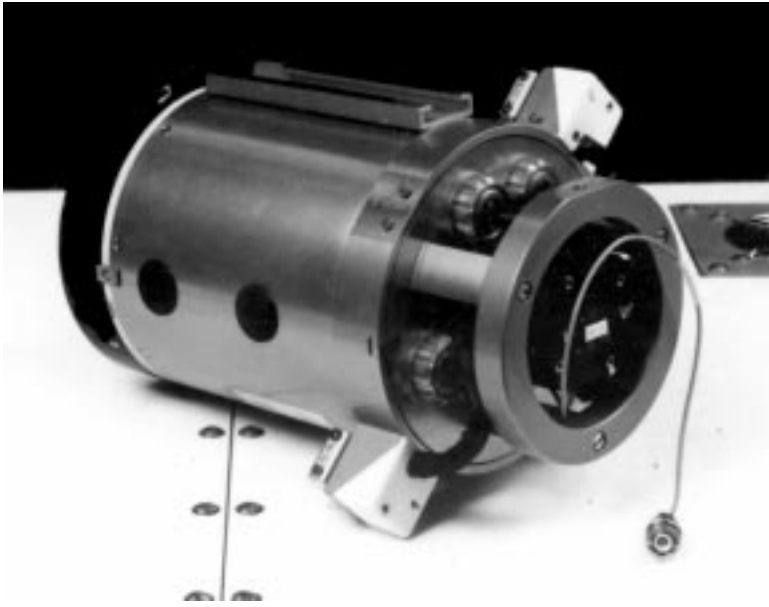
**Author:** Henry K. Nahra

**Headquarters program office:** OLMSA

**Programs/Projects:**  
 Microgravity Sciences, HEDS

**Special recognitions:**  
 Special Service Award for “Bubble Formation and Detachment,” Group Achievement Award for the “Completion of a Successful SCR for Behavior of Rapidly Sheared Bubbly Suspension Flight Definition Experiment.”

# Growth and Morphology of Supercritical Fluids Studied in Microgravity on Mir



*ALICE II thermostat for critical fluid samples. It enables stable temperature control ( $\pm 50 \mu\text{C rms}$ ) and optical diagnostics like interferometry and microscopy.*

The Growth and Morphology of Supercritical Fluids (GMSF) is an international experiment facilitated by the NASA Glenn Research Center at Lewis Field and under the guidance of U.S. principal investigator Professor John Hegseth of the University of New Orleans and three French coinvestigators—Daniel Beysens, Yves Garrabos, and Carole Chabot. In early 1999, GMSF experiments were operated for 20 days on the Russian Space Station Mir. Mir astronauts performed experiments One through Seven, which spanned the three science themes of near-critical phase separation rates, interface dynamics in near-critical boiling, and measurement of the spectrum of density fluctuation length scales very close to the critical point. The fluids used were pure  $\text{CO}_2$  or  $\text{SF}_6$ . Three of the five thermostats used could adjust the sample volume with the scheduled crew time. Such a volume adjustment enabled variable sample densities around the critical density as well as pressure steps (as distinct from the usual temperature steps) to be applied to the sample.

The French-built ALICE II facility was used for these experiments. It allows tightly thermostated (top photograph) samples (right photograph) to be controlled, viewed, and measured. Its diagnostics include interferometry, shadow graph, high-speed pressure measurements, and microscopy. Data were logged onto computer DAT tapes and PCMCIA cards and were returned to Earth only after the mission was over.

The near-critical boiling experiment worked well and produced different liquid-vapor interface dynamics than previous low-gravity results. This was due to the bubble locating with different thermal

boundary conditions for the two missions. The density fluctuation spectrum experiment did not perform well because of a hardware problem and the inability of Earth-based researchers to detect and interact with the hardware onboard Mir. The phase-separation experiments were the most successful. These required the greatest amount of data reduction, which is still in progress. The second 20 days of experiments that had been planned were cancelled when the U.S. support of Mir expired.

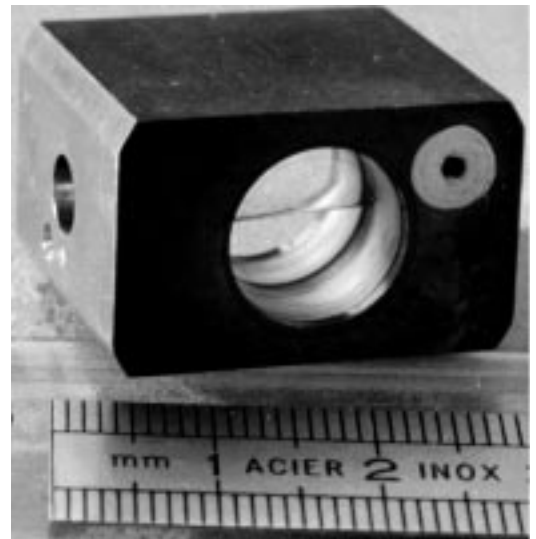
**Glenn contacts:**

Dr. R. Allen Wilkinson, (216) 433-2075, R.A.Wilkinson@grc.nasa.gov; and Monica I. Hoffmann, (216) 433-6765, Monica.I.Hoffmann@grc.nasa.gov

**Author:** Dr. R. Allen Wilkinson

**Headquarters program office:** OLMSA

**Programs/Projects:**  
Microgravity Science



*Typical copper-bodied cell with sapphire windows. It is filled with  $\text{SF}_6$  to roughly 38 atm and a density of  $0.73 \text{ g/cm}^3$ . The typical fluid volume was less than  $1 \text{ cm}^3$ .*

# Density Relaxation of Liquid-Vapor Critical Fluids Examined in Earth's Gravity

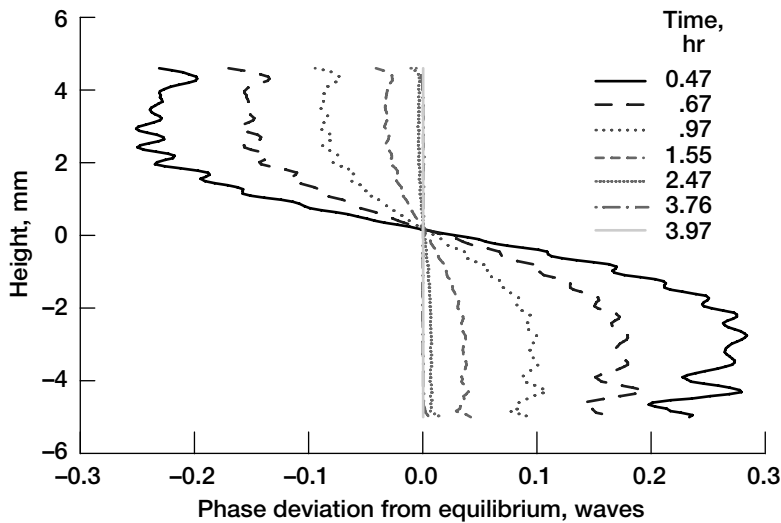
This work shows quantitatively the pronounced differences between the density equilibration of very compressible dense fluids in Earth's gravity and those in microgravity. The work was performed onsite at the NASA Glenn Research Center at Lewis Field and is complete. Full details are given in references 1 and 2.

Liquid-vapor critical fluids (e.g., water) at their critical temperature and pressure, are very compressible. They collapse under their own weight

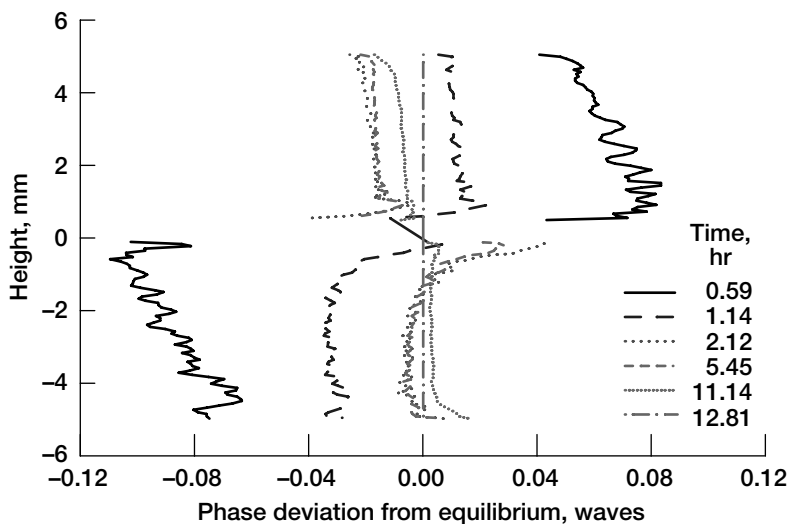
in Earth's gravity, allowing only a thin meniscus-like layer with the critical pressure to survive. This critical layer, however, greatly slows down the equilibration process of the entire sample. A complicating feature is the buoyancy-driven slow flows of layers of heavier and lighter fluid. This work highlights the incomplete understanding of the hydrodynamics involved in these fluids.

In low gravity, critical fluids equilibrate to a homogeneous density state by diffusion only. Density disturbances are very easy to induce in low gravity and are very very slow to relax away.

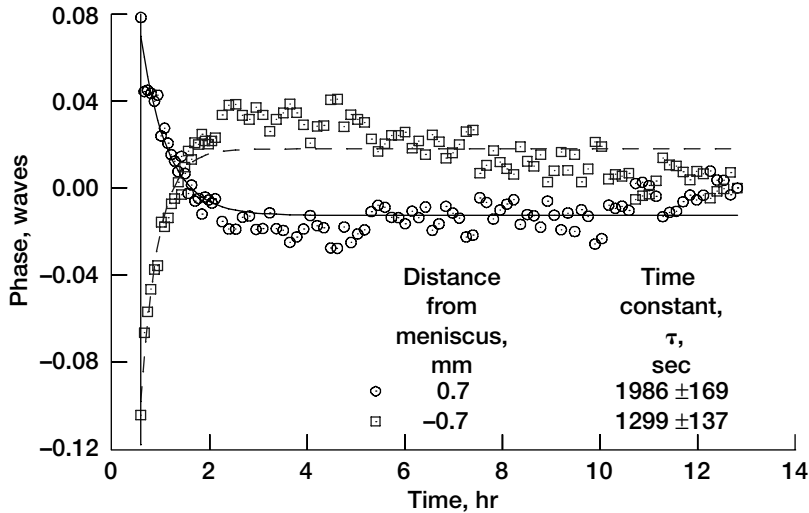
These experiments studied the density relaxation of a liquid-vapor critical fluid in Earth's gravity over a temperature regime of severe density stratification. A 10-mm-diameter, 1-mm-thick, disk-shaped sample of SF<sub>6</sub> was placed in a Twyman-Green phase-shifting interferometer with a phase uncertainty of 1/65 of a wavelength during a test period of over 60 hours. Relaxations to an equilibrium stratification were observed for a temperature range from 1.0 to 29.6 mK above the critical temperature  $T_c$ . The interferometry provided a density distribution history over the full extent of the sample cell. Two types of initial density states were established before stepping to the final temperature states for density relaxation: (1) the two-phase state at  $T_c - 50$  mK and (2) the equilibrium state at  $T_c + 100$  mK. Upper and lower portions of the cell relaxed differently for these two initial states. For the  $T_c + 100$  mK initial state, relaxation to  $T < T_c + 3$  mK showed an early density overshoot, followed by an additional long-time relaxation not



Height profiles of deviation from equilibrium with time for a run with an initial state of  $T_c - 50$  mK and a final state of  $T_c + 29.6$  mK. The earliest and latest times plotted reflect the time window when the thermostat was stable to  $\pm 50$   $\mu$ K. One wave (fringe) of phase deviation corresponds to a 0.35-percent density deviation.



Height profiles for a run with an initial state of  $T_c + 100$  mK and a final state of  $T_c + 2.8$  mK. Note the geometric time sequence of the plots. Ignore the traces in the height region  $\pm 0.5$  about 0 because the fringes were too closely packed for reliable analysis.



Relaxation at 0.7-mm above and below the meniscus for a run with an initial state at  $T_c + 100$  mK and a final state of  $T_c + 2.8$  mK. In low gravity, the time constant was  $5546 \pm 62$  sec at  $T_c + 3.4$  mK. The legend notes the fit exponential time constants and their fit uncertainties.

seen in the other relaxation sequences. Otherwise, relaxations were faster and increasingly non-diffusive (without a unique exponential description) as the final state drew closer to the critical temperature.

#### Reference

1. Wilkinson, R.A., et al.: Equilibration Near the Liquid-Vapor Critical Point in Microgravity. Phys. Rev. E, vol. 57, no. 1, 1998, p. 436.
2. Wilkinson, R.A.: Int. J. Thermophysics, vol. 19, no. 4, 1998.

#### Glenn contact:

Dr. R. Allen Wilkinson, (216) 433-2075, R.A.Wilkinson@grc.nasa.gov

**Author:** Dr. R. Allen Wilkinson

**Headquarters program office:** OLMSA

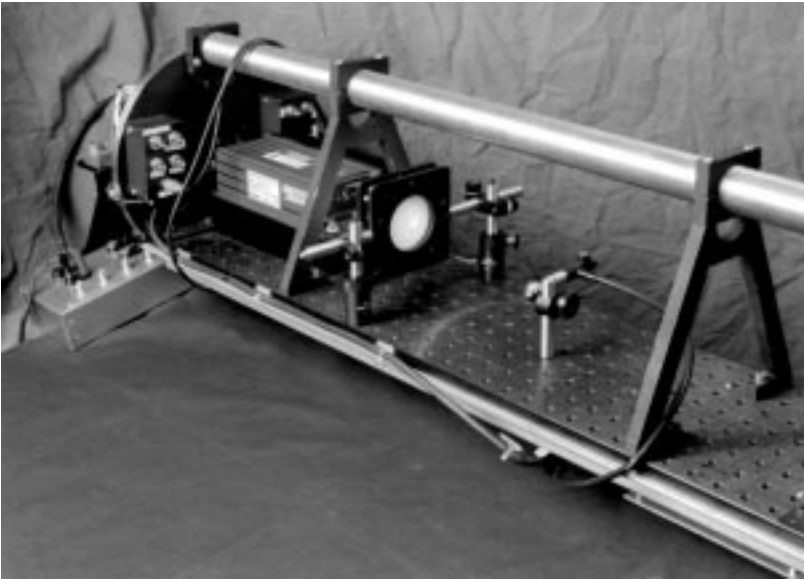
#### Programs/Projects:

Microgravity Science

## Diffusing Wave Spectroscopy Used to Study Foams

The white appearance of familiar objects—such as clouds, snow, milk, or foam—is due to the random scattering of light by the sample. As we all know, pure water is clear and easily passes a beam of light. However, tiny water droplets, such as those in a cloud, scatter light because the air and water droplet have different indexes of refraction. When many droplets, or scattering sites, are present, the incident light is scattered in random

directions and the sample takes on a milky white appearance. In a glass of milk, the scattering is due to small colloidal particles. The white appearance of shaving cream, or foam, is due to the scattering of light at the water-bubble interface.



DWS setup for studying foams on a rotating optical breadboard. A laser illuminates the foam sample, and the scattered light is fed to the detector by a fiber-optic cable.

Diffusing wave spectroscopy (DWS) is a laser light-scattering technique used to noninvasively probe the particle dynamics in systems that strongly scatter light. The technique takes advantage of the diffuse nature of light, which is reflected or transmitted from samples such as foams, dense colloidal suspensions (such as paint and milk), emulsions, liquid crystals, sandpiles, and even biological tissues.

In traditional dynamic light-scattering measurements, one measures the amount of time it takes for a particle in a suspension to move a distance comparable to

the wavelength of light  $\lambda$  ( $\sim 0.5 \mu\text{m}$ ), such as the diffusion of colloidal particles in a solution. Or one might measure the lifetime of a density fluctuation such as those that occur in fluids near the liquid-vapor critical point. In these applications, the samples should be only weakly scattering (single-scattering) for a proper interpretation of the data. DWS extends the type of systems that can be studied by exploring systems that scatter light many, many times.

When incident light is scattered many times and in random directions, the light is said to diffuse through the sample. By using the diffuse approximation, one is able to accurately interpret the small intensity fluctuations that result from particle motion in the sample. Furthermore, because the light is scattered many times, the DWS technique is very sensitive to much smaller motions in the sample. For example, if the light is scattered 100 times (on average) before it reaches the detector, average displacements as small as  $\lambda/100$  ( $\sim 5 \text{ nm}$ ) can be detected. Thus, DWS is a powerful technique for probing motion on a molecular scale.

The NASA Glenn Research Center at Lewis Field and the University of California, Los Angeles, are using DWS to study aqueous foams. Foams are a dynamic system since they evolve with time. By using DWS in conjunction with rheology measurements, the Foam Optics and Mechanics (FOAM) flight project team expects to discover how the bubble-scale motion and

structure of the foam affects its bulk rheological properties. Because these experiments will be conducted in microgravity, liquid will not drain from the foam, and we will be able to investigate the "melting transition" from dry, solidlike foams (shaving cream) to wet, liquidlike foams (bubbly water).

**National Center for Microgravity**

**Research contact:** Dr. Gregory A. Zimmerli, (216) 433-6577, Gregory.A.Zimmerli@grc.nasa.gov

**Glenn contact:**

Angela R. Becker, (216) 433-5750, Angela.R.Becker@grc.nasa.gov

**Authors:** Dr. Gregory A. Zimmerli and Professor Douglas J. Durian

**Headquarters program office:** OLMSA

**Programs/Projects:**

Microgravity Science

## Concept Defined for the International Space Station's Fluids and Combustion Facility

The Fluids and Combustion Facility (FCF) will occupy three powered racks and one stowage rack on the International Space Station (ISS). It will be a permanent modular, multiuser facility to accommodate microgravity science experiments onboard the ISS's U.S. Laboratory Module. FCF will support NASA Human Exploration and Development of Space program objectives requiring sustained, systematic research in the disciplines of fluid physics and combustion science. The two disciplines share racks and mutually necessary hardware within FCF to dramatically reduce costs and effectively use ISS resources. Even with the cost of FCF development included, experimentation using FCF on the space station will cost only half of what it did on the space shuttles.

Fluid physics processes are ubiquitous. Because the human body is composed predominantly of fluids, creating new drugs and treating disease frequently depend on fluid physics. Numerous high-value commercial processes, such as petroleum production and semiconductor production, rely on fluid physics. Unfortunately, many definitive fluid physics experiments cannot be conducted on Earth because gravitational buoyancy and settling effects interfere. Moreover, many other experiments conducted on ISS require the knowledge of microgravity fluid physics to interpret the results. Microgravity fluid physics experiments in FCF should result in the following benefits:

- Advances in public medicine and treatment of disease
- Improved commercial processes and competitiveness in a wide range of U.S. industries
- Greater success in applying the results of other experiments conducted on ISS to benefit the public

Combustion processes are also ubiquitous. We use combustion to heat our homes, power our cars, manufacture our products, and more. Combustion figures into fire safety; environmental issues, such as acid rain; health issues, such as lung disease; and more. Combustion costs U.S. taxpayers \$400 billion a year. If we knew more about combustion, we could lower that cost while improving health

and safety. Unfortunately, some definitive combustion science experiments cannot be conducted on Earth because gravitational convection interferes. Microgravity combustion experiments in FCF should result in the following benefits:

- Billions of dollars in energy costs saved every year
- U.S. commercial processes and competitiveness improved
- Incidence of fire and other public health hazards reduced
- Environmental pollution lessened

FCF has been at the forefront of new technical approaches. First, FCF pioneered the concept of low-cost, incremental development and deployment of ISS facilities—one rack at a time. This paradigm is now standard for new ISS multirack facilities. Second, FCF invented the Embedded Web Software Technology (EWT) that won the NASA Software of the Year award in 1998. This software is now recommended for all ISS facilities and has spawned commercial products that may lead to a billion-dollar-a-year industry. Third, FCF developed a practical hybrid-power switch that is now on the commercial market and is being considered for use throughout the aerospace industry (in aircraft, in satellites, and in other ISS applications).

The NASA Glenn Research Center at Lewis Field is developing FCF in partnership with local contractors. Technical feasibility has been demonstrated, the concept has been defined, and an engineering model of the first rack is nearing completion. The first rack and initial experiments will be launched in 2003. Over 100 fluids and combustion experiments are planned during the life of the ISS.

**Glenn contacts:**

Thomas H. StOnge, (216) 433-3557, Thomas.H.StOnge@grc.nasa.gov; and Robert L. Zurawski, (216) 433-3932, Robert.L.Zurawski@grc.nasa.gov

**Author:** Edward A. Winsa

**Headquarters program office:** OLMSA

**Programs/Projects:**

HEDS, Microgravity Science

## Hubble Space Telescope Program on STS-95 Supported by Space Acceleration Measurement System for Free Flyers

John Glenn's historic return to space was a primary focus of the STS-95 space shuttle mission; however, the 83 science payloads aboard were the focus of the flight activities. One of the payloads, the Hubble Space Telescope Orbital System Test (HOST), was flown in the cargo bay by the NASA Goddard Space Flight Center. It served as a space flight test of upgrade components for the telescope before they are installed in the shuttle for the next Hubble Space Telescope servicing mission. One of the upgrade components is a cryogenic cooling system for the Near Infrared Camera and Multi-Object Spectrometer (NICMOS). The cooling is required for low noise in the receiver's sensitive electronic instrumentation. Originally, a passive system using dry ice cooled NICMOS, but the ice leaked away and must be replaced. The active cryogenic cooler can provide the cold temperatures required for the NICMOS, but there was a concern that it would create vibrations that would affect the fine pointing accuracy of the Hubble platform.

The Microgravity Science Division of the NASA Glenn Research Center at Lewis Field was contacted to supply an acceleration measurement system to characterize the vibrations of the cooler. These measurement systems have traditionally supported microgravity payloads flown by Glenn. The acceleration data is provided to the experimenters so that they can evaluate the influence of the microgravity environment on their experiments. Researchers in the fluids, combustion, materials, and life science disciplines all conduct experiments in the microgravity environment of space to enhance the understanding of fundamental physical phenomena. However,

events such as spacecraft maneuvers, equipment operations, atmospheric drag, and crew movement on manned flights can disturb experiments.

The system chosen to meet the HOST requirements was the Space Acceleration Measurement System for Free Flyers (SAMS-FF). SAMS-FF is a compact, low-power system that offers high-resolution acceleration measurements and a flexible, modular system for easy adaptation to a variety of spacecraft. It also complements SAMS-II, which is being designed and developed for the International Space Station. SAMS-FF has the heritage of the original SAMS, which flew on the shuttle 20 times and on the Russian space station Mir. The system had an initial test flight of a sounding rocket in 1997 and also flew on NASA's KC-135 reduced-gravity aircraft.



*HOST payload with SAMS-FF ready for integration on the space shuttle for STS-95. The SAMS-FF control and data acquisition unit can be seen in the lower left corner.*

The SAMS-FF system flown on this flight as part of the HOST payload consisted of a control and data acquisition unit (CDU) and two triaxial sensor heads (TSH's). The CDU is a rugged PC/104-based embedded computer system, which is physically small with a modular construction. The CDU controls the flow of data from the sensors, stores data, and has ports for control and external interfaces. A real-time operating system from QNX Software Systems Ltd. was used. This version of the CDU used a Flash memory card, which has no moving parts. Power converters and filters were located in the base of the unit, supplying power to the PC/104 stack and the sensors. This system was similar to the system flown on the previous flights, except for the addition of a hermetic housing to seal the unit in dry nitrogen for protection from the vacuum of space in the shuttle's cargo bay.

The TSH consists of three AlliedSignal QA3000 accelerometers mounted orthogonally on a small housing, a 3-in. cube. The TSH contains signal conditioning and conversion circuits for processing the analog acceleration signal from the accelerometer into digital data. One 24-bit delta-sigma analog-to-digital converter is used for each accelerometer's signal. This design provides sufficient resolution to measure the small microgravity ( $<1 \times 10^{-6}$ ) acceleration forces. The TSH's were configured at a bandwidth of approximately 100 Hz to capture specific resonant frequencies in the Hubble Space Telescope's optical system. The digitized signals were processed by a microcontroller and sent back to the CDU through a serial

interface. The TSH was adapted for this flight similarly to the CDU, with a hermetic housing.

Testing conducted for the mission consisted of TSH characterization, environmental testing, and integration testing. The TSH characterization tests plotted the filter response and the noise floor. The environmental testing consisted of traditional thermal and vibration testing to test workmanship and screen infant mortality.<sup>1</sup> After the system was delivered, it was tested with the HOST payload for both proper system operation and integrated payload screening.

The HOST payload controlled the operation of the system during flight, through a discrete interface. This type of interface was chosen to allow independent development and verification of the two systems. Once power was applied to the system and the CDU was booted, controllers from the ground could command the system to record data and could observe the operating status of the system. HOST conducted a series of data sessions, each approximately 255 sec long. These data sessions corresponded to various operating cycles of the HOST cryocooler. Several discrete interface lines served as counters of the recording sessions completed to ensure that the data storage was optimally utilized.

A total of 43 measurement sessions were conducted during the HOST mission. The data gathered from each of these sessions were complete and anomaly free. They were analyzed by the Principal Investigator Microgravity Services group and then provided to the HOST team. Data gathered by SAMS-FF on STS-95 have been invaluable in determining how the

---

<sup>1</sup>Stress test it to remove early failures.



*SAMS-FF control and data acquisition unit mounted on the HOST payload.*

cryocooler may affect the precise alignment capabilities of the Hubble Space Telescope. They indicate that the vibration is not a problem, and the decision was made to install the cryocooler on the Hubble during the third servicing mission.

## Physics of Hard Spheres Experiment: Significant and Quantitative Findings Made

Direct examination of atomic interactions is difficult. One powerful approach to visualizing atomic interactions is to study near-index-matched colloidal dispersions of microscopic plastic spheres, which can be probed by visible light. Such spheres interact through hydrodynamic and Brownian forces, but they feel no direct force before an infinite repulsion at contact. Through the microgravity flight of the Physics of Hard Spheres Experiment (PHaSE), researchers have sought a more complete understanding of the entropically driven disorder-order transition in hard-sphere colloidal dispersions. The experiment was conceived by Professors Paul M. Chaikin and William B. Russel of Princeton University. Microgravity was required because, on Earth, index-matched colloidal dispersions often cannot be density matched, resulting in significant settling over the crystallization period. This settling makes them a poor model of the equilibrium atomic system, where the effect of gravity is truly negligible.

For this purpose, a customized light-scattering instrument was designed, built, and flown by the NASA Glenn Research Center at Lewis Field on the space shuttle (shuttle missions STS-83 and STS-94). This instrument performed both static and dynamic light scattering, with sample oscillation for determining rheological properties. Scattered light from a 532-nm laser was recorded either by a 10-bit charge-coupled discharge (CCD) camera

**For more information, visit us on the World Wide Web:**

<http://www.grc.nasa.gov/WWW/MMAP/SAMSFF/samsff.html>

**Glenn contact:**

Ronald J. Sicker, (216) 433-6498,  
Ronald.J.Sicker@grc.nasa.gov

**Dynacs Engineering Company, Inc., contact:**

Thomas J. Kacpura, (216) 977-1057,  
Thomas.J.Kacpura@grc.nasa.gov

**Author:** Thomas J. Kacpura

**Headquarters program office:**

OLMSA (MRPO)

**Programs/Projects:**

Microgravity Science, HST, SAMS-FF

from a concentric screen covering angles of 0° to 60° or by sensitive avalanche photodiode detectors, which convert the photons into binary data from which two correlators compute autocorrelation functions. The sample cell was driven by a direct-current servomotor to allow sinusoidal oscillation for the measurement of rheological properties.

Significant microgravity research findings include the observation of beautiful dendritic crystals, the crystallization of a "glassy phase" sample in microgravity that did not crystallize for over 1 year in 1g (Earth's gravity), and the emergence of face-centered-cubic (FCC) crystals late in the coarsening



*PHaSE hardware: an interior view of the test section without walls.*

process (as small crystallites lost particles to the slow ripening of large crystallites).

Significant quantitative findings from the microgravity experiments have been developed describing complex interactions among crystallites during the growth process, as concentration fields overlap in the surrounding disordered phase. Time-resolved Bragg scattering under microgravity captures one effect of these interactions quite conclusively for the sample at a volume fraction of 0.528. From the earliest time until the sample is almost fully crystalline, the size and overall crystallinity grow monotonically, but the number of crystallites per unit volume (number density) falls. Apparently nucleation is slower than the loss of crystallites because of the transfer of particles from small to large crystals. Thus, coarsening occurs simultaneously with growth, rather than following the completion of nucleation and growth as is generally assumed. In the same sample, an interesting signature appears in the apparent number density of crystallites and the volume fraction within the crystallites shortly before full crystallinity is reached. A brief upturn in both indicates the creation of more domains of the size of the average crystallite simultaneous with the compression of the crystallites. Only the emergence of dendritic arms offers a reasonable explanation. The arms would be "seen" by the light scattering as separate domains whose smaller radii of curvature would compress the interior phase.

In fiscal year 1999, numerous papers, a doctoral dissertation, and the PHaSE final report were produced. Although this flight project has been completed, plans are in place for a follow-on colloid experiment by Chaikin and Russel that employs a light microscope within Glenn's Fluids and Combustion Facility on the International Space Station.

PHaSE is providing us with a deeper understanding of the nature of phase transitions. The knowledge derived has added to the understanding of condensed matter. In addition, the burgeoning study of the dynamics of colloidal self-assembly may lead to the development of a range of photonic materials that control the desirable properties of light. Thus, applications of ordered colloidal structures include not only ultrastructure ceramics, but also photonic crystals and photothermal nanosecond light-switching devices. Industries dealing with semiconductors, electro-optics, ceramics, and composites stand to benefit from such advancements.

**Find out more about this research on the World Wide Web:**

<http://zeta.grc.nasa.gov/phase/>

**Glenn contact:**

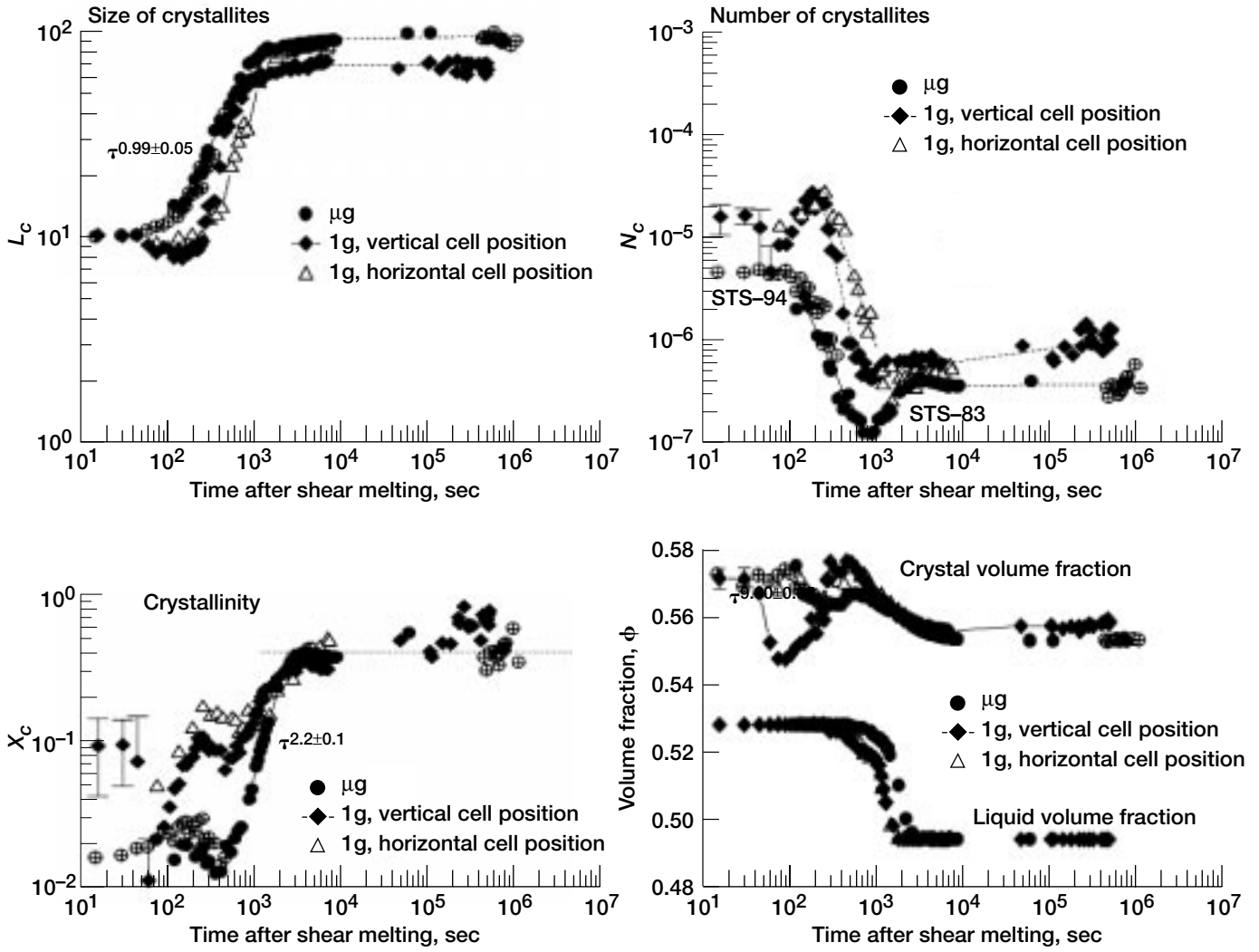
Michael P. Doherty, (216) 433-6641,  
Michael.P.Doherty@grc.nasa.gov

**Author:** Michael P. Doherty

**Headquarters program office:** OLMSA

**Programs/Projects:**

Microgravity Science



Crystallization kinetics of sample 3; volume fraction, 0.528 (where  $\tau$ , time;  $L_c$ , average crystallite size (in particle diameters),  $X_c$ , crystalline fraction, and  $N_c$ , number density).

# Colloidal Gelation-2 and Colloidal Disorder-Order Transition-2 Investigations Conducted on STS-95



*Astronauts Chiaki Mukai and Pedro Duque prepare to take photographs of the colloidal crystals on top of the glovebox during STS-95 ground training.*

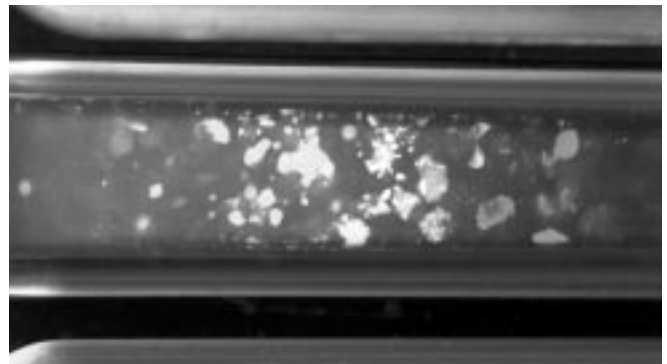
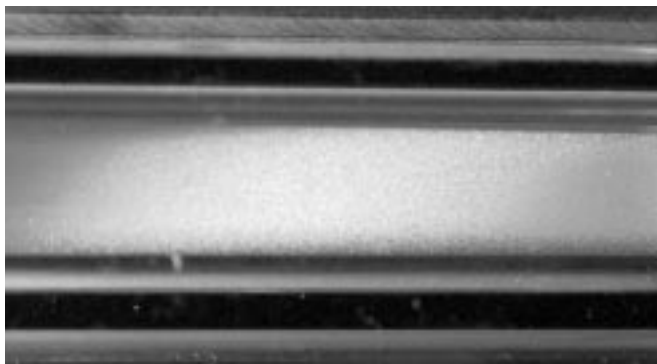
The Colloidal Gelation-2 (CGEL-2) and Colloidal Disorder-Order Transition-2 (CDOT-2) investigations flew on Space Shuttle Discovery mission STS-95 (also known as the John Glenn Mission). These investigations were part of a series of colloid experiments designed to help scientists answer fundamental science questions and reduce the trial and error involved in developing new and better materials. Industries dealing with semiconductors, electro-optics, ceramics, and composites are just a few that may benefit from this knowledge.

The goal of the CGEL-2 investigation was to study the fundamental properties of colloids to help scientists better understand their nature and make them more useful for technology. Colloids consist of very small (submicron) particles suspended in a fluid. They play a critical role in the tech-

nology of this country, finding uses in materials ranging from paints and coatings to drugs, cosmetics, food, and drink. Although these products are routinely produced and used, there are still many aspects of their behavior about which scientists know little. Understanding their structures may allow scientists to manipulate the physical properties of colloids (a process called "colloidal engineering") to produce new materials and products. Colloid research may even improve the processing of known products to enhance their desirable properties.

The CGEL-2 investigation was designed to advance colloid research through the study of three kinds of colloid systems:

- (1) Binary colloidal alloys, which are suspensions of particles of two different sizes
- (2) Colloid polymer solutions, which form gels or glasslike materials
- (3) Fractal colloid aggregates, which are colloids that have repeating structural patterns and networks



*These CGEL-2 samples taken during STS-95 show binary colloidal suspensions that have formed ordered crystalline structures in microgravity. Left: There are more particles; therefore, many, many crystallites (small crystals) form. Right: There are fewer particles; therefore, the particles are far apart, and fewer, much larger crystallites form.*

The STS-95 CGEL-2 investigation revealed that the gels formed from the colloid polymer solutions, which tend to last only a few minutes on Earth, are stable over long periods of time in microgravity. The delicate fractal colloid aggregates grow much larger without the destructive pull of gravity. The binary colloidal alloy samples studied exhibited similar growth rates on Earth and in space. The STS-95 studies brought invaluable new information that can be applied to future colloidal materials synthesis.

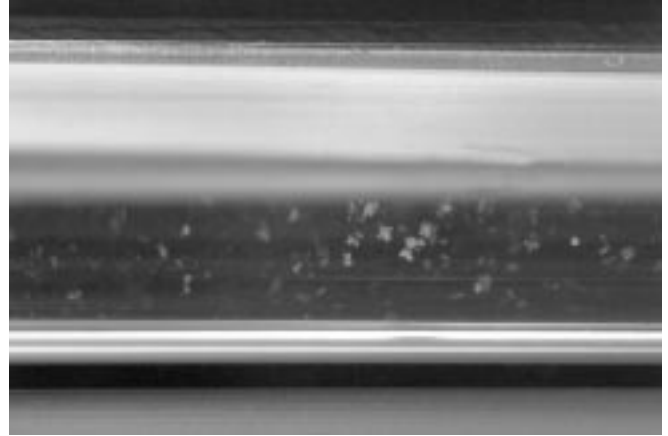
The CDOT-2 investigation also focused on the study of colloidal systems, but for different reasons. CDOT-2 used colloidal suspensions of microscopic solid plastic spheres as a model of atomic interactions. A colloidal suspension containing particles of very uniformly sized spheres that cannot penetrate each other (hard spheres) shares a fundamental characteristic with atomic systems. Under the proper conditions, both undergo a transition from a disordered liquid state to an ordered solid state, such as when water molecules become ordered to form ice.

During the STS-95 CDOT-2 investigation, dendrites were observed for a sample with a volume fraction (volume of particles per container volume) between 0.494 and 0.545. On Earth, these butterflylike structures settle to the bottom of the container and the “wings” shear off. The observation of these dendrites reveals important information about the nucleation and growth of crystals.

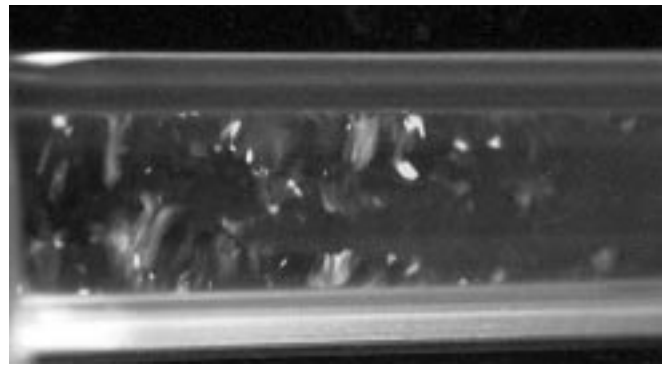
The STS-95 CDOT-2 investigation also revealed that crystallization can occur in samples that have a volume fraction larger than the formerly reported glass transition of 0.58. This has great implications for theories of the structural glass transition. These glassy samples never crystallized on Earth, but once grown in space, the crystals were strong enough to survive shuttle reentry and landing.

The CGEL-2/CDOT-2 investigations used the same experiment hardware that had been used on Earth to observe colloidal systems in orbit around the Earth, where the force of gravity is about a million times less than at the Earth’s surface (microgravity). In this reduced-gravity environment, astronauts were able to test current theories that model atomic interactions as hard sphere systems and to study the properties of colloidal structures without the problems of sedimentation and convection obscuring the true nature of the colloidal system.

Professors Paul M. Chaikin and William B. Russel of Princeton University are the principle investigators for the CDOT-2 investigation, and Professors David A. Weitz from the University of Pennsylvania and Peter N. Pusey from



*The snowflake-like crystallites, or dendrites, clustered in the center of this CDOT-2 sample taken during STS-95 have never been seen in such samples on Earth. Similar structures were seen for the first time in the CDOT experiment on STS-73. This experiment showed that dendritic growth occurs in samples with even more particles (i.e., higher volume fractions) than in those that flew on STS-73.*



*This CDOT-2 sample, which flew on STS-95, contains so many colloidal particles that it behaves like a glass. In the laboratory on Earth, the sample remained in an amorphous state, showing no sign of crystal growth. In microgravity, the sample crystallized in 3 days, as did the other glassy colloidal samples examined during the CDOT-2 experiment.*

the University of Edinburgh, Scotland, are the principal investigators for CGEL-2. The experiment hardware was designed, built, and tested at the NASA Glenn Research Center at Lewis Field with participation from Aerospace Design and Fabrication, Inc., the National Center for Microgravity Research, NYMA, Inc., the Ohio Aerospace Institute, and Princeton University.



*CGEL-2/CDOT-2 experiment hardware that flew on STS-95.*

**Glenn contacts:**

Monica I. Hoffmann, (216) 433-6765, [Monica.I.Hoffmann@grc.nasa.gov](mailto:Monica.I.Hoffmann@grc.nasa.gov);  
William V. Meyer, (216) 433-5011, [William.V.Meyer@grc.nasa.gov](mailto:William.V.Meyer@grc.nasa.gov); and  
Dr. Rafat R. Ansari, (216) 433-5008, [Rafat.R.Ansari@grc.nasa.gov](mailto:Rafat.R.Ansari@grc.nasa.gov)

**Author:** Monica I. Hoffmann

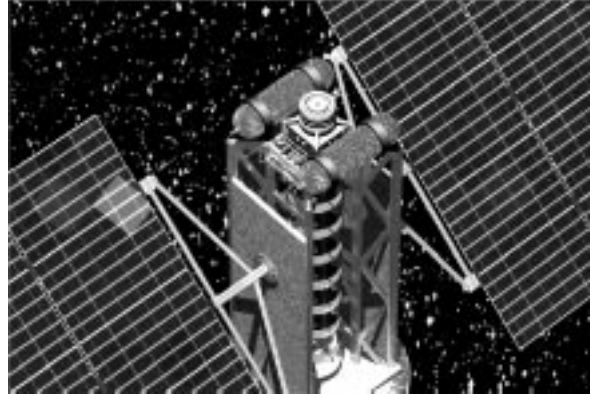
**Headquarters program office:** OLMSA (MRD)

**Programs/Projects:** Microgravity Science, Fluid Physics

# Power and Propulsion

## Power System Options Evaluated for the Radiation and Technology Demonstration Mission

The Radiation and Technology Demonstration (RTD) Mission is under joint study by three NASA Centers: the NASA Johnson Space Center, the NASA Goddard Space Flight Center, and the NASA Glenn Research Center at Lewis Field. This Earth-orbiting mission, which may launch on a space shuttle in the first half of the next decade, has the primary objective of demonstrating high-power electric thruster technologies. Secondary objectives include better characterization of Earth's Van Allen trapped-radiation belts, measurement of the effectiveness of the radiation shielding for human protection, measurement of radiation effects on advanced solar cells, and demonstration of radiation-tolerant microelectronics.



*Radiation and Technology Demonstration spacecraft.*

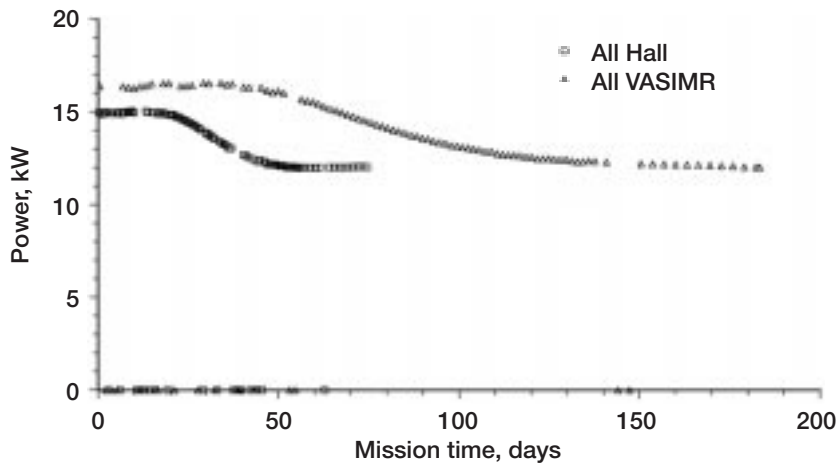
During the mission, which may continue up to 1 year, the 2000-kg RTD spacecraft will first spiral outward from the shuttle-deployed, medium-inclination, low Earth orbit. By the phased operation of a 10-kW Hall thruster and a 10-kW Variable Specific Impulse Magneto-Plasma Rocket, the RTD spacecraft will reach a low-inclination Earth orbit with a radius greater than five Earth radii. This will be followed by an inward spiraling orbit phase when the spacecraft deploys 8 to 12 microsattellites to map the Van Allen belts. The mission will conclude in low Earth orbit with the possible retrieval of the spacecraft by the space shuttle.

The preceding figure illustrates a conceptual RTD spacecraft design showing two photovoltaic (PV) array wings, the Hall thruster with propellant tanks, and stowed microsattellites. Early power system studies assessed five different PV array design options coupled with a 120-Vdc power management and distribution system (PMAD) and secondary lithium battery energy storage. Array options include (1) state-of-the-art 10-percent efficient three-junction amorphous SiGe thin-film cells on thin polymer panels deployed with an inflatable (or articulated) truss, (2) SCARLET array panels, (3) commercial state-of-the-art, planar PV array rigid panels with 25-percent efficient, three-junction GaInP<sub>2</sub>/GaAs/Ge solar cells, (4) rigid panels with 25-percent efficient, three-junction GaInP<sub>2</sub>/GaAs/Ge solar cells, in a 2x-concentrator trough configuration, and (5) thin polymer panels with 25-percent efficient, three-junction GaInP<sub>2</sub>/GaAs/Ge solar cells deployed with an inflatable (or articulated) truss.

To assess the relative merits of these PV array design options, the study group developed a dedicated Fortran code to predict power system performance and estimate system mass. This code also modeled Earth orbital environments important for accurately predicting PV array performance. The most important environmental effect, solar cell radiation degradation, was calculated from electron-proton fluence input from the industry standard AE8/AP8 trapped radiation models and the concept of damage equivalence (ref. 1). Power systems were sized to provide 10 kW of

thruster power and approximately 1 kW of spacecraft power at end of life. Of the five PV array design options, the option 1 (thin-film cells) power system was the most massive—590 kg, whereas the option 4 (trough concentrator) power system was the lightest—260 kg. Arguably, the lowest cost would come from the option 3 (commercial array panels) power system with an acceptable, albeit greater, system mass of 320 kg.

Predicted power system performance during the spiral-out mission phase is shown the following graph for the option 5 (flexible-panel) array. From the results, the radiation-induced power loss over time is evident as the spacecraft slowly spirals outward through the trapped proton belt. The importance of the spiral trip time is also evident in the two curves representing 74-day and 182-day spiral-out periods. The longer spiral time introduces a beginning-of-life power oversizing penalty greater than 1 kW. Future studies will analyze power system performance



Power to thruster and spacecraft for RTD mission.

and mass with a 50-Vdc power management and distribution architecture favorable to the VASIMR thruster and longer missions.

## Solar Power System Evaluated for the Human Exploration of Mars

The electric power system is a crucial element of any mission for the human exploration of the Martian surface. The bulk of the power generated will be delivered to crew life-support systems, extravehicular activity suits, robotic vehicles, and predeployed in situ resource utilization (ISRU) equipment. In one mission scenario, before the crew departs for Mars, the ISRU plant operates for 435 days producing liquefied methane and oxygen for ascent-stage propellants and water for crew life support. About 200 days after ISRU production is completed, the crew arrives for a 500-day surface stay. In this scenario, the power system must operate for a total of 1130 days (equivalent to 1100 Martian "sols"), providing 400 MW-hr of

### Reference

1. Anspaugh, B.E.: GaAs Solar Cell Radiation Handbook. NASA CR-203421, 1996.

### Glenn contact:

Thomas W. Kerslake, (216) 433-5373, Thomas.W.Kerslake@grc.nasa.gov

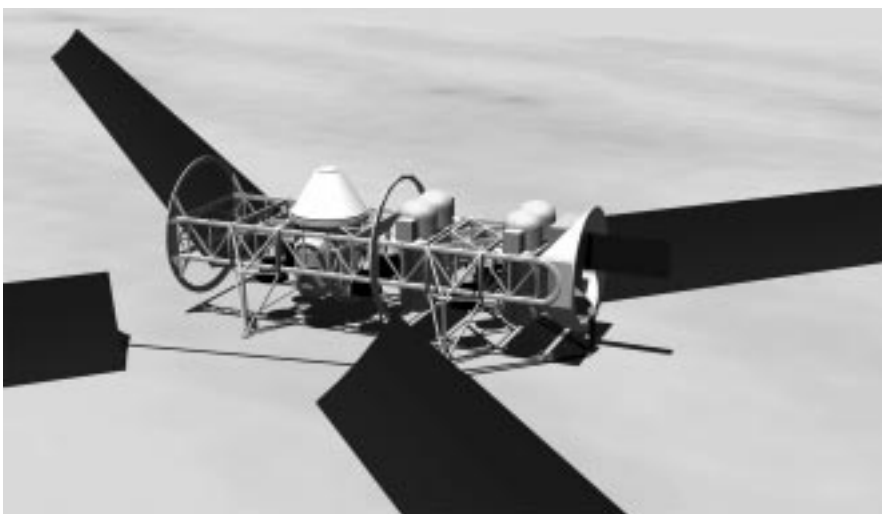
**Authors:** Thomas W. Kerslake and Scott W. Benson

**Headquarters program office:** OSF

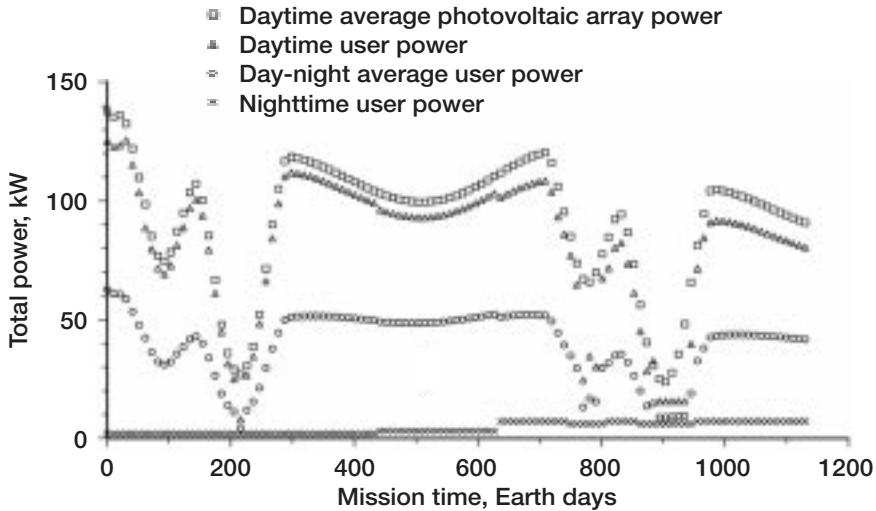
**Programs/Projects:** HEDS

energy to the ISRU plant and up to 18 kW of daytime user power.

A photovoltaic power-generation system with regenerative fuel cell (RFC) energy storage has been under study at the NASA Glenn Research Center at Lewis Field (ref. 1). The conceptual power system (shown in the illustration) is dominated by the 4000-m<sup>2</sup> class photovoltaic array that is deployed orthogonally as four tent structures, each approximately 5 m on a side and 100-m long. The structures are composed of composite members deployed by an articulating mast, an inflatable boom, or rover vehicles, and are subsequently anchored to the ground. Array panels consist of thin polymer membranes with thin-film solar cells. The array is divided into eight independent electrical sections with solar cell strings operating at 600 V. Energy storage is provided by regenerative fuel cells based on hydrogen-oxygen proton exchange



Mars surface photovoltaic-regenerative fuel cell power system.



*Mission power profile.*

membrane technology. Hydrogen and oxygen reactants are stored in gaseous form at 3000 psi, and the water produced is stored at 14.7 psi. The fuel cell operating temperature is maintained by a 40-m<sup>2</sup> deployable pumped-fluid loop radiator that uses water as the working fluid. The power management and distribution (PMAD) architecture features eight independent, regulated 600-Vdc channels. Power management and distribution power cables use various gauges of copper conductors with ethylene tetrafluoroethylene insulation.

To assess power system design options and sizing, we developed a dedicated Fortran code to predict detailed power system performance and estimate system mass. This code also modeled the requisite Mars surface environments: solar insolation, Sun angles, dust storms, dust deposition, and thermal and ultraviolet radiation. Using this code, trade studies were performed to assess performance and mass sensitivities to power system design parameters (photovoltaic array geometry and orientation) and mission parameters (landing date and landing site latitude, terrain slope, and dust storm activity).

Mission analysis cases were also run. Power results are shown in the preceding graph for an analysis case with a September 1, 2012, landing date; 18.95° North latitude landing site; two seasonal dust storms; and tent arrays. To meet user load requirements and the ISRU energy requirement, an 8-metric ton (MT) power system and 4000-m<sup>2</sup> photovoltaic array area were required for the assumed advanced CuInS<sub>2</sub> thin-film solar cell technology. In this figure, the top curve is the average daytime photovoltaic

array power, the middle curve is average daytime user load power, and the bottom curve is nighttime power. At mission day 1, daytime user power exceeds 120 kW before falling off to 80 kW at the end of the mission. Throughout the mission, nighttime user power is set to the nighttime power requirement. In this analysis, "nighttime" is defined as the 13- to 15-hr period when array power output is below the daytime power requirement. During dust storms, power system capability falls off dramatically so that by mission day 900, a daily energy balance cannot be maintained. Under these conditions, the ISRU plant is placed in standby mode, and the regenerative fuel cell energy storage is gradually discharged to meet user loads.

#### Reference

1. Kerslake, T.W.; and Kohout, L.L.: Solar Electric Power System Analyses for Mars Surface Missions. 34th Inter-society Energy Conversion Engineering Conference, SAE Paper 99-01-2482 (NASA/TM-1999-209288), 1999. (Available online: <http://gltrs.grc.nasa.gov/cgi-bin/GLTRS/browse.pl?1999/TM-1999-209288.html>)

#### Glenn contact:

Thomas W. Kerslake, (216) 433-5373,  
Thomas.W.Kerslake@grc.nasa.gov

**Author:** Thomas W. Kerslake

**Headquarters program office:** OSF

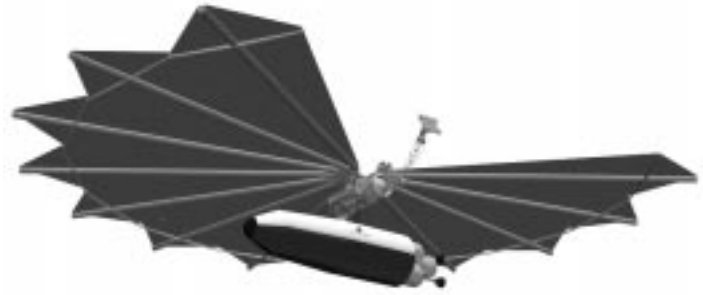
**Programs/Projects:** HEDS

# Power Systems Evaluated for Solar Electric Propulsion Vehicles

Solar electric propulsion (SEP) mission architectures are applicable to a wide range of NASA missions including the robotic exploration of the outer planets in the next decade and the human exploration of Mars (ref. 1) within the next 2 decades. SEP enables architectures that are very mass efficient with reasonable power levels (1-MW class) when aerobrake and cryogenic upper-stage transportation technologies are utilized. In this architecture, the efficient SEP stage transfers the payload from low Earth orbit (LEO) to a High Energy Elliptical Parking Orbit (HEEPO) within a period of 6 to 12 months. A high-thrust, cryogenic upper stage and payload then separate from the SEP vehicle for injection to the planetary target, allowing for fast heliocentric trip times. This mission architecture offers a potential reduction in mass to LEO in comparison to alternative all-chemical or nuclear propulsion schemes. Mass reductions may allow launch vehicle downsizing and enable missions that would have been grounded because of cost constraints.

This figure illustrates a conceptual SEP stage design for a human Mars mission (ref. 2). Researchers at the NASA Glenn Research Center at Lewis Field designed the conceptual SEP vehicle, conceived the mission architecture to use this vehicle, and analyzed the vehicle's performance. This SEP stage has a dry mass of 35 metric tons (MT), 40 MT of xenon propellant, and a photovoltaic array that spans 110 m, providing power to a cluster of eight 100-kW Hall thrusters. The stage can transfer an 80-MT payload and upper stage to the desired HEEPO. Preliminary packaging studies show that this space-station-class SEP vehicle meets the proposed "Magnum" launch vehicle mass and volume requirements with considerable margin. An SEP vehicle for outer planetary missions, such as the Europa Mapper Mission, would be dramatically smaller than a human Mars mission SEP stage. In this mission architecture, the SEP power system injects with the payload to provide spacecraft power throughout the mission.

Several photovoltaic array design concepts were considered for the SEP vehicle power system for the human mission to Mars. These include a space station derivative, a SCARLET (Solar Concentrator Arrays with Refractive Linear Element Technology) array derivative, and a hybrid inflatable-deployable thin polymer membrane array with thin-film solar cells (as shown in the concept illustration). This concept is based on a design developed for the Next Generation Space Telescope Sun shield. The array is divided into 16 independent electrical sections with 500-V, negative-grounded solar cell strings. The power system employs a channelized, 500-Vdc power management and distribution (PMAD) architecture with lithium ion batteries for energy storage for vehicle and payload secondary loads (the high-power Hall thrusters do not operate in eclipse periods). The 500-V PMAD voltage permits "direct-drive" thruster operation, greatly reducing the power processing unit size, complexity, and power loss.

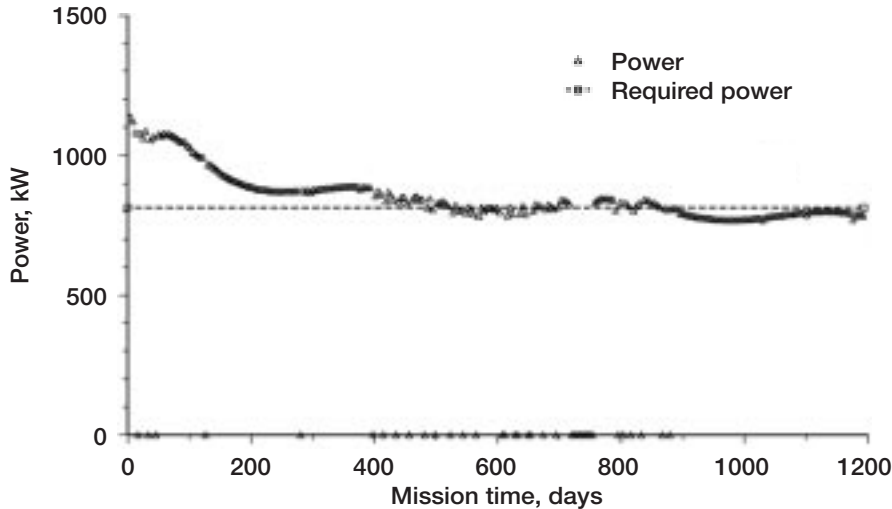


*Solar electric propulsion stage for a human mission to Mars.*

Similar power system architecture, designs, and technology are assumed for the Europa Mapper Mission SEP vehicle. The primary exceptions are that the photovoltaic array is assumed to consist of two rectangular wings and that the power system rating is 15 kW in Earth orbit and 200 W at Europa.

To size the SEP vehicle power system, a dedicated Fortran code was developed to predict detailed power system performance, mass, and thermal control requirements (ref. 2). This code also modeled all the relevant Earth orbit environments; that is, the particulate radiation, plasma, meteoroids and debris, ultraviolet radiation, contamination, and thermal conditions. Analysis results for the Human Mars Mission SEP vehicle show a power system mass of 9-MT and photovoltaic array area of 5800-m<sup>2</sup> for the thin-membrane design concept with CuInS<sub>2</sub> thin-film cells.

Power processing unit input power for a thin-membrane array design with three-junction, amorphous SiGe solar cells is shown in the graph. Power falls off rapidly in the first weeks of the mission because of light-induced (Staebler-Wronski) solar cell losses. During the next



Power to Hall thruster power processing units.

200 days, power decreases steadily as the SEP stage spirals through the proton belts and sustains the bulk of the mission radiation damage. Once the vehicle apogee is above approximately four Earth radii, little additional degradation is incurred. From 400 to 800 days, a 1100-km “parking” orbit is maintained to await the next payload transfer opportunity. This orbit is below the main proton belt, and thus, little radiation dose is accumulated during this time period. During the second LEO-to-HEEPO transfer, power degrades somewhat further, but power requirements are still met. In comparison, the Europa Mapper SEP vehicle power system had a mass of 150 kg and a thin membrane array area of 100 m<sup>2</sup>.

#### References

1. Gefert, L.P.; Hack, K.J.; and Kerslake, T.W.: Options for the Human Exploration of Mars Using Solar Electric Propulsion. STAIF Conference, Albuquerque, New Mexico, Jan. 1999.
2. Kerslake, T.W.; and Gefert, L.P.: Solar Power System Analyses for Electric Propulsion Missions. 34th Intersociety Energy Conversion Engineering Conference, SAE Paper 99-01-2449 (NASA/TM-1999-209289), 1999. (Available online: <http://gltrs.grc.nasa.gov/cgi-bin/GLTRS/browse.pl?1999/TM-1999-209289.html>)

#### Glenn contact:

Thomas W. Kerslake, (216) 433-5373,  
Thomas.W.Kerslake@grc.nasa.gov

#### Authors:

Thomas W. Kerslake and Leon P. Gefert

#### Headquarters program office: OSF

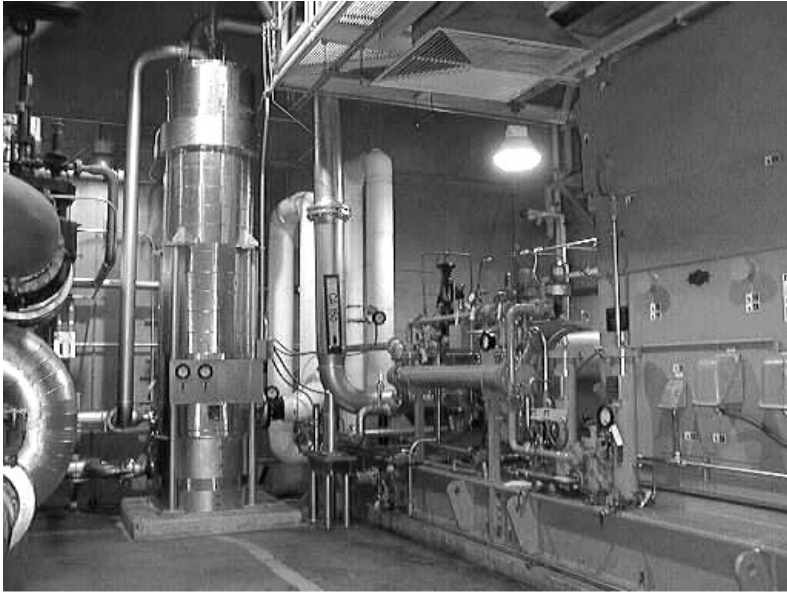
#### Programs/Projects: HEDS

# Engineering and Technical Services



# Facilities and Test Engineering

## New Compressor Added to Glenn's 450-psig Combustion Air System



*Compressor C-18 with electric drive motor and auxiliary systems.*

In September 1999, the Central Process Systems Engineering Branch and the Maintenance and the Central Process Systems Operations Branch, released for service a new high-pressure compressor to supplement the 450-psig Combustion Air System at the NASA Glenn Research Center at Lewis Field. The new compressor, designated C-18, is located in Glenn's Central Air Equipment Building and is remotely operated from the Central Control Building. C-18 can provide 40 pounds per second (pps) of airflow at pressure to our research customers. This capability augments our existing system capacity (compressors C-4 at 38 pps and C-5 at 32 pps), which

is generated from Glenn's Engine Research Building. The C-18 compressor was originally part of Glenn's 21-Inch Hypersonic Tunnel, which was transferred from the Jet Propulsion Laboratory to Glenn in the mid-1980's. With the investment of construction of facilities funding, the compressor was modified, new mechanical and electrical support equipment were purchased, and the unit was installed in the basement of the Central Air Equipment Building. After several weeks of checkout and troubleshooting, the new compressor was ready for long-term, reliable operations. With a total of 110 pps in airflow now available, Glenn is well positioned to support the high-pressure air test requirements of our research customers.

**Glenn contact:**

James F. Liebel, (216) 433-3636,  
James.F.Liebel@grc.nasa.gov

**Author:** Jeffrey A. Swan

**Headquarters program office:** OAST

**Programs/Projects:**

Propulsion Systems R&T

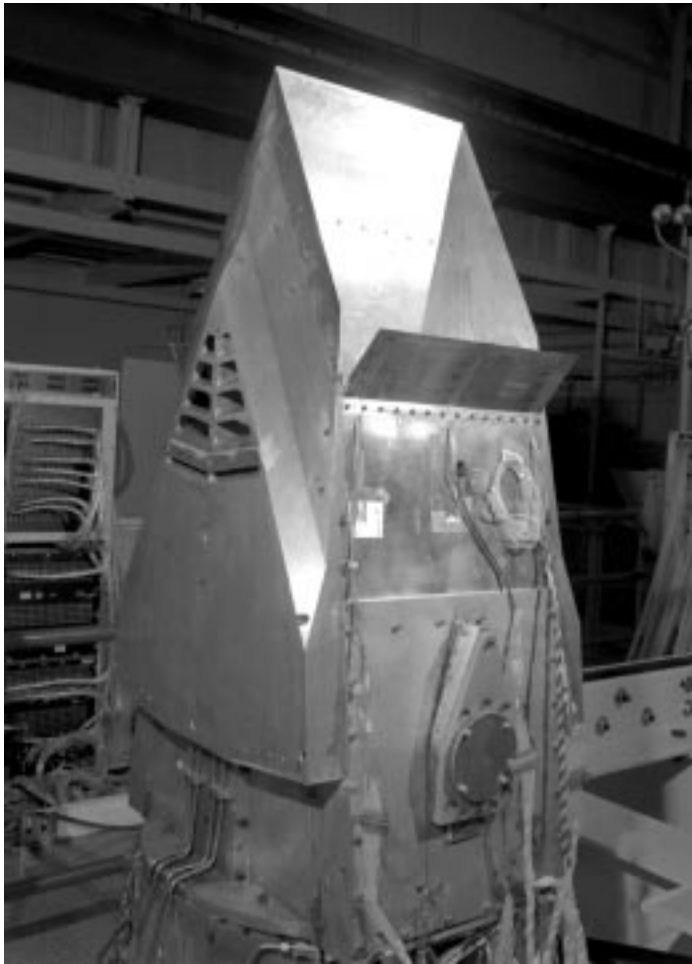
## Two-Dimensional Bifurcated Inlet Variable Cowl Lip Test Completed in 10- by 10-Foot Supersonic Wind Tunnel

Researchers at the NASA Glenn Research Center at Lewis Field successfully tested a variable cowl lip inlet at simulated takeoff conditions in Glenn's 10- by 10-Foot Supersonic Wind Tunnel (10x10 SWT) as part of the High-Speed Research Program. The test was a follow-on to the Two-Dimensional Bifurcated (2DB) Inlet/Engine test as described in reference 1.

At the takeoff condition for a High-Speed Civil Transport aircraft, the inlet must provide adequate airflow to the engine with an acceptable distortion level and high-pressure recovery. The test was conducted to study the effec-

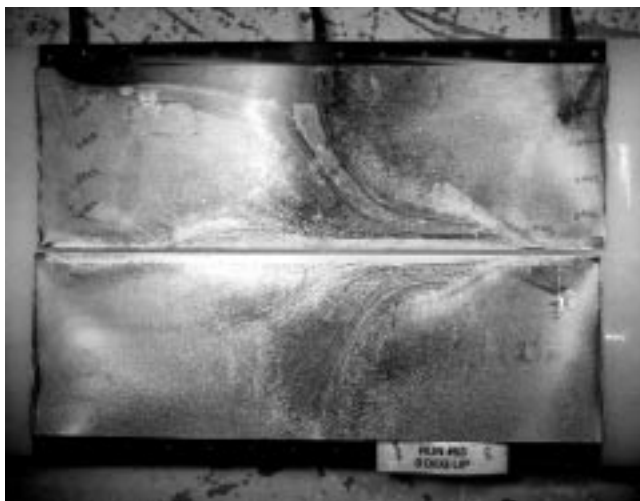
tiveness of installing two rotating lips on the 2DB Inlet cowls to increase mass flow rate and eliminate or reduce boundary layer flow separation near the lips.

Hardware was mounted vertically in the test section so that it extended through the tunnel ceil-

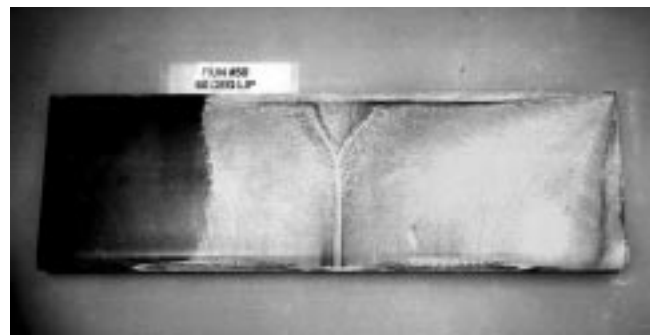


2DB Inlet with 45° cowl lips attached and exit vents open.

ing and that the 2DB Inlet was exposed to the atmosphere above the test section. The tunnel was configured in the aerodynamic mode, and exhausters were used to pump down the tunnel to vacuum levels and to provide a maximum flow rate of approximately 58 lb/sec.



Flow visualization of 0° cowl lips under ultraviolet light.



Flow visualization of 60° cowl lips under ultraviolet light. This picture shows much improvement in flow quality over the 0° baseline case.

#### *Engineering and Technical Services*

The test determined the (1) maximum flow in the 2DB Inlet for each variable cowl lip, (2) distortion level and pressure recovery for each lip configuration, (3) boundary layer conditions near variable lips inside the 2DB Inlet, (4) effects of a wing structure adjacent to the 2DB Inlet, and (5) effects of different 2DB Inlet exit configurations. It also employed flow visualization to generate enough qualitative data on variable lips to optimize the variable lip concept.

This test was a collaborative effort between the Boeing Company and Glenn. Extensive in-house support at Glenn contributed significantly to the progress and accomplishment of this test.

#### **Reference**

1. Two-Dimensional Bifurcated Inlet/Engine Tests Completed in 10- by 10-Foot Supersonic Wind Tunnel. Research and Technology 1998. NASA TM-1999-208815, 1999, p. 107. (Available online: <http://www.grc.nasa.gov/WWW/RT1998/5000/5850saunders.html>)

#### **Glenn contacts:**

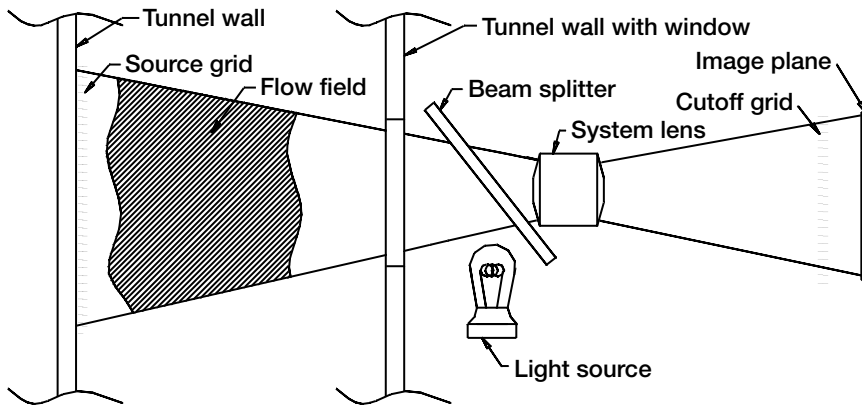
Hyun D. Kim, (216) 433-8344, Hyun.D.Kim@grc.nasa.gov;  
John D. Saunders, (216) 433-6278, John.D.Saunders@grc.nasa.gov; and  
Thomas R. Hoffman, (216) 433-5637, Thomas.R.Hoffman@grc.nasa.gov

**Author:** Thomas R. Hoffman

**Headquarters program office:** OAST

**Programs/Projects:** HSR

# Reflective Focused Schlieren System Improved for Use in 10- by 10-Foot Supersonic Wind Tunnel



Reflective focused schlieren system (not drawn to scale).

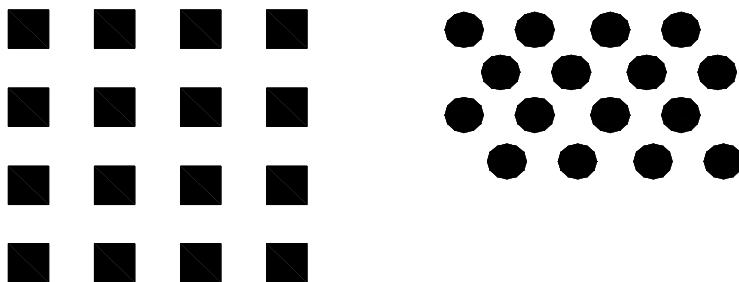
The reflective focused schlieren system that was developed for use in the 10- by 10-Foot Supersonic Wind Tunnel (10×10 SWT) at the NASA Glenn Research Center at Lewis Field as part of the Unstart Test Program was improved this past year. In April 1999, the development and use of the system was presented at the Supersonic Tunnel Association International in Bedford, England. A focused schlieren system is similar to a standard schlieren system in that shock waves coming from an object in supersonic flow can be seen using a standard video camera. Unlike the standard schlieren system, which produces a two-dimensional schlieren image, a focused schlieren system can produce a three-dimensional image. The preceding drawing shows the components of the reflective focused schlieren system being developed for use in the 10×10 SWT.

Although the system worked well for the Unstart Test Program, it was not sensitive enough to be classified as a facility capability. Therefore, a program was implemented to improve the sensitivity of the reflective focused schlieren system so that it could be a facility capability for Glenn's 10×10 SWT. Several techniques were implemented to increase the sensitivity and to improve the overall operation of the system. These included refinement of the source grid, improvement in the cutoff grid production, improvement of the source grid and cutoff grid alignment, installation of an improved light source, and incorporation of an image-enhancing system. These changes are being implemented with the system set up in the

laboratory. A checkout test of the system is planned in the 10×10 SWT in March 2000.

Of these techniques, the most developed is the refinement of the source grid. The original system had a pattern of 1/4-in. by 1/4-in. squares on 1/2-in. centers (distance between the center points of adjacent squares). This gave a ratio of light to dark (reflective to nonreflective area) of 3:1. The recommended ratio is 1:1. In order to accomplish this, a pattern of 1/4-in.-diameter dots on 3/8-in. centers was developed. Preliminary tests with this pattern showed an increase in system sensitivity and image clarity. Further testing and refinement are scheduled. The bottom figure shows the former and improved dot patterns.

The use of glass plates to produce the cutoff grid improved the cutoff grid's quality and helped to align it with the source grid. The cutoff grid, which is the negative of the source grid, is made by exposing photography film (or glass plates) to the proper light while it is installed in the focused schlieren system. The exposed film or plate is removed from the system and then developed as a photograph negative. Because the glass plates are rigid, they eliminate the risk of distortion when the negative is reinstalled in the system and realigned with the source grid.



Source grid patterns. Left: Original pattern. Right: New pattern.

**Glenn contact:**

Gary Scott Williamson, (216) 433-5717,  
Gary.S.Williamson@grc.nasa.gov

**Author:** Gary Scott Williamson

**Headquarters program office:** OAST

**Programs/Projects:** HSR, 10- by 10-Foot Supersonic Wind Tunnel

# Engineering Design and Analysis

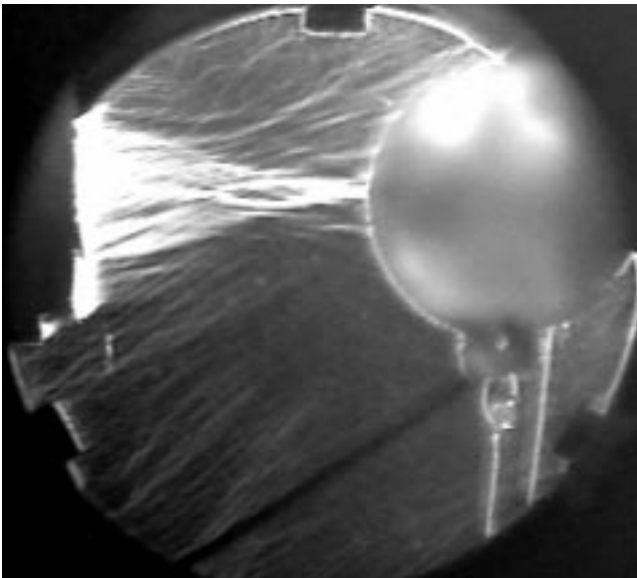
## Ultrasonic Waves in Water Visualized With Schlieren Imaging

The Acoustic Liquid Manipulation project at the NASA Glenn Research Center at Lewis Field is working with high-intensity ultrasound waves to produce acoustic radiation pressure and acoustic streaming. These effects can be used to propel liquid flows to manipulate floating objects and liquid surfaces. Interest in acoustic liquid manipulation has been shown in acoustically enhanced circuit board electroplating, microelectromechanical systems (MEMS), and microgravity space experiments. The current areas of work on this project include phased-array ultrasonic beam steering, acoustic intensity measurements, and schlieren imaging of the ultrasonic waves.

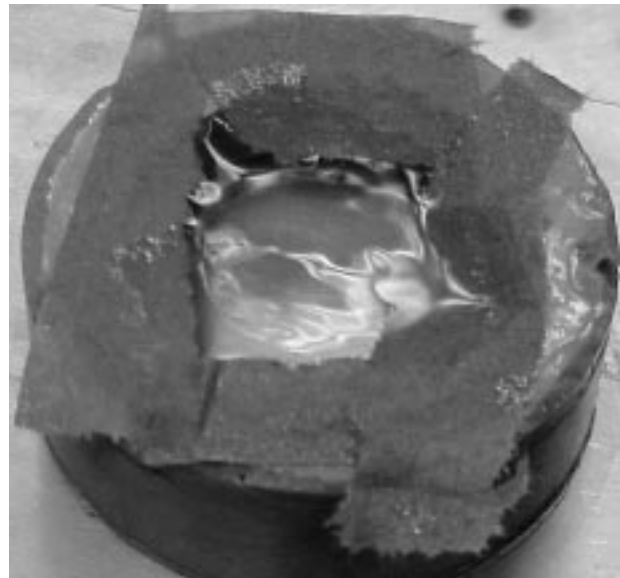
The ultrasonic waves need to be imaged for a number of reasons: to verify that the transducer producing the ultrasonic waves is functioning properly (especially at low power), to visually see the shape of the transducer's output, to help reduce reflections off the walls of the tank, and to visually verify the focal point of the transducer.

To visualize the ultrasonic field, we decided to use a schlieren imaging system because it is a well-established technique for visualizing density gradients. The system operates by sending a collimated beam of light through a test section. When areas of varying indices of refraction in the test section refract the collimated light, it is focused to the point where the light that was refracted by the index of refraction gradient in the test section is blocked, producing areas of varying brightness when the image is formed on a video camera.

For the schlieren system, a fiber light source, which is used as a point source, is collimated with a 6-in. concave spherical mirror focused offaxis. This mirror provides an economical, large field of view but produces astigmatism and field curvature. The collimated light is projected through the ultrasonic beam being studied. Since the ultrasonic beam produces pressure gradients in the water, the water's index of refraction is changed slightly. The gradient in the water's index of refraction causes the light to stray slightly from its path. The collimated beam is then focused to a point using another 6-in. concave spherical mirror. A knife-edge is placed at the focal point of the mirror to block the rays whose path has been altered by the varying index of refraction from the ultrasonic beam. A video camera is



*Schlieren image of ultrasonic waves in water deflection in an air-filled glass sphere.*



*Deformation of water surface by acoustic radiation pressure.*



*Experimental setup in the Acoustic Liquid Manipulation Lab.*

placed after the knife-edge, allowing the ultrasonic beam to be viewed on a monitor.

In the near future, the Acoustic Liquid Manipulation project plans moving to a microelectromechanical systems scale: that is, devices on the scale of hundreds of micrometers. This will require adapting the schlieren system to a much smaller scale.

## Mars Spark Source Prototype Developed

The Mars Spark Source Prototype (MSSP) hardware was developed as part of a proof of concept system for the detection of trace metals such as lead, cadmium, and arsenic in Martian dusts and soils. A spark discharge produces plasma from a soil sample, and detectors measure the optical emission from metals in the plasma to identify and quantify them.

Trace metal measurements are vital in assessing whether or not the Martian environment will be toxic to human explorers. The current method of x-ray fluorescence can yield concentrations of major species only. Other instruments are incompatible with the volume, weight, and power constraints for a Mars mission. The new instrument will be developed primarily for use in the Martian environment, but it would be adaptable for terrestrial use in environmental monitoring.

The NASA Glenn Research Center at Lewis Field initiated the development of the MSSP as part of Glenn's Director's Discretionary Fund project for the Spark Analysis Detection of Trace Metal Species in Martian Dusts and Soils. The objective of this project is to develop and demonstrate a compact, sensitive optical instrument for the detection of trace hazardous metals in Martian dusts and soils.

Glenn built the MSSP hardware, which was developed from inexpensive, readily available commercial components to minimize costs and develop-

### Bibliography

Hanafy, A.; Zanelli, C.I.; and McAvoy, B.R.: Quantitative Real-Time Pulsed Schlieren Imaging of Ultrasonic Waves. IEEE Ultrasonics Symposium, IEEE, New York, NY, 1991, pp. 1223-1227.

### Glenn contact:

Jeffrey R. Juergens, (216) 433-5460, Jeffrey.R.Juergens@grc.nasa.gov

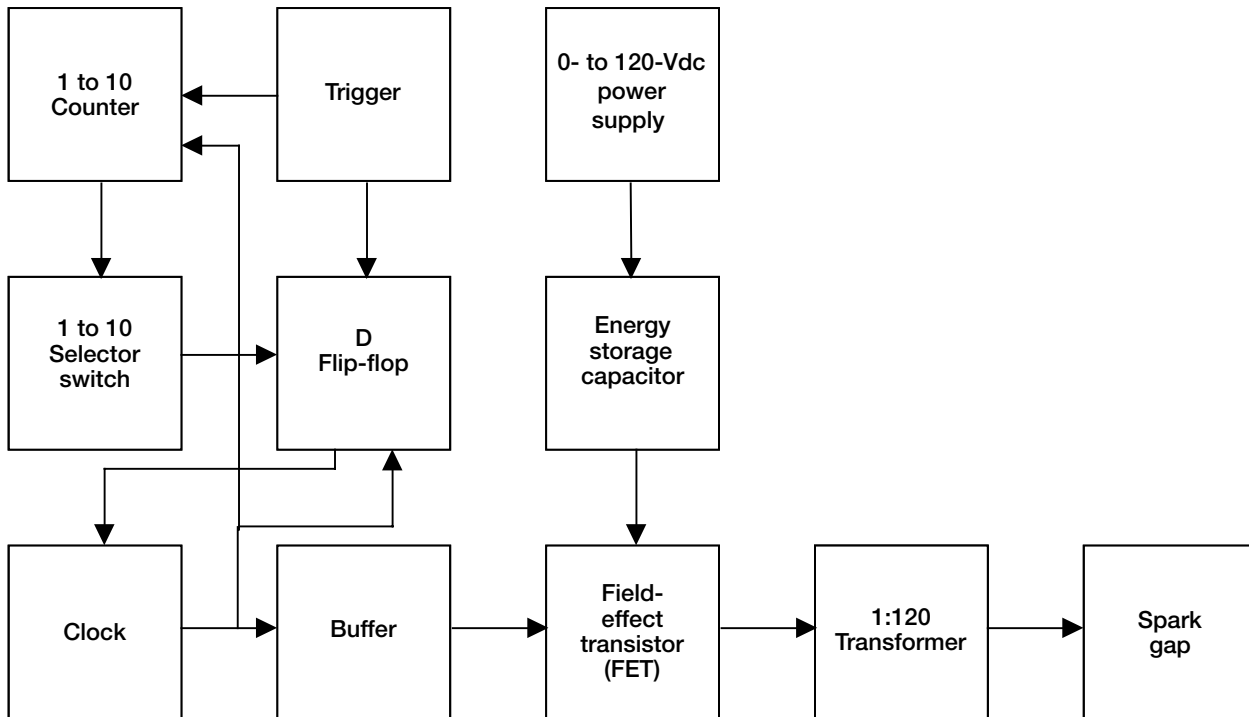
**Author:** Jeffrey R. Juergens

**Programs/Projects:** GMI

ment time. Miniaturization and optimization of the hardware will greatly improve its efficiency for space applications.

Tests were performed successfully to characterize the prototype's performance in 1 atm of air, in 10 torr of air, and in 10 torr of carbon dioxide (CO<sub>2</sub>). A pressure of 10 torr of CO<sub>2</sub> approximates the Martian atmosphere.

A block diagram of the Mars Spark Source Prototype is shown in the figure. A clock is used to provide a pulse train and adjust the pulse width. The output of the clock is taken to a counter and a flip-flop. Triggering the circuit resets both. A selector switch from the output of the counter selects the desired number of pulses from 1 to 10.



*Mars Spark Source Prototype (MSSP).*

After the preset number of pulses has been attained, the flip-flop inhibits the clock until the circuit is triggered again. The output pulses go to a buffer that drives a field effect transistor (FET), which provides power from a 0- to 120-Vdc power supply and an energy storage capacitor to the primary winding of a pulse transformer. The secondary winding of the pulse transformer is connected to the spark gap.

#### **Bibliography**

Eichenberg, D.J., et al.: Mars Spark Source Prototype. NASA/TM-1999-209448, 1999. (Available online: <http://gltrs.grc.nasa.gov/cgi-bin/GLTRS/browse.pl?/1999/TM-1999-209448.html>)

#### **Glenn contacts:**

Dennis J. Eichenberg, (216) 433-8360, [Dennis.J.Eichenberg@grc.nasa.gov](mailto:Dennis.J.Eichenberg@grc.nasa.gov); and Dr. Karen J. Weiland, (216) 433-3623, [Karen.J.Weiland@grc.nasa.gov](mailto:Karen.J.Weiland@grc.nasa.gov)

**Authors:** Dennis J. Eichenberg, Glenn R. Lindamood, Dr. Randall L. Vander Wal, and Dr. Karen J. Weiland

**Headquarters program office:** OAST

**Programs/Projects:** Microgravity Combustion Science, CDDF

# Reduced-Noise Gas Flow Design Guide Developed as a Noise-Control Design Tool for Meeting Glenn's Hearing Conservation and Community Noise Goals



*The Reduced Noise Gas Flow Design Guide enables the development and implementation of noise-control strategies such as this silencer, which reduces the noise generated by the multiple pressure relief valves associated with Glenn's Central Process Air System. This system provides high-pressure processed air and exhaust to support Glenn's experimental facilities.*

A Reduced-Noise Gas Flow Design Guide has been developed for the NASA Glenn Research Center at Lewis Field by Nelson Acoustical Engineering of Elgin, Texas. Gas flow systems are a significant contributor to the noise exposure landscape at Glenn. Because of the power of many of these systems, hearing conservation and community noise are important issues. The purpose of the Guide is to allow Glenn engineers and designers to address noise emission and control at the design stage by using readily available system parameters. Although the Guide was developed with Glenn equipment and systems in mind, it is expected to have wide application in industry.

The Guide addresses several noise-generating gas flow processes, including

- Gas and steam discharge vents, ambient air intake vents, and inlet debris screens
- Compressors, exhausters, fans, and blowers
- Turbomachinery components such as inlet fans and compressors, combustor cores, turbines, exhaust jet mixing, and exhaust jet shock cells
- Flow noise from pipe walls and at fittings

- Control valves
- Orifices and venturis

The Guide also addresses the noise control performance of elements typically associated with gas flow systems:

- The walls of pipes, ducts, and vessels
- Vent silencers and inline silencers
- Intake and discharge duct openings with flow
- Acoustical lagging

The Guide consists of two parts: a written manual and a Microsoft Excel (Microsoft Corporation) workbook. The manual explains the mechanisms of noise generation, provides low-noise design guidelines, lists design parameters required for noise estimation, and describes applicable noise control methods. The parameters of the predictive equations consist of readily available design information such as mass flow rates, gas properties, pipe diameters, and wall thickness. No manual calculations are necessary because the noise emission estimates are implemented in an easy-to-follow spreadsheet format in the accompanying software workbook.

The workbook consists of 16 spreadsheets that implement the noise-emission and noise-reduction estimates, 2 spreadsheets that perform computations for an elementary gas flow system, and a handy gas flow parameter calculator spreadsheet that includes unit conversions, decibel mathematics,

ideal gas equations, and isentropic expansions and contractions. Two linked spreadsheets that combine estimates from the individual source noise estimation spreadsheets are used to model noise emission from a gas flow system. The gas flow system also addresses radiation from pipe openings, pipe walls, and extended surfaces; the benefit of inline silencers and pipe lagging; and the influence of reverberation on indoor sound levels.

Noise emission estimates generated by the workbook are compared directly with maximum noise-emission criteria determined in accordance with Glenn's "Buy Quiet" Program. The ability to predict sound levels at any point in a gas flow system greatly facilitates the development of noise-control strategies for new experimental research facilities and support systems, thus promoting compliance with hearing conservation and community noise goals.

**Find out more about Glenn Research Center resources for noise control and hearing conservation on the World Wide Web:**

<http://acousticaltest.grc.nasa.gov>

[http://www-osma.grc.nasa.gov/oep/nmtpages/oep\\_nt.htm](http://www-osma.grc.nasa.gov/oep/nmtpages/oep_nt.htm)

**Bibliography**

Nelson, D.A.; and Cooper, B.A.: Reduced-Noise Gas Flow Design Guide for NASA Glenn Research Center. Proceedings of InterNoise 99, the International Congress on Noise Control Engineering. Institute of Noise Control Engineering, Washington, DC, 1999. (Available online: <http://acousticaltest.grc.nasa.gov>)

*Engineering and Technical Services*

Cooper, B.A.; and Nelson, D.A.: Development of a 'Quiet-by-Design' Approach to Reduced-Noise Gas Flow Systems for Experimental Research Facilities at NASA Lewis Research Center. Presented at the 136th Meeting of the Acoustical Society of America, October 12–16, 1998.

Nelson, D.A.; and Cooper, B.A.: A "Reduced-Noise Gas Flow Design Guide" for NASA Glenn Research Center. Proceedings of Internoise '99, Dec. 5–8, 1999.

**Glenn contact:**

Beth A. Cooper, (216) 433–3950,  
[Beth.A.Cooper@grc.nasa.gov](mailto:Beth.A.Cooper@grc.nasa.gov)

**Author:** Beth A. Cooper

**Headquarters program office:**

OLMSA (OH), OSMA

**Programs/Projects:** Occupational Health, Propulsion Systems R&T

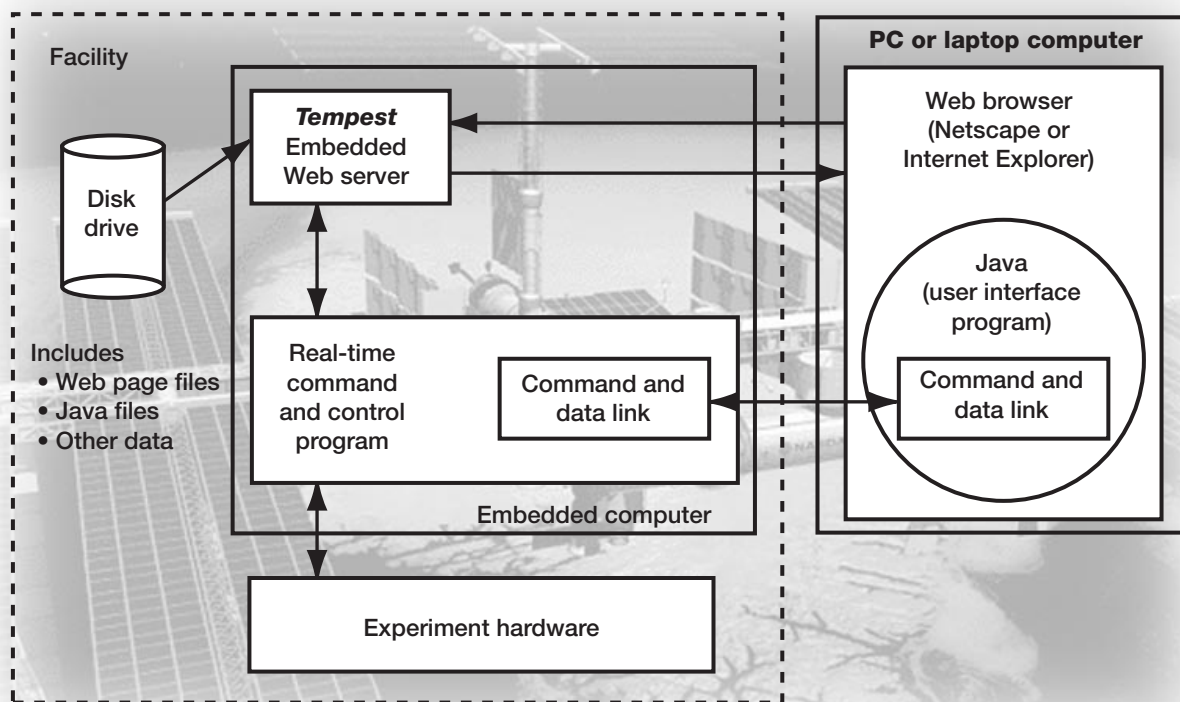
## New Web Server—the Java Version of *Tempest*—Produced

A new software design and development effort has produced a Java (Sun Microsystems, Inc.) version of the award-winning *Tempest* software (refs. 1 and 2). In 1999, the Embedded Web Technology (EWT) team received a prestigious R&D 100 Award for *Tempest*, Java Version. In this article, "*Tempest*" will refer to the Java version of *Tempest*, a World Wide Web server for desktop or embedded systems.

*Tempest* was designed at the NASA Glenn Research Center at Lewis Field to run on any platform for which a Java Virtual Machine (JVM, Sun Microsystems, Inc.) exists. The JVM acts as a translator between the native code of the platform and the byte code of *Tempest*, which is compiled in Java. These byte code files are Java executables with a ".class" extension. Multiple byte code files can be zipped together as a "\*.jar" file for more efficient transmission over the Internet. Today's popular browsers, such as Netscape (Netscape Communications Corporation) and Internet Explorer (Microsoft Corporation) have built-in Virtual Machines to display Java applets.

The popularity of Java has given Sun Microsystems, Inc., the ability to support a large number of platforms and operating systems. *Tempest* was able to leverage this popularity and make it attractive for a wide range of users to employ *Tempest* as a platform-independent web server.

*Tempest* was designed with features allowing ease of installation in embedded or desktop computers. Separate configuration files are one of these features. The user can modify the configuration files to limit client access to the server according to Internet Protocol (IP) addresses or to specific user ID and password combinations that force clients to identify themselves as valid users. Other configuration files include a file that links stored images to specific user ID's for the customization of web pages served by *Tempest* and a file that contains pseudo commands for other executables on the server. The pseudo commands work in conjunction with *Tempest's* dynamic web page feature or custom <TEMPEST> tags to modify the contents of web pages as they are served.



*Embedded Web Technology.*

Command line options allow users to specify *Tempest* port numbers and persistent or nonpersistent connections, and to enable or disable a debug feature, a logging feature, or the client ID and password authorization.

*Tempest* requires little minimum memory (< 200 kilobytes) and computer resources. Its source code is available through participation in the EWT Workshops and is well documented for those who wish to customize the code. A user manual and design manual are also available.

Existing applications of *Tempest* include remote control of video cameras (pan, tilt, zoom, and focus), science experiments for education (ref. 2), and applications in the automotive, medical, instrumentation, machine control, and communications industries. *Tempest* is being applied in-house in Glenn's Satellites and Networking Branch, Manufacturing Engineering Division, and External Programs Directorate.

**Find out more about Glenn's EWT and VIC projects on the World Wide Web:**

**Embedded Web Technology:** <http://vic.grc.nasa.gov/>

**Virtual Interactive Classroom:** <http://vic.grc.nasa.gov/virtlab/>

**References**

1. Daniele, C.J.: Embedded Web Technology: Internet Technology Applied to Real-Time System Control. Research & Technology 1997, NASA/TM-1998-206312, 1998, pp. 165-166. (Available online: <http://www.grc.nasa.gov/WWW/RT1997/7000/7750daniele.htm>)

2. York, D.W.; and Babula, M: Virtual Interactive Classroom: A New Technology for Distance Learning Developed. Research & Technology 1998, NASA/TM-1999-208815, 1999, pp. 183-184. (Available online: <http://www.grc.nasa.gov/WWW/RT1998/7000/7750york.html>)

**Glenn contacts:**

David W. York, (216) 433-3162, [David.W.York@grc.nasa.gov](mailto:David.W.York@grc.nasa.gov);  
 Maria Babula, (216) 433-5221, [Maria.Babula@grc.nasa.gov](mailto:Maria.Babula@grc.nasa.gov);  
 Joseph G. Ponyik, (216) 433-8592, [Joseph.G.Ponyik@grc.nasa.gov](mailto:Joseph.G.Ponyik@grc.nasa.gov); and  
 Lisa M. Lambert, (216) 433-3994, [Lisa.M.Lambert@grc.nasa.gov](mailto:Lisa.M.Lambert@grc.nasa.gov)

**Authors:**

David W. York and Joseph G. Ponyik

**Headquarters program office:** OLMSA

**Programs/Projects:**

VIC, EWT, SEMAA, AEL, FCF, LTP

**Special Recognition:**

*Tempest*, Java Version, received a 1999 R&D Magazine 100 Award.

# Definitions of NASA Headquarters Program Offices

<b>OAST</b>	Office of Aero-Space Technology
<b>OLMSA</b>	Office of Life & Microgravity Sciences & Applications
<b>MRD</b>	Microgravity Research Division
<b>MRPO</b>	Microgravity Research Program Office
<b>OH</b>	Occupational Health
<b>OSF</b>	Office of Space Flight
<b>OSMA</b>	Office of Safety and Mission Assurance
<b>OSS</b>	Office of Space Science
<b>ATMS</b>	Advanced Technology & Mission Studies Division
<b>SCO</b>	Space Communications Office

# Definitions of Programs and Projects

<b>AAP</b>	Advanced Aircraft Program
<b>AC/ATM</b>	Advanced Communications for Air Traffic Management
<b>ACESE</b>	Attitude Control and Energy Storage Experiment
<b>ACTS</b>	Advanced Communication Technology Satellite
<b>AEL</b>	Aeronautics Education Laboratory
<b>AITP</b>	Aerospace Industry Technology Program
<b>AOS</b>	Aviation Operations Systems
<b>ASCOT</b>	Airframes Systems Concept to Test
<b>AST</b>	Advanced Subsonic Technology
<b>ASTP</b>	Advanced Space Transportation Program
<b>AVRS</b>	Adaptive Vibration Reduction System
<b>AvSP</b>	Aviation Safety Program
<b>CDDF</b>	Center Director's Discretionary Fund
<b>CETDP</b>	Cross-Enterprise Technology Development Program
<b>COMMTECH</b>	A cooperative technology commercialization program
<b>CTO</b>	Glenn's Commercial Technology Office
<b>D<sup>3</sup></b>	Direct Data Distribution
<b>EPM</b>	Enabling Propulsion Materials
<b>EWT</b>	Embedded Web Technology
<b>FCF</b>	Fluids & Combustion Facility for the International Space Station
<b>FQE</b>	Fast Quiet Engine
<b>GMI</b>	Glennan Microsystems Initiative
<b>GPS</b>	Global Positioning System
<b>HEDS</b>	Human Exploration and Development of Space
<b>HITEMP</b>	Advanced High Temperature Engine Materials Technology Program
<b>HPCC</b>	High Performance Computing and Communications
<b>HRDD</b>	high-rate data delivery
<b>HSCT</b>	High-Speed Civil Transport
<b>HSR</b>	High-Speed Research
<b>HST</b>	Hubble Space Telescope
<b>HTD</b>	Hardware Technology Demonstration
<b>IHPTET</b>	Integrated High Performance Turbine Engine Technology
<b>IITS</b>	Integrated Instrumentation Testing Systems
<b>ISS</b>	International Space Station
<b>IT Base</b>	Information Technology Base Program
<b>JSC</b>	NASA Johnson Space Center
<b>JSF</b>	Joint Strike Fighter
<b>LEO</b>	low Earth orbit
<b>LTP</b>	Learning Technologies Project
<b>NGST</b>	Next Generation Space Telescope
<b>NSTAR</b>	NASA Solar Electric Propulsion Technology Applications Readiness
<b>PHSV</b>	Propulsion for Highly Survivable Vehicles
<b>P&amp;PM</b>	Physics and Process Modeling

<b>R&amp;T</b>	Research and Technology
<b>RLV</b>	Reusable Launch Vehicles
<b>RNSS</b>	Radionavigation Satellite Service
<b>SAMS–FF</b>	Space Acceleration Measurement System for Free Flyers
<b>SBIR</b>	Small Business Innovation Research
<b>SEMAA</b>	Science/Engineering/Mathematics & Aerospace Academy
<b>SERT</b>	Space Solar Power Exploratory Research and Technology
<b>SGE</b>	Smart Green Engine
<b>SOMO</b>	Space Operations Management Office
<b>SRF</b>	Strategic Research Fund
<b>SSP</b>	Space Solar Power
<b>STR</b>	Space Transportation Research
<b>TCT</b>	Technical Communication Terminal
<b>TDRSS H,I,J</b>	Tracking and Data Relay Satellite
<b>UAV</b>	Unmanned Aerial Vehicle
<b>UEET</b>	Ultra Efficient Engine Technology
<b>VIC</b>	Virtual Interactive Classroom
<b>VUV</b>	vacuum ultraviolet light
<b>WINCOMM</b>	Weather Information Communications
<b>X–33</b>	Replacement for space shuttles

# Index of Authors and Contacts

Both authors and contacts are listed in this index. Articles start on the page numbers following the names.

- A**  
Abel, Dr. Phillip B. 16, 107  
Abdul-Aziz, Ali 94  
Acosta, Dr. Roberto J. 128  
Addy, Harold E., Jr. 79  
Allman, Mark A. 66  
Alston, Dr. William B. 19  
Angel, Dr. Paul W. 23  
Ansari, Dr. Rafat R. 143, 160  
Arnold, Dr. Steven M. 97  
Austin, Curt 103  
Axelbaum, Professor Richard L. 140
- B**  
Baaklini, Dr. George Y. 93, 94, 103  
Babula, Maria 177  
Bakhle, Milind A. 108  
Banks, Bruce A. 42, 43, 48, 49, 53, 54  
Barth, Janet L. 49  
Bartolotta, Dr. Paul A. 98, 99, 102  
Bauer, Robert A. 129  
Becker, Angela R. 153  
Beheim, Dr. Glenn M. 57  
Bencic, Timothy J. 61  
Benson, Scott W. 163  
Berton, Jeffrey J. 2  
Bizon, Thomas P. 69  
Bodis, James R. 107  
Bowman, Dr. Randy R. 9  
Bozzolo, Dr. Guillermo H. 16  
Brady, Michael P. 6  
Breisacher, Kevin J. 63  
Bridges, Dr. James E. 116  
Bright, Michelle M. 62  
Buhro, Professor William E. 33
- C**  
Carney, Dr. Kelly S. 110  
Castelli, Michael G. 97  
Cato, Daveen R. 45  
Chamis, Dr. Christos C. 105  
Chapek, Richard M. 141  
Chao, Professor Beei-Huan 140  
Chao, Dr. David F. 146, 148  
Chen, Dr. Liang-Yu 58  
Chenault, Dr. Michelle V. 143  
Chock, Ricaurte 32
- Choi, Dr. Sung R. 100  
Choo, Dr. Yung K. 81  
Cooper, Beth A. 176  
Curry, Dr. Donald M. 24
- D**  
Darolia, Dr. Ram 9  
Datiles, Dr. Manuel B., III 143  
de Groh, Kim K. 45, 46, 49  
DeAngelo, Frank L. 59  
DeLaat, John C. 63  
Delgado, Irebert R. 117  
DellaCorte, Dr. Christopher 17  
Dever, Joyce A. 48, 49, 54  
Dhadwal, Dr. Harbans S. 109  
DiCarlo, Dr. James A. 11, 104  
Doherty, Michael P. 157  
Draper, Susan L. 103  
Dunlap, Patrick H., Jr. 123  
Durian, Professor Douglas J. 153
- E**  
Eckel, Dr. Andrew J. 12  
Eichenberg, Dennis J. 174  
Espe, Dr. Matthew P. 45
- F**  
Farmer, Dr. Serene C. 13  
Feliciano, Walber 128  
Flood, Dr. Dennis J. 34  
Friedman, Robert 137
- G**  
Gaier, Dr. James R. 45  
Gariepy, Christopher 20  
Gaugler, Dr. Raymond E. 75  
Gauntner, William 128  
Gefert, Leon P. 166  
Georgiadis, Nicholas J. 88  
Gerber, Scott S. 52  
Giel, Dr. Paul W. 75  
Gokoglu, Suleyman A. 138  
Goldberg, Robert K. 101  
Goldsby, Dr. Jon C. 14  
Greenbauer-Seng, Leslie A. 28  
Gregory, Teri 49  
Gyekenyesi, Dr. Andrew L. 93  
Gyekenyesi, Dr. John P. 100
- H**  
Halbig, Michael C. 14  
Hall, Greg 59  
Hall, Rachelle L. 45  
Hammoud, Ahmad 52  
Handschuh, Dr. Robert F. 118  
Harris, Dr. Jerry D. 33  
Hasan, Dr. Mohammad M. 146  
Hathaway, Dr. Michael D. 73  
Hatton, Kenneth S. 28  
Hehemann, Dr. David G. 33  
Heinen, Dr. Vernon O. 67  
Hendricks, J. Lynne 107  
Hepp, Dr. Aloysius F. 33  
Hoffman, Thomas R. 170  
Hoffmann, Monica I. 149, 151, 160  
Hollingsworth, Jennifer A. 33  
Hopkins, Dale A. 113  
Howard, Samuel A. 17  
Hung, Ching-cheh 50  
Hunter, Dr. Gary W. 58, 59
- I**  
Ivancic, William D. 66
- J**  
Jacobson, Dr. Nathan S. 24  
Jankovsky, Robert S. 38  
Jansen, Ralph H. 115  
Jaworske, Dr. Donald A. 51  
Johnson, Sandra K. 128  
Jones, Jeffrey A. 140  
Juergens, Jeffrey R. 173  
Juhasz, Albert J. 41
- K**  
Kacpura, Thomas J. 155  
Kautz, Harold E. 107  
Kerslake, Thomas W. 163, 164, 166  
Kim, Hyun D. 170  
Kory, Carol L. 67  
Krantz, Timothy L. 120  
Krause, David L. 98, 102  
Kuczarski, Dr. Maria A. 60  
Kurkov, Dr. Anatole P. 109

**L**

Lambert, Lisa M. 177  
 Lawrence, Dr. Charles 110  
 Lee, Ho-Jun 111  
 Lei, Dr. Jih-Fen 58  
 Lerch, Dr. Bradley A. 103, 114  
 Liebel, James F. 170  
 Lindamood, Glenn R. 174  
 Liou, Dr. Meng-Sing 92  
 Liu, Professor C.C. 59  
 Locci, Dr. Ivan E. 6, 8, 9

**M**

Makel, Dr. D. 59  
 Mallasch, Paul G. 130  
 Manzo, Michelle A. 35  
 Martzaklis, Konstantinos S. 130  
 Mason, Lee S. 38  
 McCue, Terry R. 46  
 McEntee, Kathleen M. 128  
 Meador, Dr. Mary Ann 20  
 Meador, Dr. Michael A. 20  
 Meyer, Claudia M. 65  
 Meyer, William V. 160  
 Miller, Dean R. 82  
 Miller, Dr. Robert A. 29  
 Miller, Thomas B. 36  
 Min, Dr. James B. 111  
 Mital, Subodh K. 104  
 Miyoshi, Dr. Kazuhisa 26  
 Murthy, Dr. Pappu L.N. 104, 105

**N**

Nahra, Henry K. 149  
 Neudeck, Dr. Philip G. 58, 60  
 Neville, Donna L. 141  
 Norris, Mary Jo 45  
 NPARC Alliance User Support 88

**O**

Okiishi, Dr. Theodore H. 73

**P**

Palaszewski, Bryan A. 77, 78  
 Palazzolo, Dr. Alan 115  
 Panda, Jayanta 89  
 Patnaik, Dr. Surya N. 113  
 Patterson, Richard L. 52  
 Paxson, Dr. Daniel E. 74  
 Pearlman, Dr. Howard 141  
 Penko, Paul F. 79  
 Pereira, Dr. J. Michael 101, 103, 114

Ponyik, Joseph G. 177  
 Porro, A. Robert 87  
 Potapczuk, Dr. Mark G. 84  
 Proctor, Margaret P. 117, 122  
 Provenza, Andy J. 115

**R**

Raffaella, Professor Ryne P. 33  
 Raj, Dr. Sai V. 8  
 Ratvasky, Thomas P. 82, 86  
 Rawlin, Vincent K. 40  
 Reed, Brian D. 39  
 Reehorst, Andrew L. 85  
 Retallick, William B. 6  
 Rieke, William J. 86  
 Robinson, R. Craig 28  
 Romanofsky, Robert R. 133  
 Roth, Dr. Don J. 107  
 Rutledge, Sharon K. 42, 43, 53, 54  
 Rybicki, Dr. George C. 33

**S**

Saiyed, Naseem H. 116  
 Salem, Jonathan A. 8  
 Saunders, John D. 170  
 Savage, William J. 49  
 Sayir, Dr. Ali 13  
 Scheiman, Daniel A. 19  
 Schultz, Donald 138  
 Seasholtz, Dr. Richard G. 89  
 Sebag, Dr. J. 143  
 Sechkar, Edward A. 42, 43, 48, 53, 54  
 Seigneur, Alban D. 3  
 Sicker, Ronald J. 155  
 Singh, Brijendra 3  
 Singh, Dr. Mrityunjay 15  
 Skoch, Gary J. 62  
 Smialek, Dr. James L. 6  
 Sovey, James S. 40  
 Spence, Rodney L. 131  
 Srivastava, Rakesh 108  
 Stefko, George L. 108  
 Steinetz, Dr. Bruce M. 117, 122, 123  
 Stocker, Dennis P. 140  
 St.Onge, Thomas H. 154  
 Strazisar, Dr. Anthony J. 73  
 Street, Dr. Kenneth W. 18  
 Stueber, Thomas J. 42, 43, 48, 53, 54  
 Suh, Dr. Kwang I. 143  
 Sunderland, Dr. Peter B. 140  
 Sutter, Dr. James K. 22  
 Swan, Jeffrey A. 170

**T**

Tew, Roy C. 41  
 Thieme, Lanny G. 55  
 Thomson, Shaun 49  
 Tomsik, Thomas M. 90  
 Towne, Dr. Charles E. 88  
 Townsend, Jacqueline A. 49  
 Tran, Quang K. 71

**U**

Urban, Dr. David L. 140

**V**

Valco, Dr. Mark J. 17  
 Vancil, Bernard K. 68  
 Vander Wal, Dr. Randall L. 174  
 Van Zante, Dr. Dale E. 73  
 Van Zante, Dr. Judith Foss 86  
 Vickerman, Mary B. 81

**W**

Wald, Lawrence W. 133, 134  
 Warner, Joseph D. 133  
 Weiland, Dr. Karen J. 174  
 Welch, Dr. Gerard E. 74  
 Wernet, Dr. Mark P. 62  
 Whalen, Mike F. 107  
 Whittenberger, Dr. J. Daniel 8, 9  
 Wilkinson, Dr. R. Allen 151, 152  
 Williamson, Gary Scott 172  
 Wilson, Dr. Jack 74  
 Wilt, David M. 34  
 Winsa, Edward A. 154  
 Wintucky, Edwin G. 68  
 Wood, Jerry R. 73  
 Wright, William B. 84  
 Wu, Dr. Ming-Shin 141  
 Wu, Q.H. 59

**Y**

York, David W. 177  
 Yun, Hee Mann 11

**Z**

Zakrajsek, James J. 120  
 Zakrajsek, Robert J. 135  
 Zimmerli, Dr. Gregory A. 153  
 Zhu, Dr. Dongming 29  
 Zurawski, Robert L. 154

<b>REPORT DOCUMENTATION PAGE</b>			<i>Form Approved</i> <i>OMB No. 0704-0188</i>	
Public reporting burden for this collection of information is estimated to average 1 hour per response, including the time for reviewing instructions, searching existing data sources, gathering and maintaining the data needed, and completing and reviewing the collection of information. Send comments regarding this burden estimate or any other aspect of this collection of information, including suggestions for reducing this burden, to Washington Headquarters Services, Directorate for Information Operations and Reports, 1215 Jefferson Davis Highway, Suite 1204, Arlington, VA 22202-4302, and to the Office of Management and Budget, Paperwork Reduction Project (0704-0188), Washington, DC 20503.				
<b>1. AGENCY USE ONLY (Leave blank)</b>		<b>2. REPORT DATE</b> March 2000	<b>3. REPORT TYPE AND DATES COVERED</b> Technical Memorandum	
<b>4. TITLE AND SUBTITLE</b>  Research & Technology 1999			<b>5. FUNDING NUMBERS</b>  None	
<b>6. AUTHOR(S)</b>				
<b>7. PERFORMING ORGANIZATION NAME(S) AND ADDRESS(ES)</b>  National Aeronautics and Space Administration John H. Glenn Research Center at Lewis Field Cleveland, Ohio 44135-3191			<b>8. PERFORMING ORGANIZATION REPORT NUMBER</b>  E-11969	
<b>9. SPONSORING/MONITORING AGENCY NAME(S) AND ADDRESS(ES)</b>  National Aeronautics and Space Administration Washington, DC 20546-0001			<b>10. SPONSORING/MONITORING AGENCY REPORT NUMBER</b>  NASA TM-2000-209639	
<b>11. SUPPLEMENTARY NOTES</b>  Responsible person, Walter S. Kim, organization code 9400, (216) 433-3742.				
<b>12a. DISTRIBUTION/AVAILABILITY STATEMENT</b>  Unclassified - Unlimited Subject Categories: 01 and 31  This publication is available from the NASA Center for AeroSpace Information, (301) 621-0390.			<b>12b. DISTRIBUTION CODE</b>  Distribution: Nonstandard	
<b>13. ABSTRACT (Maximum 200 words)</b>  This report selectively summarizes the NASA Glenn Research Center's research and technology accomplishments for the fiscal year 1999. It comprises 130 short articles submitted by the staff scientists and engineers. The report is organized into four major sections: Aeronautics, Research and Technology, Space, and Engineering and Technical Services. A table of contents and an author index have been developed to assist readers in finding articles of special interest. This report is not intended to be a comprehensive summary of all the research and technology work done over the past fiscal year. Most of the work is reported in Glenn-published technical reports, journal articles, and presentations prepared by Glenn staff and contractors. In addition, university grants have enabled faculty members and graduate students to engage in sponsored research that is reported at technical meetings or in journal articles. For each article in this report, a Glenn contact person has been identified, and where possible, reference documents are listed so that additional information can be easily obtained. The diversity of topics attests to the breadth of research and technology being pursued and to the skill mix of the staff that makes it possible. For more information about research at NASA Glenn, visit us on the World Wide Web ( <a href="http://www.grc.nasa.gov">http://www.grc.nasa.gov</a> ). This document is available on the World Wide Web ( <a href="http://www.grc.nasa.gov/WWW/RT/">http://www.grc.nasa.gov/WWW/RT/</a> ). For publicly available reports, visit the Glenn Technical Report Server (GLTRS) on the World Wide Web ( <a href="http://gltrs.grc.nasa.gov/GLTRS/">http://gltrs.grc.nasa.gov/GLTRS/</a> ).				
<b>14. SUBJECT TERMS</b>  Aeronautics; Aerospace engineering; Space flight; Space power; Materials; Structures; Electronics; Space experiments; Technology transfer			<b>15. NUMBER OF PAGES</b> 197	
			<b>16. PRICE CODE</b> A09	
<b>17. SECURITY CLASSIFICATION OF REPORT</b> Unclassified	<b>18. SECURITY CLASSIFICATION OF THIS PAGE</b> Unclassified	<b>19. SECURITY CLASSIFICATION OF ABSTRACT</b> Unclassified	<b>20. LIMITATION OF ABSTRACT</b>	